Development and monitoring of a novel monoclonal antibody purification strategy

TECHNISCHE
UNIVERSITÄT
DARMSTADT

Vom Fachbereich Chemie
der Technischen Universität Darmstadt

zur Erlangung des akademischen Grades eines

Doctor rerum naturalium (Dr. rer. nat.)

genehmigte
kumulative Dissertation

vorgelegt von

M.Sc. Florian Capito
aus Mainz

Referent: Prof. Dr. Harald Kolmar
Korreferent: Prof. Dr. Katja Schmitz

Tag der Einreichung: 18. Oktober 2013
Tag der mündlichen Prüfung: 20. Januar 2014

Darmstadt 2014

für meine Eltern

I think the biggest innovations of the twenty-first century will be the intersection of biology and technology. (Steve Jobs)

Danksagung

Zusammenfassung und Kontext

Therapeutische Antikörper finden eine breite Anwendung in klinischen Applikationen, Diagnostik sowie Forschung und Entwicklung. Diese Proteine werden u.a. in Säugetierzellen in Bioreaktoren produziert und müssen danach über Aufreinigungskaskaden im sogennanten „Downstream processing" von anderen, unerwünschten Proteinen sowie Verunreinigungen getrennt werden. Typischerweise erfolgt zunächst eine Klärifizierung des Zellkulturüberstandes durch Zentrifugation und Filtration und danach eine Reihe von chromatographischen Schritten sowie weitere Filtrationen. Der initiale Chromatographieschritt ist hierbei üblicherweise eine Affinitätschromatographie, basierend z.B. auf Protein A oder G. Das Zielprotein bindet dabei an die Säulenmatrix, wobei unerwünschte Störproteine, sogenannte „host cell proteins", abgetrennt werden können. Dieser Schritt beinhaltet eine Elution des gebundenen Zielproteins durch pH-Erniedrigung und kann mit einem Virusinaktivierungsschritt verknüpft werden. Danach folgen typischerweise Ionenaustauschchromatographie, z.B. Kationenaustauschchromatographie zur Abreicherung von Antikörperaggregaten, sowie hydrophobe Interaktionschromatographie. Nach einer finalen Filtration und zusätzlichen Virusinaktivierung kann das gereinigte Protein als „Drug Substance" Verwendung finden.

Bei diesem Herstellungsprozess wurden in den letzten Jahrzehnten erhebliche Fortschritte erzielt, was zu Steigerungen bei der Ausbeute geführt hat. Die höheren Volumenausbeuten haben jedoch gleichzeitig zu einer Verlagerung des Engpasses bei der Produktion weg vom Upstream, hin zum Downstream Bereich geführt. Dieser Engpass findet sich also nun in der Aufreinigung. Herkömmliche Chromatographie-basierte Systeme stoßen hierbei an ihre Kapazitätsgrenzen. Zusätzlich kann z.B. der Elutionsschritt bei der Affinitätschromatographie in der Aufreinigungskaskade unerwünschte Aggregate erzeugen.

Diese Aspekte sowie steigender wirtschaftlicher Druck auf die Hersteller verlangen die Entwicklung alternativer nicht Chromatographie-basierter Aufreinigungsverfahren, um diesen Problemen - zumindest teilweise- entgegenzuwirken. Möglichkeiten hierfür sind z.B. größere Chromatographiesäulen, eine größere Kapazität der Säulenmaterialien, Wegwerfsäulen oder gezielte Fällung der Proteine in Batch-Verfahren.

Beispiele für diese Fällung sind die Fällung von Immunglobulinen mit Caprylsäure, das Aussalzen mittels Ammoniumsulfat sowie die Fällung mit Polyethylenglykol (PEG). Die Verwendung dieser Fällungsmittel hat jedoch einige Nachteile. Einige dieser Präzipitantien müssen in größeren Konzentrationen eingesetzt werden und führen dadurch zu größeren Abfallmengen, andere erfordern bestimmte Mindestkonzentrationen der zu fällenden Proteine. Daher sind Polyelektrolyte als Kopolymere in den wissenschaftlichen Fokus gelangt. Diese erlauben eine gerichtete Anpassung an die biophysikalischen Eigenschaften des Zielproteins, indem neben dissoziierbaren Gruppen (Eigenschaft der Polyelektrolyte) auch Gruppen mit ausgeprägten hydrophoben bzw. hydrophilen Eigenschaften ins Kopolymer eingefügt werden. Diese „mixed-mode" Eigenschaften ermöglichen eine selektivere Präzipitation des Zielproteins, als dies durch Polymere mit rein elektrostatischen bzw. rein hydrophoben Wechselwirkungen möglich wäre (siehe Journalbeiträge [4] und [6]). Die Verwendung dieser Kopolymere soll u.a. dazu dienen, den initialen Affinitätschromatographieschritt zu ersetzen. Durch direkte Zugabe der Kopolymere in die klärifizierte Fermentationsbrühe kann in einem Batch-Verfahren eine selektive bzw. semi-selektive Fällung des Zielproteins erreicht werden. Nach Präzipitation und Rücklösung des Zielproteins in einem definierten Volumen kann zusätzlich eine Aufkonzentrierung erzielt werden und weitere folgende Chromatographieschritte teilweise ersetzt bzw. deren Kapazität erhöht werden. Dies kann idealerweise Aufreinigungsdauer und Aufwand verringern und gleichzeitig Ausbeute, Lebensdauer von Säulenmaterialien sowie Reinheit des Zielproteins erhöhen.

Dafür müssen solche Kopolymere jedoch speziellen Anforderungen genügen wie:
(a) geringe Herstellungskosten; (b) hohe Selektivität und Ausbeute bei der Fällung; (c) einfache Anpassung an jeweilige Zielproteine; (d) gute Rückgewinnung bzw. Abtrennung vom Präzipitat; (e) sinnvollerweise geringere oder vergleichbare Kosten im Bezug zu etablierten Aufreinigungsverfahren.

Im Rahmen dieser Arbeit wurden verschiedene Kopolymere neu synthetisiert und für die spezifischen Anforderungen der Proteinaufreinigung untersucht. Durch systematische Variation der Kopolymerzusammensetzung gelang es, einen optimierten Präzipitationsprozess zu etablieren, welcher auch als Patentanmeldung eingereicht wurde. Die mit diesem Prozess assoziierten Kosten wurden hierbei mit Protein A Affinitätschromatographie verglichen und zeigten die Wirtschaftlichkeit der Präzipitation gegenüber Chromatographie ab einem bestimmten Antikörpertiter in der Produktion (Journalbeitrag [4]). Parallel zur Entwicklung eines Kopolymer-basierten Proteinaufreinigungsverfahrens wurden grundlegende Mechanismen der Kopolymer- Protein- Interaktion untersucht, auch um die Selektivität und Ausbeute zu verbessern und ein tiefergehendes Verständnis der Präzipitation zu schaffen (Journalbeiträge [3] und [7]).

Die Abhängigkeit der Präzipitation von physiko-chemischen Eigenschaften der zu fällenden Proteine an Hand eines eingeführten binären Proteintestsystems war Gegenstand weiterer Untersuchungen (Journalbeitrag [6]). Als analytische Methode zur Untersuchung des Präzipitationsprozesses wurde die Infrarotspektroskopie eingesetzt [Journalbeiträge [1], [2], [4], [5], [7], Buchkapitel [8]). Sie erlaubte nicht nur eine Aussage über die Zusammensetzung der verwendeten Kopolymere sondern auch über die Präzipitationsausbeute und Selektivität der Fällung. Dabei wurden in einem at-line Verfahren der Titer des zu präzipitierenden Antikörpers, die Bildung von Aggregaten sowie der Gehalt an unerwünschten „host cell proteins" bestimmt. Zusätzlich zur Nutzung der IR im speziellen Rahmen der Präzipitationsprozessentwicklung konnte gezeigt werden, dass diese Technik auch im Allgemeinen für die Quantifizierung kritischer Prozessparameter bei der Proteinaufreinigung Nutzung finden kann. Diese kritischen Prozessparameter beinhalten neben den oben genannten Parametern z.B. auch Endotoxine und exakte Konzentration an Antikörperaggregaten. Spezielle Anwendungsbeispiele dazu wurden in Publikationen und einer Patentanmeldung beschrieben (Journalbeiträge [1], [2] und [5]).

Die Ergebnisse der vorliegenden Arbeit wurden an folgenden Stellen vorgestellt, veröffentlicht oder zur Veröffentlichung eingereicht:

Journalbeiträge

[1] Capito, F., Skudas, R., Kolmar, H., & Stanislawski, B. (2012). Host cell protein quantification by fourier transform mid infrared spectroscopy (FT-MIR). *Biotechnology and Bioengineering*, 110(1), 252-259. **DOI: 10.1002/bit.24611**

[2] Capito, F., Skudas, R., Stanislawski, B., & Kolmar, H. (2012). Matrix effects during monitoring of antibody and host cell proteins using attenuated total reflection spectroscopy. *Biotechnology progress*, 29(1), 265-274. **DOI: 10.1002/btpr.1643**

[3] Capito, F., Skudas, R., Stanislawski, B., & Kolmar, H. (2013). Polyelectrolyte–protein interaction at low ionic strength: required chain flexibility depending on protein average charge. *Colloid and Polymer Science*, 291(7), 1759-1769. **DOI: 10.1007/s00396-013-2911-3**

[4] Capito, F., Bauer, J., Rapp, A., Schröter, C., Kolmar, H., & Stanislawski, B. (2013). Feasibility study of semi-selective protein precipitation with salt-tolerant copolymers for industrial purification of therapeutic antibodies. *Biotechnology and bioengineering*, 110(11), 2915-2927. **DOI: 10.1002/bit.24950**

[5] Capito, F., Skudas, R., Kolmar, H., & Hunzinger, C. (2013). Mid-infrared spectroscopy-based antibody aggregate quantification in cell culture fluids. *Biotechnology journal*. 8(8), 912-917. **DOI: 10.1002/biot.201300164**

[6] Capito, F., Skudas, R., Kolmar, H., & Stanislawski, B. (2013) Customization of copolymers to optimize selectivity and yield in polymer-driven antibody purification processes. *Biotechnology Progress. in press* **DOI: 10.1002/btpr.1813**

[7] Capito, F., Kolmar, H., Stanislawski, B., & Skudas, R. (2013) Determining the defined length of a polymer chain required per precipitated protein molecule: studying interactions between anionic polymers and four physicochemically different proteins. *Journal of Polymer Research. submitted*

Buchkapitel

[8] Capito, F., Skudas, R. (2013) Applications and limitations of FT-MIR for monitoring critical process parameters during downstream processing of therapeutic proteins, in *Infrared Spectroscopy: Theory, Developments and Applications* (ed. D. Cozzolino), Nova Publishers, Hauppauge, New York. *submitted*

Tagungsbeiträge

[9] Florian Capito, Romas Skudas, Bernd Stanislawski, Harald Kolmar (2012), *Kurzvortrag*, „Attenuated total reflection spectroscopy for quantification and monitoring of antibody and host cell proteins in mammalian cell culture - a feasibility study", Interdisziplinäres Doktorandenseminar des DASp und des A.M.S.El. an der Johannes Gutenberg-Universität Mainz, GDCh, Mainz, Germany

[10] Florian Capito (2012), *Kurzvortrag und Poster*, "Feasibility of attenuated total reflection spectroscopy in monitoring and quantification of antibody and host cell proteins using mammalian cell culture", EUCheMS, Prague.

[11] Florian Capito (2013), *Kurzvortrag,* "Mid Infrared spectroscopy for quantification of mAbs and their aggregates in bioprocess samples", BioProcess International European Conference, Düsseldorf/Neuss

[12] Florian Capito (2013), *Poster*, "Mid infrared spectroscopy for quantification of mAbs and their aggregates in bioprocess samples", GDCh-Wissenschaftsforum Chemie, Darmstadt.

[13] Florian Capito, Christian Hunzinger, Romas Skudas, Bernd Stanislawski, Harald Kolmar (2013), *Kurzvortrag,* "Fourier transform mid infrared spectroscopy- a cost-effective tool for monitoring mAb titer and mAb aggregates in bioprocess samples", Advanced Analytics for Therapeutic Proteins: from Research to Manufacturing, Dechema e.V., Irsee.

[14] Florian Capito (2013), *Kurzvortrag und Poster*, "Semi-selective protein precipitation using salt-tolerant copolymers for industrial purification of therapeutic antibodies", Euroscicon: Recovery and purification of biosynthetic products: Downstream processing for the 21st century, London.

Patentanmeldungen

[15] Florian Capito, Johann Bauer, Almut Rapp, Bernd Stanislawski, Copolymers for protein precipitation, EP 12008475.1 submitted 20/12/2012

[16] Florian Capito, Romas Skudas, Christian Hunzinger, IR analysis of protein aggregates, EP 13001626.4 submitted 28/03/2013

Table of contents

List of abbreviations

ABZ	acrylamidobenzoic-acid
AEX	anion exchange chromatography
AMPS	2-acrylamido-2-methylpropane sulfonic acid
ATR	attenuated total reflectance infrared spectroscopy
ATR-IR	attenuated total reflectance infrared spectroscopy
BSA	bovine serum albumin
BzAAm	benzylacrylamide
CCF	cell culture fluid
CD	circular dichroism
CEX	cation exchange chromatography
CHO	Chinese hamster ovary cell line
CPP	critical process parameter
CTA	chain transfer agent
CV	coefficient of variation
DMF	dimethylformamide
DMSO	diemthylsulfoxide
DSP	downstream processing
ELISA	enzyme linked immunosorbent assay
FDA	Federal Drug Administration (USA)
FIR	far infrared spectroscopy
FTIR	Fourier transfrom infrared spectroscopy
FT-MIR	Fourier transfrom mid infrared spectroscopy
GPC	gel permeation chromatography
HCP	host cell protein
HIC	hydrophobic interaction chromatography
IEX	ion exchange chromatography
IR	infrared spectroscopy
L_{def}	length of defined polymer chain length per precipitated protein molecule
mAb	monoclonal antibody
MIR	mid infrared spectroscopy
Mw	weight average molecular weight
Mn	number average molecular weight
NIR	near infrared spectroscopy
NMR	nuclear magnetic resonance
NS0	murine myeloma cell line
PAA	poly acrylic acid
PASA	poly anethole sulfonic acid
PCA	principal component analysis
PEG	poly ethylene glycol
pH	*pondus hydrogenii*
pI	isoelectric point
PLS	partial least squares regression
PSS	poly styrene sulfonic acid
PVS	poly vinyl sulfonic acid
RMSECV	root mean square error of cross validation
RMSE-IT	root mean square error of independent test-set
RPD	relative predictive deviation
SEC	size exclusion chromatography
SP2/0	murine myeloma cell line
TEA	triethylamine
TMAE	trimethylaminoethyl (quarternary ammonia)
USP	upstream processing
UV	ultraviolet

Aims and scope

Within recent years, production of biotherapeutic proteins such as monoclonal antibodies (mAbs) has increased and is rising further. An elevation in cell culture titers during production of these proteins has led to the shift of a manufacturing bottleneck away from the upstream part to the downstream part of processing. This purification bottleneck is mainly associated with chromatography based purification and requires either implementation of new, even larger chromatography columns, or the invention of alternative non-chromatography based purification strategies. One such alternative technique is protein purification via precipitation. This is based on solid-liquid phase separation and has been known for a long time.

Additionally, regulatory and governmental authorities impose more stringent limits on production, also demanding better quality control strategies. One potential technique allowing permanent monitoring of production and purification is mid- infrared- spectroscopy (MIR). It allows identification of a compound based on specific absorbance patterns within the infrared spectrum and can be used for at-line as well as on-line monitoring, allowing for fast and cost-effective results.

The aims of this thesis were to

a) Develop and optimize a precipitation-based industrial protein purification process (see articles 3-4, 6-7)

b) Establish MIR to determine precipitation yield and selectivity, monitoring antibody and host cell protein amount during precipitation process development (see articles 1-2, 5)

c) Additionally, enable monitoring of critical process parameters within biotherapeutic protein production (see book chapter)

These aims can be divided into the following parts

a) Characterization of in-house synthesized copolymers

b) Evaluation of precipitation conditions depending on ionic strength, polymer chain length as well as composition of copolymers

c_1) Homology modeling and *in silico* calculations of antibody structures, charge densities and charge distribution on antibody surfaces

c_2) Optimization of precipitation conditions using different antibodies, cell culture fluids as well as test protein systems

d) Establishing MIR as a cost-effective tool to measure mAb titer, mAb aggregate amount and host cell protein level in precipitation process development samples to optimize yield and selectivity

e) Implementing a polyelectrolye-driven protein purification process including a cost comparison to alternative purification techniques

2. Introduction

2.1. General steps during purification of therapeutic proteins

Therapeutic proteins are typically produced in a bioreactor. To allow their later use within medical treatments and research applications, impurities, such as host cell proteins, aggregated proteins, endotoxins, viruses, leachables and nucleic acids have to be removed to meet regulatory requirements and safety aspects.[1-2] This is done during **downstream processing** (DSP) referring to the recovery and purification of biosynthetic products such as biopharmaceuticals and therapeutic proteins, using a series of different purification techniques to remove impurities (overview of typical DSP-process see figure 1). DSP can be divided into different stages, the so-called CiPP stages (capture, intermediate purification and polishing).[3-4] The first steps in downstream processing include mainly high-throughput low-resolution techniques while the latter stages use high-resolution low-throughput techniques. Removal of insolubles and recovery is performed during the first stage, **capture**, capturing the target protein. To prevent blockage of subsequent chromatography steps, cell debris as well as other particulates need to be removed from the target protein.[5] This is mainly done by employing centrifugation and several filtration steps. Contaminants with different and similar properties as the target protein are then separated from clarified harvest pool during **intermediate purification**. These steps are usually the bottleneck during large-scale protein production and mainly involve chromatography based systems such as affinity chromatography, ion-exchange chromatography or hydrophobic interaction chromatography.[5] Addtionally, virus inactivation and removal need to be done, e.g. by low pH-treatment, which can follow e.g. affinity chromatography. Afterwards, a higher than 98% purity of the product compared to HCP's in solution is typically achieved.[6] Additionally, specific impurities such as endotoxins and antibody dimers and other antibody aggregates are removed. Finally, within the so-called **polishing,** sterilization, pyrogen and virus removal are done before the protein is formulated in an according buffer, crystallized or lyophilized. For purification of an antibody, yields vary usually between 60-80%, depending on the number of purification steps.[7] A further description of purification steps during biotherapeutic protein production can be found in the chapter "protein production and monitoring techniques".
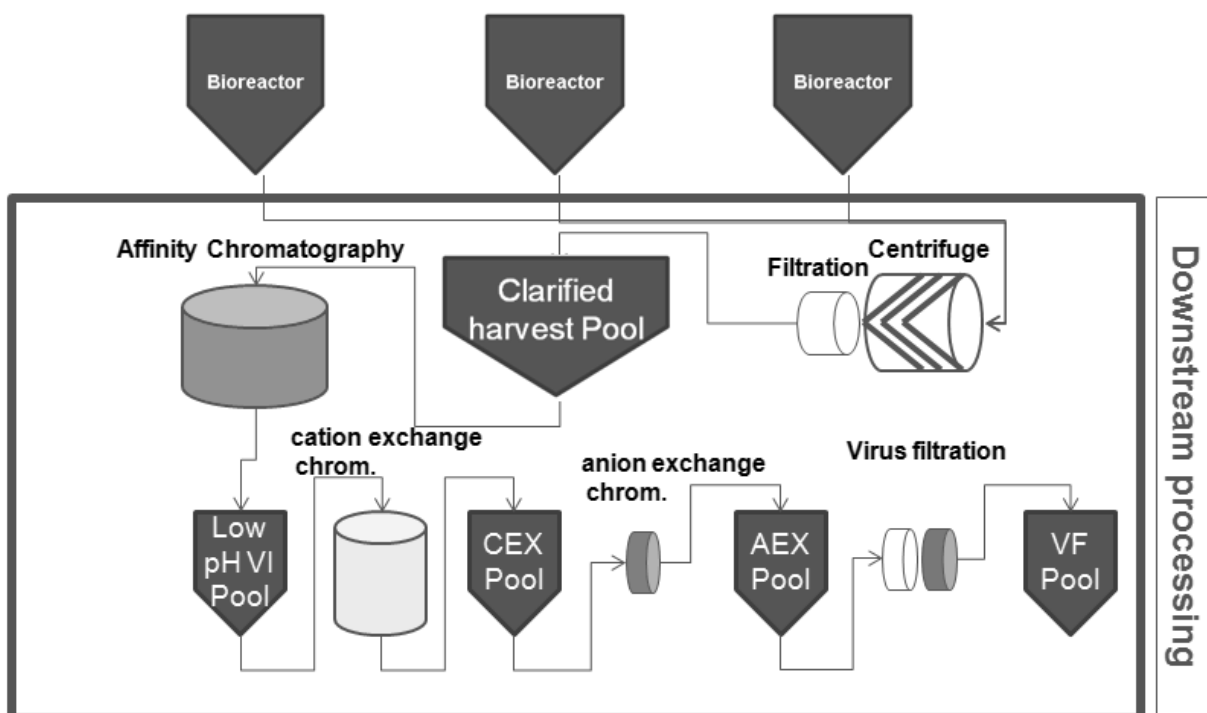
Fig. 1: Exemplary overview typical downstream process.

2.2. Current challenges and bottlenecks during therapeutic protein purification

There are several problems associated with downstream processing in general and specific purification steps in particular: Affinity chromatography for antibody capture that makes use of cell wall proteins A from *Staphylococcus aureus* and protein G from *Streptococcus*, includes the inherent risk of leaching protein A and is quite expensive.[8] Additionally, the rather harsh elution conditions during this purification step as well as the low pH virus inactivation step can induce aggregates, which have to be removed.[9] As with most chromatography systems, large buffer volumes are required, also leading to a higher waste load. While in the past the production bottleneck was localized within protein expression and upstream processing, it now shifts towards downstream processing. Rising economic pressure as well as increased cell culture titers require improved manufacturing processes, enhanced throughput and optimized purification yield.[10-11]

There are several options to meet these criteria: chromatography column material capacity can be increased as well as dimensions of columns. Alternatively, different means of purification, not chromatography-based, can be implemented, however requiring comparable yields and purities but with lower costs and better scalability.[7, 12-13] Disposable columns represent one option, reducing costs and eliminating excessive cleaning as well as cleaning documentation, however, limiting the number of purification cycles per column lifetime.[14] Alternatively, batch purification methods have been developed, allowing precipitation of the desired protein out of the fermentation broth. Common precipitants thereby are ammonium sulphate,[15] polyethylene glycol (PEG) or caprylic acid.[16-17] Yet, they lack selectivity.[18] Therefore, improvements in protein and antibody purification are urgently required.[10, 12] As one option, membrane chromatography, charged ultrafiltration membranes and flocculation agents can be used.[9] Another option is the use of affinity macroligands with attached polymers precipitating in dependence on pH or temperature changes.[18-22]

However, additionally to the need of creating a customized macroligand for each target, the use of these macroligands is costly due to the requirement of antibody binding proteins.[23] Therefore, a similar but more cost-effective way can be the use of customizable polyelectrolytes to allow semi-selective precipitation of the respective target protein, not requiring additional binding proteins as ligands.

2.3. Protein purification and precipitation using polyelectrolytes

Proteins can interact with each other and other molecules via electrostatic forces, hydrophobic forces as well as van der Waals forces. This can be used in precipitation, a solid-liquid phase separation. Common precipitants include polyethylene glycol (PEG), ammonium sulphate, organic solvents and caprylic acid.[4, 24] PEG separates proteins via an excluded volume effect, excluding proteins sterically from the solvent until protein concentration exceeds solubility and they precipitate. Although PEG can precipitate immunglobulins with some specificity from serum, it is generally difficult to selectively precipitate proteins as this precipitant increases the effective concentration of all proteins in solution.[25] Ammonium sulphate removes the shell of hydrating water around proteins, allowing them to aggregate as their hydrophobic surfaces are not shielded anymore.[26-27] This technique is cost-effective and the salt can be removed easily by centrifugation, however, precipitation selectivity is limited due to similar protein solubility.[28] Another precipitation technique uses organic solvents as precipitants, which displace molecules around hydrophobic areas of proteins and lower the dielectric constant, increasing electrostatic dipole-dipole- attraction and interaction between charged molecules which leads to protein aggregation.[29] An example is the so-called Cohn fractionation which has been used since 1946 and is still employed today for purification of plasma proteins.[30]

However, as these techniques have some disadvantages such as the amount of precipitant required, the risk of denaturation, or reduced precipitation selectivity,[27] polyelectrolytes as protein precipitants came into the scientific focus some time ago and were already studied in the 1950's by the working group of Morawetz.[31-32] Polyelectrolytes are polymers which have charged groups in their repeating units. Important polyelectrolytes in biology are proteins, DNA and ionic polysaccharides such as alginate and pectin. Examples for synthetic polyelectrolytes include poly vinyl sulfonic acid (PVS), poly acrylic acid (PAA) and polystyrene sulfonic acid (PSS), which can be used to separate and fractionate proteins.[21, 33] Other polyelectrolytes find applications in water treatment and food technology.[34-35]

Generally, there are two main problems associated with using polyelectrolytes for protein purification. The first problem is the recovery of the protein after precipitation and potential re-use of the polyelectrolyte. Another problem is how to obtain a sufficient selectivity to enable the use within purification.[22] Although polyelectrolytes can interact in a so-called mixed-mode principle, exhibiting both electrostatic as well as e.g. hydrophobic interaction, for strong polyelectrolytes such as polystyrene sulfonic acid, which dissociate completely in solution, fine-tuning is not possible. In contrast, for weak polyelectrolytes, dissociation and thereby switching from e.g. hydrophobic to electrostatic interaction can be controlled by pH and ionic strength. However, while fine-tuning and thereby modulation of precipitation selectivity for these weak polyelectrolytes can be achieved, required changes in pH and ionic strength do also affect the charge presentation and distribution of the target as well as impurity proteins, making it difficult to find optimal conditions as both, polyelectrolyte and protein charge are altered at the same time. These problems of selectivity can, however, partly be solved when choosing a protein system with a discriminating power, e.g. where the target protein has a very distinct feature compared to (most) of the impurity proteins.[22]

One such system would be e.g. a mammalian cell culture solution, containing many impurity proteins, the majority with an isoelectric point below 7 and a target protein, e.g. an antibody with an isoelectric point between 8- 9. Such a system has been employed by McDonald et al.,[23] using polyelectrolytes PAA, PSS and PVS for purification, however requiring additional dilution of the cell culture fluid. PSS as strong polyelectrolyte did not allow recovery of the protein due to bad redissolution behavior.

Thus, the use of copolymers as precipitants, polymers composed of polyelectrolytes as well as permanently non-charged groups, allowing the permanent introduction of hydrophobic groups, came into the focus. The underlying idea is that they would allow even better fine-tuning of selectivity, not necessarily by pH change but by changing the composition of the copolymer optimized for the respective target protein and conditions. Although the properties of these copolymers can still be modulated by pH-changes, the main "fine-tuning" is done during synthesis, allowing customization for

---

the respective target protein. An additional benefit of these copolymers is their ability to withstand high salt concentrations, as e.g. required for precipitation in cell culture fluid at physiological ionic strength.

These high salt concentrations can shield the charges at the polyelectrolyte chains and lead to polymer chain collapse during a coil- globule transition. The introduced hydrophobic groups in copolymers displace surrounding water molecules. Thereby, screening effects due to salt as seen with polyelectrolytes are reduced, allowing the use of these copolymers at higher ionic strength compared to polyelectrolytes.

There are several factors influencing protein- polyelectrolyte interaction. For example, it is known that protein- polyelectrolyte interaction exhibits a non-monotonic ionic strength dependence. While for low ionic strength, interaction is impeded, an optimum is found in the medium salt concentration between 5- 30 mM NaCl [36] whereas further salt addition leads to worse interaction again.[37-38] Furthermore, polyelectrolyte- protein interaction also depends on the polymer chain length as shown by Houska et al. and Izumrudov et al.[22, 39] An increase in the chain length, i.e. higher polymerization degree, allows these polyelectrolytes to form complexes even at higher salt concentrations compared to same polyelectrolytes of lower chain length.[40] Further parameters are temperature, physico-chemical properties of polymer and protein, e.g. charge distribution and charge density, hydrophobicity and polymer chain stiffness.[41-42] Highlighting the underlying principles behind protein-polyelectrolyte interaction, a wide range of experiments has been performed including in silico studies.[43-44] These experiments also showed a redissolution of complexes when adding excess polymer.[45]

How does protein purification via precipitation of a target protein work? The pH of a cell culture solution is adjusted so that the target protein has the opposite charge as most of the impurity proteins. Afterwards a concentrated copolymer solution is added, obtaining a charge opposite the one of the target protein, allowing interaction with that respective target protein. As the copolymer has the same charge as most of the impurity proteins, interaction is minimized. A complex between target protein and copolymers is formed, leading to precipitation and allowing to separate the precipitate, e.g. via centrifugation. Afterwards, the non-precipitated proteins in the cell culture fluid are discarded together with the supernatant. The complex of target protein and copolymer is then redissolved via pH-change, and the protein recovered by a suitable method which can be chromatography or filtration. Copolymer can be removed, e.g. adding beads or flakes with opposite charge to selectively bind the copolymer. Another advantage of this principle is that by adjusting the volume for redissolving the protein-copolymer complex, the concentration of the target protein can be adjusted to the demands, also allowing up-concentrating the protein. This principle, employing polyelectrolytes for purification of target proteins has been pursued by the industry, found its way into patent databases[46-47] and could be a promising technique, allowing now to reduce the purification bottleneck as described in the previous section.

Compared to chromatography-based purification, precipitation can be more cost-effective for high protein titer expressing cell cultures. Purifying these high titer mAbs with protein A chromatography would mainly suffer from high media and buffer costs. While for low mAb titers, chromatography is the method of choice, purification of higher titers would require several loadings and runs due to limited resin capacity.[10] For precipitation, costs are mainly due to larger mAb loss during precipitation. However, upstream production costs are decreased for increased product titers, due to economy of scale.[10] Thus, using higher titers during precipitation, the contribution of costs due to mAb loss to overall costs in precipitation can be reduced. Therefore, depending on the product titer, either of the two techniques can be more cost-effective. Protein A chromatography is more suitable for low titer systems, while precipitation is better suitable for titers above 5-6 g l^{-1} also allowing scalability. Comparing both techniques for purification of cell culture fluid with a mAb titer of 10 g l^{-1}, precipitation could save costs between 30-50% compared to the protein A chromatography step.[48]

2.4. Infrared Spectroscopy

During process development, analysis of protein quality and process parameters is very important to understand and optimize a process. Spectroscopy is widely used for protein analysis, e.g. UV-spectroscopy for protein quantity. While this does not allow for selective quantification, infrared spectroscopy presents a fast and cost-effective tool with the possibility for selective quantification and analysis of proteins as well as other process parameters during process development, also in the context of this thesis. Thus it was used to help in designing a precipitation-based protein purification process.

Generally, infrared spectroscopy (IR) is a spectroscopic method, making use of the interaction between irradiation and matter at wavenumbers (number of waves per cm; λ^{-1}). It can be divided into near-infrared (NIR), mid-infrared as used within the context of this thesis (MIR) and far-infrared (FIR). It is used to study fundamental vibrations, thereby elucidating the structure of molecules such as proteins. Protein secondary structure can be analyzed measuring IR spectra near the Amide I absorption band (1600- 1690 cm^{-1}). This technique gives better results for proteins with high β-sheet content, such as antibodies, compared to circular dichroism.[49] Dipole changes have to occur for a molecule to be IR-active; of diatomic molecules, only non-symmetrical bonds can be observed. Molecules absorb frequencies of irradiation matching their resonance vibration frequency. The vibration frequency thereby depends on the bond strength which is related to the bound atoms and the shape of the molecular potential energy surfaces.[50] Complex molecules have more bonds and can vibrate in different vibrational modes, leading to different peaks in the spectra. Typically, a beam of infrared light is passed from a Helium-neon laser through a cuvette containing the sample. Using Fourier transformation, the transmission of all the wavelengths is measured at once, analysing the amount of energy absorbed at each wavelength. The recorded signal represents light output as a function of mirror position in the so-called interferometer. Fourier transformation then converts the raw data into a spectrum.[50] A reference spectrum, typically water, is subtracted from the sample spectrum to account for instrument effects such as light sources and detector differences. A transmittance or absorbance spectrum is plotted, revealing the wavelengths at which the sample absorbs. Resolution-enhancing methods such as supersmoothing can be used to determine the position of the band components. After that the amount of secondary structure components can be adjusted with their absorption maxima, amplitudes and half-widths. Assignment of those components is done by analyzing reference proteins with similar structural properties, whereby using proteins from the same batch can facilitate comparison. Protein stability and protein folding properties are analyzed using denaturing agents or different temperatures during IR-spectrum aquisition. Thereby spectra can reveal information about the content of the sample and enable to identify unknown substances by comparing their spectra to known ones. Transmission measurements using infrared spectroscopy at the spectral area between 500 cm^{-1} and 1800 cm^{-1} require very thin coat thicknesses of maximum 10-15 µm. This is due to the fact of high background absorption by water molecules at 1645 cm^{-1}, which is an order of magnitude higher than the absorption of the Amide I band.[51] Thereby the amount of water in the beam path length can be reduced and by using high protein concentrations it is possible to obtain good spectra. Cuvettes are made of different IR-transparent materials with coating thicknesses of 5- 50 µm, allowing precise coating thickness adjustment, BaF_2 or CaF_2 windows are one example.[50] Other means of sample preparation include hydrated films, similar to the principle used by Direct Detect™ spectrophotometer, which contain concentrated sample after water removal. Another technique uses attenuated total reflection (ATR) (figure 2). The IR beam passes through material with a high refraction index, leading to multiple total reflections, creating an evanescent wave, which can penetrate the optical thinner area with the sample. Immobilised protein on the surface of ATR-crystals can thereby be analyzed.[50] Special ATR-cells can be used for high-throughput analysis of ingredients of drinks and reactions during fermentation processes in real-time. More detailed applications of MIR and ATR can be found in the next chapter "protein production and monitoring techniques".
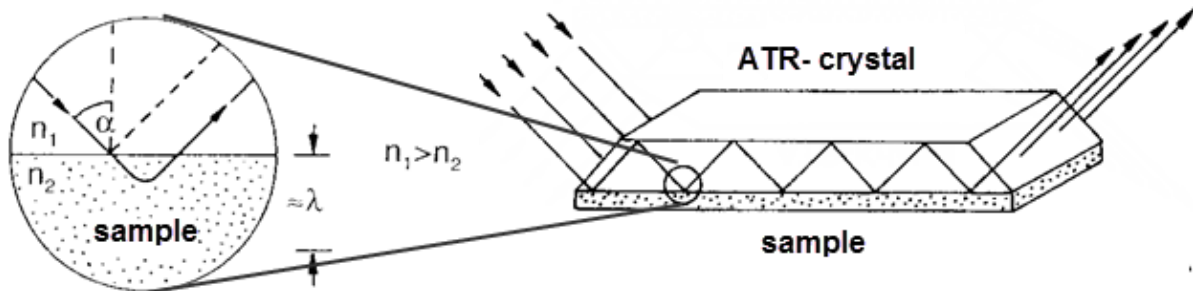
Fig. 2: principle of attenuated total reflection for infrared spectroscopy. An IR beam passes through a crystal, being reflected at the boundary phases and revealing information of the sample being coated to the crystal. own drawing

Within the mid-infrared, proteins are mainly characterized via the so-called Amide I band, although several other bands can be used (see next chapter "protein production and monitoring techniques").[50] This is mainly due to the carbonyl bond, interacting with hydrogen bonds of the secondary structure and leading to different bands at specific wavenumbers within the Amide I region, depending on the secondary structure involved. Strong hydrogen bonds weaken the C=O bond, thereby reducing the oscillation frequency.[51] As these smaller bands are also present in the Amide I band, mathematical data analysis methods can yield information about the secondary structure of a protein. These methods include Fourier self-deconvolution, partial least-squares analysis and second derivative analysis.

Second derivative analysis is usually performed, employing an algorithm derived from Savitzky and Golay,[52] whereby a polynom is fit into the spectral course. A defined number of vertices help to cut noise-derived minipeaks and attenuate background noise by "smoothing" the spectral course.[52] Smoothing, however, can lead to a falsification of spectral intensities as a reduction of associated peaks occurs. Yet, derivatives of spectra are suitable for qualitative spectral interpretation, as the intensities of derived spectra depend mainly on half-widths, not the intensities of the respective original bands.[53] At the first derivation of a spectrum, extreme values or peaks are present as roots. In contrast, after the second derivative, inflection points of a spectrum become roots. Derivation leads to worse signal to noise ratios as peaks show stronger decrease than background noise.[54] The first derivative serves as a means of baseline correction, whereby second and higher derivatives have the function of band separation and lead to an apparent resolution enhancement as they present broad spectral bands more narrow, however, also with reduced band intensity.[54]

Cumulative part

This part consists of manuscripts submitted to different journals and publishing companies. The chapter "protein production and monitoring techniques", still belonging to the introduction, is based on a book chapter contribution, written on behalf of invitation by Nova Science Publishers Inc, New York. The then following "experiments" chapter is based on eight articles, six of them accepted and either published as early-view or in printed journal volumes. Two articles have been submitted to journals or are going to be submitted as soon as possible.

Following contributions are included in the cumulative part of this thesis:

Introduction

Capito, F., Skudas, R. (2013) Applications and limitations of FT-MIR for monitoring critical process parameters during downstream processing of therapeutic proteins, in *Infrared Spectroscopy: Theory, Developments and Applications* (ed. D. Cozzolino), Nova Publishers, Hauppauge, New York. *Submitted by invitation*

Experimental

Capito, F., Bauer, J., Rapp, A., Kolmar, H., & Stanislawski, B. Synthesis and characterization of customized 2-acrylamido-2-methylpropane sulfonic acid - benzylacrylamide /acrylamidobenzoic-acid copolymers for semi-selective protein purification.

Capito, F., Skudas, R., Stanislawski, B., & Kolmar, H. (2013). Polyelectrolyte–protein interaction at low ionic strength: required chain flexibility depending on protein average charge. *Colloid and Polymer Science*, 291(7), 1759-1769. **DOI: 10.1007/s00396-013-2911-3**

Capito, F., Kolmar, H., Stanislawski, B., & Skudas, R. (2013) Determining the defined length of a polymer chain required per precipitated protein molecule: studying interactions between anionic polymers and four physicochemically different proteins. *Journal of Polymer Research. submitted*

Capito, F., Skudas, R., Kolmar, H., & Stanislawski, B. (2013) Customization of copolymers to optimize selectivity and yield in polymer-driven antibody purification processes. *Biotechnology Progress. in press* **DOI: 10.1002/btpr.1813**

Capito, F., Skudas, R., Kolmar, H., & Stanislawski, B. (2013). Host cell protein quantification by fourier transform mid infrared spectroscopy (FT-MIR). *Biotechnology and Bioengineering*, 110(1), 252-259. **DOI: 10.1002/bit.24611**

Capito, F., Skudas, R., Stanislawski, B., & Kolmar, H. (2012). Matrix effects during monitoring of antibody and host cell proteins using attenuated total reflection spectroscopy. *Biotechnology progress*, 29(1), 265-274. **DOI: 10.1002/btpr.1643**

Capito, F., Skudas, R., Kolmar, H., & Hunzinger, C. (2013). Mid-infrared spectroscopy-based antibody aggregate quantification in cell culture fluids. *Biotechnology journal*. 8(8), 912-917. **DOI: 10.1002/biot.201300164**

Capito, F., Bauer, J., Rapp, A., Schröter, C., Kolmar, H., & Stanislawski, B. (2013). Feasibility study of semi-selective protein precipitation with salt-tolerant copolymers for industrial purification of therapeutic antibodies. *Biotechnology and bioengineering*. 110(11), 2915-2927. **DOI: 10.1002/bit.24950**

2.5. Protein production and monitoring techniques

Book chapter: Applications and limitations of FT-MIR for monitoring critical process parameters during downstream processing of therapeutic proteins

Florian Capito, Dr. Romas Skudas

Submitted 30/04/2013

in D. Cozzolino: Infrared Spectroscopy: Theory, Developments and Applications, Nova Science Publishers Inc., Hauppauge, USA.

Short summary:

This part is based on a book chapter contribution and describes applications of FTIR in general and MIR as well as ATR in particular for monitoring critical process parameters in bioproduction. An introduction explains current purification strategies for protein production and monitoring techniques used for surveillance of these processes. Detailed case studies are given, showing the suitability of IR spectroscopy to quantify several critical process parameters, e.g. mAb titer, mAb aggregate amount and host cell protein level. Furthermore, besides glycosylation analysis, the applicability to analyze protein secondary structure and e.g. distiniguish protein A from mAb is shown.
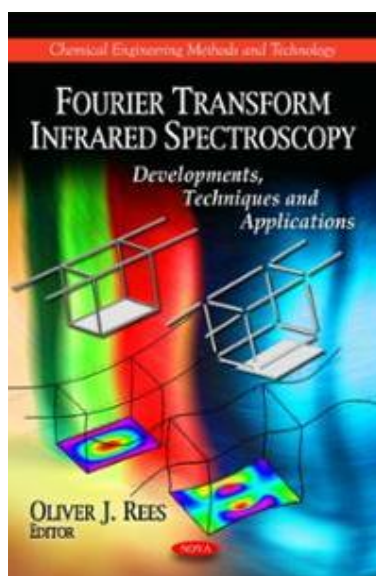
Fig. 3: Cover of last edition of a book at Nova, depicting FTIR.

Chapter: Applications and limitations of FT-MIR for monitoring critical process parameters during downstream processing of therapeutic proteins (15,680 words)

Contributors: Florian Capito[1][2], Dr. Romas Skudas[2]

1 Institute for Organic Chemistry and Biochemistry, Technische Universität Darmstadt, Germany

2 Merck KGaA, Frankfurter Strasse 250, 64293 Darmstadt, Germany

Correspondence to: Florian Capito (E-mail: florian.capito@external.merckgroup.com)

phone: 0049 6151 72 7168

fax: 0049 6151 72 917510

Abstract

1. Introduction to biotherapeutic molecule downstream processing and monitoring of critical process parameters (CPP's)

General procedure for quantification of a CPP

Aspects to consider before choosing FT-MIR as monitoring technique in downstream processing

Elucidation of protein structure, differentiation and quantification of protein secondary structure using MIR

2. Case studies: Using FT-MIR for monitoring critical process parameters in downstream processing

a) Quantification of antibody levels in cell culture fluid using FT-MIR

b) Quantification of impurity protein levels in cell culture fluid using FT-MIR

c) Antibody aggregate quantification using FT-MIR

d) Quantification of leaching protein A in cell culture fluid using FT-MIR

3. Other possible applications

a) Quantification of endotoxins, lipids and polysaccharides by FT-MIR

b) Quantification of nucleic acids by FT-MIR

c) Detection of glycosylation patterns by FT-MIR

4. CONCLUSION

ABSTRACT

This chapter outlines Fourier transform mid infrared spectroscopy (FT-MIR) applications in monitoring critical therapeutic protein process quality parameters, taking antibody (mAb) production as an example.

Being the most profitable group of new therapeutic proteins generated, mAbs are still gaining great interest. But the pressure on production cost reduction, emerging biosimilars and regulatory concerns requires a process optimization. Upon all, this is achieved through better process control and monitoring, avoiding batch failures and assuring product quality attributes throughout the whole production line. Critical process parameters, such as mAb titer, impurity contamination and mAb aggregate levels are to be monitored throughout the mAb production process to fulfill therapeutic protein quality and regulatory requirements. Besides, this constant in-time monitoring is required to obtain high product yields and minimize manufacture costs by reducing the risk for production errors.

The state-of-the-art techniques for monitoring mAb and impurity levels are HPLC, ELISA and SDS-PAGE. These methods provide a low limit of detection but are time-consuming and laborious.

As alternative, FT-MIR can be used for mAb and HCP level monitoring as it enables quantification of proteins due to their structure-specific vibrational modes and wavelength specific energy absorption, resulting in a protein-structure specific sample spectrum, allowing differentiation of protein types, e.g. mAb and protein A. Moreover, process information is obtained promptly, thereby enabling the ability to react adequately to manufacture changes. Other process related impurities, such as aggregate levels, are mainly quantified by size exclusion chromatography and dynamic light scattering, whereby FT-MIR has been proven by numerous publications to be a suitable tool for aggregate amount estimation.

Application of this technology for monitoring critical process parameters during mammalian cell culture based antibody production might benefit from direct sample application (no sample preparation), quantitative critical process parameter estimation from a single measurement, and application to different cell cultures *in situ*. Impurity levels (*e.g.* HCP's) between 5,000- 300,000ng ml^{-1} and mAb titer between 0.2- 1.7g l^{-1} were successfully quantified, using FT-MIR and adequate chemometric models for multivariate data analysis. Antibody aggregates were quantified in the low percent range, meeting the FDA's limit of < 5%. Therefore, FTIR is applicable as cost-effective, simple, fast and non-invasive process monitoring technique.

INTRODUCTION

Protein production

Monoclonal antibodies (mAb) are widely used in clinical applications, diagnostic systems and different research fields. To date, there are more than 350 antibodies in development worldwide, and their number is rising (Vunnum, Vedantham, and Hubbard, 2009). mAbs are very efficient but among the most expensive drugs as well, with costs mounting to $ 35,000 per year for mAbs used in cancer treatment, involving high dosage treatment (Farid, 2009). Additionally, demands per product can annually mount to several hundreds of kilograms. With patents running out, and biosimilar molecules making their way to clinical trials, the production of antibodies requires process optimization. Besides the economic pressure, healthcare providers and governmental regulations tend to put certain limits on pricing and marketing possibilities of new therapeutics.

These factors require pharmaceutical companies to focus on material consumption, e.g. buffers, consumables, utilities, labor and work force as cost-intensive examples.

Thereby cost-effective production facilities and processes need to be achieved and processes require to be optimized and developed within shorter time- periods, reducing time to market due to lower overall process development and lowering development costs (Farid, 2009; Kamarck, 2006; Farid, Washbrook, and Titchener-Hooker, 2005).

Typically, mAb expression is performed in genetically modified mammalian cell cultures, e.g. chinese hamster ovary cells (CHO), murine myeloma cells, e.g. NS0 and SP2/0, in genetically modified bacterial cell cultures, *e.g. Escherichia coli*, in yeast, *e.g. Pichia pastoris* or *Saccharomyces cerevisiae* and other protein expression systems. The production process starts with the so-called upstream processing phase. This encompasses optimization of cell growth, usually within a bioreactor. A small scale bioreactor is used to elucidate optimum bioreactor design, feeding rate, agitation speed, stirring rate, gas supply, waste removal and temperature while fermentation within the bioreactor can be done as either batch, fed- batch or continuously.

Following small- scale feasibility experiments, typically, a large- scale production process is established, covering a size of several hundred to several thousand liters. Today, typical bioreactor scales are between several thousand litres up to 25,000 litres and more with antibody titers in the mg per ml scale (Farid, 2009; Birch and Racher, 2006; Werner, 2005).
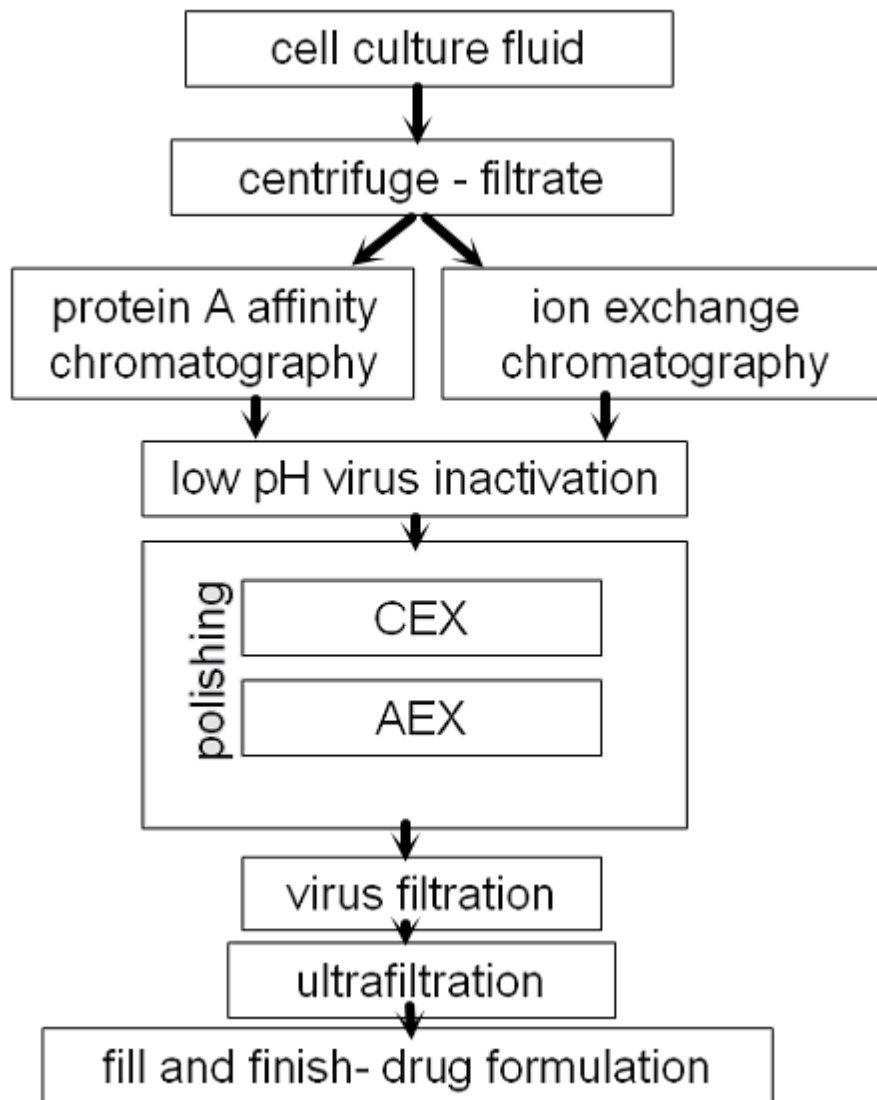
Figure 1: Overview typical downstream process in antibody manufacture.

Following the upstream processing phase, cell culture is harvested (figure 1). In mAb expression, usually the product is secreted into the cell culture; therefore cells and cellular debris have to be removed. This can be achieved by centrifugation or depth filtration, leaving the antibody together with impurities such as proteins, nucleic acids and protein variants in solution. It marks the beginning of the so- called downstream processing phase. Within this phase, the desired biopharmaceutical product, *e.g.* a mAb, needs to be purified to a desired yield to meet product and regulatory quality criteria, using a sequence of orthogonal purification strategies. Within downstream processing, this can be separated into several stages: the so-called RIPP stages (Recovery, Isolation, Purification and Polishing) (Gosh, 2006) or CiPP scheme (capture, intermediate purification and polishing) (Antibody Purification Handbook, Amersham Biosciences).

The first two steps include mainly high-throughput low-resolution techniques while the last two stages use high-resolution low-throughput techniques. Removal of insolubles and recovery is done during the first step, recovery, by capturing the target as a solute in a particulate-free liquid. Cells, cell debris and

other particulate matter have to be removed from the fermentation broth containing the target protein, to prevent blockage of the chromatography columns. This can be done by filtration, centrifugation, sedimentation, flocculation, precipitation or crystallization. During product isolation impurities with properties varying a lot to the ones of the target and bulk proteins are removed. As water is the main impurity for most products, isolation steps are designed to remove most of it, thereby concentrating the target and reducing the material volume to be handled. This involves adsorption, solvent extraction, ultrafiltration and precipitation. Contaminants with similar properties as the target are separated during product purification. Steps may be repeated to increase product purity after partial purification. After affinity chromatography, ion-exchange chromatography and gel-filtration are typically used to obtain a higher than 98% purity of the product compared to HCPs in solution. These chromatography steps also need to remove specific impurities such as endotoxins, nucleic acids, antibody dimers and other antibody aggregates as well as leaching protein A, from *e.g.* affinity chromatography.

The final processing stage is the so-called product polishing which ends with packaging of the product in a stable, easily transportable containment and can involve buffer changes, crystallization and lyophilization. Sterilization, pyrogen and virus removal, and removal of trace contaminants to ensure product safety also have to be done during the polishing step. To avoid the risk of virus contamination working with cell lines, several virus removal steps are included. These can be based on filtration, UV irradiation, low pH treatment and use of detergents and solvents (Birch and Racher, 2006; Sommerfeld and Strube, 2005).

Some of these stages can be combined using special methods. Insolubles are removed and the product is isolated in a single step during expanded bed adsorption or using affinity chromatography. Typical yields for antibody purification are around 60-80%, varying with the number of purification steps (Farid, 2009; Werner, 2004).

Monitoring techniques

Having a look at above mentioned parameters, one can easily see that a large set of experiments is necessary to allow for optimum growth conditions and high product quality and purity. Using wrong agitation speed can lead to increased cell death due to shear forces or decreased oxygen and nutrient supply. Using wrong reactor design can also impede gas and nutrient distribution within the cell culture broth. Within downstream processing, the correct choice of e.g. filter pore sizes and correct pH- adjustment for ion exchange chromatography are vital to obtain high yields and high purity of the final biotherapeutic product. Also, the correct pH for virus inactivation needs to be chosen so as to obtain virus inactivation but prevent excessive antibody aggregate formation due to pH and pH- incubation time. Removal of HCP and DNA needs to be monitored to adjust the corresponding chromatography systems (Fontes and van Reis, 2009). Thus, a number of so-called critical process parameters need to be monitored throughout the entire production process. Within upstream

processing, these critical process parameters can comprise glucose, lactate and ammonia levels, oxygen level, optical density and live cell counts. For the downstream part, these parameters can comprise target protein titer, e.g. antibody levels at different purification stages, impurity protein level, e.g. host cell protein concentrations, antibody aggregate level, glycosylation patterns as well as detection of leachables, *e.g.* residual protein A from purification steps involving affinity chromatography. Monitoring of these critical process parameters is vital to obtain high product quality while at the same time ensuring low production costs and minimizing production errors.

This monitoring can be done off-line, at-line and on-line. With off-line monitoring, a sample is regularly withdrawn from the bioreactor or from different purification stages and then analyzed outside the bioreactor.

At-line monitoring is similar, however, the sample is analyzed next to the bioreactor, reducing analysis time. The third technique is on-line or in-line monitoring.In-line monitoring is done *in-situ* directly in the reactor within the fermentation broth, while on-line monitoring is done *ex-situ*, in a bypass or loop, making use of filters to remove cells and unwanted particles prior to sample analysis (Vojinović, Cabral, and Fonseca, 2006; Garn *et al.*, 1989).

For the upstream part, analysis of critical process parameters is mainly done by using sensors. These can comprise, but are not limited to standard potentiometric ion selective glass electrodes for pH-measurement, Clark amperometric electrodes for oxygen level monitoring and Severinghaus type electrodes for CO_2 monitoring (Vojinović, Cabral, and Fonseca, 2006).

However, their overall use is impeded by contamination- and long- term stability risks, requiring the implementation of non-invasive sensors (Rhiel *et al.*, 2002). Additionally, UV as a standard sensor within process analysis can track protein levels, however, is unable to differentiate between product and impurities (Pujar, Low, and O'Leary, 2009).

Within downstream processing, critical process parameters are mainly analyzed with off-line techniques such as enzyme linked immunosorbent assays (ELISA), SDS-PAGE and western blotting or isoelectric focussing. These techniques have the advantage of obtaining a low to very low limit of detection. However, they are quite expensive, with ELISA plates mounting to several hundred euros per plate. Furthermore, it takes several hours to obtain the results, thus information on the process is obtained retrospectively. Thereby, adequate process adjustments cannot be made on time, increasing the risk for process failures and thereby higher production costs and longer process development times.

Protein aggregation is usually monitored by size exclusion chromatography, differentiating proteins according to their hydrodynamic radius, or using dynamic light scattering to analyze the size of a protein and thereby identify protein dimers, multimers and other forms of protein aggregates. Some of these techniques can be done at-line, allowing for sample analysis next to the bioreactor, e.g. using lab-on-the chip techniques. Thereby, results are obtained slightly faster.

However, the use of non-invasive techniques for monitoring would reduce workload significantly, not requiring regular sample withdrawal anymore and leading to faster analysis time. Additionally, batch

success rates could be increased, eliminating operator errors and contamination risks, associated with sample withdrawal.

FTIR as technique within process development and monitoring

One alternative non-invasive technology is Fourier transform infrared spectroscopy (FTIR) which can give structural information and identity confirmation of an (un)known sample, based on the interaction between irradiation and matter at different wavelengths (Kong, 2007).

This is achieved as molecules absorb frequencies of irradiation matching their resonance vibration frequency depending on their bond strength, hydrogen bonding pattern and surrounding molecule bonds.

Complex molecules have more bonds and can thus vibrate in different vibrational modes, resulting in fundamental vibrations as well as overtones via specific energy absorption at different wavelengths. Thereby, a specific sample spectrum is obtained, which provides the opportunity for identifying functional groups and molecules (Griffiths and de Haseth, 2007), *e.g.* proteins and protein structures.

Infrared spectroscopy can be separated into two, for structure analysis and quantification relevant subtypes: near- infrared spectroscopy (NIR), already largely employed in monitoring processes, and mid- infrared spectroscopy, used *e.g.* for studying protein structures. While NIR covers the wavenumber range between 4,000- 13,000cm^{-1}, MIR extents across the range of 200- 4,000cm^{-1} (Landgrebe *et al.*, 2010). The advantage of IR as analytical tool is the relatively low amount of sample required, between 10- 100µg and down to 50ng, its short measuring time, obtaining results within less than 1-2 minutes and its cost- effectiveness (Barth, 2007).

Both, NIR as well as MIR have advantages and disadvantages. However, they both enable structural analysis of molecules, based on the molecule's specific absorbance. While NIR detects overtones, MIR allows detection of more fundamental vibrations in a molecule. For NIR, quantification is not that straight-forward, as relatively large sample sets are required and calibration is not that simple to achieve and can also not be transferred from one instrument to another one (Cen and He, 2007). Additionally, bands in NIR are highly overlapping and need to be deconvoluted by mathematical steps- visual confirmation of results is not possible. In contrast, MIR also allows to visually identifying bands which correlate or seem to correlate with the concentration of an analyte, thus leading to higher confidence of a user when designing a new quantification method. Calibration in MIR is also more straightforward and information about a molecule's structure is more clearly visible, due to usually well-separated bands of different functional groups and the additive effect of different groups within spectra of molecule mixtures.

Although in principle both, NIR as well as MIR, lead to the same results and can be used for quantification purposes, most information about a molecule's structure can be found in the MIR range, also with the ability to quantify substances at significantly lower concentrations compared to NIR (Landgrebe *et al.*, 2010). Yet, the advantage of NIR is the low absorbance of water in that region, which imposes additional equipment effort, using MIR, in order to minimize water absorbance. There

the problem is that usually very thin thicknesses in the µm- range are required for flow-through cells, as otherwise total absorbance within the Amide region would occur, due to water absorbing at the same regions as proteins. While for NIR, low-cost materials, *e.g.* quartz and glass can be used to transmit radiation, similar materials used for MIR irradiation transmittance are still very expensive.

Despite this, in the following chapter MIR will be discussed as it facilitates the design of calibration models, and also allows visual identification of potentially useful wavenumber ranges within the spectra, thereby allowing process monitoring through increase or decrease of a specific band within the IR spectra. Furthermore, for protein structural analysis, which will also be the foundation for some of the monitoring applications described here, MIR is primarily used already.

MIR has the ability to perform at-line analysis without destroying the analytes. Even in-line and on-line measurements are possible, e.g. using a sub-type of MIR, ATR (Fahrenfort, 1961; Harrick, 1960).

To date, it is widely used for analysis of liquid samples, e.g. fuel composition, drinks, food composition as well as educts for chemical reactions (Fernanda Pimentel *et al.*, 2006; Moros *et al.*, 2005; Pillonel *et al.*, 2003; Doak and Philips, 1999).

MIR can be used to differentiate different proteins, *e.g.* protein A from mAb, or host cell proteins from mAb as well as aggregated mAb from non- aggregated antibodies. In the past, MIR has therefore been used to analyze protein secondary structures as well as elucidate changes in antibody formulations upon storage and formulation type (Skrdla, Harrington, and Lin, 2010; Barth, 2007; Yoshioka and Aso, 2007; Matheus, Mahler, and Fries, 2006; Gupta *et al.*, 2002; Breen *et al.*, 2001; Goormaghtigh,Raussens, and Ruysschaert, 1999; Jackson and Mantsch, 1995) and analyze compounds in various cell culture compositions (Mazarevica *et al.*, 2004; Doak and Phillips, 1999). Furthermore, it has been used to determine protein levels

(Capito *et al.*, 2013; Capito *et al.* 2012; Sellick *et al.*, 2010; Etzion *et al.*, 2004; Oberg and Fink, 1998) and to quantify polysaccharides in bacterial samples (Marcotte *et al.*, 2007).

Pistorius et *al.* (2008) were able to quantify lipid, carbohydrate and protein content in biomass of different origin, using a single MIR measurement (Pistorius, DeGrip, and Egorova-Zachernyuk, 2009).

Also IR-based classification of micro-organisms is possible, if they show differences in exposure of their surface proteins and composition (Preisner *et al.*, 2010; Winder *et al.*, 2004).

Furthermore, besides NIR, MIR can be used to quantify single amino acids, differentiating them because of minor differences in their IR spectra. This allows amino acid quantification in the millimolar range (Barth, 2007; Riley *et al.*, 2001).

The suitability of MIR for quantification of recombinant protein levels was shown by various groups. Gross-Selbeck *et al.* (2007) and McGovern *et al.* (1999) used this technique to quantify protein in microbial cell cultures while Sellick *et al.* (2010) quantified protein in mammalian cell cultures. Timmins *et al.* (1998) utilized MIR to differentiate baker's yeast strains.

With ATR, the sample is coated to a crystal consisting of material with a high refractive index, usually zinc selenide, germanium, diamond or silicon. Instead of a crystal, immersion probes can be used such as chalcogenide and silver halide based autoclavable ATR probes fitting into a bioreactor port

(Landgrebe *et al.*, 2010). Alternatively, glass fibers for ATR, made of Telur, Arsen and Selen can be used, passing through a bioreactor (Capito *et al.*, 2013). For at-line analysis, either ATR instruments or flow-through cells can be used.

ATR was already used for overall protein quantification as well as to elucidate differences in protein secondary structure (Landgrebe *et al.*, 2010; Goormaghtigh, Ruysschaert, and Raussens, 2006; Doak and Phillips, 1999; Jackson and Mantsch, 1995).

Additionally, due to its suitability for multivariate data analysis and process control, NIR, MIR in general as well as ATR all fit into the FDA's guideline for process analytical technology (PAT) and will likely be increasingly used for process monitoring in the future with different applications already (FDA, 2004; Lopes *et al.*, 2004).

Within the here discussed middle infrared region [4,000–200cm^{-1}] nine characteristic IR bands are used to allow for quantitative and qualitative protein analysis. Besides the mainly used Amide I and II these bands comprise Amide A, Amide B and Amide 3- 7 (table I) (Krimm and Bandekar, 1986). NH-stretching leads to formation of the Amide A band which is insensitive to polypeptide backbone conformation (Barth and Zscherp, 2002). The Amide I band originates mainly from C-O stretching vibrations, with small contributions from CN stretching and NH- bending and provides information on a protein's secondary structure, but is almost not influenced by amino acid side chains.

Similarly to the Amide I band, also the Amide II band is only to a minor extent affected by amino acid side chains. Yet, the correlation of the protein secondary structure with the Amide II band shape is not as well established as with the Amide I region. The Amide II band is generated due to CN stretching and NH bending vibrations as well as CO bending and CC stretching.

Also the Amide III band has been suggested to allow for protein analysis (table II continued; (Cai and Singh, 2004; DeOliveira *et al.*, 1994).

Similarly, different bands are generated due to different vibrations, exemplary shown in table I, and thus can be related to the structure causing these vibrations.

The protein secondary structure affects the hydrogen bonding pattern, which on the other hand, influences the C=O stretching vibration frequency. Thus, proteins with high beta-sheet content, *e.g.* monoclonal antibodies, differ in their Amide I band from proteins with high alpha-helix content, *e.g.* protein A from *Staphylococcus aureus*. While beta-sheet structures shift the band maximum of the Amide I to lower wavenumbers, alpha-helix rich structures shift this maximum to higher wavenumbers. Depending on the protein secondary structure, there are different shifts of band maxima as well as appearance of new bands. While aggregated strands manifest themselves in peak maxima at 1,615 and 1,685cm^{-1}, beta-sheets are related to band maxima visible in a smaller band at 1,675-1,695cm^{-1} as well as a main band at 1,620-1,635cm^{-1}. Even irregular structures, turns and loops can be detected and also be quantified; using specific wavenumber regions (tables II and III).

Using infrared spectroscopy for monitoring of critical process parameters, there are some hurdles, which, however, are mostly possible to be solved.

One such hurdle is to separate the important information within the spectra, originating from critical process parameters from the non- important spectral information. Cell cultures consist of many different components such as amino acids, supplements such as BSA, vitamins, antibiotics, cholesterol, growth factors, proteins, lipids and nucleic acids (Chu and Robinson, 2001). These components result in complex overlapping spectra, making it not easy to identify the relevant information.

Table I: Amide bands, their corresponding wavenumber ranges and associated molecule vibrations.

Designation	wavenumber range (cm^{-1})	Assigned to
Amide A	3,300	NH stretching
Amide B	3,100	NH stretching
Amide I	1,600- 1,690	C=O stretching
Amide II	1,480- 1,575	CN stretching, NH bending
Amide III	1,229- 1,301	CN stretching, NH bending
Amide IV	625- 767	OCN bending
Amide V	640- 800	out-of-plane NH bending
Amide VI	537- 606	out-of-plane C=O bending
Amide VII	200	skeletal torsion

Table II: comparison of Amide I and Amide III band with associated secondary structure elements in proteins.

	Amide I	Amide III
secondary structure element	wavenumber (cm^{-1})	
aggregated strands	~ 1,615; 1,619	
β-sheet	1,620-1,635; 1,624-1,642	1,224-1,255
Irregular	1,640-1,650	1,256-1,288
3_{10} helix	~ 1,640	
α-helix	1,650-1,658	1,289-1,328
3_{10}-helix	~ 1,660-1,663	
turns & loops	1,655-1,685	
antiparallel β-sheet	1,675-1,695; 1,691-1,696	1,224-1,255
aggregated strands	~ 1,685	

Therefore, using chemometrics and algorithms such as partial least squares regression, univariate or multivariate data analysis, software is then used to identify the resulting IR bands originating from these specific molecule structures and separate overlapping bands. Using data processing, first and second derivative treatment according to Savitzky- Golay (Gorry, 1990) results in a mathematical resolution enhancement, allows the differentiation of minor band maxima shifts and thus selective quantification. Fourier self-deconvolution and normalization helps to enhance the spectra resolution and reveal information, *e.g.* about secondary structure elements of proteins (Kong and Yu, 2007; Dong *et al.*, 2002).

For univariate analysis, a relationship is established between the absorbance of a single peak height or peak area, and the concentration of an analyte corresponding to that absorbance. This works well if there is no or little interference and no or little band overlap. Otherwise, multivariate methods need to be used. These techniques can comprise PCA or different types of PLS (Esbensen, 2002; Naes *et al.*, 2002; Wold, Sjöström, and Eriksson, 2001).

Using PCA with PLS, an algorithm thereby extracts variables **T** and **U** by compressing the information from factors **X** (*e.g.* spectral intensities within spectra, formula (1)) and results **Y** (reference values, formula (2)), respectively.

Irrelevant information is disregarded and the score matrix T is then used to predict the matrix U, which contains the Y-scores. Thereby the results Y are predicted (Sjöström *et al.*, 1983). The loadings P and q are estimated by regression and explain the relation between the **T**-matrix and X as well as the **U**-matrix and Y, respectively. The first PLS component is then used to explain for most of the covariance, with the succeeding components explaining less covariance. The succeeding components may also explain spectral noise, therefore the use of PLS models with fewer components reduces the risk of overfitting a model to a certain set of spectra, otherwise being another hurdle (Naes *et al.*, 2002; Martens and Martens, 2000; Sjöström *et al.*, 1983).

$$X = T \times P^T + E \quad \textbf{(1)}$$

$$Y = U \times q^T + f \quad \textbf{(2)}$$

This approach is already used for several parameters within upstream processing, including pH, conductivity, ion concentration, temperature etc. For downstream processing, it can be used to correlate buffer pH, conductivity, residence time and similar input parameters with peak volume and shape, purity, overall yield and other output parameters (Kirdar *et al.*, 2007).

General procedure for quantification of a critical process parameter

Before using FT-MIR for quantification of an analyte or critical process parameter, a model needs to be designed. A set of samples comprising several hundred samples is split into a training set, a

calibration set and a validation set (figure 2). If the number of available samples is limited, cross-validation, *e.g.* one-out- cross validation can be used. The corresponding analytes to be detected by MIR need to be quantified by a reference method, *e.g.* ELISA for host cell proteins as impurities or leaching protein A. Target protein concentrations can be quantified by affinity chromatography for antibodies, size exclusion chromatography (SEC) or other suitable tools. It is also possible to label the analyte of interest and quantify the label to indirectly quantify then the analyte, *e.g.* by fluorescence. However, using this step, labeling an analyte to simplify the generation of reference values, one has to assure that the label does not interfere with the spectral window area to be used for detection and quantification in FT-MIR. Best is, *e.g.* to measure an IR spectrum of the label without any other substance such as protein, to exclude potential interference and erroneous results.

Having established a reference method, the training set comprising the samples is measured with FT-MIR, using the analyte concentrations determined by the reference method for calibration. PCA can be used to simplify identification of relevant spectral wavenumber ranges which contain information about the analyte and thus allow potential quantification. PCA thereby converts the observations of putatively correlated variables, using orthogonal transformation, into linearly not correlated principal components. The first principal components have most of the variance within the data set, whereby the succeeding principal components have less variance and are all independent from the preceding principal components (Naes *et al.*, 2002; Warnes *et al.*, 1996).

Using PCA, outliers, differing a lot from other spectra, can be removed.

Alternatively to this procedure, wavenumber ranges can be selected manually, using wavenumber ranges which are known to be related to certain protein secondary structures or specific analytes. Also, wavenumber ranges which contain bands, whose intensities correlate with concentrations as determined by reference values, can be used to establish a quantification model, proven that there is a clear correlation.

Afterwards, an initial quantification model, e.g. based on the PLS algorithm, is validated using a set of samples for validation. If the prediction accuracy is not acceptable, different wavenumber ranges can be chosen or combined to obtain better results. Alternatively, different mathematical pre-treatment steps for the spectra can be performed before doing spectral analysis, *e.g.* using first and second derivative, *e.g.* based on Savitzky- Golay algorithm, vector normalization and smoothing.

In the end, an unused set of samples, a so-called independent test-set is used to elucidate the robustness and general prediction ability of the quantification model. Once the robustness of a specific model for using FT-MIR within a specific process is established, this technique can then be used to replace existing techniques or be used as stand-alone process control tool, thereby reducing process development time, leading to a cost-effective process and minimizing the effort for process development.
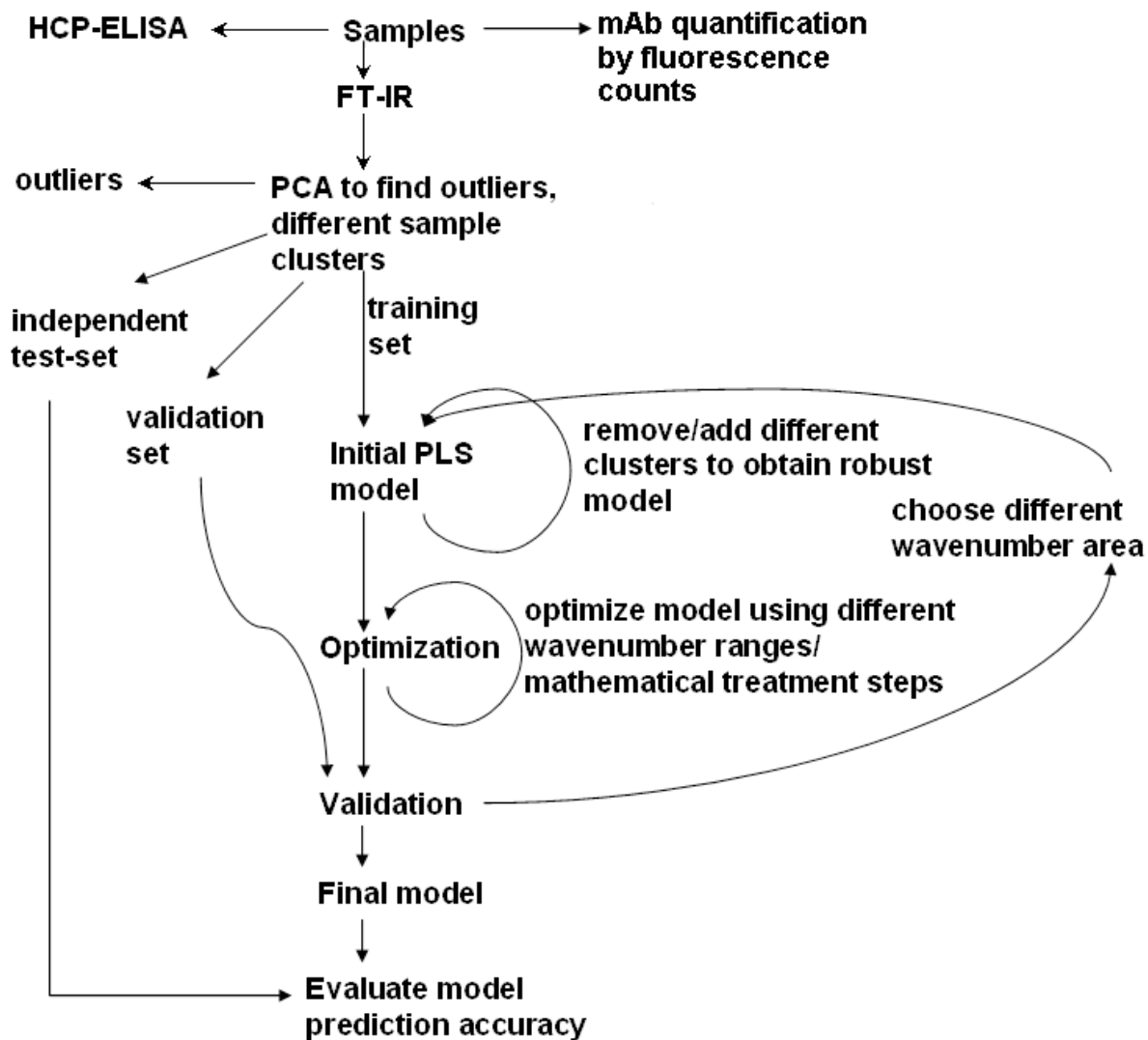
Figure 2: General set-up to establish a quantification model for critical process parameter estimation.

Aspects to consider before choosing FT-MIR as monitoring technique in downstream processing

Before deciding to use FT-MIR for quantification of critical process parameters, a user should be aware that this technique is not applicable if processes are prone to regular changes. While monitoring of constant downstream processes using FT-MIR is working well, results of process surveillance are less accurate and even irrelevant, if there are process changes, which can greatly affect the background matrix of a sample. Process changes can be *e.g.* any changes which affect the composition of the cell culture broth, *e.g.* an additional filtration step or using different chromatography systems for one IR calibration system. If these aspects apply, a user should consider using the to-date monitoring techniques such as ELISA, affinity chromatography, light scattering and SEC. The problem with FT-MIR is, that *e.g.* a change in the buffer can interfere with the chosen wavenumber range for analyte quantification.

However, for process monitoring applied to regular continuous purification processes, not subjective to changes, such as established downstream purification processes, MIR can be used, provided that

a careful quantification model is established, calibrated for a specific portion of the process chain with a specific background matrix (*e.g.* one calibration for analyzing samples after affinity chromatography and the other calibration for analyzing samples after the virus inactivation step) and carefully analyzed for potential interference. If a user follows these principles, this hurdle can be circumnavigated.

Now that we described how and when FT-MIR can be used for monitoring critical process parameters, the next section will describe the use of FT-MIR for protein structure analysis as differences in protein structure, and thus differences in the absorbance spectrum are the foundations for the here presented monitoring applications.

By describing potentials of FT-MIR for distinguishing relative amounts of protein secondary structure, as well as monitoring *e.g.* protein denaturation, we try to give the reader an introduction to the topic before giving examples of how to distinguish mAb from impurity proteins, mAb from protein A, aggregated mAb from non-aggregated etc.

Elucidation of protein structure, differentiation and quantification of protein secondary structure using MIR

IR- spectroscopy can be used to elucidate the relative amount of secondary structure within a protein of interest, e.g. beta-sheet and alpha-helix amounts or gain insight into reaction mechanisms, *e.g.* within photosynthesis (Berthomieu and Hienerwadel, 2009). However, it can also be used to state the protonation state of aspartate and glutamate groups, which *e.g.* have a shift from 1,680cm^{-1} to 1,580-1,560cm^{-1} as well as 1,420-1,395cm^{-1} upon deprotonation or characterize His and Tyr residues, *e.g.* in photosystem II or in bacteriorhodopsin (Barth, 2007; Berthomieu and Hienerwadel, 2009).

IR spectroscopy can provide information on the hydrogen bonding pattern of a protein. While increasing hydrogen- bonding leads to lower frequencies of stretching vibrations, bending vibrations are increased (Barth and Zscherp, 2002). Additionally, it can be used to identify side chains in proteins, although not straight-forward due to largely overlapping bands. However, due to band overlap, *e.g.* between alpha-helix and random structures, or with alpha-helix side chains and beta-sheets, errors can occur which can be reduced, *e.g.* using D_2O instead of water as solvent (DeOliveira *et al.*, 1994).

Additionally to the difficulties described above, side chains are estimated to contribute to up to 30% to the Amide I absorbance, thus contributing to a protein secondary structure estimation error. Yet, the average error compared to X-ray crystallographic data with respect to secondary structure estimation is about 4-10% and thereby similar to other structure elucidating techniques, such as circular dichroism (Barth and Zscherp, 2002).

Using second derivative, it is possible to identify secondary protein structures and quantify the corresponding secondary structure composition within a protein using FT-MIR (Dong, Huang, and Caughey, 1990; Kalnin, Baikalov, and Venyaminov, 1990; Venyaminov and Kalnin, 1990; Susi and Byler, 1986; Susi and Byler, 1983).

The position and shape of the Amide I band can also be used to estimate the length of the alpha-helix or the number of strands in beta-sheets. Increasing length of alpha-helix as well as increasing number of strands in parallel beta-sheets both lead to shifting of the Amide I peak to lower wavenumbers (Barth, 2007).

However, these above mentioned insights require usually protein concentrations of > 10mg ml^{-1} and short path lengths.

One possibility is to use a library of proteins with known structures to build a secondary structure quantification model. This has been done by Capito *et al.* (2013; 2012) using a set of protein spectra with known secondary structure composition for establishing a protein secondary structure prediction model. Proteins at a concentration of 12mg ml^{-1} were measured, using a flow-through cell with a path length of 7µm (Aqua spec Flow cell, Microbiolytics GmbH, Esslingen, Germany) and correlated with relative secondary structure amounts, determined by Server- based secondary structure prediction tool Jpred III (Cole, Barber, and Barton, 2008). The obtained models for predicting relative amount of beta-sheet and alpha-helix, respectively, showed low RMSECV of 4.3 and 4.7%, respectively, similar to validation errors by Goormaghtigh et *al.* (2006) who used only three specific wavenumbers and first derivative to selectively quantify relative amounts of secondary structure in protein (table III).

Table III. Protein secondary structure composition determined by MIR in comparison to known composition. SD: Standard deviation of the prediction compared with the actual structure component, using a linear model including different proteins. Goormaghtigh *et al.*, 2006.

secondary structure	wavenumbers	SD
alpha-helix	1,545- 1,655- 1,613	5.4
beta-sheet	1,656- 1,634- 1,691	6.6
beta-turn	1,677- 1,528- 1,577	3.2
random	1,544- 1,627- 1,691	7.9
3_{10}-helix	1,631- 1,694- 1,625	2.9
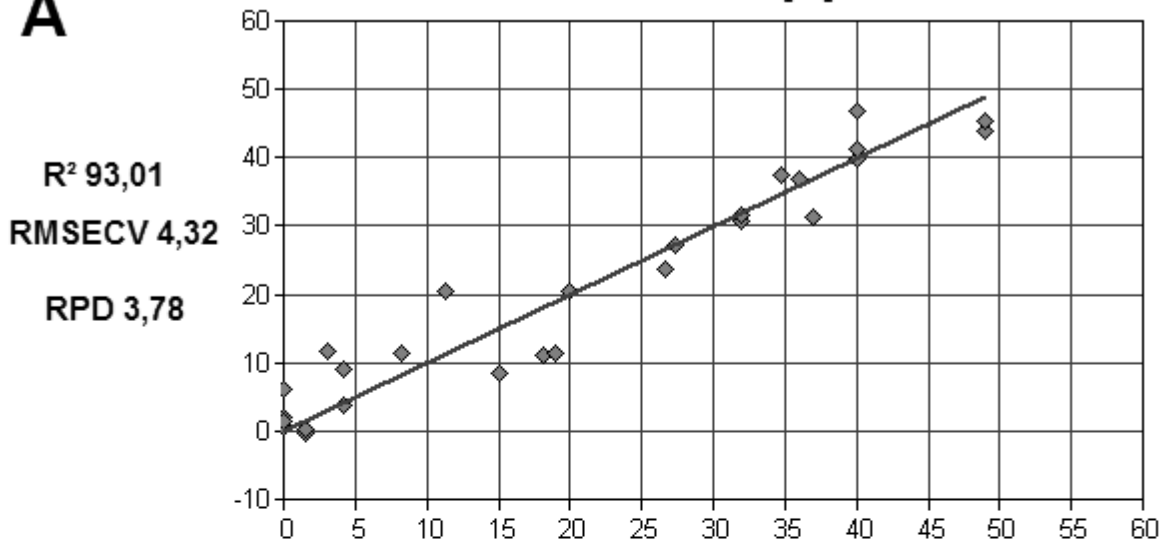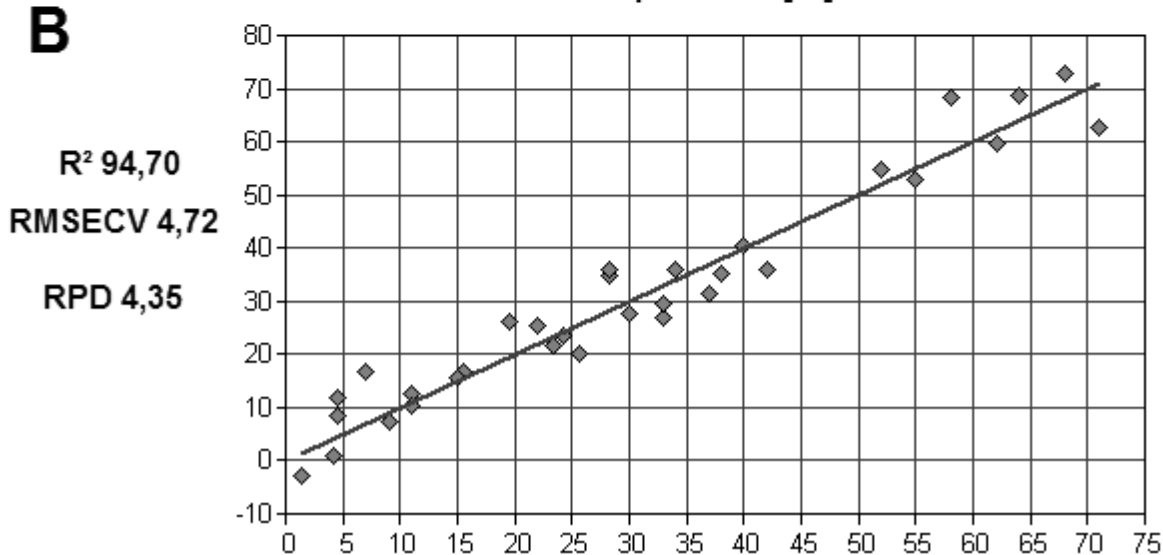
Figure 3: Capito *et al.* (unpublished results): quantification models for predicting A: beta-sheet content and B: alpha-helix content in proteins. Prediction as relative content in %. R^2 and root mean square error of cross-validation (RMSECV) given. RPD: relative predictive deviation.

Besides above described secondary structure quantification, FT-MIR can also be used to monitor secondary structure changes, *e.g.* upon thermal heating leading to denaturation.

In such an approach, first the aqueous mAb solution is measured at temperatures between 25°C and 95°C, using Bio ATR cell II (Bruker Optik GmbH, Ettlingen, Germany). Afterwards, water spectra are measured at the same temperature range and subtracted from the aqueous protein spectra, using corresponding water spectra at same temperature as measured protein spectra. This is done to account for spectral changes at different temperatures. Antibody secondary structure changes, e.g.

temperature dependent aggregation behavior can then be evaluated using second derivative for the Amide I wavenumber range (figure 4).
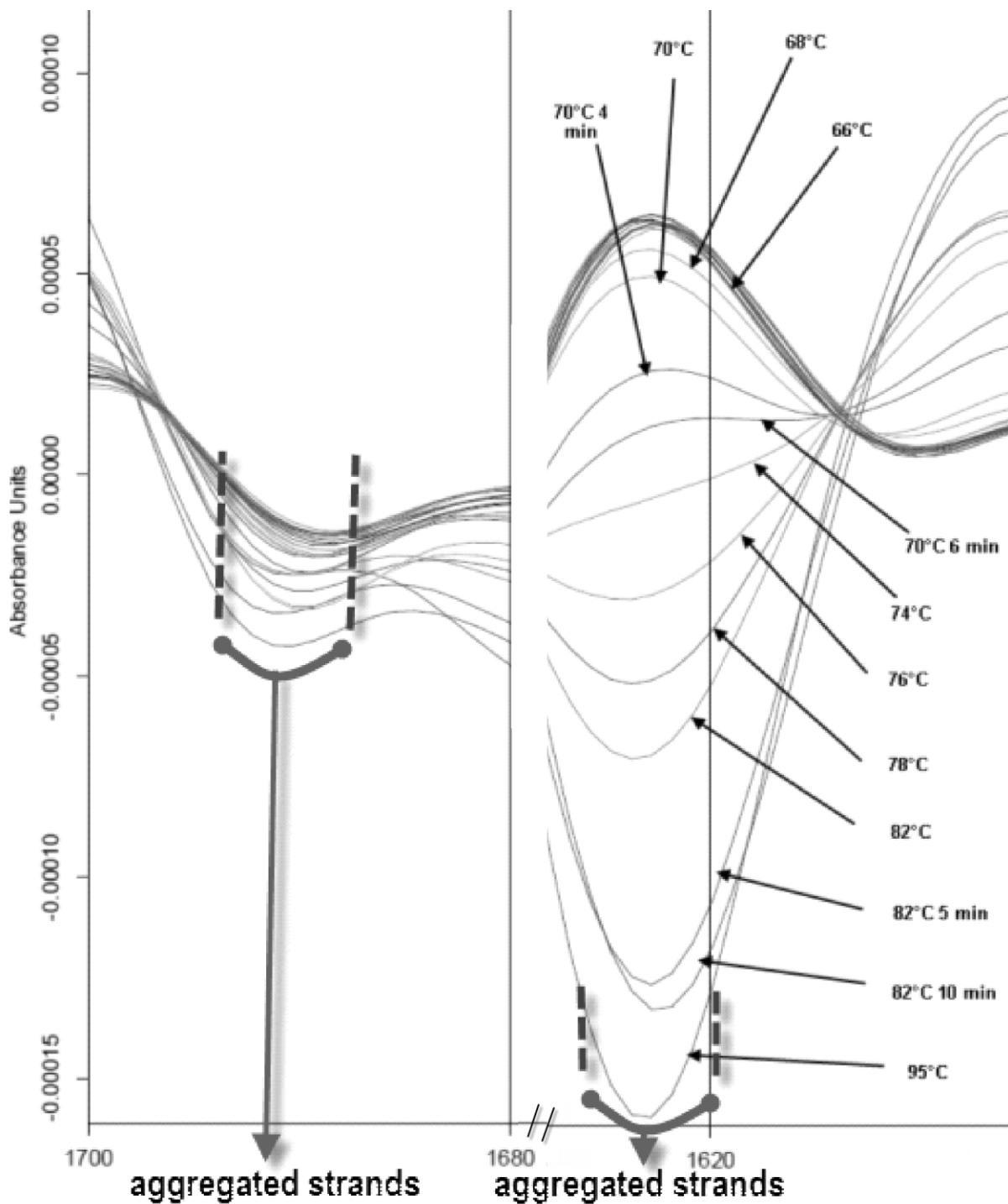
Figure 4: Capito *et al.* (unpublished results): Second derivative of temperature stressed mAb at wavenumber range 1,630- 1,610cm^{-1} and 1,700-1,680cm^{-1}, showing increased presence of aggregated strands at temperatures above 68°C.

Having a look at the spectra, a strong beta-sheet associated peak at 1,625- ~ 1,650cm^{-1} can be observed. Although this band is slightly shifted compared to table I, it is associated to beta-sheet, due to the high beta-sheet content of IgG- type antibodies of approximately 70%.

Additionally, it might also refer to so-called beta-barrel structures, forming the different domains within light and heavy chains (Furtado *et al.*, 2004; Chen *et al.*, 2003).

When exposing the mAb to increasing temperature, denaturation is visible through decrease of ordered beta-sheet structures, with simultaneous increase in bands, assigned to intermolecular beta-sheet aggregated strands exhibited at wavenumbers below 1,620cm^{-1} and around 1,690cm^{-1} (Dong, Randolph, and Carpenter, 2000). First, significant spectral differences are obvious at temperatures above 68°C, and larger differences appear around 70°C, being relatively similar to described denaturation temperatures of mAbs of around 70- 74°C (Matheus, Mahler, and Friess, 2006; Li, Bomser, and Zhang, 2005; Chen *et al.*, 2003; Welfle *et al.*, 1999).

Similar results were achieved by Natalello *et al.* (2005), who investigated effects of heat treatment on lipase from *Candida rugosa*. At temperatures above 50°C a decrease was noticed in the intensities of both: alpha-helix as well as beta-sheet associated bands in the Amide I and Amide II regions. Additionally, new bands appeared around 1,625 and 1,696cm^{-1}, associated to aggregated protein structures. These results suggested to use FT-MIR as a tool to monitor protein conformational changes, *e.g.* due to induced aggregation, site-directed mutagenesis and processing steps.

Case studies: Using FT-MIR for monitoring critical process parameters in downstream processing

a) Quantification of antibody levels in cell culture fluid using FT-MIR

Using PCA and PLS with FT-MIR, levels of recombinant expressed protein in cell culture fluid can be quantified via related spectral bands, e.g. those within the Amide I region between 1,600- 1,700cm^{-1} or using different appropriate regions.

Similarly, this has been done by Harthun *et al.* (1997), who quantified human antithrombin III levels in CHO cell culture. While the authors used near infrared spectroscopy with wavenumbers between 10,000cm^{-1}- 4,000cm^{-1}, they were able to quantify protein levels between 0.1- 5µg ml^{-1}, with a standard error of prediction of less than 0.5µg ml^{-1}, despite using background matrices with slight differences. The same technique is also used for quantification of drug substance in the final drug product (Christiansen *et al.*, 2007). Similarly, the use of FT-MIR for monitoring biomanufacturing processes, is also covered by a patent (Naughton, Rohrer, and Gentz, 2000) as well as quantifying antibody levels of different antibodies in serum (Iley, McClure, and Shaw, 2008).

Alternatively, Etzion *et al.* (2004) showed the applicability of ATR for quantification of protein content in liquid samples with slightly varying matrix. They quantified total protein content in milk samples from cow milk, using protein related Amide I and Amide II bands. Their results showed the suitability

of ATR for possible on-line protein quantification in milk, however using samples with relatively high protein concentration, when compared to concentrations in downstream processing, of 24.7-39.0mg ml^{-1} for model setup. Standard errors of prediction were 0.22% and less, using either PLS or PCA.

Monitoring of antibody levels throughout different parts of downstream processing is important to adjust *e.g.* residence times on chromatography columns, use correct elution and binding pH in buffers and monitor column lifetime based on its binding and separation efficacies.

When using a software and the PLS algorithm, reference values need to be obtained. For mAb levels, a good reference is *e.g.* antibody quantification via protein A affinity chromatography as the protein A shows selective binding towards the Fc part of an IgG monoclonal antibody while having low affinity for other substances, such as impurity proteins. The reference values for a given set of samples are then used as training set to obtain a good mAb titer prediction model.

The same set is then analyzed via FT-MIR and mAb related spectral window areas are selected. This can be done either by PCA or by visual inspection, looking for band maxima which correlate with the measured mAb level in those samples. When performing this work, one can *e.g.* use spectral window areas within the Amide I region, *e.g.* beta-sheet associated bands as well as alpha-helix associated bands as shown by Capito *et al*. (2012). As mAbs are known for their elevated beta-sheet content of about 70%, one can then look for strong beta-sheet bands, *e.g.* in the wavenumber range of 1,620-1,635cm^{-1} for parallel beta-sheets and 1,675-1,695cm^{-1} for antiparallel beta-sheets and at the same time for weak alpha-helix bands. The latter is important as the mAbs should only give low signals regarding alpha-helix content. It might be necessary to modify the wavenumber ranges to be used, *e.g.* using wavenumber range 1,614-1,660cm^{-1} and 1,680-1,690cm^{-1} for mAb quantification which has been shown to give good results. Of course, there are several different analytes within cell culture fluid, therefore one has to assure that there is no interference with other analytes. Polysaccharides for example, are known to lead to associated bands at 1,610cm^{-1}, therefore the use of these bands within a quantification model needs to be excluded.

This approach has been used to develop specific calibrations for ATR based mAb quantification in liquid samples, using either filtered and unfiltered samples to simulate ex-situ and in-situ measurements (figure 5). Resulting models showed coefficients of determination between 83.0% and 89.9% with a rank of 2 (figure 5). mAb concentrations between 0.17- 1.7g l^{-1} were quantified.
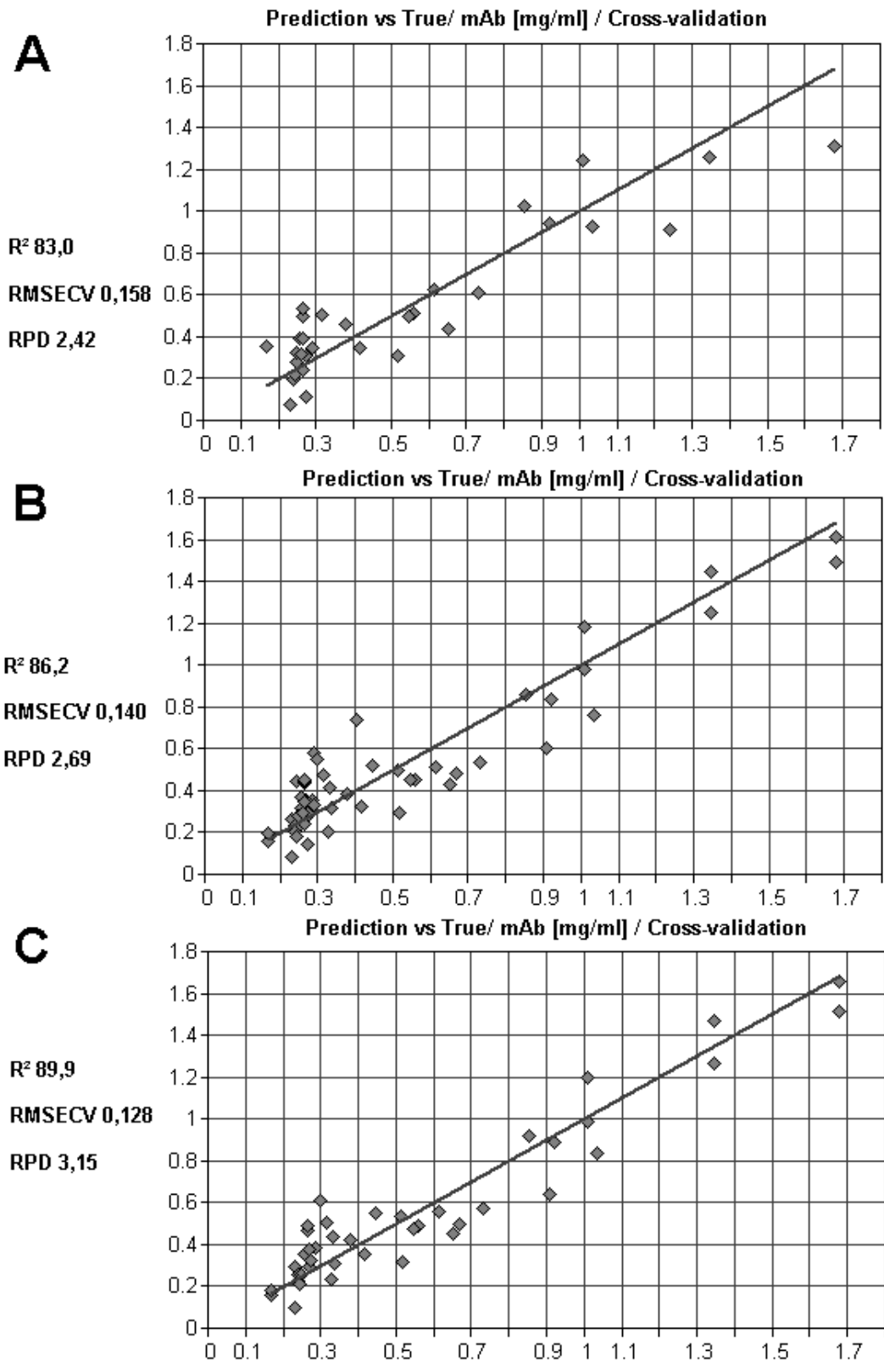
Figure 5: Capito *et al.* (unpublished results and 2012): Comparison of correlation of mAb titers predicted using PLS models covering Amide I region. Reference values measured by ELISA- assay. A: mAb quantification in unfiltered samples. B: PLS model for measuring mAb titer in both, filtered and unfiltered samples. C: mAb quantification in filtered samples.

Regarding prediction accuracy of FT-MIR and ATR based mAb titer monitoring, improvements can still be made. Currently, achievements are published enabling to predict 60-70% of samples with a CV equal to the acceptable variation in an ELISA assay, when using models specified for a specific background matrix during mAb quantification.

Using a non-optimized calibration model, based on filtered and unfiltered samples and thus differing background matrix, only 50% of test-set samples could be predicted with a CV < 25%. Yet, for some quantification procedures, even a general quantification model can be applied to different phases within downstream processing. This has successfully been shown by Rodrigues *et al.* (2008) who used a PLS model, involving NIR for quantification of an active pharmaceutical ingredient after applying different kinds of filtration steps, at approximate concentrations of 2- 4.5mg ml^{-1}. It was shown that a careful calibration design can help to use quantification models, even if the background matrix is slightly changed as is the case with different filtration systems.

Sellick *et al.* (2010) quantified mAb levels in CHO and NS0 cell cultures, using 96 well microtiterplates with dried samples for high-throughput analysis, with scanning times of 45 seconds. The cross-validation was used after splitting the samples into a training, a calibration and an independent test-set, investigating two mAb producing cell lines as well as one non-producing Null cell line, for CHO and NS0, respectively, to design quantification models. The Null cell line was thereby used to prevent incorporation of accumulated protein, other than mAb, to be identified as mAb titer. Thus, samples taken from the non-producing Null cell line, at different time points, were included in the PLS model and assigned to 0mg ml^{-1} mAb, also to avoid PLS model accidentally predicting cell growth instead of antibody titer, as both of course increase during cell culture incubation.

Afterwards, additional detection methods, such as ELISA, are used to validate PLS models designed for mAb titer prediction in either CHO or NS0 cell culture, respectively. While the RMS errors for prediction were below 10%, a relatively high-number of up to 8 factors was selected (table IV). Plotting either the Amide I band area or band height at 1,655cm^{-1} vs. the antibody titer as determined by ELISA, the achieved coefficient of correlation R² was between 92-96 percent for both cell cultures. To allow for normalization when predicting the mAb titer, a spectral background region at 2,000cm^{-1} was used.

Using this approach, mAb titer down to 10,000ng ml^{-1} was quantified. Additionally lactate and glucose were measured, at levels as low as 1g l^{-1} or less, thereby again showing the suitability of FT-MIR for simultaneous measurement of multiple analytes, using a single measurement. These findings suggest to apply FT-MIR within the early development phase, *e.g.* to elucidate high-producing cell lines after FTIR analysis using a cost-effective, fast and simple analysis technique.

Table IV: Details of PLS prediction for mAb titer in NS0 and CHO cell culture fluid as determined by FT-MIR (Sellick *et al.,* 2010). RMS: root mean square (in mg L^{-1}).

	factor (rank)	RMS error of training set	RMS error of validation set	RMS error of test-set
NS0 cell culture fluid	8	3.94 (4.9%)	7.07 (8.8%)	5.97 (7.4%)
CHO cell culture fluid	8	8.27 (2.1%)	37.82 (9.6%)	37.88 (9.6%)

b) Quantification of impurity protein levels in cell culture fluid

Another critical process parameter which can be monitored by FT-MIR is host cell protein (HCP) amount. These impurity proteins represent a major process related impurity group in cell culture supernatant during the production of biopharmaceuticals. They originate from host cells, *e.g.* mammalian CHO, NS0 or SP2/0 cells as well as bacterial and insect cells, which are used for the production of the desired biopharmaceutical substance. While a minor source is secretion into the cell culture broth, the main origin is due to cell lysis or release during cell disruption and harvesting (Tait *et al.*, 2012). The number of HCPs can exceed hundreds to thousands of proteins (Hoffman, 2000). As HCPs are potentially immunogenic and have antigenic functions (Champion *et al.*, 2005; Dotzel, 1999; Zoon, 1997) they need to be removed to levels of <1-100ppm during downstream processing (Tait *et al.*, 2012; Wang, Hunter, and Mozier, 2009; Champion *et al.*, 2005; Wolter and Richter, 2005; Eaton, 1995).

Various orthogonal methods are used to remove these impurities based on differences in their physicochemical attributes such as isoelectric point, charge at specific pH, hydrophobicity and size (Wang, Hunter, and Mozier, 2009), resulting in final HCP levels below 100ppm (Arunakumari and Wang, 2009). These orthogonal methods are usually established within a set of different methods within the purification chain during downstream processing.

The potential of a chosen set of purification strategies for HCP clearance as well as impacts of upstream parameters on HCP secretion needs to be monitored and elucidated. This is preferably to be done by continuous process surveillance, requiring many HCP analyses or alternative tools for real-time monitoring. As FT-MIR is one technique allowing real-time monitoring due to fast data acquisition and analysis, this part will discuss the use of FT-MIR for HCP impurity monitoring.

HCP- ELISA is the standard method of choice for quantification of host cell proteins and can detect less than 1ng ml^{-1} of proteins (Hoffman, 2000). However, the use of polyclonal antibodies and requirement of several immunization steps in the immunogen- producing animal makes ELISA assays expensive. Special chemicals used within the assay also contribute to additional costs. Although ELISA assays are very sensitive, they require quite some time for sample preparation and assay incubation, additionally adding dilution errors to the sample to be analyzed. 2D- SDS-PAGE combined

with western blotting has slightly lower sensitivity compared to ELISA but is time consuming, as well (Flatman *et al.*, 2007). HPLC can be used, also at- or online to the bioreactor, but it shows lower sensitivity and results are subjective to interpretation (Hoffman, 2000).

HCP quantification using FT-MIR can be done similar to mAb quantification. Elucidating wavenumber ranges which contain spectral information regarding HCP levels, a quantification model can be established. Before, training samples need to be generated. This can be achieved by using *e.g.* activated carbon to remove different amounts of HCP from cell culture fluid, depending on the pH. Alternative techniques can be semi- selective protein precipitation (Capito *et al.*, 2013; Capito *et al.*, 2012) or ion exchange chromatography. The important aspect with all of these methods is, to avoid co-linearity between HCP concentration and the concentration of other analytes within the samples, *e.g.* antibody titer. This training set of samples is then analyzed with the ELISA assay to obtain reference values to be used within the IR quantification software. Afterwards, samples are measured on MIR and analyzed either by PCA or visual inspection of spectra to find bands whose intensity correlates with the reference values, similar to the above described principles for mAb quantification.

Using this approach, several spectral window areas correlating with the HCP concentration can be used for multivariate data analysis and model design. The benefit of using a so-called multiple spectral window approach is that interference by other substances can be minimized. In case a substance interferes with *e.g.* one of these spectral windows, there are several other "windows" left, thus still allowing for good prediction ability. However, one should be aware, that if the interfering substance has structural similarities very close to the impurity proteins, the interference would most likely occur with all "windows".

Performing this multiple spectral window approach, five wavenumber ranges which correlate with ELISA values, can be identified (figure 6). These ranges are 1,557.49-1,546.88; 1,514.092-1,505.412; 1,424.403-1,417.653, 1,410.9-1,395.47 and 1,352.07-1,341.47cm^{-1}. The wavenumber ranges 1,557-1,545cm^{-1} and 1,514-1,505cm^{-1} may be assigned to the Amide II band at 1,575-1,480cm^{-1}, corresponding to CN stretching and NH bending vibrations as well as minor contributions from CO bending and CC stretching (Barth, 2007). Two other ranges (1,424- 1,417cm^{-1} and 1,410-1,394cm^{-1}) may be assigned to C-O-H bending (table V). The wavenumber range 1,352-1,341cm^{-1} may be assigned to a carboxyl group. Using this approach, HCPs can be quantified between 5,000-300,000ng ml^{-1} with CVs similar to ELISA assays (table VI and figure 7) and coeeficients of correlation between 87- 98%., However, the detection limit is slightly lower as the reported 17,000ng ml^{-1} for polysaccharides and 10,000ng ml^{-1} for mAbs (Sellick *et al.*, 2010; Marcotte *et al.*, 2007). Yet, the possible quantification range also encompasses the relevant HCP titer after ion exchange chromatography, when using this technique instead of protein A affinity chromatography as initial purification step (Arunakumari and Wang, 2009). Therefore, FT-MIR can in principle be used to semi-selectively quantify HCPs in upstream processing as well as early downstream processing.

However, after affinity chromatography, HCP levels vary usually between 500-10,000 ng per mg mAb (Eriksson *et al.*, 2009), thus currently impeding the use of FT-MIR based impurity quantification for this part of the purification chain.

Table V: Functional groups assigned to wavenumbers used for the model building in HCP quantification.

Wavenumber range cm^{-1}	Assigned
1,557 - 1,545	Amide II
1,514 - 1,505	Amide II
1,424 - 1,417	C-O-H bending
1,410 - 1,394	C-O-H
1,352 - 1,341	C-O carboxylic acid

Table VI: Capito *et al.* (unpublished results): Prediction accuracy of calibration model for independent test-set samples taken from CHO cell culture fluid.

Sample	HCP titer determined by ELISA (ng ml^{-1})	HCP titer predicted with model (ng ml^{-1})	**precision**: % CV (* ELISA precision < 10% CV)	within limitation of ELISA
1	6,763	10,346	37.46	no
2	7,476	9,188	16.19	yes
3	8,015	9,453	12.69	yes
4	24,470	27,287	8.14	yes
5	26,006	27,370	3.71	yes
6	42,562	51,660	15.12	yes
7	60,503	62,230	2.02	yes
8	73,675	71,209	2.37	yes
9	85,908	84,905	0.83	yes
10	93,443	79,741	10.37	yes
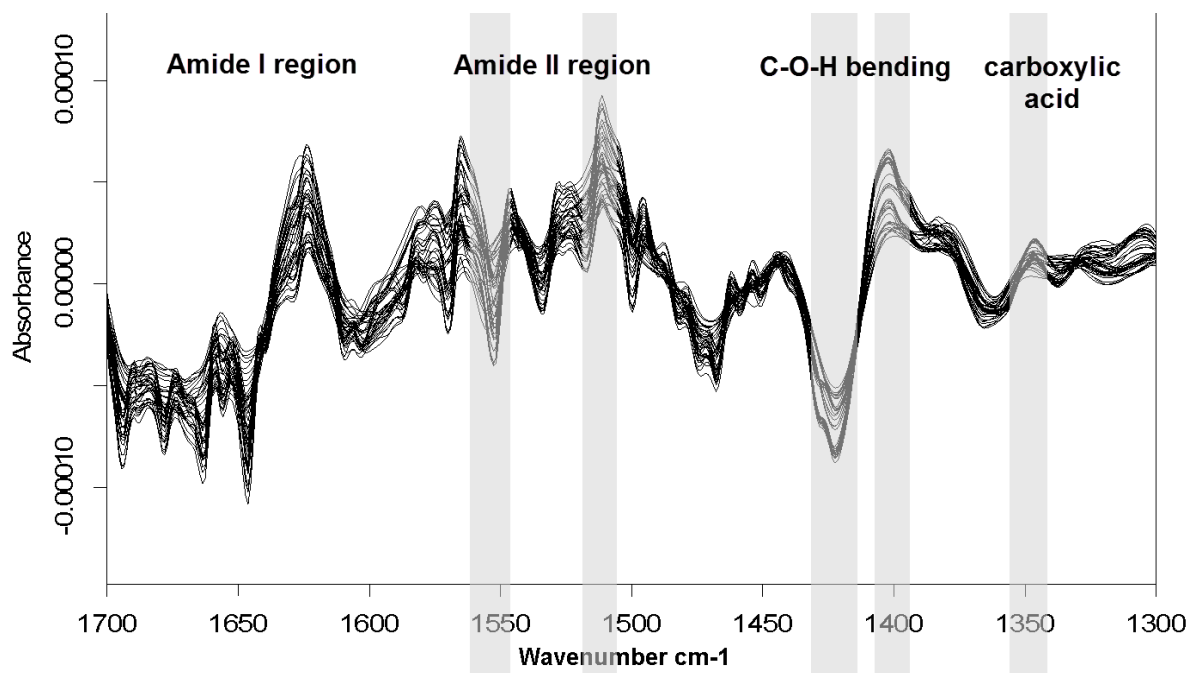
Figure 6: Capito *et al.* (2013): Spectral overview and wavenumber ranges used for HCP quantification, with assigned structural information.
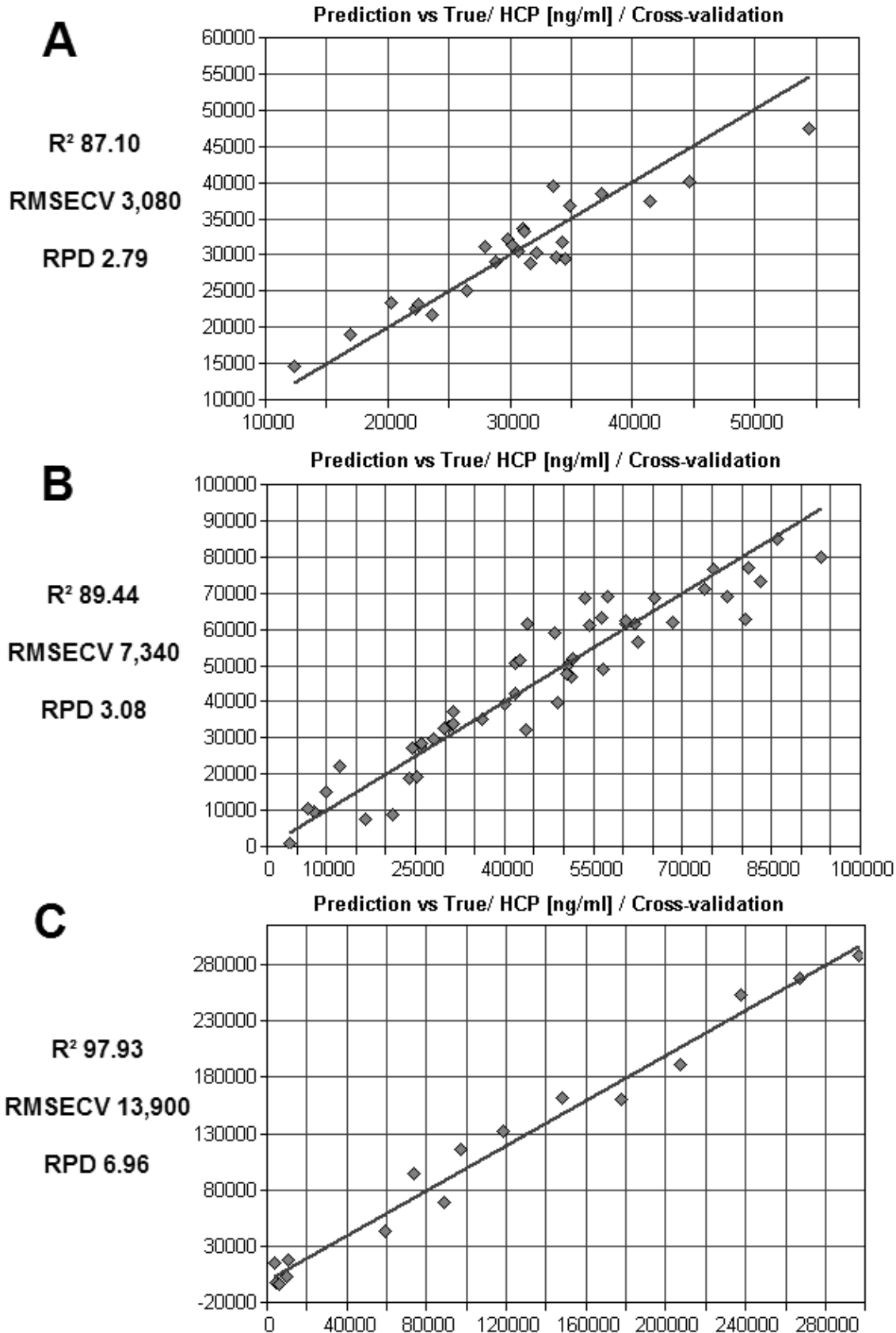
Figure 7: Capito *et al.* (unpublished results and 2012, 2013): Comparison of correlation of HCP titers predicted using ELISA and ATR by application of different PLS models for different cell culture fluids. Models optimized for A: samples taken from CHO cell culture fluid; B: samples taken from NS0 cell culture fluid; C: samples taken from SP2/0 cell culture fluid.

c) Antibody aggregate quantification using FT-MIR

Antibody aggregation can occur at different steps during the mAb production process and needs to be monitored to meet regulatory limits. One source for aggregation is affinity chromatography, requiring low pH-elution which can then result in aggregate formation (Vunnum, Vedantham, and Hubbard, 2009). Other causes are the low- pH- virus inactivation step during downstream processing, shear stress in tangential flow filtration as well as shear stress due to agitation and aeration in suspension cell cultures within the upstream phase (Chu and Robinson, 2001).

mAb aggregation can also be induced by factors influencing protein-protein interaction such as freeze-thawing, pH-shifts, shaking, long-term storage or lyophilization (Wang *et al.*, 2007) as well as mAb formulations of highly concentrated protein which may lead to concentration-induced aggregation of antibodies (Shire, Shahrokh, and Liu, 2004).

Antibody aggregates are a challenging impurity as they closely resemble the product (Arunakumari and Wang, 2009). To date, they are measured using SEC-HPLC and SDS-PAGE as robust routine analysis techniques and also by light scattering as semi-quantitative and qualitative method (Brorson and Phillips, 2005). Other techniques involve analytical ultracentrifugation, field-flow fractionation and electrophoresis (Hawe *et al.*, 2009; Brorson and Phillips, 2005).

However, these techniques, especially HPLC and SDS-PAGE are not suitable for rapid monitoring of process development (Flatman *et al.*, 2007), although they have a higher sensitivity compared to the faster dynamic light scattering. Typical aggregation levels in antibody purification can vary between 0.5%- 25% and reach even up to 40-60% (Vunnum, Vedantham, and Hubbard, 2009; Shukla and Han, 2007; Harinarayan *et al.*, 2006; Ishihara *et al.*, 2005).

These aggregates need to be removed as they can result in anaphylactoid side reactions and renal failure due to increased immunogenicity with lower activity (Wang *et al.*, 2007; Rosenberg, 2006; Demeule, Gurny, and Arvinte, 2005; Hermeling *et al.*, 2004 ; Braun *et al.*, 1997; Ryan, Webster, and Statler, 1996). Thus, a common acceptance criterion for aggregates during early development of mAbs, also used by FDA, is "<5%" (Brorson and Phillips, 2005)

However, this accepted level can be more stringent if expertise on the manufacture of such mAbs is available and therefore should not be used as a general acceptance criterion.

Of potential techniques to be used in aggregate monitoring, MIR is one of the most- promising ones, providing a good balance between measurement speed and sensitivity (Flatman *et al.*, 2007). The approach, using MIR for aggregate analysis is not new. Several research groups have used this technique already for aggregate quantification (Joubert *et al.*, 2007; Ami *et al.,* 2006; Maruyama *et al.*, 2001; Seshadri *et al.,* 1999; Dong *et al.*, 1995) and it has been proposed as a potential replacement technique for protein aggregation and conformation analysis (Flatman *et al.*, 2007).

MIR was used to elucidate changes in antibody formulations upon storage and formulation type, as formulations containing aggregated mAbs are known to exhibit a band shift of beta-sheet associated bands from $1,690 cm^{-1}$ to $1,694 cm^{-1}$ as well as broadening of bands, indicative for the increase of

disordered structures (Skrdla, Harrington, and Lin, 2010; Yoshioka and Aso, 2007; Matheus, Mahler, and Friess, 2006; Andya, Hsu, and Shire, 2003; Gupta *et al.,* 2002; Breen *et al.*, 2001; Surewicz, Mantsch, and Chapman, 1993).

Andya *et al.* compared the secondary structure of native mAb with that of mAb after undergoing lyophilization (Andya, Hsu, and Shire, 2003). Comparing assigned secondary structures within the Amide I region, a band broadening, appearance of a broad band at 1,650cm^{-1} which they saw as indicator of protein unfolding to unordered structures as well as band shifts from 1,690 cm^{-1} to 1,694cm^{-1} were discovered (compare figure 8).

Furthermore, the authors showed evidence for more native-like mAb secondary structures, if adding specific carbohydrates before formulation and storage, thereby showing the suitability of FT-MIR for formulation monitoring

Hawe *et al.* (2009) showed strong bands at wavenumbers 1,635 and 1,690cm^{-1}, using non-aggregated mAb while the aggregated-denatured mAb, subjected to heat-denaturation at 77°C exhibited bands at 1,655cm^{-1} and 1,619cm[-1](compare figure 8), attributed to intermolecular beta-sheets within the mAb aggregates and was consistent to results obtained by complementary techniques.
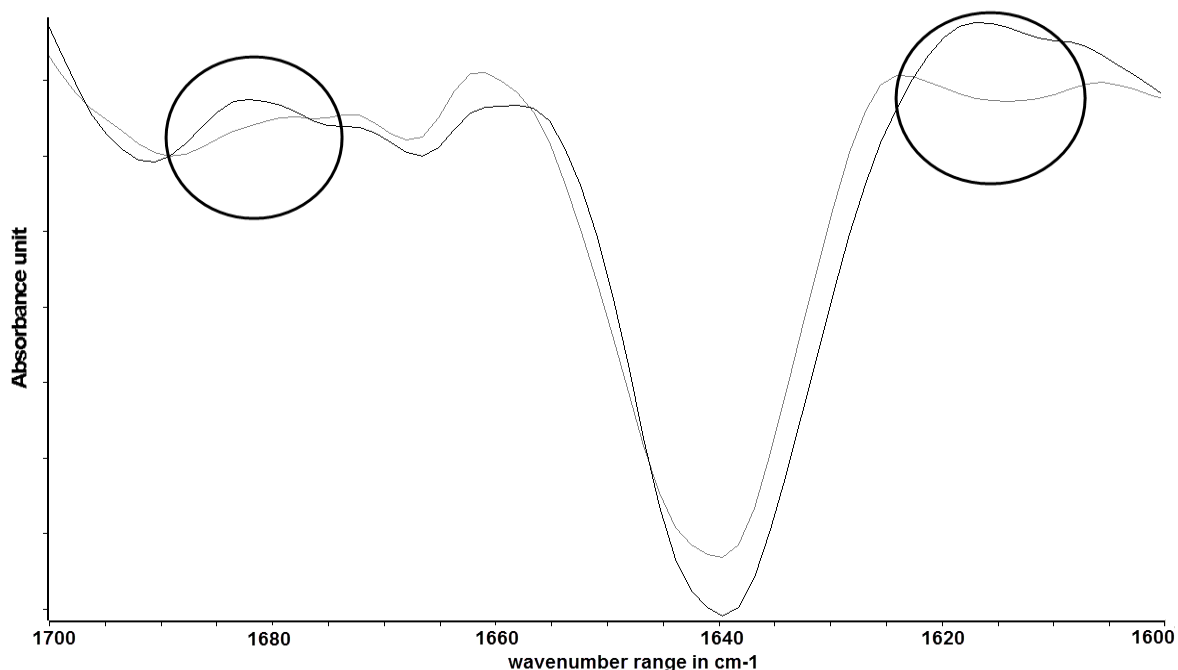
Figure 8: Second derivative of samples containing aggregated mAb (black) and native mAb (grey). Encircled in black: a distinct peak at 1,619cm^{-1} visible with the aggregated mAb as well as a strong band around 1,694cm^{-1}. Results by Capito *et al.* (*unpublished*) similar to Hawe *et al.* (2009) and Andya *et al.* (2003).

As aggregates are mainly occurring in the intermediate and late phases of downstream processing, such as after affinity chromatography, virus inactivation or even after formulation of the purified drug product, they can easily be measured using FT-MIR. Interfering substances such as other impurity

proteins are already removed to >98% after affinity chromatography. This allows for relatively straightforward aggregate quantification using FT-MIR without having to consider significant interference by impurity proteins. As aggregates are detected at slightly different wavenumber ranges compared to protein A quantification, there is also no cross-interference between these two analytes within FT-MIR. Depending on the concentration of aggregated mAb within the overall mAb concentration, different models can be used to optimize prediction accuracy. This approach has been used to quantify aggregated mAb within mAb drug solution to concentrations of less than 5% (w/w), using the wavenumber range 1,660-1,642cm^{-1} and 1,620-1,610cm^{-1} (figure 9 A). Additionally, for a second mAb, a model optimized for quantification of aggregates down to 1% (w/w) could be achieved, using wavenumber ranges 1,665-1,654; 1,580-1,567; 1,502-1,496; 1,360-1,346cm^{-1} (figure 9 B). Therefore, FT-MIR can be a method of choice for aggregate quantification as it requires low workforce, no materials, no buffer and obtains fast data analysis, compared to conventional techniques.
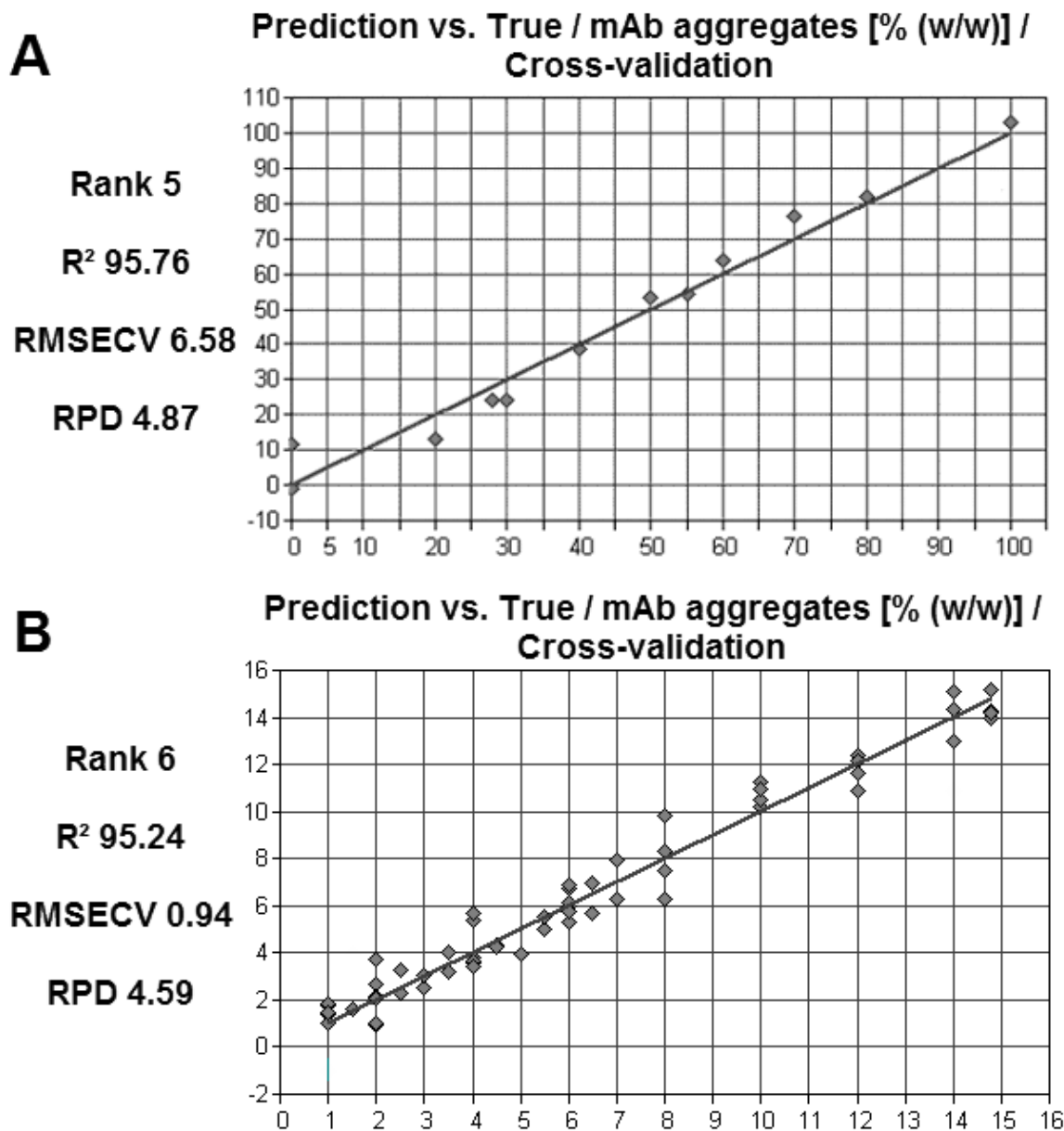
Figure 9: A: Results by Capito *et al.* (unpublished): aggregate quantification in mAb1 mixing aggregated mAb1 with non-aggregated mAb1. Rank of 5. Model covering a wide aggregate titer range with R² of 95.76, RMSECV of 6.58 and RPD of 4.87, showing good prediction of the model based on the entire calibration range. Data pre-processing done removing outliers according to PCA, performing multiplicative scatter correction and using wavenumber range 1,660- 1,642cm^{-1} as well as 1,620-1,610cm^{-1}, covering secondary structure associated wavenumber ranges. B: Model for aggregate quantification in mAb2, optimized for quantification down to 1% (w/w) relative aggregate amount, using first derivative and wavenumber ranges 1,665-1,654; 1,580-1,567; 1,502-1,496; 1,360-1,346cm^{-1}. Rank of 6, R² 95.24 and RMSECV 0.94%.

d) Quantification of leaching protein A in cell culture fluid using FT-MIR

Protein A is a cell-wall anchored protein in *Staphylococcus aureus*. It is exposed on the surface of this pathogenic bacterium and binds antibodies of the IgG- type, due to its affinity to the Fc region of these antibodies. By that, it leads to "wrong binding" of the antibodies, which are then not able to initiate an immune reaction.

In antibody purification, protein A is used within downstream processing in affinity chromatography due to its selective binding towards the mAb's Fc region. The protein itself has a molecular weight of about 54kDa and consists of five domains, all of which are composed of an anti-parallel three-helix bundle motif and tow inter-helical loops, but no beta-sheets (Vunnum, Vedantham, and Hubbard, 2009).

Protein A can leach into cell culture when using affinity chromatography involving this protein. Leaching arises due to proteolytic cleavage between domains by proteases present in cell culture fluid, resulting in segments between 6- 40kDa being present in the purified eluate (Vunnum, Vedantham, and Hubbard, 2009). Residual protein A levels after affinity chromatography are approximately between 2-40ppm (Horenstein *et al.*, 2003; Godfrey *et al.*, 1992) and thus meet FDA regulations (Vunnum, Vedantham, and Hubbard, 2009).

Although these levels are low, protein A can lead to immunogenic reactions in a patient, therefore removal needs to be monitored. To-date, leached protein A is detected using immunoassays, such as ELISA with limits of detection less than 1ng per mg mAb. Although these assays have the potential for at-line analysis, using appropriate automation procedures, alternative non-invasive techniques would be beneficial (Flatman *et al.,* 2007; Dertzbaugh *et al.,* 1985).

Yet, not with that low limit of detection, protein A can therefore, in principle, be differentiated from antibody, using FT-MIR, due to structural differences and thus differences in the absorbance spectra.

This is done similar to the above described mAb quantification procedure. Amide I regions associated to alpha-helix and beta-sheet secondary structures are used which allow differentiation of the proteins. The advantage for protein A quantification is, that it does not contain beta-sheet structures as mentioned before, but is mainly composed of alpha-helix secondary structures (figure 10).

Therefore, FT-MIR can in principle be used for monitoring leaching protein A levels after applying protein A chromatography (Vunnum, Vedantham, and Hubbard, 2009).

This has been shown in a feasibility experiment, spiking aqueous protein A into aqueous mAb solution, allowing protein A quantification down to 0.01mg ml^{-1} with low prediction errors down to either 0.05mg ml^{-1}and even 0.01mg ml^{-1} (figure 11 A and B).

Unfortunately the quantified Prot A levels are much higher as usually observed after Prot A affinity step thus not enabling direct FT-MIR application. Even though, sample enrichment to concentrate protein A within the sample can be a way to enable its use. These techniques include using centrifugal filters, allowing to enrich protein A levels and thus visualize residual protein A levels in purified product after affinity chromatography. By these approaches, FT-MIR can be an alternative to conventional ProtA Elisa although more investigations are necessary.
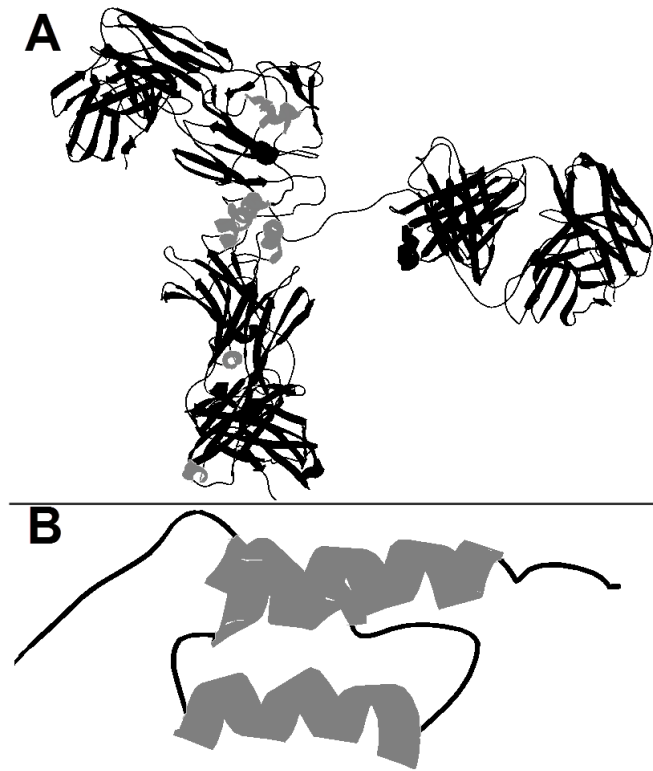
Figure 10: A mAb (Pdb accession code 1igt) secondary structure with low amount of alpha-helices (in grey) and high beta-sheet content (in black). B: secondary structure of B domain of *staphylococcus aureus* protein A (Uniprot ID **P38507)** only showing alpha-helices (in grey) and absence of beta-sheet.
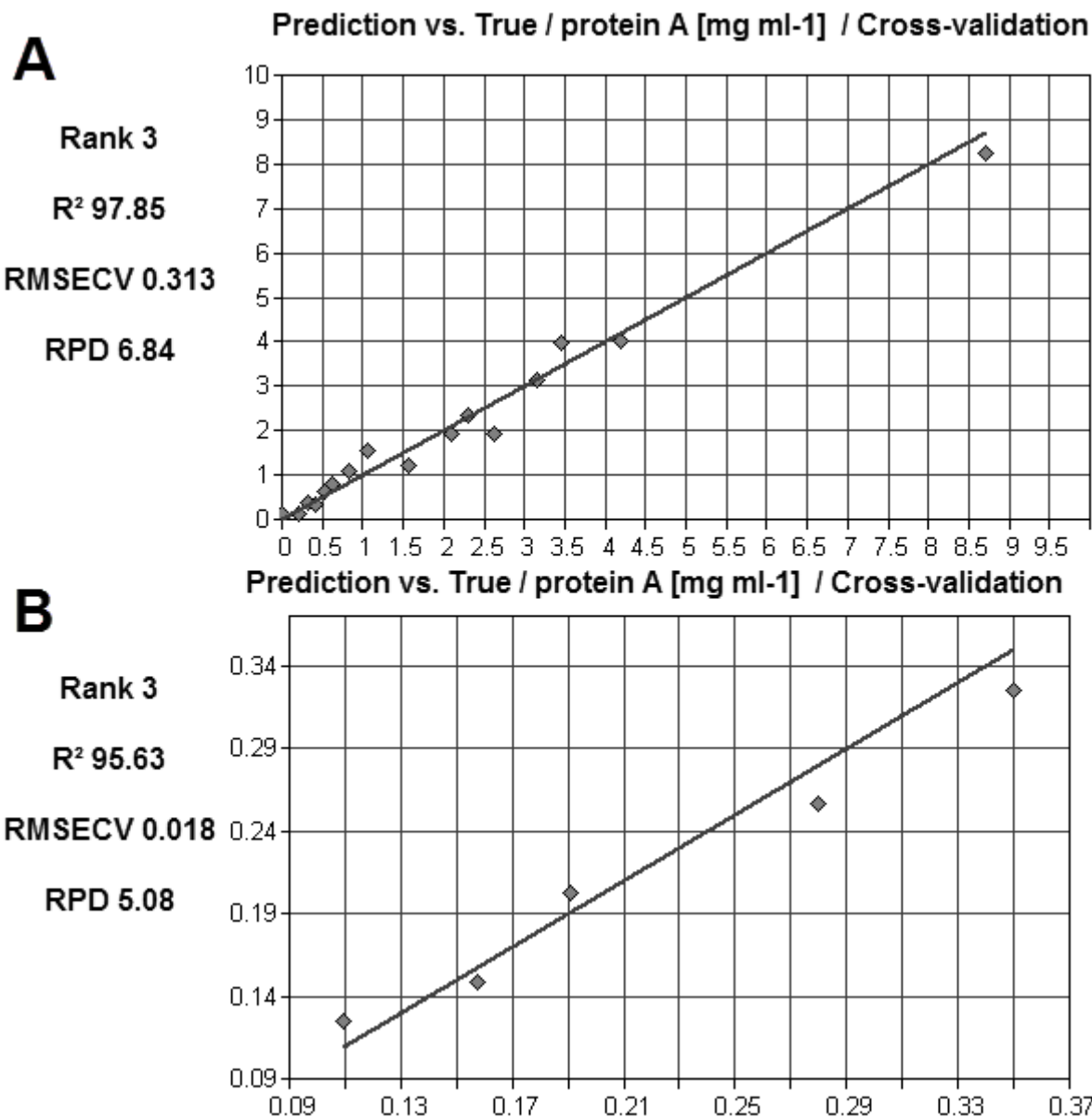
Figure 11: A: Results by Capito *et al.* (unpublished): protein A quantification in mAb2 solution after spiking protein A to mAb. Rank 3. Protein A levels between 0.01mg ml^{-1} to 9.0mg ml^{-1} were spiked to mAb solution with C_{mAb} = 0.33 mg ml^{-1}. First derivative of spectra used encompassing Amide region between 1,600-1,700cm^{-1}. R² 97.85, RMSECV 0.313mg ml^{-1} and RPD 6.84, indicating model to be reliable. Low prediction error only possible down to 0.05 mg ml^{-1} protein A in cell culture fluid. B: model optimized for predicting protein A in range of 0.1-0.4mg ml^{-1}, using portions of wavenumber range 1,700-1,600cm^{-1}. Rank 3. Quantification possible to 0.01mg ml^{-1} protein A.

3. Other possible applications

Quantification of endotoxins, lipids and polysaccharides by FT-MIR

Another parameter to be controlled and its presence in the drug product to be minimized are endotoxins which are lipolysaccharides or pyrogens. Endotoxins are composed of three, chemically different, parts:one part is so-called lipid A, being exposed to the cell interior, the other part is so-called core-oligosaccharide and the third part is the O-antigen, being the surface antigen, composed of a heteropolysaccharide (Petsch and Anspach, 2000) (see figure 12). The O-antigen thereby differs between different bacterial strains while the core-polysaccharide is more conserved and lipid A being very conserved among different strains (Petsch and Anspach, 2000). Both, core-structure and lipid A are additionally phosphorylated.
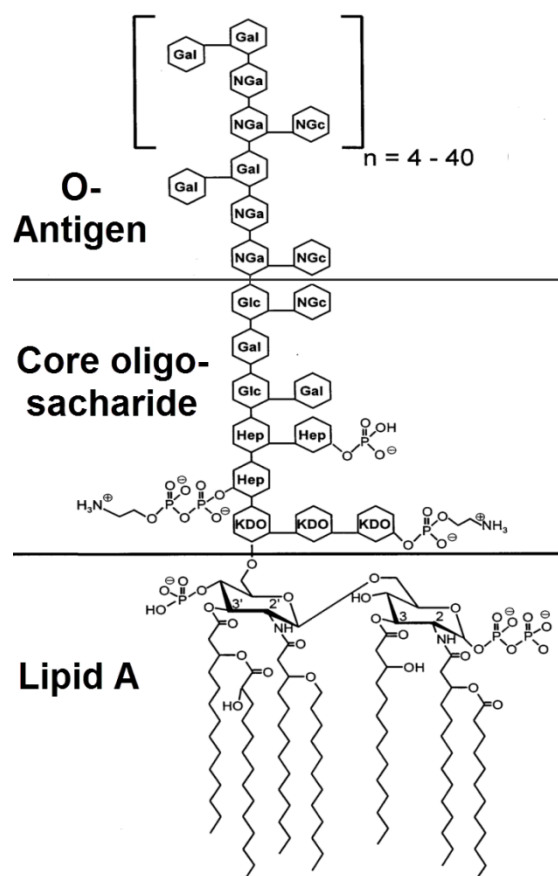
Figure 12: Schematic view of the chemical structure of endotoxin from *E. coli* O111:B4.
Reprinted from *Journal of biotechnology*, *76*(2), Petsch, D., & Anspach, F. B., Endotoxin removal from protein solutions, p.99, © 2000, with permission from Elsevier.

They originate from the outer cell membrane of gram negative bacteria, forming about 75% of their surface, are responsible for stability but also interaction with other bacteria and can lead to harmful effects in humans (Varaa and Nikaido, 1984).

Such effects may be fever, modified hemodynamics, shock, organ and cell changes. Thus, their presence in drug products is limited (European Pharmacopea, 3rd Edition, 1997; Rietschel et al., 1994; Martich, Boujoukos, and Suffredini, 1993).

Currently, endotoxin levels in *E. coli* cell culture supernatant can vary between 10ng ml^{-1} to 100,000ng ml^{-1} (Horenstein et al., 2003; Petsch and Anspach, 2000). Removal is usually accomplished using ion-exchangers, phase-extraction systems, as well as tailor-made selective endotoxin adsorbers, however, all with different efficacy and applications (Petsch and Anspach, 2000). In some cases, the level of endotoxin can be high as shown by Rantze (1996), who measured more than 2300ng ml^{-1} endotoxin after applying ion exchange chromatography during purification of basic fibroblast growth factor from high density *E. coli* cultivation.

The state-of-art way of endotoxin level monitoring is use of either the *Limulus* amoebocyte lysate assay, the galactosamine-primed mice lethality assays or the chicken embryo lethality assay with the first showing a sensitivity of 0.02 endotoxin units ml^{-1}, similar to a detection limit of 2pg ml^{-1} (Galanos and Freudenberg, 1993; Galanos et al., 1971). However, these assays may suffer from interference by many substances and they can fail in samples with complex matrix, e.g. blood and biological fluids with certain proteins (Petsch and Anspach, 2000), thus requiring alternative techniques.

In principle, FT-MIR can be applied to detect endotoxin levels as well, however, at higher concentrations, *e.g.* within the bioreactor, shortly after harvesting or within the early phases of downstream processing. As endotoxins are composed of polysaccharides and lipid, they can, in principle, be quantified by specific absorbance bands of these compounds within IR spectroscopy. These absorbance bands have already been used within FT-MIR, *e.g.* to classify micro-organisms according to their lipopolysaccharides (Kim, Reuhs, and Mauer, 2005), and study the interaction of lipopolysaccharides with different surfaces (Parikh and Chorover, 2008; Reiter et al., 2002). Synthetic lipid A and glycolipids were analyzed by FT-MIR (Brandenburg and Seidel, 1998; Brandenburg, Kusumoto, and Seydel, 1997) as well as endotoxins and their interaction with lipoproteins (Brandenburg et al., 2002; Petsch and Anspach, 2000).

Following the line of lipid quantification, the C-O groups of lipid esters can be identified between 1,700-1,750cm^{-1} and lipid acyl chains at 2,800-3,000cm^{-1} (table VII) (Chapman et al., 1967). As lipids differ vastly in their structure and biochemical composition, they can also be differentiated due to unique IR absorbance signature. Polysaccharides can also be quantified, thereby allowing possible detection of endotoxins. This has been shown by Marcotte et al. (2007) who used FT-MIR to quantify different polysaccharides present on bacterial biofilm, using the wavenumber range of 970-1,182cm^{-1} (Marcotte et al., 2007). The limit of detection was 17,000ng ml^{-1} for different dried polysaccharide samples, including xanthan, alginate and mannan. Using a similar wavenumber range between 1,180-1,133cm^{-1}, Pistorius et al. (2008) used C-O and C-O-C stretching vibrations to quantify carbohydrates (Pistorius, DeGrip, and Egorova-Zachernyuk, 2009; Tewari and Irudayaraj, 2004; Hineno, 1977).

Therefore, all through no direct endotoxin quantification during downstream processing has been described, these impurities may be monitored using FT-MIR, combining the knowledge and applications described above.

Table VII: wavenumber ranges to be used for lipid quantification in MIR.

Vibration	wavenumber range in cm^{-1}
CH$_3$ asymmetric stretch	2,956
CH$_2$ asymmetric stretch	2,920
CH$_3$ symmetric stretch	2,870
CH$_2$ symmetric stretch	2,850
C=O stretch	1,740
CH$_2$ scissoring	1,463-1,468; 1,472-1,473
CH$_3$ asymmetric bend	1,460
CH$_3$ symmetric bend	1,378
PO$_2$- asymmetric stretch	1,228
PO$_2$- symmetric stretch	1,085
CH$_2$ rocking	720-730

Quantification of nucleic acids by FT-MIR

Nucleic acids are one of the impurities which also require monitoring. They can arise from cell disrupture within the bioreactor and levels may vary depending on cell type and density, harvesting time and conditions (Flatman *et al.*, 2007). Regulations state, that the amount of cellular DNA should not exceed 100pg per dose of a therapeutic protein (Flatman *et al.*, 2007), employing methods which can detect DNA down to 10pg. Typically, DNA levels after using ion exchange chromatography as initial purification step, are less than 3pg DNA per mg of antibody.

To date, residual nucleic acid amounts are determined using quantitative polymerase chain reaction (QPCR) as method of choice, allowing detection of 0.1 pg DNA per mg mAb within reasonable amount of time (Gijsbers *et al.*, 2005). As this technique does not allow for at-line measurements, lab-on-the chip methods, *e.g* Agilent's Bioanalyzer allow for even faster data acquisition and thus faster process development. These techniques are also able to perform at- and on-line analysis of nucleic acids based on microfluidic systems and can detect DNA down to the nanogram scale (Flatman *et al.*, 2007).

As for FT-MIR, it can, in principle, also be used to detect and quantify nucleic acids, although not with that high sensitivity: FT-MIR has been used to study single-stranded, double-stranded and triple-stranded nucleic acid structures, at higher concentrations in the double-digit milligram scale, or at least, using a total amount of nucleic acids of more than 0.2mg per sample (Banyay, Sarkar, and

Gräslund, 2003; Lindqvist and Gräslund, 2001; Geinguenaud *et al.*, 2000; Lindqvist *et al.*, 2000; Gousset *et al.*, 1998; Mohammadi *et al.,* 1998; Dagneaux, Liquier, and Taillandier, 1995a; Dagneaux, Liquier, and Taillandier, 1995b; White and Powell, 1995; Ouali *et al.,* 1993; Akhebat *et al.*, 1992; Liquier *et al.*, 1991; Urpi *et al.,* 1989; Miles, 1964).

Dovbeshko *et al.* (2000) have shown the ability of FT-MIR to detect changes within the primary, secondary and tertiary structure of nucleic acids, linked to base and sugar modifications as well as alterations of the hydrogen-bonding pattern. The wavenumber ranges between 1,350-1,000cm^{-1} were used to elucidate phosphate vibrations, 1,800-1,550cm^{-1} to see changes in the base structure and 3,800-2,300cm^{-1} to elucidate OH-NH-CH stretching vibrations. Having assigned specific wavenumber ranges to the four different bases, sugar and phosphate backbone, relative concentration differences of the four bases between different samples were detected.

Additionally, nucleic acids can also be quantified via the wavenumber range 1,700-1,400cm^{-1} and 1,120-940cm^{-1} however only at high concentrations of about 1mg ml^{-1} (Amara *et al.*, 2012). In contrast, DNA levels after protein A affinity chromatography vary usually between 0.01- 1ng per mg mAb (Eriksson *et al.*, 2009), thus not allowing FT-MIR-based monitoring. While semi-selective enrichment of DNA within samples might pave the way for using IR also for nucleic acid impurity quantification within process monitoring, the enrichment factor would be very high, also introducing errors. Thus, although FT-MIR can be used for nucleic acid quantification and analysis, to date it cannot be used successfully within the scope of bioprocess monitoring of residual nucleic acid contamination.

Detection of glycosylation patterns by FT-MIR

At the position of Asn297, a well conserved amino acid in IgG- type mAbs, an oligosaccharide chain is usually attached via N-linkage (Janeway *et al.,* 2001). The composition of this oligosaccharide and thus glycosylation can vary, depending on the chosen cell line for mAb production, the bioreactor itself as well as the chosen downstream purification scheme (Harris, Shire, and Winter, 2004; Roque, Lowe, and Taipa, 2004; Wright and Morrison, 1997).

Correct glycosylation as well as composition of glycosylation is important for mAb efficacy and can also influence mAb conformation (Shinkawa *et al.*, 2003; Wright and Morrison, 1997; Tao and Morrison, 1989).

Besides above described applications of using FT-MIR for monitoring of various critical process parameters, it can, in principle, also be used to analyze glycosylation, mainly differentiating highly glycosylated protein from non-glycosylated protein. This has been shown by Natalello et *al.* (2005) that used the so-called fingerprint region for carbohydrate detection between 1,200-900cm^{-1}.

The authors employed a normalization step based on the intensities within the Amide I region before comparing the carbohydrate-associated spectral range between 1200-900cm^{-1}. Comparing the band intensities between glyosylated samples as well as samples being treated by glycosidase PNGase F,

the latter samples exhibited a strongly reduced band intensity compared to the glycosylated protein (figure 13).

These results were confirmed by orthogonal techniques such as SDS-PAGE, MALDI-MS and GC-MS and the authors also concluded, that differences within the glycosylation pattern might be visible within the IR spectrum (Natalello *et al.,* 2005). Although they used a protein concentration of their investigated lipase of 10-20 mg ml^{-1}, this can also be performed at lower concentrations. Khajehpour et *al.* (2006) confirmed their results, showing the suitability of FT-MIR to detect protein glycosylation, using mucin, soybean peroxidase, collagen IV, cytochrome c and avidin at concentrations of 5mg ml^{-1} (figure 14). Additionally they were able to distinguish different sugars if no blends were used and identified a band at 1,050cm^{-1}, within the carbohydrate fingerprint region, which allowed comparing the relative glycosylation of proteins after normalization to the Amide I region. Thus they were able to detect protein glycosylation even lower than 10%.

Consequently, both groups show the principal suitability of FT-MIR for detecting the presence as well as relative concentration of glycosylation among different proteins. While Khajehpour *et al.* (2006) additionally were able to elucidate the approximate composition of glycosylation in their investigated proteins, this can only be regarded as a helpful indication for further analysis, however is difficult to perform for complex glycosylation patterns. Yet, general monitoring of protein glycosylation using FT-MIR is a useful application, allowing differentiation between glycosylated and non-glycosylated protein. Thus, it can also be used within process monitoring, e.g. for verification of successful treatment after incubation with a glycosidase.

decrease of band intensity
after treatment with
glycosidase
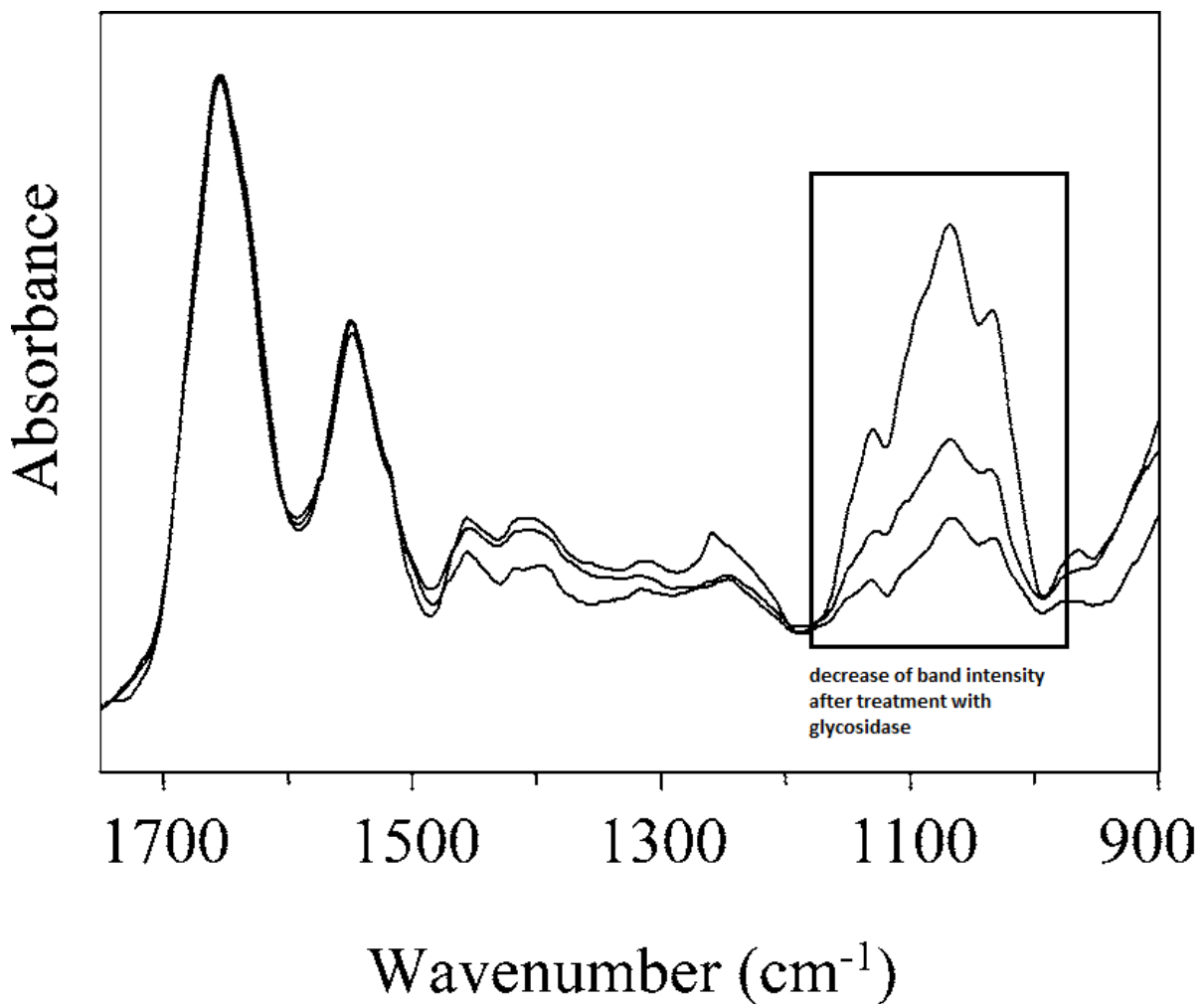
Figure 13: Carbohydrate region (1,200-900cm^{-1}) shows differences in band intensity after treatment of samples with glycosidase. Reproduced and adapted with permission, from Natalello A., Ami D., Brocca S., Lotti M., Doglia S.M., 2005, Biochemical Society, 385, 511-517. © the Biochemical Society.
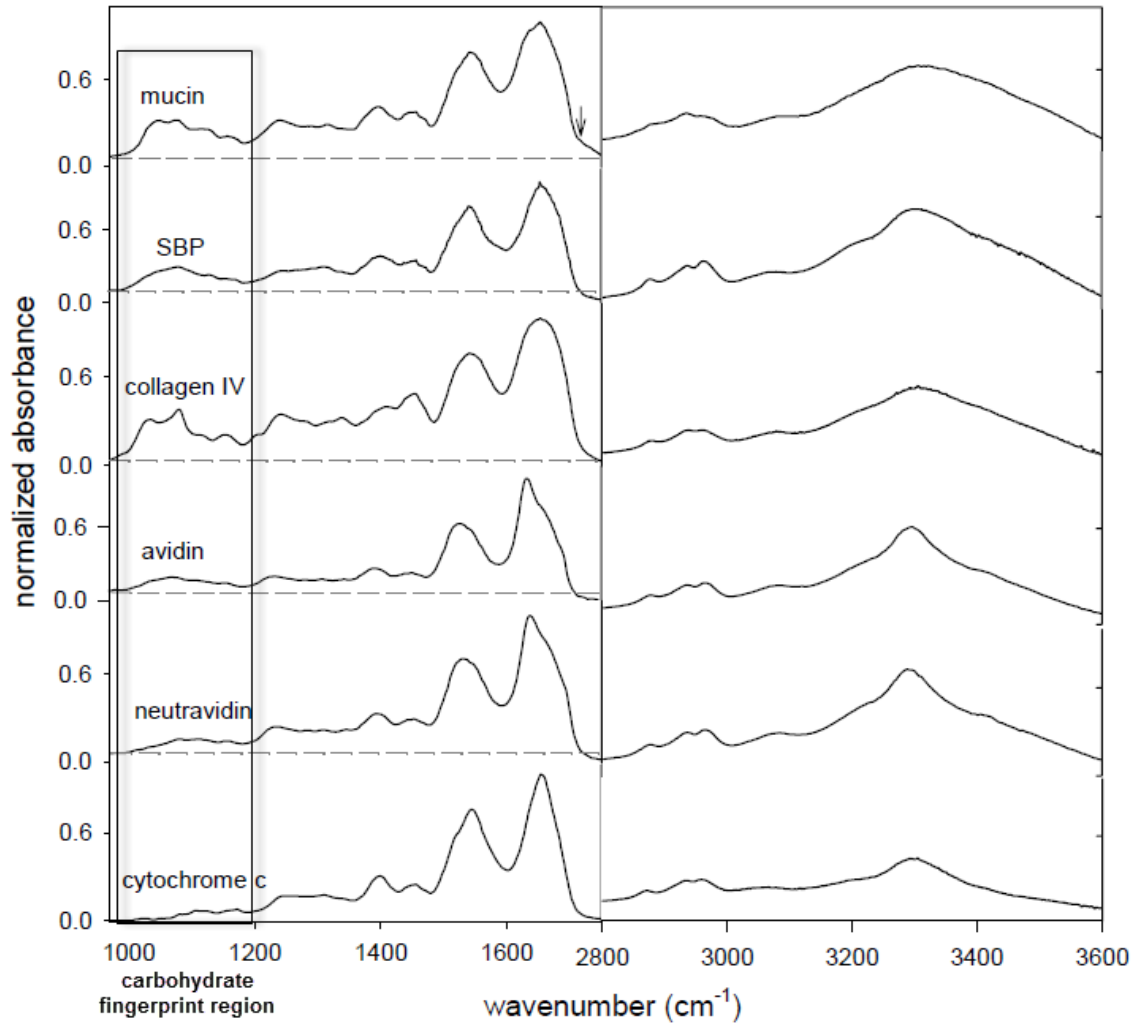
Figure 14: Comparison of spectra of proteins with different degrees of glycosylation as measured on a ZnS plate in dried state. SBP: soybean peroxidase. Reprinted from *Analytical Biochemistry*, *348*, Khajehpour, Mazdak, Jennifer L. Dashnau, and Jane M. Vanderkooi, Infrared spectroscopy used to evaluate glycosylation of proteins, p.46, © 2006, with permission from Elsevier.

CONCLUSION

This chapter shows the potential of mid infrared spectroscopy to be used for critical process parameter estimation during various phases in downstream processing, allowing the quantification of target protein titer, impurity protein levels, aggregation amount. While these parameters are directly applicable and were shown in case studies, additional parameters might be measured, however requiring further development and sample preparation.

The principal suitability of FT-MIR to differentiate protein A from mAb, and thus allowing potential leaching protein A quantification, was shown as well as examples of how to analyze effects of process steps on *e.g.* mAb secondary structure.

Other parameters which can, in principle, be monitored by FT-MIR include the presence of glycosylation and differentiation of glycosylated as well as non-glycosylated protein; detection of endotoxin and nucleic acid, both however at high concentrations only.

Although FT-MIR exhibits a lower sensitivity, when compared to conventional tools such as ELISA and western blotting, the use of infrared spectroscopy within process development, especially within the early downstream processing phases, serves as a fast and cost-effective monitoring technique without extensive sample preparation. FT-MIR can simplify screening in the initial and intermediate steps of downstream processing, involving capture, recovery, product isolation and partly, purification. So far, FT-MIR is not fully suitable for HCP quantification of samples after using affinity chromatography in the late purification phase and the polishing phase of downstream processing due to higher LOD and LOQ, compared to other techniques. However, the use of selective sample enrichment techniques, e.g. centrifugal filters, can help to further extend its applicability, even for monitoring leaching protein A levels.

Compared to HPLC for target protein titer monitoring, it is faster, does not require costly equipment and no solvent consumption, otherwise leading to higher waste load. Although SEC and DLS are well-accepted techniques for aggregate quantification, the use of FT-MIR can hereby replace these techniques, allowing aggregate quantification below the FDA's limit of 5% with the ability to quantify less than 1%.

The unique advantage of FT-MIR is its ability to determine multiple critical process parameters within a single simple measurement. Thereby, instead of using several instruments, these critical process parameters can be determined by just one FT-MIR instrument, reducing maintenance and investment costs. Although higher LOD and LOQ are the drawbacks of current IR instruments, their applicability might be increased by concentrating samples before measurement. Development of disposable equipment with connecting devices to allow for simple IR analysis as well as quality by design developments, can help to enhance the usage of FT-MIR within process development and process monitoring. Additionally, development of new IR instrumentation with higher sensitivity can help to obtain even lower quantification limits in the future, enabling the wide-spread acceptance of FT-MIR within these disciplines.

REFERENCES

Akhebat, A., Dagneaux, C., Liquier, J., Taillandier, E., (1992). Triple-helical polynucleotidic structures: an FTIR study of the Cq*GC triplet, *J. Biomol. Struct. Dyn.* 10, 577–588.

Amara, R., Chernokalskaya, E., Clark, P., Joshi, V., Rider, T.S., Utzat, C. EP 2511692 A2 (02.04.2012) Devices and methods for infrared (IR) quantitation of biomolecules.

Ami, D., Natalello, A., Taylor, G., Tonon, G., Doglia, S.M., (2006). Structural analysis of protein inclusion bodies by Fourier transform infrared microspectroscopy. *BBA* 1764, 793-799.

Andya, J., Hsu, C., Shire, S., (2003). Mechanisms of aggregate formation and carbohydrate excipient stabilization of lyophilized humanized monoclonal antibody formulations. AAPS J. 5, 21-31.

Antibody Purification Handbook, Amersham Biosciences, Amersham, UK.

Arunakumari, A., Wang, J. (2009). Purification of human monoclonal antibodies: non-protein A strategies, in *Process Scale purification of antibodies* (ed. U. Gottschalk), John Wiley & Sons, Inc., Hoboken, New Jersey.

Banyay, M., Sarkar, M., Gräslund, A., (2003). A library of IR bands of nucleic acids in solution. *Biophys. Chem.* 104, 477-488.

Barth, A., Zscherp, C., (2002). What vibrations tell us about proteins. *Q. Rev. Biophys.* 35, 369-430.

Barth A., (2007). Infrared spectroscopy of proteins. *BBA.* 1767, 1073-1101.

Berthomieu, C., Hienerwadel, R., (2009). Fourier transform infrared (FTIR) spectroscopy. *Photosynth. Res.* 101, 157-170.

Birch, J.R., Racher, A.J., (2006). Antibody production. *Adv. Drug Deliv. Rev.* 58, 671-685.

Brandenburg, K., Kusumoto, S., Seydel, U., (1997). Conformational studies of synthetic lipid A analogues and partial structures by infrared spectroscopy. *BBA* 1329, 183-201.

Brandenburg, K., Seydel, U., (1998). Infrared spectroscopy of glycolipids. *Chem. Phys. Lipids* 96, 23-40.

Brandenburg, K., Jürgens, G., Andrä, J., Lindner, B., Koch, M.H.J., Blume, A., Garidel, P., (2002). Biophysical characterization of the interaction of high-density lipoprotein (HDL) with endotoxins. *Eur. J. Biochem.* 269, 5972-5981.

Braun, A., Kwee, L., Labow, M.A., Alsenz, J., (1997). Protein aggregates seem to play a key role among the parameters influencing the antigenicity of interferon alpha (IFN-alpha) in normal and transgenic mice. *Pharm. Res.* 14, 1472–1478.

Breen, E.D., Curley, J.G., Overcashier, D.E., Hsu, C.C., Shire, S.J., (2001). Effect of Moisture on the Stability of a Lyophilized Humanized Monoclonal Antibody Formulation. *Pharm. Res.* 18, 1345-1353.

Brorson, K., Phillips, J., (2005). Defining Your Product Profile and Maintaining Control Over It, Part 4 Product-Related Impurities: Tackling Aggregates; Technical Bioprocess; *BioProcess Int.* 3, 50-54.

Byler, D.M., Susi, H., (1986). Examination of the secondary structure of proteins by deconvolved FTIR spectra. *Biopolymers* 25, 469–487.

Cai, S., Singh, B.R., (2004). A distinct utility of the amide III infrared band for secondary structure estimation of aqueous protein solutions using partial least squares methods. *Biochemistry* 43, 2541-2549.

Capito, F., Skudas, R., Stanislawski, B., & Kolmar, H., (2012). Matrix effects during monitoring of antibody and host cell proteins using attenuated total reflection spectroscopy. *Biotechnol. Prog.* DOI: 10.1002/btpr.1643.

Capito, F., Skudas, R., Kolmar, H., Stanislawski, B., (2013). Host cell protein quantification by fourier transform mid infrared spectroscopy (FT-MIR). B*iotechnol. Bioeng.* 110, 252-259.

Cen, H., and He, Y., (2007). Theory and application of near infrared reflectance spectroscopy in determination of food quality. *Trends. Food. Sci Tech.* 18, 72-83.

Champion, K., Madden, H., Dougherty, J., Shacter, E., (2005). Defining your product profile and maintaining control over it, part 2. *Bioprocess Int.* 5, 52–57.

Chapman, D., Williams, R.M., Ladbrooke, B.D., (1967). Physical studies of phospholipids. VI Thermotropic and lyotropic mesomorphism of some 1,2-diacyl-phosphatidylcholines (lecithins). *Chem. Phys. Lipids* 1, 445–475.

Chen, B., Bautista, R., Yu, K., Zapata, G.A., Chamow, S.M., (2003). Influence of histidine on the stability and physical properties of a fully human antibody in aqueous and solid forms. *Pharm. Res.* 20, 1952-1960.

Christiansen, C.P., Ploss, H.J., Merten, R., Prinz, H. US7755051B2 (14.06.2007) Method and device for the quantitative analysis of solutions and dispersions by means of near infrared spectroscopy.

Chu, L., Robinson, D.K., (2001). Industrial choices for protein production by large-scale cell culture. *Curr. Opin. Biotechnol.* 12, 180-187.

Cole, C., Barber, J.D. Barton, G.J., (2008). The Jpred 3 secondary structure prediction server. *Nucleic Acids Res.* 36, 197-201.

Dagneaux, C., Liquier, J., Taillandier, E., (1995a). FTIR study of a non-classical dA=dA$_{10}$ydT$_{10}$ intramolecular triple helix. *Biochemistry* 34, 14815-14818.

Dagneaux, C., Liquier, J., Taillandier, E., (1995b). Sugar conformations in DNA and RNA–DNA triple helices determined by FTIR spectroscopy: role of backbone composition. *Biochemistry* 34, 16618–16623.

Demeule, B., Gurny, R., Arvinte, T., (2005). Where disease pathogenesis meets protein formulation: Renal deposition of immunoglobulin aggregates. *Eur. J. Pharm. Biopharm.* 62, 121-130.

DeOliveira, D.B., Trumble, W.R., Sarkar, H.K., Singh, B.R., (1994). Secondary structure estimation of proteins using the amide III region of Fourier transform infrared spectroscopy: application to analyze calcium-binding-induced structural changes in calsequestrin. *Appl. Spectrosc.* 48, 1432-1441.

Dertzbaugh, M.T., Flickinger, M.C., Lebherz, I.W.B., (1985). An enzyme immunoassay for the detection of staphylococcal protein A in affinity-purified products. *J. Immunol. Methods* 83, 169-177.

Doak, D.L., Phillips, J.A., (1999) In Situ Monitoring of an Escherichia coli Fermentation Using a Diamond Composition ATR Probe and Mid-infrared Spectroscopy. *Biotechnol. Prog.* 15, 529-539.

Dong, A.C., Huang, P., Caughey, W.S., (1990). Protein secondary structures in water from second-derivative amide I infrared spectra. *Biochemistry* 29, 3303-3308.

Dong, A., Prestrelski, S.J., Allison, S.D., Carpenter, J.F., (1995). Infrared spectroscopic studies of lyophilization- and temperature-induced protein aggregation. *J. Pharm. Sci.* 84, 415-424.

Dong, A., Randolph, T.W., Carpenter, J.F., (2000). Entrapping intermediates of thermal aggregation in α-helical proteins with low concentration of guanidine hydrochloride. *J. Biol. Chem.* 275, 27689-27693.

Dong, A., Malecki, J.M., Lee, L., Carpenter, J.F., Lee, J.C., (2002). Ligand-Induced Conformational and Structural Dynamics Changes in Escherichia coli Cyclic AMP Receptor Protein. *Biochemistry* 41, 6660-6667.

Dotzel, M.M., (1999). International conference on harmonisation of technical requirements for registration of pharmaceuticals for human use, ''Guidance on Specifications: Test Procedures and Acceptance Criteria for Biotechnological/Biological Products'' (Geneva, Switzerland). Fed Regist 64, 44928–44935.

Dovbeshko, G. I., Gridina, N. Y., Kruglova, E. B., Pashchuk, O. P., (2000). FTIR spectroscopy studies of nucleic acid damage. *Talanta* 53, 233-246.

Eaton, L.C., (1995). Host-cell contaminant protein assay development for recombinant biopharmaceuticals. *J. Chromatogr. A* 705, 105–114.

Eriksson, K., Ljunglöf, A., Rodrigo, G., Eggert, B., (2009). MAb Contaminant Removal with a Multimodal Anion Exchanger; A Platform Step to Follow Protein A. *BioProcess Int.* 7, 52-56.

Esbensen, K.H., (2002). in *Multivariate data analysis-in practice: An introduction to multivariate data analysis and experimental design* (eds. Guyot, D., Westad, F., Houmøller, L.P.) CAMO Software, Oslo.

Etzion, Y., Linker, R., Cogan, U., Shmulevich, I., (2004). Determination of Protein Concentration in Raw Milk by Mid-Infrared Fourier Transform Infrared/Attenuated Total Reflectance Spectroscopy. *J. Dairy Sci.* 87 2779-2788.

European Pharmacopea, 3rd Edition, (1997). Council of Europe, Strasburg. Biological Tests. 2.6.8 Pyrogens; 2.6.14 Bacterial Endotoxins.

Fahrenfort, J., (1961). Attenuated total reflection: A new principle for the production of useful infra-red reflection spectra of organic compounds. *Spectrochim. Acta* 17, 698-709.

Farid, S.S., Washbrook, J., Titchener-Hooker, N.J., (2005). Decision-support tool for assessing bio-manufacturing strategies under uncertainty: stainless steel versus disposable equipment for clinical trial material preparation. *Biotechnol. Prog.* 21, 486-497.

Fernanda Pimentel, M., Ribeiro, G.M., da Cruz, R.S., Stragevitch, L., Pacheco Filho, J.G.A.,

Teixeira, L.S., (2006). Determination of biodiesel content when blended with mineral diesel fuel using infrared spectroscopy and multivariate calibration. *Microchem. J.* 82, 201-206.

Flatman, S., Alam, I., Gerard, J., Mussa, N., (2007). Process analytics for purification of monoclonal antibodies. *J. Chromatogr. B* 848, 79-87.

Fontes, N., van Reis, R., (2009). Advances in technology and process development for industrial-scale monoclonal antibody purification, in *Process Scale purification of antibodies* (ed. U. Gottschalk), John Wiley & Sons, Inc., Hoboken, New Jersey.

Furtado, P.B., Whitty, P.W., Robertson, A., Eaton, J.T., Almogren, A., Kerr, M.A., Woof, J.M., Perkins, S.J., (2004). Solution structure determination of monomeric human IgA2 by X-ray and neutron scattering, analytical ultracentrifugation and constrained modelling: A comparison with monomeric human IgA1. *J. Mol. Biol.* 338, 921-941.

Galanos, C., Rietschel, T.E., Lüeritz, O., Westphal, O., (1971). Interaction of pipopolysaccharide and lipid A with complement. *Eur. J. Biochem.* 19, 143.

Galanos, C., Freudenberg, M.A., (1993). Mechanisms of endotoxin shock and endotoxin hypersensitivity. *Immunobiology* 187, 346–356.

Garn, M., Gisin, M., Thommen, C., Cevey, P., (1989). A flow injection analysis system for fermentation monitoring and control. *Biotechnol. Bioeng.* 34, 423-428.

Geinguenaud, F., Liquier, J., Brevnov, M. G., Petrauskene, O. V., Alexeev, Y. I., Gromova, E. S., Taillandier, E., (2000). Parallel selfassociated structures formed by T-, C-rich sequences at acidic pH. *Biochemistry* 39, 12650-12658.

Ghosh R., (2006). Principles of Bioseparations Engineering (ed. R. Gosh), World Scientific Pub Co, Singapore.

Gijsbers, L., Kolb, B., Weggeman, M., Goudsmit, J., Havenga, M., Marzio, G., (2005). Quantification of Residual Host Cell DNA in Adenoviral Vectors Produced on PER. C6® Cells. *Hum. Gene Ther.* 16, 393-398.

Godfrey, M.A., Kwasowski, P., Clift, R., Marks, V., (1992). A sensitive enzyme-linked immunosorbent assay (ELISA) for the detection of staphylococcal protein A (SpA) present as a trace contaminant of murine immunoglobulins purified on immobilized protein A. *J. Immunol. Methods* 149, 21– 27.

Goormaghtigh, E., Raussens, V., Ruysschaert, J.M., (1999). Attenuated total reflection infrared spectroscopy of proteins and lipids in biological membranes. *BBA* 1422, 105-185.

Goormaghtigh, E., Ruysschaert, J.M., Raussens, V., (2006). Evaluation of the Information Content in Infrared Spectra for Protein Secondary Structure Determination. *Biophys. J.* 90, 2946-2957.

Gorry, P., (1990). General least-squares smoothing and differentiation by the convolution (Savitzky–Golay) method. *Anal. Chem.* 62, 570–573.

Gousset, H., Liquier, J., Taillandier, E., Sanghvi, Y.S., Peoch, D., (1998). Conformational study of DNA-RNA duplexes containing MMI substituted phosphodiester linkages by FTIR spectroscopy, *J. Biomol. Struct. Dyn.* 15, 931-936.

Griffiths, P.R. and de Haseth, J.A. (2007). Fourier Transform Infrared Spectrometry (eds. Griffiths, P.R. and de Haseth, J.A.), Wiley-Interscience, Hoboken, New Jersey.

Gross-Selbeck, S., Margreiter, G., Obinger, C., Bayer, K., (2007). Fast Quantification of Recombinant Protein Inclusion Bodies within Intact Cells by FT-IR Spectroscopy. *Biotechnol. Prog.* 23, 762-766.

Gupta, M.K., Tseng, Y.C., Goldman, D., Bogner, R.H., (2002). Hydrogen Bonding with Adsorbent During Storage Governs Drug Dissolution from Solid-Dispersion Granules. *Pharm. Res.* 19, 1663-1672.

Harinarayan, C., Mueller, J., Ljunglof, A., Fahrner, R., Van Alstine, J., Van Reis, R., (2006). An exclusion mechanism in ion exchange chromatography. *Biotechnol. Bioeng.* 95, 775- 787.

Harrick, N.J., (1960). Surface chemistry from spectral analysis of totally internally reflected radiation. *J. Phys. Chem.* 64, 1110-1114.

Harris, R.J., Shire, S.J., Winter, C., (2004). Commercial manufacturing scale formulation and analytical characterization of therapeutic recombinant antibodies. *Drug. Dev. Res.* 61, 137-154.

Harthun, S., Matischak, K., Friedl, P., (1997). Determination of Recombinant Protein in Animal Cell Culture Supernatant by Near-Infrared Spectroscopy. *Anal. Biochem.* 251, 73-78.

Hawe, A., Kasper, J.C., Friess, W., Jiskoot, W., (2009). Structural properties of monoclonal antibody aggregates induced by freeze-thawing and thermal stress. *Eur. J. Pharm. Sci.* 38, 79-87.

Hermeling, S., Crommelin, D.J.A., Schellekens, H., Jiskoot, W., (2004). Structure-immunogenicity relationships of therapeutic proteins. *Pharm. Res.* 21, 897–903.

Hineno, M., (1977). Ir-spectra and normal vibrations of beta-D-glucopyranose. *Carbohydr. Res.* 56, 219–227.

Hoffman, K., (2000). Strategies for Host Cell Protein Analysis. *Biopharm* 13, 38-45.

Horenstein, A.L., Crivellin, F., Funaro, A., Said, M., Malavasi, F., (2003). Design and scaleup of downstream processing of monoclonal antibodies for cancer therapy: from research to clinical proof of principle. *J. Immunol. Methods* 275, 99-112.

Iley, C.B., McClure, J.T., Shaw, R.A. US20100012844A1 (17.07.2008) Identification of immunoglobulin (Ig) disorders using fourier transform infrared spectroscopy.

Ishihara, T., Kadoya, T., Yoshida, H., Tamada, T., Yamamoto, S., (2005). Rational method for predicting human monoclonal antibody retention in protein A chromatography and cation exchange chromatography: Structural- based chromatography design for monoclonal antibodies. *J. Chromatogr. A* 1093, 126-138.

Jackson, M., Mantsch, H.H., (1995). The use and misuse of FTIR spectroscopy in the determination of protein structure. *Crit. Rev. Biochem. Mol. Biol.* 30, 95–120.

Janeway, C.A., Travers, P.A., Walport, M., Shlomchik, M.J., (2001), in *Immunobiology* (eds. Janeway, C.A., Travers, P.A., Walport, M., Shlomchik, M.J.), Garland Publishing, New York.

Joubert, M.K., Luo, Q., Nashed-Samuel, Y., Wypych, J., Narhi, L.O., (2011). Classification and Characterization of Therapeutic Antibody Aggregates. *Biol Chem.* 286, 25118-25133.

Kalnin, N.N., Baikalov, I.A., Venyaminov, S.Y., (1990). Quantitative IR spectrophotometry of peptide compounds in water (H_2O) solution. III. Estimation of the protein secondary structure. *Biopolymers* 30, 1273-1280.

Kamarck, M.E., (2006). Building biomanufacturing capacity – The chapter and verse. *Nat. Biotechnol.* 24, 503-505.

Khajehpour, M., Dashnau, J.L., Vanderkooi, J.M. (2006). Infrared spectroscopy used to evaluate glycosylation of proteins. *Anal. Biochem.* 348, 40–48.

Kim, S., Reuhs, B.L., Mauer, L.J., (2005). Use of Fourier transform infrared spectra of crude bacterial lipopolysaccharides and chemometrics for differentiation of Salmonella enterica serotypes. *J. Appl. Microbiol.* 99, 411-417.

Kirdar, A., Conner, J., Baclaski, J., Rathore, A., (2007). Application of multi-variate analysis toward biotech processes: case study of a cell-culture unit operation. *Biotechnol. Progr.* 23, 61-67.

Kong, J., Yu, S., (2007). Fourier Transform Infrared Spectroscopic Analysis of Protein Secondary Structures. *ABBS* 39, 549-559.

Krimm, S., Bandekar, J., (1986). Vibrational Spectroscopy and Conformation of Peptides, Polypeptides, and Proteins, in *Advances in Protein Chemistry* (eds .B. Anfinsen, J.T. Edsall and F.M. Richards), Academic, San Diego, CA.

Landgrebe, D., Haake, C., Höpfner, T., Beutel, S., Hitzmann, B., Scheper, T., Rhiel, M., Reardon, K., (2010). On-line infrared spectroscopy for bioprocess monitoring. *Appl. Microbiol. Biotechnol.* 88, 11-22.

Li, S.Q., Bomser, J.A., Zhang, Q.H., (2005). Effects of pulsed electric fields and heat treatment on stability and secondary structure of bovine immunoglobulin G. *J. Agric. Food. Chem.* 53, 663-670.

Lindqvist, M., Sarkar, M., Winqvist, A., Rozners, E., Strömberg, R., Gräslund, A., (2000). Optical spectroscopic study of the effects of a single deoxyribose substitution in a ribose backbone: implications in RNA–RNA interaction. *Biochemistry* 39, 1693–1701.

Lindqvist, M., Gräslund, A., (2001). An FTIR and CD study of the structural effects of G-tract length and sequence context on DNA conformation in solution, *J. Mol. Biol.* 314, 423–432.

Liquier, J., Coffinier, P., Firon, M., Taillandier, E., (1991). Triplehelical polynucleotidic structures: sugar conformations determined by FTIR spectroscopy. *J. Biomol. Struct. Dyn.* 9, 437–445.

Lopes, J.A., Costa, P.F., Alves, T.P., Menezes, J.C., (2004). Chemometrics in bioprocess engineering: process analytical technology (PAT) applications. *Chemom. Intell. Lab. Syst.* 74, 269-275.

Marcotte, L., Kegelaer, G.g., Sandt, C., Barbeau, J., Lafleur, M., (2007). An alternative infrared spectroscopy assay for the quantification of polysaccharides in bacterial samples. *Anal. Biochem.* 361, 7-14.

Martens, H., Martens, M., (2000). in *Multivariate Analysis of Quality- An Introduction* (eds. Martens, H., Martens, M.), Wiley, Chichester 2000.

Martich, G.D., Boujoukos, A.J., Suffredini, A.F., (1993). Response of man to endotoxin. *Immunobiology* 187, 403–416.

Maruyama, T., Katoh, S., Nakajima, M., Nabetani, H., Abbott, T.P., Shono, A., Satoh, K., (2001). FT-IR analysis of BSA fouled on ultrafiltration and microfiltration membranes. *J. Membr. Sci.* 192, 201-207.

Matheus, S., Mahler, H.C., Friess, W., (2006). A critical evaluation of Tm (FTIR) measurements of high-concentration IgG1 antibody formulations as a formulation development tool. *Pharm. Res.* 23, 1617-1627.

Mazarevica, G., Diewok, J., Baena, J.R., Rosenberg, E., Lendl, B., (2004). On-Line Fermentation Monitoring by Mid-infrared Spectroscopy. *Appl. Spectrosc.* 58, 804-810.

McGovern, A.C., Ernill, R., Kara, B.V., Kell, D.B., Goodacre, R., (1999) Rapid analysis of the expression of heterologous proteins in Escherichia coli using pyrolysis mass spectrometry and Fourier transform infrared spectroscopy with chemometrics: application to a-interferon production. *J. Biotechnol.* 72, 157-168.

Miles, H.T. (1964). The structure of the three-stranded helix, poly (Aq2U), *PNAS* 51,1104–1109.

Mohammadi, S., Klement, R., Shchyolkina, A. K., Liquier, J., Jovin, T. M., Taillandier, E., (1998). FTIR and UV spectroscopy of parallel-stranded DNAs with mixed AT/GC sequences and their AT/IC analogues. *Biochemistry* 37, 16529-16537.

Moros, J., Iñón, F.A., Garrigues, S., de la Guardia, M., (2005). Determination of the energetic value of fruit and milk-based beverages through partial-least-squares attenuated total reflectance-Fourier transform infrared spectrometry. *Anal. Chim. Acta* 538, 181-193.

Naes, T., Isaksson, T., Fearn, T., Davies, T., (2002). in *A user-friendly guide to Multivariate Calibration and Classification. NIR Publications* (eds Naes, T., Isaksson, T., Fearn, T., Davies, T.), Chichester, UK.

Natalello, A., Ami, D., Brocca, S., Lotti, M., Doglia, S.M., (2005). Secondary structure, conformational stability and glycosylation of a recombinant Candida rugosa lipase studied by Fourier-transform infrared spectroscopy. *Biochem. J.* 385, 511-517.

Naughton, R.A., Rohrer, T.R., Gentz, R. US6395538B1 (14.07.2000) Method and device for providing real-time, in situ biomanufacturing process monitoring and control in response to IR spectroscopy.

Oberg, K.A., Fink, A.L., (1998). A New Attenuated Total Reflectance Fourier Transform Infrared Spectroscopy Method for the Study of Proteins in Solution. *Anal. Biochem.* 256, 92-106.

Ouali, M., Letellier, R., Sun, J. S., Akhebat, A., Adnet, F., Liquier, J., Taillandier, E., (1993). Determination of G* G. cntdot. C triple-helix structure by molecular modeling and vibrational spectroscopy. *J. Am. Chem. Soc.* 115, 4264-4270.

Parikh, S.J., Chorover, J., (2008). ATR-FTIR study of lipopolysaccharides at mineral surfaces. Colloids and Surfaces B: *Biointerfaces* 62, 188-198.

Petsch, D., Anspach, F.B., (2000) Endotoxin removal from protein solutions. *J. Biotechnol.* 76, 97-119.

Pillonel, L., Luginbühl, W., Picque, D., Schaller, E., Tabacchi, R., Bosset, J., (2003). Analytical methods for the determination of the geographic origin of Emmental cheese: mid-and near-infrared spectroscopy. *Eur. Food Res.* 216, 174-178.

Pistorius, A., DeGrip, W.J., Egorova-Zachernyuk, T.A., (2009). Monitoring of biomass composition from microbiological sources by means of FT-IR spectroscopy. *Biotechnol. Bioeng.* 103, 123-129.

Preisner, O., Guiomar, R., Machado, J., Menezes, J.C., Lopes, J.A., (2010) Application of Fourier Transform Infrared Spectroscopy and Chemometrics for Differentiation of Salmonella enterica Serovar Enteritidis Phage Types. *Appl. Environ. Microbiol.* 76, 3538-3544.

Pujar, N., Low, D., O'Leary, R., (2009). Antibody purification: drivers of change, in Gottschalk, Process Scale purification of antibodies, in *Process Scale purification of antibodies* (ed. U. Gottschalk), John Wiley & Sons, Inc., Hoboken, New Jersey.

Rantze, E., (1996). Neue Pyrogen-spezifische Liganden auf der Basis von immobilisierten Polymeren, Diploma thesis, Technical University of Hannover, Germany.

Reiter, G., Siam, M., Falkenhagen, D., Gollneritsch, W., Baurecht, D., Fringeli, U.P., (2002). Interaction of a Bacterial Endotoxin with Different Surfaces Investigated by in Situ Fourier Transform Infrared Attenuated Total Reflection Spectroscopy. *Langmuir* 18, 5761-5771.

Rhiel, M., Cohen, M.B., Murhammer, D.W., Arnold, M.A., (2002). Nondestructive near-infrared spectroscopic measurement of multiple analytes in undiluted samples of serum-based cell culture media. *Biotechnol. Bioeng.* 77, 73-82.

Rietschel, E.T., Kirikae, T., Schade, F.U., Mamat, U., Schmidt, G., Lippnow, H., Ulmer, A.J., Zähringer, U., Seydel, U., di Padova, F., Schreier, M., Brade, H., (1994). Bacterial endotoxin: molecular relationship of structure to function. *FASEB J.* 8, 217–225.

Riley, M.R., Crider, H.M., Nite, M.E., Garcia, R.A., Woo, J., Wegge, R.M., (2001). Simultaneous measurement of 19 components in serum-containing animal cell culture media by Fourier transform near-infrared spectroscopy. *Biotechnol. Progr.* 17, 376-378.

Rodrigues, L.O., Cardoso, J.P., Menezes, J.C., (2008). Applying Near-Infrared Spectroscopy in Downstream Processing: One Calibration for Multiple Clarification Processes of Fermentation Media. *Biotechnol. Prog.* 24, 432-435.

Roque, A.C.A., Lowe, C.R., Taipa, M.A., (2004). Antibodies and genetically engineered related molecules: Production and purification. *Biotechnol. Prog.* 20, 639-654.

Rosenberg, A.S., (2006). Effects of protein aggregates: an immunologic perspective. *AAPS J.* 8, 501–507.

Ryan, M.E., Webster, M.L., Statler, J.D., (1996). Adverse effects of intravenous immunoglobuin therapy. *Clin. Pediatr.* 35, 23–31.

Sellick, C.A., Hansen, R., Jarvis, R.M., Maqsood, A.R., Stephens, G.M., Dickson, A.J., Goodacre, R., (2010). Rapid monitoring of recombinant antibody production by mammalian cell cultures using fourier transform infrared spectroscopy and chemometrics. *Biotechnol. Bioeng.* 106, 432-442.

Seshadri, S., Khurana, R., Fink, A.L., Ronald, W., (1999). Fourier transform infrared spectroscopy in analysis of protein deposits, in *Methods in Enzymology* (ed. W.F. Marshall), Academic Press, Waltham, MA.

Shinkawa, T., Nakamura, K., Yamane, N., Shoji-Hosaka, E., Kanda, Y., Sakurada, M., Uchida, K., Anazawa, H., Satoh, M., Yamasaki, M., Hanai, N., Shitara, K., (2003). The absence of fucose but not the presence of galactose or bisecting N-acetylglucosamine of human IgG1 complex-type oligosaccharides shows the critical role of enhancing antibody-dependent cellular cytotoxicity. *J. Biol. Chem.* 278, 3466-3473.

Shire, S.J, Shahrokh, Z., Liu, J., (2004). Challenges in the development of high protein concentration formulations. *J. Pharm. Sci.* 93, 1390-1402.

Shukla, A.A, Han, X.S., (2007). Screening of chromatographic stationary phases, in *Process Scale Bioseparations for the Biopharmaceutical industry* (eds. Shukla, A.A., Etzel, M.R., Gadam, S.), CRC Press, Boca Raton, Florida.

Sjöström, M., Wold, S., Lindberg, W., Persson, J.A.k., Martens, H.A., (1983). multivariate calibration problem in analytical chemistry solved by partial least-squares models in latent variables. *Anal. Chim. Acta* 150, 61-70.

Skrdla, P.J., Harrington, C., Lin, Z., (2010). Use of real-time FT-IR monitoring of a pharmaceutical compound under stress atmospheric conditions to characterize its solid-state degradation kinetics. *Int. J. Chem. Kinet.* 42, 25-36.

Sommerfeld, S., Strube J., (2005). Challenges in biotechnology production--generic processes and process optimization for monoclonal antibodies. *Chem. Eng. Process.* 44, 1123-1137.

Surewicz, W.K., Mantsch, H.H., Chapman, D., (1993). Determination of protein secondary structure by Fourier-transform infrared-spectroscopy—A critical-assessment. *Biochemistry* 32, 389–394.

Susi, H., Byler, D.M., (1983). Protein structure by fourier transform infrared spectroscopy: Second derivative spectra. *Biochem. Biophys. Res. Comm.* 115, 391-397.

Susi, H., Byler, D.M., (1986). Resolution-enhanced fourier transform infrared spectroscopy of enzymes. *Methods. Enzymol.* 130, 290−311.

Tait, A.S., Hogwood, C.E.M., Smales, C.M., Bracewell, D.G., (2012). Host Cell Protein Dynamics in the Supernatant of a mAb Producing CHO Cell Line. *Biotechnol. Bioeng.* 109, 971-982.

Tao, M.H., Morrison, S.L., (1989). Studies of aglycosylated chimeric mouse-human IgG. Role of carbohydrate in the structure and effector functions mediated by the human IgG constant region. *J. Immunol.* 143, 2595–2601.

Tewari, J., Irudayaraj, J., (2004). Quantification of saccharides in multiple floral honeys using Fourier transform infrared microattenuated total reflectance spectroscopy. *J. Agric. Food. Chem.* 52, 3237–3243.

Timmins, É.M., Quain, D.E., Goodacre, R., (1998). Differentiation of brewing yeast strains by pyrolysis mass spectrometry and Fourier transform infrared spectroscopy. *Yeast* 14, 885-893.

Urpi, L., Ridoux, J.P., Liquier, J., Verdaguer, N., Fita, I., Subirana, J.A., (1989). Conformations in crystals and solutions of d(CACGTG), d(CCGCGG) and d(GGCGCC) studied by vibrational spectroscopy. *Nucleic Acids. Res.* 17, 6669-6680.

U.S. Food and Drug Administration, (2004). Guidance for Industry, PAT—A Framework for Innovative Pharmaceutical Development, Manufacturing, and Quality Assurance. Rockville, MD: Office of Training and Communication, Division of Drug Information, HFD-240. Center for Drug Evaluation and Research, Food and Drug Administration.

Vaara, M., Nikaido, H., (1984). Outer membrane organization, in *Handbook of Endotoxin* (ed. E.T. Rietschel), Elsevier, Amsterdam.

Venyaminov, S.Y., Kalnin, N.N., (1990). Quantitative IR spectrophotometry of peptide compounds in water (H_2O) solution. II. Amide absorption bands of polypeptide and fibrous protein in α-, β- and random coil conformations. *Biopolymers* 30, 1259-1271.

Vojinović V., Cabral, J.M.S., Fonseca, L.P., (2006). Real-time bioprocess monitoring: Part I: In situ sensors. Sensors and Actuators B: *Chemical* 114, 1083-1091.

Vunnum, S., Vedantham, G., Hubbard, B., (2009). Protein A-based affinity chromatography, in *Process Scale purification of antibodies* (ed. U. Gottschalk), John Wiley & Sons, Inc., Hoboken, New Jersey

Wang, W., Singh, S., Zeng, D.L., King, K., Nema, S., (2007). Antibody structure, instability, and formulation. *J. Pharm. Sci.* 96, 1-26.

Wang, X., Hunter, A.K., Mozier, N.M., (2009). Host cell proteins in biologics development: Identification, quantitation and risk assessment. *Biotechnol. Bioeng.* 103, 446-458.

Warnes, M.R., Glassey, J., Montague, G.A., Kara, B., (1996). On data-based modelling techniques for fermentation processes. *Process. Biochem.* 31, 147-155.

Welfle, K., Misselwitz, R., Hausdorf, G., Hohne, W., Welfle, H., (1999). Conformation, pH-induced conformational changes, and thermal unfolding of anti-p24 (HIV-1) monoclonal antibody CB4-1 and its Fab and Fc fragments. *BBA* 1431, 120-131.

Werner, R.G., (2004). Economic aspects of commercial manufacture of biopharmaceuticals. *J. Biotechnol.* 113, 171-182.

Werner, R.G., (2005). The development and production of biopharmaceuticals: Technological and economic success factors. *BioProcess International* 3 (9), S6-15.

White, A.P., Powell, J.W., (1995). Observation of the hydrationdependent conformation of the (dG)20*(dG)20(dC)20 oligonucleotide triplex using FTIR spectroscopy. *Biochemistry* 34, 1137-1142.

Winder, C.L., Carr, E., Goodacre, R., Seviour, R., (2004). The rapid identification of Acinetobacter species using Fourier transform infrared spectroscopy. *J. Appl. Microbiol.* 96, 328-339.

Wold, S., Sjöström, M., Eriksson, L., (2001). PLS-regression: a basic tool of chemometrics. *Chemom. Intell. Lab. Syst.* 58, 109-130.

Wolter, T., Richter, A., (2005). Assay for controlling host-cell impurities in biopharmaceuticals. *Bioprocess Int.* 3, 40–46.

Wright, A., Morrison, S.L., (1997). Effect of glycosylation on antibody function: Implications for genetic engineering. *Trends. Biotechnol.* 15, 26–32.

Yoshioka, S., Aso, Y., (2007). Correlations between molecular mobility and chemical stability during storage of amorphous pharmaceuticals. *J. Pharm. Sci.* 96, 960-981.

Zoon, K.C., (1997). Points to consider in the manufacture and testing of monoclonal antibody products for human. Rockville: Center for Biologics Evaluation and Research, FDA.

3. Experimental part

3.1. Synthesis and characterization of copolymers

Paper: Synthesis and characterization of 2-acrylamido-2-methylpropane sulfonic acid - benzylacrylamide /acrylamidobenzoic-acid copolymers for semi-selective protein purification

Florian Capito, Johann Bauer, Almut Rapp, Harald Kolmar and Bernd Stanislawski

Short summary:

This part describes synthesis and composition analysis of copolymers to be used for selective protein precipitation.

These copolymers are composed of 2-acrylamido-2-methylpropane sulfonic acid and either acrylamidobenzoic-acid or benzylacrylamide. Use of chain transfer agent allowed control of copolymer chain length while different ratios of monomers were employed to obtain copolymers with different composition. Additionally, an ATR-based method is described which allowed fast and relatively accurate copolymer composition analysis, similar to ^{1}H-NMR-based analysis but with the potential of being more cost- and work-effective. Obtained copolymers were used for trial experiments within protein precipitation to confirm their suitability for the later intended use as precipitants. Compared to homopolymers, these copolymers showed increased precipitation yields and higher salt tolerance, thus being likewise superior to homopolymer-driven protein purification.

Synthesis and characterization of 2-acrylamido-2-methylpropane sulfonic acid - benzylacrylamide /acrylamidobenzoic-acid copolymers for semi-selective protein purification

Florian Capito*[1][2], Johann Bauer*[2], Almut Rapp*[2], Harald Kolmar[1] and Bernd Stanislawski[2]
*These authors contributed equally to this project and should be considered co-first authors

[1] Clemens-Schöpf Institute, Technische Universität Darmstadt, Germany

[2] Merck KGaA, Frankfurter Strasse 250, 64293 Darmstadt, Germany

Abstract

2-acrylamido-2-methylpropane sulfonic acid (AMPS) as strongly charged polyelectrolyte has recently gained interest in protein precipitation, due to its permanently dissociated sulfonic acid group. However, polymers with conjoint hydrophobic and electrostatic properties showed increased precipitation yield and higher salt tolerance, being likewise superior in protein precipitation. This contribution describes characterization of copolymers, consisting of either acrylamidobenzoic-acid (ABZ) and AMPS or benzylacrylamide (BzAAm) and AMPS, synthesized by radical polymerization. These copolymers may be used for protein purification, modulating their selectivity towards different target proteins by changing weight average molecular weight (Mw) or composition of the copolymer, thereby obtaining copolymers with difference in hydrophobicity, chain length and charge density. Synthesized copolymers were analyzed using attenuated total reflection infrared spectroscopy (ATR-IR) and ^{1}H-NMR regarding their composition as well as gel permeation chromatography to elucidate Mw distribution. Subsequent results show comparable applicability of ^{1}H-NMR and ATR-IR for analyzing these copolymers. A wide variety of customized copolymers for different target proteins in precipitation was obtained; AMPS composition (w/w) in both copolymer types varied between 20- 95 %, with Mw ranging from 9,000- 140,000 g mol^{-1}. These copolymers showed increased precipitation yields and higher salt tolerance, thus being likewise superior to homopolymer-driven protein purification.

Introduction

Nowadays, polymers find widespread use in biotechnological and biomedical applications. Examples are biodegradable polymers [1], polymers for water treatment purposes [2] and for pharmaceutical applications as drug delivery [3-7]. In recent years, in addition to long known usage of *e.g.* poly-(ethylene glycol) as precipitant [8], electrically conductive homopolymers, so-called polyelectrolytes have gained increasing interest to be used for protein purification purposes [9-10]. Copolymers, consisting of more than one type of monomer subunit are expected to have the intrinsic benefit of modulating defined copolymer properties, *e.g.* hydrophobicity, charge density and flexibility [11-13]. This is particularly important since a conjoint effect of hydrophobic interactions together with electrostatic attraction has been shown to be beneficial for protein precipitation [12-13]. 2-acrylamido-2-methylpropane sulfonic acid (AMPS) as polymer has recently gained interest because of its fully deprotonated sulphonate group, which is dissociated over nearly the entire pH- range [14]. Thus AMPS serves as a polyelectrolyte with strong charge densities similar to poly- (styrene sulfonic acids). This allows for strong electrostatic interactions to occur between polyelectrolyte and target protein, resulting in good precipitation behavior [15-17]. AMPS being a strong polyelectrolyte, does however not exhibit dedicated hydrophobic properties. In this paper we describe the synthesis of copolymers with electrostatic and hydrophobic properties. The copolymers consist of AMPS and either acrylamidobenzoic acid (ABZ) or benzylacrylamide (BzAAm). In this way, hydrophobic properties are introduced into the copolymer. BzAAm is easily available and synthesis can be scaled- up with relatively little effort [18]. Recently, copolymers comprising AMPS and BzAAm have been employed in cation exchange chromatography due to their increased binding capacity compared to homopolymeric stationary phases [19]. ABZ was chosen for copolymer synthesis because of its exceptionally good precipitation performance in protein purification screening experiments, previously conducted by our group.

NMR as non-invasive technique has the advantage of giving qualitative and quantitative results on polymer analysis. It requires however a certain infrastructure and purchase of the rather expensive spectrometers with costs > 600,000 €. Additionally, high operation costs due to liquid helium and liquid nitrogen consumption prevent the wide applicability of NMR for small start-up companies with restricted budget. Low concentration impurity quantification is difficult due to its limited sensitivity and operation expenses [20-21].

Deuteron NMR spectroscopy is widely used, especially for polymer analysis, however, requires additional sample preparation in D_2O or other deuterated samples [22].

Polymer composition can be studied in aqueous solution without extensive preparation steps, *e.g.* by vibrational spectroscopy such as Fourier transform infrared spectroscopy (FTIR), which simplifies analysis costs and time [23-28]. FTIR spectrometers can be purchased for reasonably lower costs, and are widely used even in smaller companies and laboratories. This means that samples do not have to be shipped to service analytics laboratories and analysis time is shortened. Similar to NMR, FTIR allows multi-component analysis with a single measurement, enabling on-line monitoring [20]. Thus it has been used for process control during polymerization, analyzing physical properties of polymers or copolymer composition [29-33]. Once a calibration is established, FTIR has the advantage of simple and fast composition analysis, similar to NMR but with considerably lower operation costs.

Attenuated total reflection infrared spectroscopy (ATR-IR) as one FTIR technique has been widely used to elucidate bioadhesion at polymer films [34], analyze polyelectrolyte multilayers [35], or to characterize carboxylate terminations as well as poly- (4-vinylpyridine) polymer [36-38].

Comparing composition analysis of poly[3-[2-(methacryloylethyl)dimethylammonium] propane sulfonate], using ATR-IR and ^{1}H-NMR, ATR-IR estimation errors were < 1.5 % with absolute errors < 10 %, showing the applicability of ATR-IR for composition analysis similar to NMR [39].

The goal of this work is to design customized copolymers with defined hydrophobicity and charge density to be used for semi-selective protein precipitation within purification processes. Additionally, NMR and ATR-IR, both being suitable tools for copolymer composition analysis, are compared to obtain detailed information on copolymer composition.

Materials and methods

Chemicals

All chemicals including the monomers 4-aminobenzoic acid, acrylic acid chloride, 2-acrylamido-2-methylpropane sulfonic acid, the solvent dimethylformamide, acid neutralizer triethylamine, initiator disodium sulfonatooxy sulfate and chain transfer agent 1-butanthiol were used as obtained from Merck KGaA, Darmstadt, Germany.

Synthesis

ABZ-AMPS

In a first step 4-aminobenzoic acid and acrylic acid chloride were used to synthesize ABZ at 3°C during three hours reaction time, using triethylamine (TEA) as acid neutralizing agent during the reaction (figure 1 A step 1).

82.29 g (0.6 mol) 4-aminobenzoic acid were dissolved in 600 mL dimethylformamide (DMF) while cooling to below 5 °C. Maintaining that temperature, 59.49 g (0.588 mol) TEA and 52.68 g (0.582 mol) acrylic acid chloride were slowly added over a period of 80 minutes.

Temperature was kept below 5 °C for an additional 3 hours and the precipitate was removed by vacuum filtration. The reaction solution was added to 10 °C cold water, and cooled to 8 °C for 14 hours for the product to precipitate. Solvent was evaporated using a vacuum drying oven at 30 °C and 40 mbar for 48 hours.

In a second step, AMPS, used as obtained, was copolymerized with ABZ (see above) (figure 1 A step 2). The ratio of the monomers was varied to synthesize copolymers consisting of varying amounts ABZ and AMPS. 50 % (v/v) dimethylformamide- water (DMF/H_2O) was used as solvent and $Na_2O_8S_2$ as initiator (table I).

Copolymer chain length was controlled by using initiator at different amounts of either 0.035 mmol or 0.915 mmol, respectively.

Additionally, 1-butanthiol as chain transfer agent (CTA) was added during some reactions to elucidate whether this would enable control of chain length distribution and polydispersity. Molar ratio of overall monomer concentration vs. CTA within these samples was varied between 1: 0.0075- 1: 0.06. The reaction was performed using inert conditions at pH 9.0 and 50 °C for 5 h before cooling to room temperature. Additionally, AMPS homopolymer was synthesized using the above described process without using a second type of monomer, also not using CTA. Residual solvent DMF was removed using gel filtration (PD-10 column; Sephadex G25 column material; Amersham Biosciences AB, Uppsala) and polymers adjusted to pH 5.0 before further analysis.

Exemplary, the synthesis of pol15 is described: 10.89 g (52.55 mmol) AMPS were dissolved in 215 mL H_2O, after degassing with N_2, maintaining a temperature < 10 °C. 6.72 g (35.15 mmol) ABZ were dissolved in 225 mL DMF and added to the AMPS solution, after degassing with N_2. The pH was adjusted to pH 9.0, using NaOH. CTA was added at a molar ratio of 1: 0.03 compared to overall monomer concentration. 0.22 g (0.915 mmol) $Na_2S_2O_8$, dissolved in 10 mL H_2O was added. The reaction system was under N_2 atmosphere and heated to 50 °C. After 5 hours, the reaction solution was cooled to room temperature and purified using gel filtration (PD-10 column; Sephadex G25 column material; Amersham Biosciences AB, Uppsala), according to the manufacturers instructions.

AMPS- BzAAm

Copolymers consisting of varying amounts of BzAAm and AMPS (figure 1 B), were synthesized, using DMF/H_2O as solvent and $Na_2S_2O_8$ as initiator (table I). Reaction was performed using inert conditions at pH 9.0 and 50 °C for 5 h before cooling to room temperature. By varying the ratio of the two

monomers, copolymers with different composition were obtained. Copolymer chain length was controlled by using different amounts of initiator of either 0.16 mmol or 0.915 mmol, respectively. Residual solvent DMF was removed using gel filtration (PD-10 column; Sephadex G25 column material; Amersham Biosciences AB, Uppsala) and copolymers adjusted to pH 5.0 before further analysis.

Exemplary, synthesis of pol21 is described: 5.79 g (27.94 mmol) AMPS were dissolved in 105 mL H_2O, after degassing with N_2, maintaining a temperature < 10 °C. 3.00 g (18.61 mmol) BzAAm were dissolved in 115 mL DMF and added to the AMPS solution, after degassing with N_2. pH was adjusted to pH 9.0, using NaOH. 0.218 g (0.915 mmol) $Na_2S_2O_8$, dissolved in 10 mL H_2O was added. The reaction system was under N_2 atmosphere heated to 50 °C. After 5 hours, the reaction solution was cooled to room temperature and purified using gel filtration (PD-10 column; Sephadex G25 column material; Amersham Biosciences AB, Uppsala), according to the manufacturers instructions.

Table 1: Synthesis overview of AMPS- ABZ and AMPS- BzAAm copolymers. parameters kept constant for all reactions: reaction duration 5 h; reaction pH 9.0; solvent: 50 % (v/v) DMF- H_2O; intiatior $Na_2S_2O_8$.

(co-) polymer	polymer designation	AMPS (w/w %)	ABZ/ BzAAm (w/w %)	chain transfer agent used	ratio overall monomer vs CTA mM	$Na_2S_2O_8$ initiator (mmol)
AMPS homopolymer	AMPS homopolymer	100	0	no	-	0.915
AMPS- ABZ	pol1	44	56	no	-	0.035
AMPS- ABZ	pol2	44	56	no	-	0.915
AMPS- ABZ	pol3	29	71	no	-	0.915
AMPS- ABZ	pol4	76	24	no	-	0.915
AMPS- ABZ	pol5	62	38	no	-	0.915
AMPS- ABZ	pol6	45	55	no	-	0.915
AMPS- ABZ	pol7	44	56	no	-	0.915
AMPS- ABZ	pol8	44	56	yes	1:0.0075	0.915
AMPS- ABZ	pol9	44	56	yes	1:0.015	0.915
AMPS- ABZ	pol10	44	56	yes	1:0.03	0.915
AMPS- ABZ	pol11	44	56	yes	1:0.06	0.915
AMPS- ABZ	pol12	62	38	no	-	0.915
AMPS- ABZ	pol13	62	38	yes	1:0.0075	0.915
AMPS- ABZ	pol14	62	38	yes	1:0.015	0.915
AMPS- ABZ	pol15	62	38	yes	1:0.03	0.915

AMPS-BzAAm	pol16	95	5	no	-	0.160
AMPS-BzAAm	pol17	93	7	no	-	0.160
AMPS-BzAAm	pol18	82	18	no	-	0.160
AMPS-BzAAm	pol19	49	51	no	-	0.160
AMPS-BzAAm	pol20	46	54	no	-	0.915
AMPS-BzAAm	pol21	66	34	no	-	0.915
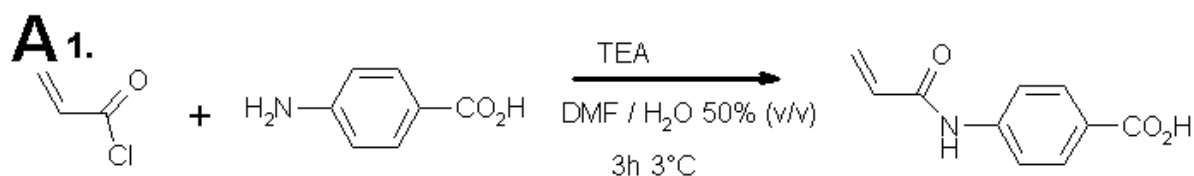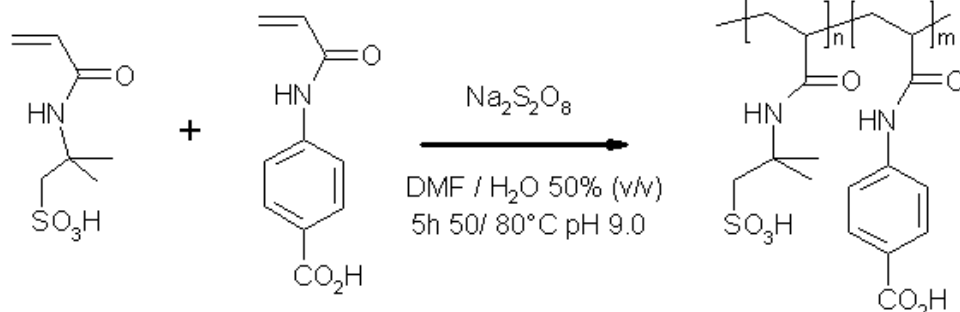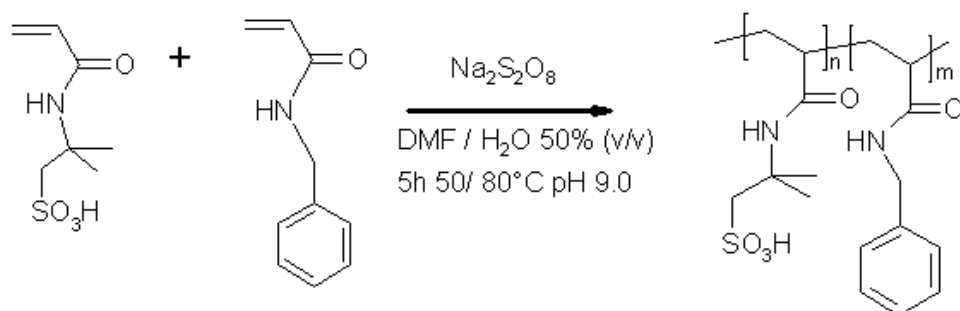
Figure 1: Synthesis steps of A: AMPS- ABZ copolymer in a two-step reaction, using TEA as acid neutralizing agent; B: AMPS- BzAAm copolymer in a single-step reaction.

Copolymer characterization

Gel permeation chromatography

Weight average molecular weight (Mw) and number average molecular weight (Mn) of copolymers and AMPS homopolymer were determined using gel permeation chromatography on a LaChrom Elite system (VWR-Hitachi, Darmstadt, Germany) employing LaChrom refractive index detector L-2490, Licrograph L-2400 UV detector, isocratic pump L-2130 and autosampler L-2200, using a set of 10 µm MCX columns (pre-column, 10^3 Å, 10^6 Å). The system was run at a flow rate of 1 mL min^{-1} at 40 °C with an injection volume of 200 µL, using an elution buffer prepared of 20 % acetonitrile (AcCN), 50 mM $NaNO_3$ and 10 mM Na_2HPO_4 after calibration with Polystyrenesulfonate (Polymer Standard Service, Mainz, Germany) in 20 % AcCN. Molecular weight determination was performed with WinGPC software package (Polymer Standard Service, Mainz, Germany).

^{1}H- NMR spectroscopy

^{1}H-NMR analysis of copolymers was performed using a Bruker DRX 400 MHz NMR spectrometer with Bruker NMR JCAMP-DX v2.0 software (Bruker Biospin GmbH, Ettlingen, Germany). Dried copolymer samples were dissolved in D_2O and tetramethylsilane- salt was used as standard.

Attenuated total reflection infrared spectroscopy

Copolymer composition was determined using attenuated total reflection infrared spectroscopy (ATR-IR) and compared to defined monomer blends of BzAAm and AMPS or ABZ and AMPS. 20 µL of each polymer sample as well as monomer blends (all C = 5 mg ml^{-1}) were analyzed with GoldenGate™ MkII series ATR (Specac Inc, Cranston, RI, USA), using a diamond (type IIa, 45°C, refractive index at 1000 cm^{-1}: 2.4; 0.8 mm diameter of active sampling area; 2 µm penetration depth for a sample of refractive index 1.5 at 1,000 cm^{-1}; diameter 2 mm x 2 mm) at 20 °C. For ABZ-AMPS copolymers and monomer blends, H_2O was used as background.

Since BzAAm monomer is insoluble in water, corresponding AMPS- BzAAm monomer blends as well as AMPS- BzAAm copolymers were dissolved in dimethyl sulfoxide (DMSO) before ATR-IR measurements, also using DMSO as background.

All spectra were recorded with a Bruker Tensor 27 (Bruker Optik GmbH, Ettlingen, Germany); samples were scanned in absorbance mode with 120 scans at a spectral resolution of 4.0. Detector was a Bruker LN-MCT photovoltaic internal detector (Bruker Optik GmbH, Ettlingen, Germany), aperture was set to 6 mm. Atmospheric compensation was performed and samples smoothed using 17 smoothing points.

Copolymer solutions were adjusted to pH 11-12, using defined molarity of NaOH solution and different composition analysis methods for AMPS- ABZ and AMPS- BzAAm copolymers were evaluated using OPUS software v. 6.5 (Bruker Optik GmbH, Ettlingen, Germany).

Quant 2 software package within OPUS software was used for multivariate calibration to allow for copolymer composition analysis. This was achieved using multivariate data analysis and partial least

squares regression (PLS) to compress the information from factors (in this case spectral intensities of several peaks within spectra) and the reference values (AMPS, ABZ or BzAAm amount in copolymers), respectively, while removing irrelevant information [40]. The PLS algorithm thereby makes use of ranks to explain the covariance between the factors and the reference values, with first ranks explaining lots of covariance and latter ranks explaining less covariance [41]. Therefore, the risk of overfitting is reduced, using PLS models with lower ranks. Errors due to wrong determination of monomer amount within a copolymer or interference of other substances, having a potential impact on the predictability of e.g. univariate calibration, are significantly reduced in Quant 2 as several factors are correlated with several reference values, thereby leading to robust models.

Copolymer composition analysis by ATR-IR

AMPS-ABZ copolymers

Copolymer composition analysis was done using Quant 2 multivariate analysis software package simultaneously for peaks associated to AMPS as well as to ABZ. To simplify spectral peak identification, first derivative with 17 smoothing points was applied. For AMPS quantification, the sulfonic acid associated peak between 1,045- 1,040 cm^{-1} was used. As Poly-AMPS did not exhibit any peak at 1,389 cm^{-1}, in contrast to a distinct peak with poly-ABZ, this peak at 1,389 cm^{-1}, likely originating from C-O stretching vibration of carboxylic acid functionalities, was used for ABZ quantification.

BzAAm-AMPS copolymers

Monomer blends showed an increase in peak height of 1,690- 1,650 cm^{-1} peak, if relative AMPS concentration was decreased and amount of BzAAm within monomer blend was increased. This likely originated from overtone and combinatorial vibrations of the benzyl ring within BzAAm. The distinct sulfonic acid associated peak at 1,045- 1,040 cm^{-1}, which we chose for AMPS quantification in AMPS-ABZ copolymers, was very close to a peak also visible in BzAAm spectra (figure 2). Thus, for AMPS quantification, another peak around 1,244- 1,217 cm^{-1} was chosen [42], also including the wavenumber range 1,230 cm^{-1}, previously used by Durmaz et al. [14] for AMPS quantification. Copolymer solutions were analyzed using these peaks for Quant 2 multivariate data analysis, after first derivative with 17 smoothing points, to simplify spectral peak identification.

Pilot experiments elucidating suitability of copolymers for polymer- based protein purification strategies

In pilot experiments, the above copolymers (table I) were used for polymer- based protein precipitation, elucidating precipitation efficiency, yield and selectivity for later intended use in protein purification processes. As protein purification processes are also performed at high salt concentrations, including physiological ionic strength, the precipitation efficiency of the above copolymers was analyzed at various ionic strengths, elucidating copolymer salt tolerance. This salt

tolerance or ionic strength tolerance was then compared to AMPS homopolymer. Experiments were carried out using a monoclonal antibody (mAb), obtained from Merck Millipore, Bedford, USA as well as BSA (Merck KGaA, Darmstadt, Germany), labelled with the fluorescent dyes Alexa 546 and 488 (Molecular Probes, Carlsbad, USA), respectively, according to the manufacturers protocol. Unbound fluorophore was removed using gel filtration (PD-10 column; Sephadex G25 column material; Amersham Biosciences AB, Uppsala), according to the manufacturers instructions. mAb and BSA solutions were then adjusted to pH 5.0. For salt tolerance experiments, mAb solution was used without added BSA solution. Salt concentration within mAb solution was adjusted, using different amounts of NaCl in 20 mM sodium-acetate buffer at pH 5.0. Gel filtered and pH- adjusted copolymer stock solutions as well as AMPS homopolymer stock solution were then added to mAb samples, leading to a final salt concentration between 125- 225 mM NaCl, final mAb concentration of 1 mg ml^{-1} and (co-) polymer concentration of 0.1- 1.5 mg ml^{-1}. Samples were incubated on a lab shaker for 1 hour at 300 rpm to allow for precipitation and then centrifuged for 15 minutes at 2500 rcf. Relative fluorescence in supernatant was then compared to mAb standards, using a Tecan reader M200 (Tecan Instruments, Männedorf, Switzerland). Thus, the relative amount of mAb, present in the supernatant was determined and the percentage of precipitated mAb could be calculated.

For precipitation selectivity experiments, the procedure was similar to the above described procedure. However, mAb and BSA were mixed before the experiments, yielding final mAb concentration of 1 mg ml^{-1} and BSA concentration of 1 mg ml^{-1}. After the precipitation steps, the relative amounts of mAb and BSA in supernatant were determined, using the corresponding excitation and emission maxima of Alexa 546 and 488, respectively, in comparison to mAb and BSA protein standards.

Results and Discussion

Gel permeation chromatography

Molecular weight analysis of copolymers and homopolymer was carried out by GPC. Copolymers with polydispersity between 1.06 and 3.86 were obtained (table II), with Mw ranging from 9,200 to 141,000 g mol^{-1} and polydispersity < 2.00 for > 90 % of all obtained copolymers. Using copolymers with specific chain length and low polydispersity for polymer-based protein precipitation experiments facilitates the modulation of selectivity as well as ionic strength tolerance [10, 12, 43-49]. However, variation of copolymer chain length by using different initiator concentrations did not result in expected chain length distributions. For pol1 and pol2, a higher amount of initiator resulted in shorter chain lengths, as expected. Yet, comparing pol2- pol7, all with same amount of initiator, Mw varied between 75,000 and 114,000 g mol^{-1}; thus control of chain length distribution by using different amounts of initiator did not lead to satisfactory results. In contrast, use of chain transfer agent reduced polymer chain length; a higher concentration of CTA during the reaction resulted, for most of the copolymers, in lower Mw and Mn, as expected and also enabled a control of polymerization products. Increasing amount of CTA resulted in polydispersity index reduction from 1.29- 1.42 down to 1.06- 1.08 (compare pol7- pol11 and pol12- pol15), analyzing AMPS- ABZ and BzAAm- AMPS copolymers

(table II). Observed discrepancies with pol7 and pol8 are due to Mw determination errors of SEC. Therefore, to obtain copolymers with narrow polydispersity, the use of CTA was clearly beneficial, with smallest polydispersities obtained for those copolymers, synthesized using CTA. For BzAAm-AMPS copolymers, CTA was not used during synthesis; instead it was attempted to control chain length distribution by adding different amount of initiator only. While pol16- pol19, exhibited Mw between 56,000- 99,000 g mol^{-1}, despite using same amount of initiator, the use of higher amount of initiator during synthesis of pol20 and pol21 resulted in significantly reduced Mw and Mn of those copolymers. Therefore, adding different amounts of initiator during synthesis still leads to some control of polymer chain length distribution, however, not at acceptable levels.

Table II: Comparison Mw and Mn of different copolymers as determined by GPC. Ratio overall monomer vs. chain transfer agent only given, if chain transfer agent used.

type of (co-) polymer	polymer designation	Mw (g mol^{-1})	Mn (g mol^{-1})	polydispersity	ratio overall monomer vs chain transfer agent(mM)
AMPS homopolymer	AMPS homopolymer	50,000	25,000	2.00	-
AMPS- ABZ	pol1	141,000	76,000	1.86	-
AMPS- ABZ	pol2	75,000	56,000	1.34	-
AMPS- ABZ	pol3	108,000	74,000	1.46	-
AMPS- ABZ	pol4	111,000	68,000	1.63	-
AMPS- ABZ	pol5	114,000	79,000	1.44	-
AMPS- ABZ	pol6	95,000	62,000	1.53	-
AMPS- ABZ	pol7	81,000	57,000	1.42	-
AMPS- ABZ	pol8	84,000	61,000	1.38	1:0.0075
AMPS- ABZ	pol9	59,000	47,000	1.26	1:0.015
AMPS- ABZ	pol10	54,000	44,000	1.23	1:0.03
AMPS- ABZ	pol11	35,000	33,000	1.06	1:0.06
AMPS- ABZ	pol12	67,000	52,000	1.29	-
AMPS- ABZ	pol13	64,000	50,000	1.28	1:0.0075
AMPS- ABZ	pol14	49,000	42,000	1.17	1:0.015
AMPS- ABZ	pol15	39,000	36,000	1.08	1:0.03
AMPS- BzAAm	pol16	56,000	17,000	3.24	-
AMPS- BzAAm	pol17	99,000	50,000	1.98	-
AMPS- BzAAm	pol18	78,000	63,000	1.25	-
AMPS- BzAAm	pol19	63,000	43,000	1.47	-
AMPS- BzAAm	pol20	9,200	2,500	3.68	-
AMPS- BzAAm	pol21	9,800	5,500	1.78	-

¹H- NMR spectroscopy

¹H-NMR spectra of 15 AMPS- ABZ and six AMPS- BzAAm polymers were analyzed. Exemplary spectra of pol7 and pol20 can be seen in figure 2.
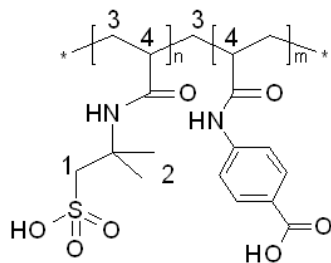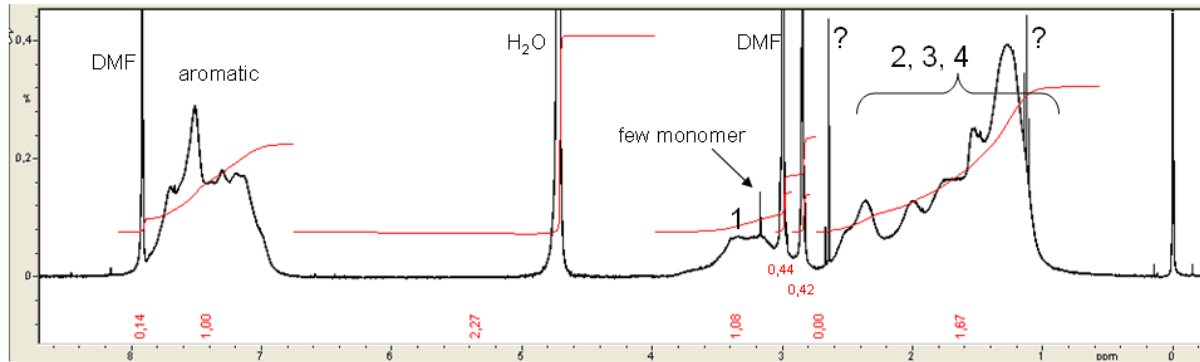
ABzA: 4H (aromatic) = 1,0-0,14 = 0,86 → 1H = 0,86/4 = 0,215

AMPS: 2H (proton1) = 1,08-0,44-0,42 = 0,22 → 1H = 0,22/2 = 0,11

AMPS : ABzA = 1 : 2,0
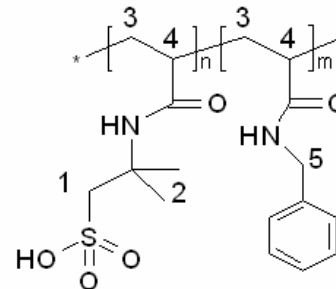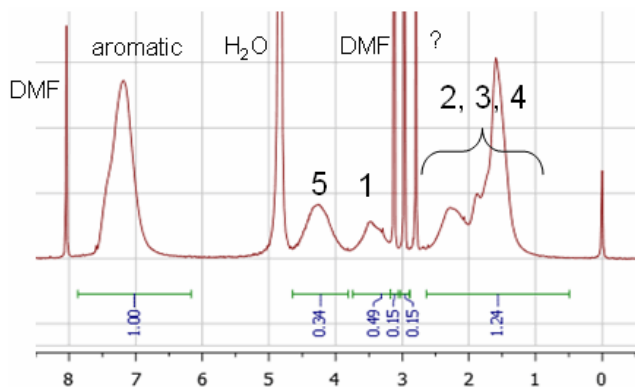
BzA: 4H (aromatic) = 1,0   → 1H = 1,0/5 = 0,20   → AMPS : BzA = 1 : 2,1
BzA: 2H (proton5) = 0,34   → 1H = 0,34/2 = 0,17 → AMPS : BzA = 1 : 1,8

AMPS: 2H (Proton1) = 0,49 – 0,15 – 0,15 = 0,19   → 1H = 0,19/2 = 0,095

AMPS : BzA = 1 : 2,0

Figure 2: NMR spectra of pol7 (above) and pol20 (below).

Attenuated total reflection infrared spectroscopy

ATR-IR was used for copolymer composition analysis, comparing different composition analysis models. Defined monomer blends were used to identify characteristic peaks (figures 3 and 4). These peaks were then used for quantification of relative monomer amounts using multivariate calibration

and quantification based on corresponding PLS models for simultaneous quantification of AMPS and either BzAAm or ABZ, thus allowing copolymer composition analysis (figure 5 A and B) as described above.
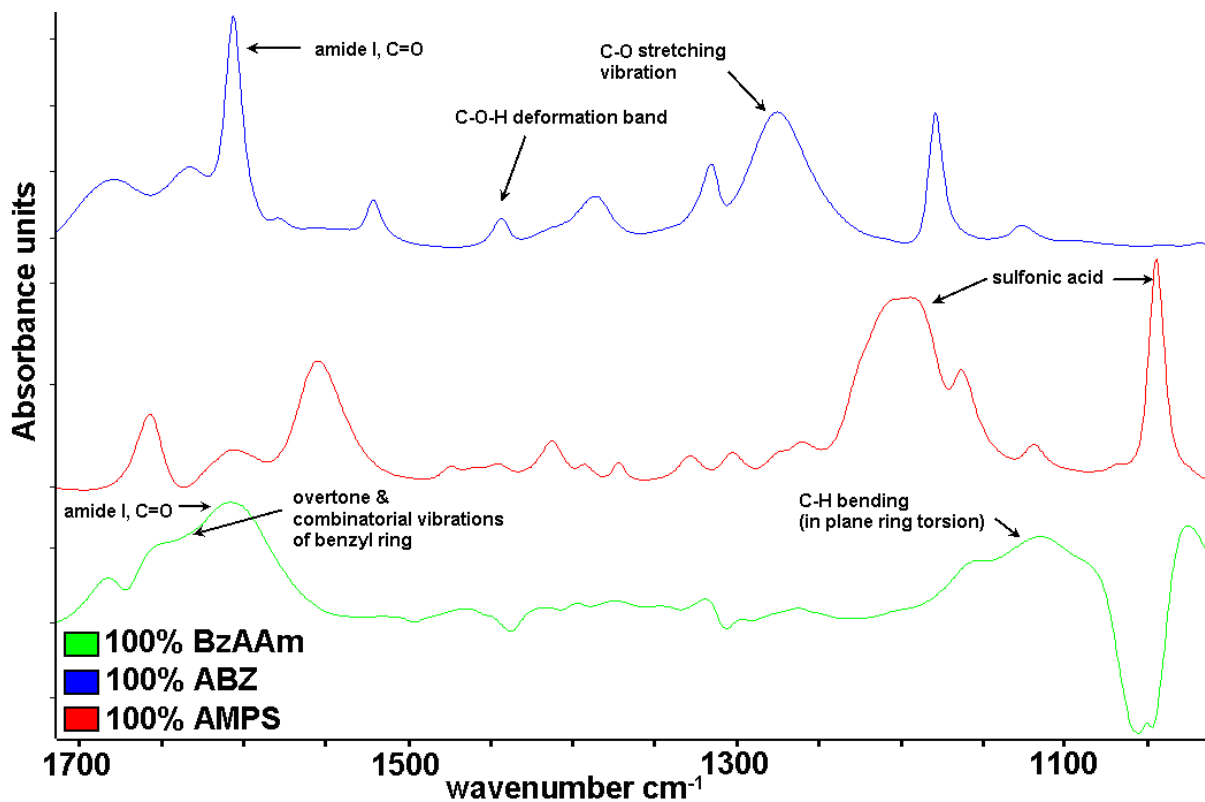
Figure 3: Comparison unmodified IR spectra of BzAAm, ABZ and AMPS.
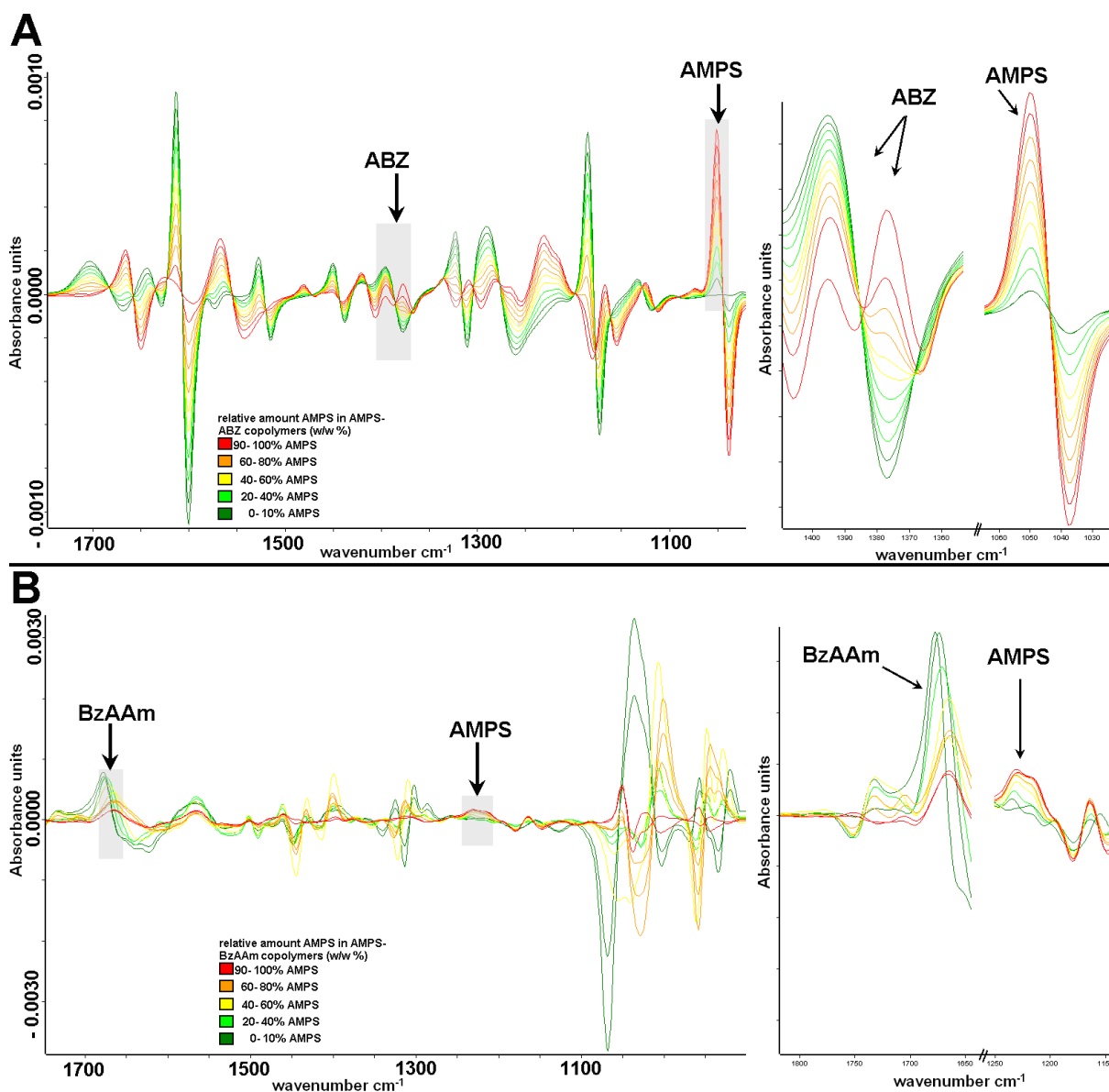
Figure 4: First derivative IR- spectra of defined monomer blends as calibration standards. Highest relative AMPS amount labelled in red, followed by intermediate AMPS concentrations in orange and yellow. Lowest AMPS amounts labelled in light green and dark green if 0- 10 % AMPS. A: spectral overview and focus on relevant wavenumber range for AMPS- ABZ composition analysis using Quant 2 method; B: spectral overview and focus on relevant wavenumber range for AMPS- BzAAm composition analysis.
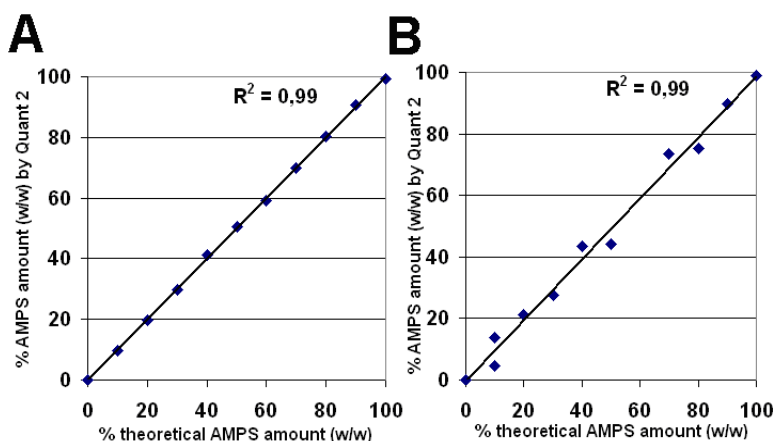
Figure 5: Determination of relative AMPS content using defined monomer blends. A: multivariate PLS model (Quant 2) for copolymer composition analysis in AMPS- BzAAm copolymers; B: multivariate PLS model (Quant 2) for copolymer composition analysis in AMPS- ABZ copolymers.

Composition analysis by ATR-IR revealed relative AMPS amounts between 20- 83 % within AMPS- ABZ copolymers as well as 36- 95 % within AMPS- BzAAm copolymers (tables III- IV). These results show that copolymers with different charge density as well as various hydrophobicity, both important in modulating and optimizing target protein precipitation conditions, were obtained [12-13, 43].

To simplify comparison with ATR-IR results, molar ratios obtained by ^{1}H-NMR analysis were transferred to weight ratios, using the corresponding molar masses of AMPS and ABZ. Comparing relative AMPS amounts determined by ATR-IR and by ^{1}H-NMR shows similar results (table III).

Taking copolymer "pol6" as an example, ATR-IR composition analysis revealed 43 % AMPS compared to 46 % AMPS as determined by NMR. Generally, for AMPS- ABZ copolymer analysis, ATR-IR measurements resulted in 90-126 % of AMPS determination compared to reference values determined by NMR.

Although these deviations are slightly higher than those obtained by Bomfim *et al.* [39], two-thirds of tested samples showed ATR-IR results being between 90- 110 % of NMR results, thus showing that both techniques are comparable (table III). Comparison of monomer ratios used during synthesis and final composition showed similar ratios for most of obtained samples.

Copolymer composition analysis of AMPS- BzAAm copolymers using ATR-IR was also compared to NMR. Taking copolymer "pol20" as an example, ATR-IR analysis resulted in 36 % AMPS content compared to 39 % as determined by NMR. Except for one sample, ATR-IR results were between 90- 110 % of those composition results obtained by NMR, showing that both techniques are comparable regarding composition determination. Monomer ratios employed during synthesis and final composition were similar for most of obtained samples.

Table III: comparison of initial AMPS monomer amount in reaction solution and relative (w/w) AMPS amounts in AMPS- ABZ copolymers determined by ATR-IR.

polymer designation	initial AMPS monomer ratio (w/w %) in reaction solution	experimental AMPS ratio (w/w %) multivariate model	NMR AMPS ratio (w/w %)
pol1	44	39	41
pol2	44	40	37
pol3	29	20	19
pol4	76	83	86
pol5	62	65	61
pol6	45	43	46
pol7	44	44	35
pol8	44	46	41
pol9	44	49	42
pol10	44	53	42
pol11	44	59	50
pol12	62	59	59
pol13	62	59	58
pol14	62	63	58
pol15	62	63	70

Table IV: comparison of initial AMPS monomer amount in reaction solution and relative (w/w) AMPS amounts in AMPS- BzAAm copolymers determined by ATR-IR.

polymer designation	initial AMPS monomer ratio (w/w %) in reaction solution	experimental AMPS ratio (w/w %) multivariate model	NMR AMPS ratio (w/w %)
pol16	95	85	94
pol17	93	92	88
pol18	82	82	74
pol19	49	49	35
pol20	46	36	39
pol21	66	54	54

Precipitation efficiency of obtained copolymers

Salt tolerance of tested copolymers and AMPS homopolymer

Pilot experiments, analyzing mAb precipitation yield, using different copolymers as well as AMPS homopolymer, were carried out. As precipitation behavior of different polymers within one type (e.g. within AMPS- BzAAm or AMPS- ABZ copolymer type) was similar, a summary of precipitation results, showing selected polymers of these different types is shown in figure 6 A. Generally, precipitation yields of AMPS- BzAAm and AMPS- ABZ copolymers were in a comparable range and were found to depend on the composition and length of the respective copolymer as well as the polymer concentration.

Both the AMPS- BzAAm and the AMPS- ABZ copolymers gave precipitation yields > 70 % at salt concentrations of 225 mM which corresponds to an ionic strength of 22.5 mS cm^{-1}. Precipitation yield increased further to > 80 %, if salt concentration was reduced to 175 mM NaCl and yields of 85- 90 % and higher were obtained at salt concentrations of 150 mM NaCl, similar to physiological ionic strength. In contrast to these results, AMPS homopolymer clearly showed low precipitation yields at salt concentrations of 150 mM NaCl, which decreased to almost no precipitation at all, using higher salt concentrations than 150 mM NaCl. Thus AMPS homopolymer does not exhibit an adequate physiological ionic strength tolerance, in contrast to the higher salt tolerance of the here synthesized copolymers.

Precipitation selectivity of tested copolymers and AMPS homopolymer

Copolymers as well as AMPS homopolymer were used for precipitation selectivity studies using an monoclonal antibody as target protein and BSA as model impurity protein. For later anticipated precipitation in cell culture fluid samples, a high precipitation yield for mAb and low precipitation yield for impurity proteins would be desirable.

Clear differences in the protein precipitation capablility of AMPS homopolymer and synthesized copolymers were seen. At 125 mM NaCl the AMPS homopolymer precipitated almost no BSA and mAb precipitation yields were only around 30 %. In contrast, AMPS- ABZ as well as AMPS- BzAAm copolymers displayed high precipiation yields, likely due to conjoint electrostatic and hydrophobic interactions. However, while BSA impurity protein co-precipitation for AMPS- ABZ copolymers was around 10 %, co-precipitation of BSA increased to up to 45 %, using similar long BzAAm-AMPS copolymers (figure 6 B). This is likely due to the more hydrophobic nature of this copolymer compared to ABZ which has an additional carboxylic acid group, resulting in enhanced hydrophobic interaction with BSA during precipitation.
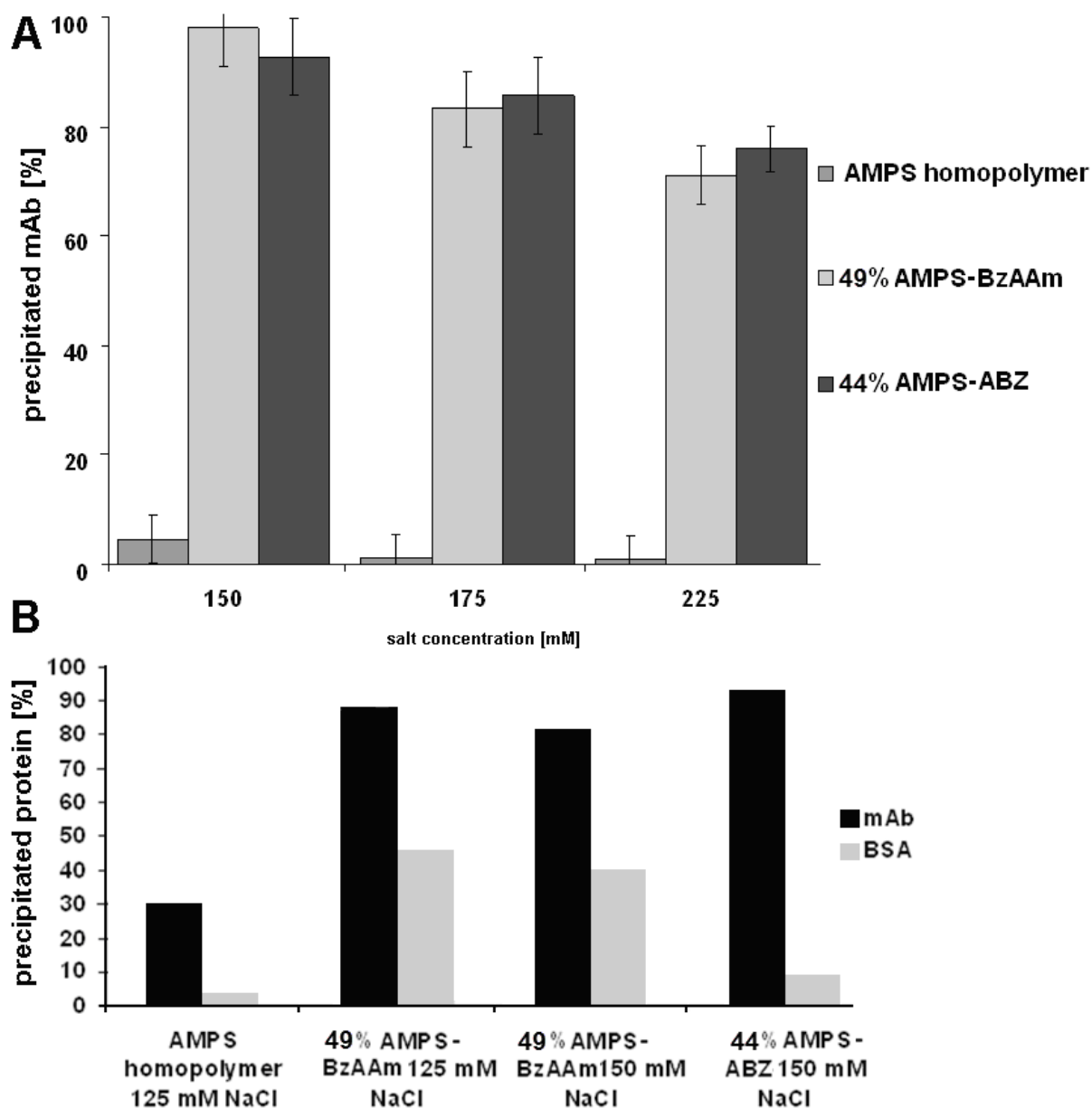
Figure 6: A: precipitation strength of similar long (Mw 59,000- 63,000 g mol^{-1}) AMPS- ABZ and AMPS- BzAAm copolymers at at pH 5.0, depending on ionic strength and copolymer composition, in comparison to AMPS homopolymer (Mw 50,000 g mol^{-1}). All polymers were used at a concentration of 0.6 mg ml^{-1}. B: precipitation selectivity of AMPS- ABZ and AMPS- BzAAm copolymers as well as AMPS homopolymer at pH 5.0, using mAb- BSA protein mixture at different ionic strength with polymer concentration of 0.6 mg ml^{-1}.

Conclusion

Obtained set of copolymers was synthesized aimed at customizing semi-selective protein precipitation. These copolymers showed higher salt- tolerance compared to AMPS homopolymer and, besides lower selectivity, overall higher mAb precipitation yields, performing initial pilot experiments. Unlike expected, copolymer chain length could not be largely varied by using different concentrations

of initiator. However, the use of different concentrations of chain transfer agent 1-butanthiol clearly helped to obtain copolymers with small polydispersity index and control copolymer Mw. Copolymer composition as determined by ATR-IR and NMR revealed relative AMPS content between 36- 95 % (w/w) for AMPS- BzAAm copolymers as well as 20- 83 % (w/w) AMPS for AMPS- ABZ copolymers. Direct comparison of copolymer composition, determined by ATR-IR and NMR, showed good agreement for most of obtained results, using a multivariate composition analysis method within OPUS software. Although some samples showed larger deviations between both techniques, requiring further method refinement, ATR-IR seems promising as a simple, cost-effective and fast copolymer analysis technique.

Acknowledgement

Conflict of interest

The authors declare that there is no conflict of interest regarding this work and publication.

References

[1] Gross RA, Kalra B (2002) Biodegradable polymers for the environment. Science 297:803-807

[2] Bolto B, Gregory J (2007) Organic polyelectrolytes in water treatment. Water Res 41:2301-2324

[3] Nart Z, Kayaman-Apohan N (2011) Preparation, characterization and drug release behavior of poly (acrylic acid–co-2-hydroxyethyl methacrylate-co-2-acrylamido-2-methyl-1-propanesulfonic acid) microgels. Journal of Polymer Res 18:869-874

[4] Schmaljohann D (2006) Thermo-and pH-responsive polymers in drug delivery. Adv Drug Deliv Rev 58:1655-1670

[5] Gillies ER, Frechet JM (2005) Dendrimers and dendritic polymers in drug delivery. Drug discovery today 10:35-43

[6] Allen TM, Cullis PR (2004) Drug delivery systems: entering the mainstream. Science 303:1818-1822

[7] Jeong B, Bae YH, Lee DS, Kim SW (1997) Biodegradable block copolymers as injectable drug-delivery systems. Nature 388:860-862

[8] Hönig W, Kula MR (1976) Selectivity of protein precipitation with polyethylene glycol fractions of various molecular weights. Anal Biochem 72:502-512

[9] Peram T, McDonald P, Carter-Franklin J, Fahrner R (2010) Monoclonal antibody purification using cationic polyelectrolytes: an alternative to column chromatography. Biotechnol Prog 26:1322-1331

[10] McDonald P, Victa C, Carter-Franklin JN, Fahrner R (2009) Selective antibody precipitation using polyelectrolytes: a novel approach to the purification of monoclonal antibodies. Biotechnol Bioeng 102:1141-1151

[11] Capito F, Skudas R, Stanislawski B, Kolmar H (2013) Polyelectrolyte–protein interaction at low ionic strength: required chain flexibility depending on protein average charge. Colloid Polym Sci 1-11

[12] Cooper CL, Dubin PL, Kayitmazer AB, Turksen S (2005) Polyelectrolyte–protein complexes. Curr Opin Colloid Interface Sci 10:52-78

[13] Tribet C (2001) In: Radeva T (ed) Physical chemistry of polyelectrolytes, surfactant science series, 10th edn. Marcel Dekker Inc., New York

[14] Durmaz S, Okay O (2000) Acrylamide/2-acrylamido-2-methylpropane sulfonic acid sodium salt-based hydrogels: synthesis and characterization. Polymer 41:3693-3704

[15] Mattison KW, Dubin PL, Brittain IJ (1998) Complex formation between bovine serum albumin and strong polyelectrolytes: effect of polymer charge density. J Phys Chem B 102:3830-3836

[16] Xia J, Dubin PL, Kim Y, Muhoberac BB, Klimkowski VJ (1993) Electrophoretic and quasi-elastic light scattering of soluble protein-polyelectrolyte complexes. J Phys Chem 97:4528-4534

[17] Fisher LW, Sochor AR, Tan JS (1977) Chain Characteristics of Poly (2-acrylamido-2-methylpropanesulfonate) Polymers. 1. Light-Scattering and Intrinsic-Viscosity Studies. Macromolecules 10:949-954

[18] Yahaya GO, Ahdab AA, Ali SA, Abu-Sharkh BF, Hamad EZ (2001) Solution behavior of hydrophobically associating water-soluble block copolymers of acrylamide and N-benzylacrylamide. Polymer 42:3363-3372

[19] Graalfs H, Patent US2010/0181254A1, Merck KGaA

[20] Miller-Chou BA, Koenig JL (2003) A review of polymer dissolution. Prog Polym Sci 28:1223-1270

[21] Hyde TM, Gladden LF, Mackley MR, Gao P (1995) Quantitative nuclear magnetic resonance imaging of liquids in swelling polymers. J Polym Sci, Part A: Polym Chem 33:1795-1806

[22] Spiess HW (1983) Molecular dynamics of solid polymers as revealed by deuteron NMR. Colloid Polym Sci 261:193-209

[23] Su YL, Liu HZ, Wang J, Chen JY (2002) Study of salt effects on the micellization of PEO-PPO-PEO block copolymer in aqueous solution by FTIR spectroscopy. Langmuir 18:865-871

[24] Inoue T, Kawamura H, Matsuda M, Misono Y, Suzuki M (2001) FT-IR and ESR Spin-Label Studies of Mesomorphic Phases Formed in Aqueous Mixtures of Heptaethylene Glycol Dodecyl Ether. Langmuir 17:6915-6922

[25] Maeda Y, Nakamura T, Ikeda I (2001) Changes in the hydration states of poly (N-alkylacrylamide) s during their phase transitions in water observed by FTIR spectroscopy. Macromolecules 34:1391-1399

[26] Maeda Y, Higuchi T, Ikeda I (2000) Change in hydration state during the coil-globule transition of aqueous solutions of poly (N-isopropylacrylamide) as evidenced by FTIR spectroscopy. Langmuir 16:7503-7509

[27] Wong PTT, Mantsch HH (1989) Effects of internal and external pressure on the structure and dynamics of micelles: A FTIR study of sodium and potassium decanoates in D_2O. J Colloid Interface Sci 129:258-269

[28] Yang PW, Mantsch HH (1986) The critical micellization temperature and its dependence on the position and geometry of the double bond in a series of sodium octadecenoates. J Colloid Interface Sci 113:218-224

[29] Ngadaonye JI, Cloonan MO, Geever LM, Higginbotham CL (2011) Synthesis and characterisation of thermo-sensitive terpolymer hydrogels for drug delivery applications. Journal of Polymer Res 18:2307-2324

[30] Fei M, Jin B, Wang W, Liu L (2010) Synthesis and characterization of AB block copolymers based on polyhedral oligomeric silsesquioxane. Journal of Polymer Res 17:19-23

[31] Lee RS, Huang YT (2010) Synthesis and characterization of amphiphilic triblock-graft PEG-(b-PαN3CL-g-Alkyne) 2 degradable copolymers. Journal of Polymer Res 17:697-706

[32] Bunding Lee KA, Johnson SC (1993) Comparison of mid-ir with nir in polymer analysis. Appl Spectrosc Rev 28:231-284

[33] Toft J, Kvalheim OM, Karstang TV, Christy AA, Kleveland K, Henriksen A (1992) Analysis of nontransparent polymers: mixture design, second-derivative attenuated total internal reflectance FT-IR, and multivariate calibration. Appl Spectrosc 46:1002-1008

[34] Chittur KK, Fink DJ, Leininger RI, Hutson TB (1986) Fourier transform infrared spectroscopy/attenuated total reflection studies of protein adsorption in flowing systems: Approaches for bulk correction and compositional analysis of adsorbed and bulk proteins in mixtures. J Colloid Interface Sci 111:419-433

[35] Müller M (2002) In: Tripathy SK, Kumar J, Nalwa HS (eds) Handbook of Polyelectrolytes and Their Applications, American Scientific, Stevenson Ranch

[36] Sukhishvili SA, Dhinojwala A, Granick S (1999) How polyelectrolyte adsorption depends on history: a combined Fourier transform infrared spectroscopy in attenuated total reflection and surface forces study. Langmuir 15:8474-8482

[37] Cheng SS, Scherson DA, Sukenik CN (1995) In Situ Attenuated Total Reflectance Fourier Transform Infrared Spectroscopy Study of Carboxylate-Bearing, Siloxane-Anchored, Self-Assembled Monolayers: A Study of Carboxylate Reactivity and Acid-Base Properties. Langmuir 11:1190-1195

[38] Frantz P, Granick S (1995) Infrared dichroism, chain flattening, and the bound fraction histogram in adsorbed poly (methyl methacrylate) layers. Macromolecules 28:6915-6925

[39] Bomfim JA, Mincheva R, Beigbeder A, Persenaire O, Dubois P (2009) Quaternized/betainized) amino-based amphiphilic block copolymers: quantitative composition characterization via FTIR and thermogravimetry. e-Polymers 35. http://www.e-polymers.org/journal/abstract.cfm?abstract_Id=2843. Accessed 05 May 2013

[40] Naes T (2002) Multivariate Calibration and Classification. NIR Publications, Chichester

[41] Wold S, Martens H, Wold H (1983) The multivariate calibration problem in chemistry solved by the PLS method. Matrix pencils 973:286-293

[42] Huglin MB, Rego JM (1990) Study of polymer blends based on poly (vinylpyridines) and acidic polymers. Polymer 31:1269-1276

[43] Carlsson F, Malmsten M, Linse P (2003) Protein-polyelectrolyte cluster formation and redissolution: A monte carlo study. J Am Chem Soc 125:3140-3149

[44] Izumrudov VA, Galaev IY, Mattiasson B (1998) Polycomplexes–potential for bioseparation. Bioseparation 7:207-220

[45] Houska M, Brynda E (1997) Interactions of proteins with polyelectrolytes at solid/liquid interfaces: sequential adsorption of albumin and heparin. . J Colloid Interface Sci 188:243-250

[46] Pergushov DV, Izumrudov VA, Zezin AB, Kabanov VA (1995) Stability of interpolyelectrolyte complexes in aqueous saline solutions: effect of the degree of polymerization of polyions. J Polym Sci, Part A: Polym Chem 37:1081-1087

[47] Shieh JY, Glatz CE (1994) In: Dubin PL (ed) Macromolecular Complexes in Chemistry and Biology. Springer, Berlin

[48] Papisov IM, Litmanovich AA (1989) Conducting Polymers/Molecular Recognition. Springer, Berlin

[49] Tsuchida E, Abe K (1986) In: Wilson AD (ed) Developments in Ionic Polymers, 2nd edn. Elsevier, New York

3.2. Effects of ionic strength on precipitation

**Paper: Polyelectrolyte-protein interaction at low ionic strength:
Required chain flexibility depending on protein average charge**

Florian Capito, Romas Skudas, Bernd Stanislawski and Harald Kolmar

Short summary:

In order to understand protein-polyelectrolyte interactions and find ways to optimize precipitation efficiency, experiments were carried out at very low as well as very high salt concentrations. These findings of lower precipitation efficiency at both ionic strength regimes led us analyze precipitation depending on polymer chain flexibility at the very low salt concentration range. It is known that polymer chains obtain a more rigid-like structure at these conditions, due to the absence of shielding charges between polymer units. Using three different antibodies and lysozyme, a qualitative correlation between required chain flexibility and protein hydrophobicity as well as protein charge density was discovered. Antibodies with lower average charge and less hydrophobicity required more flexible polyelectrolytes to have sufficient precipitation compared to more hydrophobic antibodies with higher charge density.
These highlights are useful for the intended development of a polymer-driven protein precipitation process, as polymers with specific chain flexibility could help to improve precipitation behavior towards specific target proteins.

ORIGINAL CONTRIBUTION

Polyelectrolyte–protein interaction at low ionic strength: required chain flexibility depending on protein average charge

Florian Capito · Romas Skudas · Bernd Stanislawski · Harald Kolmar

Abstract The effect of low ionic strength leading to reduced polyelectrolyte–protein interactions has been shown by in silico and in vitro experiments, suggesting polyelectrolyte rigidity increasing at low ionic strength, thus leading to reduced interactions with proteins. This contribution elucidates polyelectrolyte–protein precipitation in the 0–2.6-$mS\,cm^{-1}$ ionic strength regime with polyelectrolyte rigidity determinations, using viscosimetry at these conditions, also considering protein charge distributions, using different proteins. Precipitation yields increased from 5 to 40 % at low ionic strength to up to 90 % at intermediate ionic strength, depending on protein and polyelectrolyte type, using lysozyme and three different monoclonal antibodies. Comparing precipitation behavior of the monoclonal antibodies, a qualitative correlation between required polyelectrolyte flexibility to enhance protein precipitation and protein average charge as well as hydrophobicity of the antibodies was discovered. Antibodies with lower average charge and less hydrophobicity required more flexible polyelectrolytes to enhance precipitation behavior by allowing interaction of the polyelectrolytes with proteins, attaching to positively charged protein patches while "circumnavigating" negatively charged protein areas. In contrast, antibodies with higher protein average charge showed increasing precipitation yields up to 90 % already at lower ionic strength, associated with then more rigid polyelectrolyte structures. Therefore,

designing polyelectrolytes with specific chain flexibility could help to improve precipitation behavior toward specific target proteins in polyelectrolyte-driven purification techniques.

Keywords Polyelectrolyte flexibility · Proteins · Structure–property relations · Viscosity

Introduction

Charged and non-charged polymers find widespread use in food technology, in environmental chemistry as biopolymers, in water treatment, and in biological applications, e.g., delivery of drugs to specific targets [1–10]. Applications in the field of protein and cell purification range from immobilized polymers in chromatography to the use as flocculation agents, such as poly(ethylenimine) [11–15]. Furthermore, their use as precipitants, e.g., poly(ethylene glycol), has been known for a long time and is also further investigated by various companies [16–21]. Recent investigations in this field include the evaluation of poly(acrylic acid) (PAA), poly(vinyl sulfonic acid) (PVS), and poly(styrene sulfonic acid) (PSS) as precipitants to semi-selectively precipitate target proteins or impurities from cell culture fluid [21, 22]. Polyelectrolyte–protein interaction has been studied using infrared spectroscopy and circular dichroism spectroscopy to elucidate polyelectrolyte-induced damage to proteins. Further investigations made use of turbidity measurements to evaluate polyelectrolyte-driven protein precipitation. Extensive Monte Carlo (MC) simulations were performed aimed at predicting the contribution of various polyelectrolyte properties such as chain stiffness, charge distribution, polyelectrolyte molecular weight, and

F. Capito (✉) · H. Kolmar
Institute for Organic Chemistry and Biochemistry, Technische Universität Darmstadt, Darmstadt, Germany
e-mail: florian.capito@external.merckgroup.com

R. Skudas · B. Stanislawski
Merck KGaA, Frankfurter Strasse 250,
64293, Darmstadt, Germany

🙆 Springer

chain length to protein interaction and precipitation. These studies provide a fundament for deeper knowledge and understanding of polyelectrolyte–protein interaction and parameter effects and may serve as a tool to further optimize polyelectrolyte–protein interactions. MC simulations and preparative experiments indicate a pH and ionic strength-dependent protein precipitation behavior using charged polymers. Both very low and very high salt concentrations decrease protein–polyelectrolyte interaction while an optimum is found in the medium ionic strength range around 1–2 mScm^{-1} [23–30]. These findings are attributed to screening effects due to counterions, forming a diffuse double layer around the polymer side chain charges and thereby neutralizing them, also leading to flexible polymer chains and collapsing polymers [31]. While high ionic strength effects on precipitation have been analyzed, due to their relevance during protein purification using precipitation [21, 22], low ionic strength effects have been of minor interest so far. MC simulations at very low ionic strength show the low presence of Debye–Hückel screening effects; charges are less shielded and maximize their distance among each other, leading to stiff expanded polymers, causing weaker binding to proteins [24, 32, 33]. Intermediate ionic strength leads to "tennisball-like" conformations of polyelectrolytes when interacting with colloids of opposite charges [24, 32]. These in silico simulations indicate that while binding loosely at the center parts of polymer chains, counterions bind strongly to the outer sections of chains, making polymer outer-chain segments more flexible than inner-chain segments [34]. This can lead to contractions in form of a kink or "horseshoe shape" [35]. Further increase of the ionic strength can lead to self-contraction of polymers, impedes electrostatic attraction between proteins and polymers and thereby precipitation as elucidated by MC simulations [36, 37]. The effect of polymer chain rigidity on polymer–protein and polymer–sphere–model interaction evaluated by various in silico methods shows loosely wrapped or collapsed flexible chains, semiflexible tennisball-like chains, and rodlike stiff chains with inter-sphere separations, when complexing polymers to particles of opposite charge [33, 38, 39]. Cluster formation is elevated for very flexible and semiflexible chains, the latter being favored compared to rigid chains [40]. At very low ionic strength, less rigid chains show a more rod-like structure to minimize electrostatic energy between monomer units [32]. Flexible chains also allow colloid binding at larger ionic strength and exhibit lower desorption, compared to stiffer chains [23, 25, 32, 41]. The polymer chain rigidity depends on the intrinsic chain stiffness due to the chemical structure of the polymer backbone and on the chain stiffening due to the confinement energy of the polyelectrolyte chain. The latter originates from electrostatic repulsion between the charges in the side chains of the polyelectrolyte monomers

[32]. Therefore, an increase of the ionic strength in solution leads to a decrease of the effective stiffness of rigid chains as the persistence length decreases [42]. The intrinsic rigidity is thereby dependent on the chain length and the type of polyelectrolyte, e.g., dextran sulfate obtains higher intrinsic chain stiffness than PVS and PSS [43]. Longer polymer chains with a higher monomer number exhibit an increase in the repulsion between monomer side chains, leading to more rigid chains [44]. Also, increasing the temperature, using non-thermoactive polymers, reduces polymer adsorption onto spherical particles while an increase of radius and charge density of the spherical particle leads to higher adsorption [45, 46]. Viscosity measurements of polymer solutions show an increased viscosity at low ionic strength that can be explained with the expansion of polymer chains induced by repulsive electrostatic forces at the backbone or side chains, due to the absence of otherwise shielding counterions [47]. Even though few scientists, Seyrek et al. [25] and Hattori et al. [26], analyzed in vitro protein–polyelectrolyte interaction at low ionic strength conditions, the polyelectrolyte chain stiffness at precipitation conditions has not been determined.

Therefore, the objective of this study is to compare the above summarized numerous in silico results governing protein–polyelectrolyte interaction behavior, with experimental results involving viscometric measurements at precipitation conditions as well as perform protein precipitation experiments at low ionic strength, providing a link between polyelectrolyte chain stiffness studies, in vitro precipitation experiments, existing computer simulation data, and taking protein surface charge distribution as well as estimated average charges into account. The results of this study would help in designing polyelectrolytes with specific chain flexibility, thus improving precipitation behavior toward target proteins in polyelectrolyte-driven precipitation techniques.

Experimental

Proteins

Lysozyme was obtained from Merck KGaA, Darmstadt, Germany. IgG1 monoclonal antibodies (mAb) B, mAb C, and mAb D were produced by Merck Millipore, Bedford, MA, USA.

Fluorophore labeling

All proteins were labeled with fluorophores; mAb B, mAb C, and mAb D (all molecular weight 150 kDa) were labeled with Alexa Fluor® 546 fluorophore (Invitrogen, Carlsbad, CA, USA); lysozyme (molecular weight 14.3 kDa) was labeled with Alexa Fluor® 680 fluorophore (Invitrogen, Carlsbad, CA, USA). For labeling, 1 mg of fluorophore

was dissolved in 500 μL DMSO and added to 1 g of protein, dissolved in aqueous buffer solution. After stirring for 1 h, unbound fluorophore was removed using a PD-10 column (Amersham Biosciences AB, Uppsala, Sweden) for gel filtration with Sephadex G25 column material. Protein solutions were adjusted to pH 5.0, obtaining 2 mg ml^{-1} stock solutions. Protein solutions showed no aggregation in the ionic strength regime of 0–5 mS cm^{-1}, when adding NaCl to elucidate polyelectrolyte-independent protein aggregation behavior at low ionic strength.

Polyelectrolytes

Anionic polyelectrolytes PSS (Polymer Standards Service, Mainz, Germany) and PAA (Polysciences, Warrington, FL, USA; Polymer Standards Service, Mainz, Germany) were dissolved in deionized water and adjusted to pH 5.0 to achieve stock solutions for each polyelectrolyte, respectively. Molecular weight of polyelectrolytes was 976, 145, 15.2, and 2.22 kDa for PSS and 958, 225, and 60 kDa for PAA. Polyelectrolyte solutions showed no aggregation in the ionic strength regime of 0–5 mS cm^{-1}, when adding NaCl to elucidate salt-dependent polyelectrolyte aggregation behavior.

Precipitation buffer

Sodium acetate buffer pH 5.0 with ionic strength of 1.10, 2.00, 3.25, 4.50, 7.40, and 13.00 mS cm^{-1}, respectively, was prepared, and ionic strength was measured at 22 °C using Mettler Toledo Inlab 731 conductivity sensor.

Precipitation experiments

Precipitation experiments were performed in Eppendorf tubes, using 600 μL of protein stock solution, 240 μL of buffer, and 360 μL of polyelectrolyte solution. Final concentrations in each sample were 1.0 mg ml^{-1} protein, 0.04 mg ml^{-1} polyelectrolyte, and sodium acetate buffer pH 5.0 with ionic strength of 0.22, 0.40, 0.65, 0.90, 1.48, or 2.60 mS cm^{-1}, respectively. Buffer, polyelectrolyte, and protein were mixed and incubated on lab shaker for 1 h at 300 rpm. Afterward, samples were centrifuged at 2,500 rcf for 15 min and supernatant transferred to microtiter plates (Nunc, Langenselbold, Germany). Protein concentration in supernatant was determined by fluorescence measurements in comparison to calibration standards using a Tecan fluorescence plate reader M200 (Tecan Instruments, Männedorf, Switzerland). Decrease of protein concentration in supernatant in comparison to initial protein concentration was used to calculate percentage of precipitated protein. Procedure was repeated for all five different proteins, using lysozyme, mAb B, mAb C, or mAb D as protein.

Homology modeling of mAb B, mAb C, and mAb D

Homology model based on known mAb B primary amino acid sequence was designed using program DeepView 4.0.1 (Swiss Institute of Bioinformatics) and the "iterative Magic fit" option [48]. Template used was pdb-file 1igt of a monoclonal antibody from RCSB Protein data bank. Homology model was built by iteratively superimposing best matching fragments of primary sequences of mAb B and 1igt using a PAM200 matrix, followed by a structural alignment to minimize the RMS deviation of carbon alpha and backbone atoms of the template and the model, using SWISS-MODEL structure homology-modeling server [48–50]. Same procedure was applied for primary sequences of mAb C and mAb D using 1igt as template.

Calculation of electrostatic potential of protein surfaces

pdb-file of lysozyme (2LYZ) from RCSB Protein data bank as well as homology models of mAb B, mAb C, and mAb D were used in DeepView 4.0.1 to compute the electrostatic potential at pH 7.0 using Coulomb potential with one dielectric constant for protein exterior and interior and atomic partial charges from the GROMOS43A1 force field [51, 52]. Protein surface was calculated using a probe size of 1.4 Å and electrostatic potential mapped to surface with a contour plot of sigma ±4.05.

Estimation of protein average charge, expressed as charge per amino acid, depending on pH

Protein average charges at different pH values were estimated using the primary amino acid sequences of lysozyme, mAb B, mAb C, and mAb D, respectively. Program protein calculator version 3.3 (Chris Putnam, Scripps Institute) was used and protein charge estimated according to Henderson–Hasselbalch equation using pKa's for isolated residues and termini as: N terminus 8.0, C terminus 3.1, lysine 10.0, arginine 12.0, histidine 6.5, glutamic acid 4.4, aspartic acid 4.4, tyrosine 10.0, and cysteine 8.5.

$$pH = pK_i + \log\left[\frac{\alpha_i}{1 - \alpha_i}\right] \qquad (1)$$

The fractional dissociation α of each amino acid was estimated according to Henderson–Hasselbalch and the net charge of the protein with n ionizable groups of type i estimated as

$$Z_p = \sum n_i \times z_i \times \alpha_i \qquad (2)$$

under the assumption that the pKa of the amino acids is not altered by the local protein and solvent environment [53].

Estimation was done for pH 5.0 and 7.0 and charge normalized by dividing overall charge Z_p by the number of amino acids to estimate average charge per amino acid (Z_c/a) and thereby compare average charge of proteins.

$$Z_c/a = Z_p \times \sum \alpha_i^{-1} \qquad (3)$$

There is an error in this estimation as effects of protein and solvent environment on pKa are not taken into account, interactions between protein molecules as well as hydrogen bonding between residues are not considered, and the estimated average charge is based on all protein residues, not only the residues present at the protein surface which are the ones interacting with polyelectrolytes. Estimating the average charge will result in small numbers, as most of the charges within the analyzed pH range neutralize themselves, with only few charges remaining. Additionally, the calculation does not consider if, e.g., one side of the protein is mainly positively charged and the other one mainly negatively charged. While this would still allow precipitation to happen, results of the calculation would only show low average charge due to charge neutralization. Yet, these estimated average protein charges are only used for better understanding of precipitation results, providing a more indicative than absolute basis of comparing precipitation results. Furthermore, similar antibody molecules with similar charge patterns are compared, not exhibiting the above-described division into a positively charged side and a mostly negatively charged side, thereby minimizing the risk charge neutralization. Therefore, the introduced errors in these estimations are seen as acceptable for the scope of this publication.

Viscosity measurements of polyelectrolyte solutions

The specific viscosity of PSS and PAA polyelectrolyte solutions, except for small PAA and PSS polyelectrolyte chains and PAA with weight average molecular weight of 958 kDa, was determined at different salt concentrations without added protein. The gained information on the extension or collapse of polyelectrolyte chains depending on the ionic strength is associated with a decrease in viscosity [54]. Viscosity was measured by dissolving the polyelectrolytes in sodium acetate buffer pH 5.0 to obtain final polyelectrolyte concentrations of 1.67 mg ml^{-1} and a final ionic strength of 0.65 or 2.6 mS cm^{-1}, respectively; additionally, polyelectrolytes were dissolved in water to obtain an ionic strength of almost 0 mM NaCl equivalents and final polyelectrolyte concentrations of 1.67 mg ml^{-1}. Viscosity was measured at 25 °C in a rheometer DV-III ultra using a CPE40 cone (viscosity range 0.1–3.07) (Brookfield, Middleboro, MA, USA). To take into account changes of viscosity occurring

with non-Newtonian fluids, measurements were performed at an initial cone rotation speed of 30 rpm, using 10 s intervals at each step and a speed increment of 1 rpm per step. Fifty steps were measured to cover rotation speeds of 30–80 rpm and analyze viscosity at different shear rates. Viscosity of polyelectrolytes depending on salt concentration was determined as average viscosity using the mean value of results of steps 3–50 obtained by each polyelectrolyte and specific salt concentration. Measurements were performed for all polyelectrolytes. Viscosities were presented as relative viscosity compared to the initial viscosity at 0 mM NaCl equivalents (set to 100 %) of each polyelectrolyte, respectively.

Results and discussion

Calculation of electrostatic potential of protein surfaces

The electrostatic potential of lysozyme (pI 10.7) as well as mAb B, mAb C, and mAb D (all pI 8–9) was calculated at pH 7.0 using a GROMOS43A1 force field for partial charges and the Coulomb potential in DeepView to correlate precipitation results with protein surface charge distribution and protein average charge estimation. Lysozyme obtained mainly positive surface charge (Fig. 1a). The three antibody homology models exhibited larger stretches of negative surface charges (indicated in red in Fig. 1b, d), mainly distributed at the Fc region of the antibodies, prevailed by positive surface potentials (indicated in blue in Fig. 1b, d) in the Fab region. mAb B (Fig. 1b) showed slightly more negative charge stretches than mAb C (Fig. 1c) and mAb D (Fig. 1d). Comparing mAb C with mAb D, mAb C showed negative stretches, both within the Fab region as well as the Fc region, while mAb D showed negative stretches only within the Fc region.

Estimation of protein average charge, expressed as charge per amino acid, depending on pH

Table 1 shows the protein average charge of the different antibodies, expressed as charge per amino acid, in correlation with the corresponding pH. Lysozyme shows the highest average charge at pH 5.0 (Table 1). A comparison of the different antibodies reveals a slightly higher average charge of mAb D compared to mAb C, also seen in cation exchange chromatography experiments, with mAb B obtaining the least average charge among the tested antibodies.

A comparison of the protein average charge at pH 7.0 shows a correlation between the surface charge potential calculations performed in DeepView and protein average charges estimated by protein calculator. The mostly positively charged lysozyme shows the highest average charge,

Fig. 1 Electrostatic potential of proteins at pH 7.0 calculated by DeepView v. 4.0.1 and SWISS-MODEL structure homology-modeling server, using GROMOS43A1 force field and Coulomb potential (protein sizes not to scale). Potential mapped to surface using contour plot sigma 4.05. *Red* -1.8 kTe^{-1}; *blue* $+1.8$ kTe^{-1}. **a** Lysozyme; **b** homology model of mAb B; **c** homology model of mAb C; **d** homology model of mAb D. Fab and Fc regions of mAbs additionally indicated
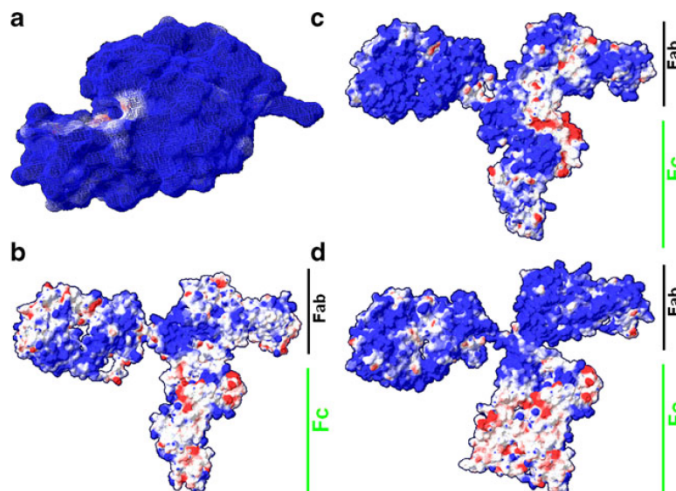
followed by mAb D, mAb C, and then mAb B, also reflected by surface charge potential presentations in Fig. 1.

Precipitation experiments

Comparing the precipitation yields of PSS and PAA polyelectrolytes of different weight average molecular weight at increasing ionic strength, we saw low precipitation yields for ionic strength less than 0.65 mS cm^{-1} (Figs. 2 and 3), which increased with higher ionic strength until a maximum phase was achieved around 1–2.6 mS cm^{-1}, depending on the type of protein, type of polyelectrolyte, as well as polyelectrolyte chain length (Figs. 2 and 3). The absolute measurement error at low ionic strength was approximately ±3 % on the *y*-axis, using a concentration line for protein concentration determination in the supernatant. Yet, including the measurement errors, the trend of increased precipitation yield at higher ionic strength compared to very low ionic strength is obvious for all tested proteins. The observed non-monotonic ionic strength dependence is known from various theoretical and practical experiments, as

protein precipitation decreases again with high ionic strength [24, 26–30]. It has also been confirmed by experiments using electrophoretic light scattering (ELS) analyzing PVS-BSA precipitation at pH 3.0 with then positively charged BSA and ionic strength ranging from $I=0.001$ mS cm^{-1} to $I=0.2$ mS cm^{-1} [55]. These ELS experiments showed free (non-precipitated) BSA at $I=0.001$–0.1 mS cm^{-1}, which was not visible at $I=0.2$ mS cm^{-1}, indicating a lower precipitation efficiency at low ionic strength compared to higher ionic strength.

Comparing the different proteins, a qualitative correlation of the precipitation yield with the estimated average charge of the corresponding proteins as well as their surface charge distribution of positively and negatively charged patterns, determined by DeepView, is visible. mAb D obtains the highest precipitation yield, using PSS, followed by mAb C and lysozyme. Unlike expected from protein average charge estimations, the yield for lysozyme is lower, most likely due to the suboptimal ratio of lysozyme molecules to polyelectrolyte molecules, which is due to the different molecular weights of lysozyme compared to the antibodies and thus a different molar ratio. mAb B shows the lowest precipitation, likely due to the presence of larger negative stretches at pH 5.0, thus leading to repulsion of the polyelectrolytes and thereby preventing sufficient precipitation.

Precipitation with mAb D, using PSS as polyelectrolytes, increased from 40 to 60 % at 0.22 mS cm^{-1} to >80 % at 0.98 mS cm^{-1} (Fig. 2a) using longer PSS 976 and 145 kDa polyelectrolyte chains. Shorter polyelectrolytes (15.2, 2.22 kDa) did not show large differences in precipitation yields, indicating good protein–polyelectrolyte interaction in the investigated ionic strength range. A comparison with the weak polyelectrolyte PAA showed lower mAb D precipitation yields of maximum

Table 1 Comparison of protein average charges, expressed as charge per amino acid, estimated using program Protein calculator v. 3.3 at pH 5.0 to compare lysozyme, mAb D, mAb C, and mAb B in experimental conditions

Protein average charge	Lysozyme	mAb D	mAb C	mAb B
pH 5.0	8.37×10^{-02}	4.57×10^{-02}	4.49×10^{-02}	4.34×10^{-02}
pH 7.0	6.12×10^{-02}	1.31×10^{-02}	1.20×10^{-02}	1.16×10^{-02}

Average charge at pH 7.0 given to compare to surface charge potential calculations with DeepView
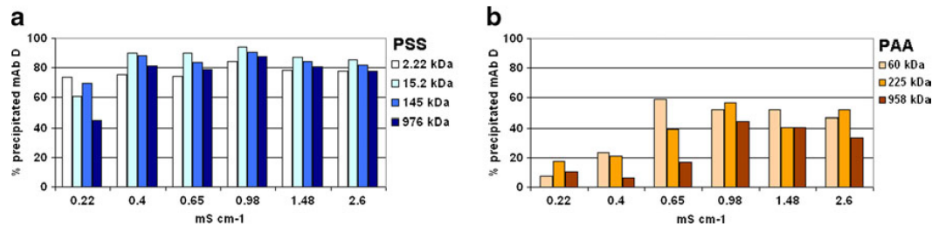
Fig. 2 Precipitation of mAb D with PSS (**a**) and PAA (**b**) polyelectrolytes at 0.4 mgml^{-1} per 1 mgml^{-1} protein (w/w) and ionic strengths from 0.22 to 2.6 mScm^{-1}. pH remained constant among the samples and was confirmed by pH measurements. Polyelectrolyte weight average molecular weight given, absolute error in measurement approximately ±3 % in low salt concentrations, and less at higher salt concentrations

60 % at 0.98 mScm^{-1} despite the visibility of increasing precipitation with increasing ionic strength (Fig. 2b). Additionally, it was observed with the three PAA polyelectrolytes that the larger the PAA polyelectrolyte, the higher ionic strength was required to achieve precipitation yield increase. For PAA 60 kDa, precipitation yield increase was observed at 0.4 mScm^{-1}, for PAA 225 kDa at 0.65 mScm^{-1} and for PAA 958 kDa at 0.98 mScm^{-1}. This indicates that higher ionic strength is required to achieve partial charge shielding and thereby polyelectrolyte flexibility for longer polyelectrolytes compared to shorter ones. In comparison to the weak polyelectrolyte PAA, the strong polyelectrolyte PSS exhibits stronger electrostatic forces which are likely able to overcome the loss of entropy associated with precipitation and absorption of particles [44]. In contrast, PAA shows an approximately 20 % lower charge density at pH 5.0 due to protonation of the carboxyl group (pKa~4.3).

mAb C precipitation increased from 20–40 % at 0.22 mS cm^{-1} to 40–80 % at 0.98 mScm^{-1} for PSS polyelectrolytes 2.22 and 15.2 kDa. PSS 145 and 976 kDa showed precipitation increase only at 2.6 mScm^{-1} (Fig. 3a). For lysozyme, precipitation increased from 5 % at 0.22 mScm^{-1} to approximately 40 % at 0.98 mScm^{-1} with obviously ionic strength difference only for the smallest PSS 2.22-kDa polyelectrolyte, showing increase already at 0.65 mScm^{-1} (Fig. 3b).

For mAb B, precipitation increased from 15–20 % at 0.22 mScm^{-1} to 20–40 % at 2.6 mScm^{-1} whereby the largest increase in precipitation yield was noticed with PSS 15.2 kDa (Fig. 3c). This indicates that the investigated ionic strength range was just enough to see effects for increasing
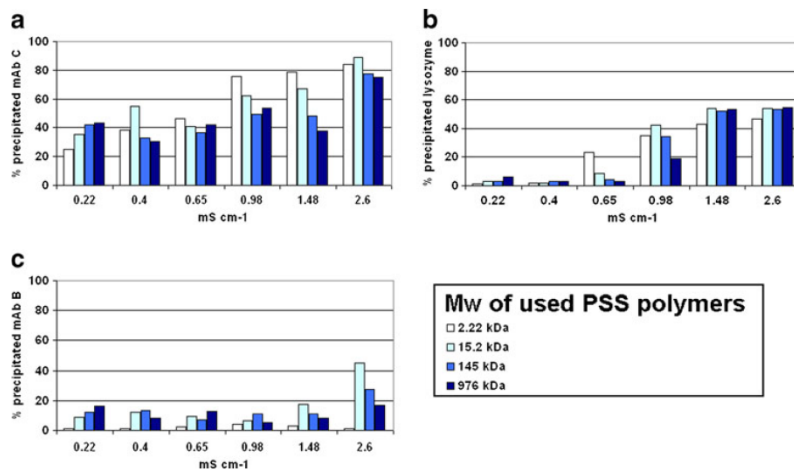
Fig. 3 Precipitation of different proteins using PSS polyelectrolytes at 0.4 mgml^{-1} per 1 mgml^{-1} protein (w/w) and ionic strengths from 0.22 to 2.6 mScm^{-1}. pH remained constant among the samples and was confirmed by pH measurements. Figures sorted according to precipitation yield using PSS polyelectrolytes, respectively: **a** mAb C; **b** lysozyme; **c** mAb B. PSS polyelectrolyte weight average molecular weight given. Absolute error in measurement was approximately ±3 % in low salt concentrations and less pronounced at higher salt concentrations. Lysozyme shows lower precipitation yields than expected according to protein average charge estimations due to suboptimal ratio of protein to polyelectrolyte compared to the monoclonal antibodies

$\underline{\textcircled{\tiny 2}}$ Springer

yield with small polyelectrolytes and proteins during precipitation. PSS 2.22 kDa did not show any increase in precipitation yield and almost no precipitation, likely due to difficulties in interacting with the less-charged mAb due to its relatively short length.

The first reason for the precipitation differences among the proteins might be the average charge of the different proteins and their isoelectric point, lysozyme with a pI of 10.7 still has sufficient positive charges distributed at pH 5.0, while the antibodies have different average charges, mAb B showing the lowest average charge and lowest precipitation yield compared with the other two mAb's. Secondly, the observed differences between polyelectrolytes of different chain length interacting with proteins could be related to different polyelectrolyte flexibility in different ionic strength.

Correlation between polyelectrolyte chain flexibility required for enhanced precipitation yields, with estimated average charge and hydrophobicity of the monoclonal antibodies

The three tested antibodies show almost similar molecular weight, shape, and size with similar pI's of 8–9 with mAb D having a ~0.2 U higher pI than mAb C and mAb B having a ~0.2 U lower pI than mAb C (data not shown). This is also reflected in the slightly higher positive protein average charge of mAb D at pH 5.0 compared to mAb C and mAb B according to bioinformatic estimations by protein calculator (Table 1) and thereby stronger electrostatic attraction, leading to better precipitation yields for mAb D. Additionally, according to hydrophobic interaction chromatography as well as the grand average of hydropathicity index, mAb D is more hydrophobic than mAb C and mAb B (data not shown), implying the additional presence of hydrophobic forces in precipitation with polyelectrolytes, shown by various experiments [56–58].

Comparing two different polyelectrolyte types and their precipitation yield for mAb D showed that higher ionic strength was required for PAA (0.65 mS cm^{-1}) compared to PSS (4 mS cm^{-1}), likely to obtain a flexibility, sufficient for leading to increasing precipitation yields (compare Fig. 2a, b). According to viscosimetry experiments in the literature, PAA exhibits a higher persistence length compared to PSS, due to the rigidity of the backbone, in the ionic strength regime of 0.5–10 mM NaCl equivalents, although the part of the persistence length due to electrostatic repulsion between neighboring charges of PSS is higher compared to PAA [43, 59, 60]. This has indirectly been confirmed in our experiments, as mAb D precipitation with PAA led to significantly lower precipitation yields compared to PSS.

To elucidate general ionic strength influence on mAb precipitation, precipitation in correlation with ionic strength for PSS 15.2 kDa was compared for the three antibodies (Fig. 4). PSS of intermediate M_w was chosen as it showed increasing precipitation yields for all mAbs, within the ionic strength range analyzed by our group. Larger PSS polyelectrolytes would have required higher ionic strength to obtain degrees of flexibility, allowing precipitation increase for mAbs, similar to the above-described PAA polyelectrolytes, while shorter chains would have been influenced by low precipitation efficiency due to chain length limitations.

Comparing precipitation with PSS 15.2 kDa, precipitation yields of around 90 % for mAb D are already found at ionic strength of 0.4 mS cm^{-1}, and precipitation with mAb C at that ionic strength is only at approximately 40–60 %. To achieve similar precipitation yields of 90 %, mAb C requires an ionic strength of 2.6 mS cm^{-1} (Fig. 4). In contrast, precipitation for mAb B is very low and starts to increase only at 1.5 mS cm^{-1}, however does not exceed 45 % within the ionic strength range analyzed. Expecting a somehow linear increase of mAb B precipitation with further increase of ionic strength, a theoretical ionic strength of around 4.5 mS cm^{-1} would be required, to achieve 90 % precipitation yields as seen with the two other mAbs (Fig. 4).
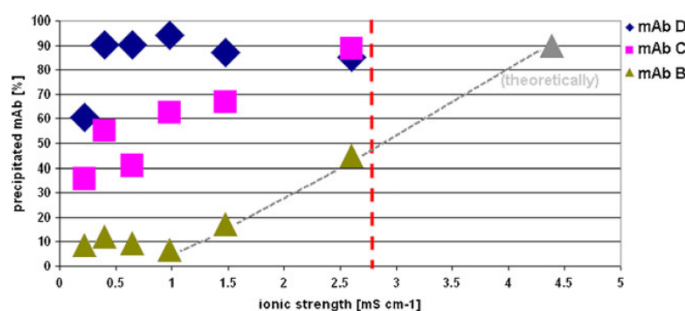
Fig. 4 Comparison of mAb precipitation yields, using PSS 15.2 kDa, at different ionic strengths. While mAb D obtains 90 % precipitation yield already at 0.4 mS cm^{-1}, mAb C requires 2.6 mS cm^{-1} to obtain similar high yields. Within the ionic strength range analyzed, mAb B obtained yields of only 45 % at 2.6 mS cm^{-1}. Extrapolating precipitation yield increase for mAb B, a theoretical yield of 90 % would be expected at around 4.5 mS cm^{-1} (highlighted in *gray*)

Comparing these results to the average charges of the mAbs, a qualitative correlation can be seen, with mAb D of higher average charge showing 90 % precipitation yields already at 0.4 mS cm^{-1}, mAb C with intermediate average charge obtaining 90 % precipitation at 2.6 mS cm^{-1}, and mAb B with lower average charge being expected to obtain precipitation yields of 90 % at around 4.5 mS cm^{-1}. Considering higher ionic strength leading to more flexible polyelectrolyte chains, a negative qualitative correlation of "required" polyelectrolyte chain flexibility depending on the estimated average charge at pH 5.0 and hydrophobicity of the monoclonal antibody can be concluded. This effect of required chain flexibility can also be observed comparing the ionic strength differences in precipitation yield increase depending on polyelectrolyte chain length. For mAb D, precipitation increase was noticed at similar ionic strength for all polyelectrolytes (regardless of M_{w}). For mAb C, the investigated ionic strength range indicated PSS 145 and 976 kDa showing an increase in precipitation yield at 2.6 mS cm^{-1}, in contrast to the two shorter PSS polyelectrolytes with an increase to 60–80 % at 0.98 mS cm^{-1} already. Additionally, mAb B with the lowest average charge required the highest ionic strength and polyelectrolyte flexibility to show increase of precipitation yields, however only to up to 45 %. Actually, in the investigated ionic strength range, only PSS 15.2 kDa was flexible enough to show precipitation yield increase. Similar behavior, showing increasing precipitation efficiency with polyelectrolyte chains of higher flexibility, has also been confirmed by Cooper et al. [61]. Reason for this is most likely that flexible polyelectrolytes can obtain chain conformations, allowing them to interact with positively charged surface patches of the antibody, while avoiding or "circumnavigating" negatively charged patches, e.g., via loop formation. Although mAb D shows presence of larger negative stretches within its Fc part, it allows direct interaction with the polyelectrolyte, likely at the Fab part, as the positively charged patches within the Fab region are all connected and not interrupted by negatively charged areas, compared to the two other mAbs (Fig. 1d). Thus, mAb D might allow precipitation similar to a necklace-like structure with the polymer annealing to the Fab region in a linear-like fashion, not requiring further loop formation. This is not the case for mAb B, showing disruption of the positively charged patches, both within Fc and Fab region, by large patches of negative surface potential (Fig. 1b). Thus, to allow strong interaction between polyelectrolyte and protein, a higher degree of polyelectrolyte flexibility is required to avoid these negative patches in mAb B, e.g., by formation of polyelectrolyte loops.

mAb C requires an intermediate polyelectrolyte flexibility, and minor loop formation might be needed to allow sufficient interaction, as both, Fab and Fc part, exhibit small negatively charged stretches interrupting the positively charged areas (Fig. 1c). Additionally to the qualitative correlation, a quantitative correlation might be expected, however, cannot surely be proven due to influences of mAb hydrophobicity and different degrees of charged residues present at mAb surfaces, not considered within the estimated protein average charges.

Viscosity measurements of polyelectrolyte solutions to analyze chain rigidity

Viscosity of polyelectrolyte solutions (except for PAA 958 kDa, PAA 123 kDa, PAA 2.1 kDa, and PSS 2.22 kDa) was measured in a rheometer at low, intermediate, and high ionic strength. Results showed a decrease in viscosity occurring when exposing the polyelectrolytes to higher salt concentrations. Viscosity of higher weight average molecular weight polyelectrolytes decreased from initially 100 to 50–70 %. A general trend of showing a decrease in viscosity of polyelectrolyte solutions when exposed to increasing ionic strength, as described in various literature sources, was obvious (Fig. 5) [54, 62]. This reduced viscosity is associated with a decrease in chain stiffness, also seen in MC simulations showing the rigidity of polyelectrolyte chains, depending on the ionic strength [32]. While viscosity decrease with longer polyelectrolytes was larger, shorter polyelectrolyte chains showed less decrease and lower influence of ionic strength on viscosity. This can be linked to our precipitation experiments, showing higher ionic strength required to achieve precipitation increase, likely due to polyelectrolyte rigidity changes for longer
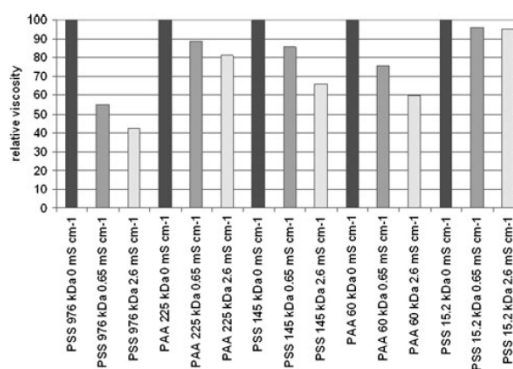

Fig. 5 Decrease in viscosity of different polyelectrolytes compared to initial viscosity of each polyelectrolyte (set to 100 %), at ionic strength of 0, 0.65, and 2.6 mS cm^{-1}, respectively. A general trend of decreasing viscosity when increasing the ionic strength is seen

chains. Shorter chains however, as in the case with mAb D (Fig. 3a) are less prone to ionic strength influence on rigidity, thus showing lower decrease in viscosity and minor ionic strength influence on precipitation yield only.

Conclusions

Using three different monoclonal antibodies and lysozyme, all with different isoelectric point and surface charge distributions, our precipitation experiments confirmed the effect of low ionic strength leading to reduced precipitation yields due to impeded polyelectrolyte–protein interaction, compared to medium and high ionic strength. Precipitation yields increased from 5–40 % at 0–0.65 mS cm^{-1} to up to >80 % at ionic strengths of 0.98 mS cm^{-1} or higher. Polyelectrolyte viscosity determinations at precipitation conditions showed higher viscosity at 0 mM NaCl equivalents and 0.65 mS cm^{-1} compared to 2.6 mS cm^{-1}, associated with elevated stiffness, leading to worse protein–polyelectrolyte interaction and reduced ability of polyelectrolytes to conform to protein surfaces as predicted by Monte Carlo simulations. PAA polyelectrolytes with higher intrinsic chain stiffness compared to PSS, according to the literature, and lower charge density than PSS showed reduced precipitation yields. Higher salt concentrations were required to achieve certain polyelectrolyte flexibility for PAA and thus an increase in precipitation yield, when compared to PSS. Comparing precipitation results of three different monoclonal antibodies, a qualitative negative correlation of ionic strength induced polyelectrolyte flexibility required for high precipitation yields, depending on the estimated average charge and hydrophobicity of the monoclonal antibody, was observed. While mAb D with higher hydrophobicity and higher average charge showed precipitation yields of 90 % already at 0.4 mS cm^{-1}, mAb C required 2.6 mS cm^{-1}, thus leading to higher degree of polyelectrolyte flexibility, to achieve high similar high precipitation yields. mAb B required even higher polyelectrolyte flexibility and thus higher ionic strengths, outside the ionic strength range tested by us; extrapolation of results led to theoretical yields of 90 % at around 4.5 mS cm^{-1}. Additionally, precipitation increase with longer polyelectrolytes was shown to require higher ionic strength due to chain rigidity. In contrast, shorter chains with lower intrinsic rigidity achieved increasing precipitation yields already at lower ionic strength. These insights might help to further improve precipitation processes; design polyelectrolytes with defined flexibility to, e.g., obtain ionic strength triggered semi-selective protein precipitation behavior, avoid salt concentration associated precipitation difficulties and design polyelectrolytes interacting semi-selectively with surface charge distributions of specific target proteins.

References

1. Shahidi F, Synowiecki J (1991) Isolation and characterization of nutrients and value-added products from snow crab (*Chionoecetes opilio*) and shrimp (*Pandalus borealis*) processing discards. J Agric Food Chem 39:1527–1532. doi:10.1021/jf00008a032
2. Sudharshan NR, Hoover DG, Knorr D (1992) Antibacterial action of chitosan. Food Biotechnol 6:257–272. doi:10.1080/08905439209549838
3. Papineau AM, Hoover DG, Knorr D, Farkas DF (1991) Antimicrobial effect of water-soluble chitosans with high hydrostatic pressure. Food Biotechnol 5:45–57. doi:10.1080/08905439109549790
4. Gross RA, Kalra B (2002) Biodegradable polymers for the environment. Science 297:803–807. doi:10.1126/science.297.5582.803
5. Muzzarelli RAA, Weckx M, Fillipini O, Lough C (1989) Characteristic properties of N-carboxybutyl chitosan. Carbohydr Poly 11:293–296. doi:10.1016/0144-8617(89)90005-2
6. Bolto B, Gregory J (2007) Organic polyelectrolytes in water treatment. Water Research 41:2301–2324. doi:10.1016/j.watres.2007.03.012
7. Allen TM, Cullis PR (2004) Drug delivery systems: entering the mainstream. Science 303:1818–1822. doi:10.1126/science.1095833
8. Jeong B, Bae YH, Lee DS, Kim SW (1997) Biodegradable block copolymers as injectable drug-delivery systems. Nature 388:860–862. doi:10.1038/42218
9. Schmaljohann D (2006) Thermo- and pH-responsive polymers in drug delivery. Adv Drug Delivery Rev 58:1655–1670. doi:10.1016/j.addr.2006.09.020
10. Gillies ER, Fréchet JM (2005) Dendrimers and dendritic polymers in drug delivery. J Drug Discovery Today 10:35–43. doi:10.1016/S1359-6446(04)03276-3
11. Svec F, Fréchet JM (1992) Continuous rods of macroporous polymer as high-performance liquid chromatography separation media. J Anal Chem 64:820–822. doi:10.1021/ac00031a022
12. Šmigol V, Švec F, Hosoya K, Wang Q, Fréchet JM (1992) Monodisperse polymer beads as packing material for high-performance liquid chromatography. Synthesis and properties of monodisperse polystyrene and poly(methacrylate) latex seeds. Die Angewandte Makromolekulare Chemie 195:151–164. doi:10.1002/apmc.1992.051950112
13. Barrande M, Beurroies I, Denoyel R, Tatárová I, Gramblička M, Polakovič M, Joehnck M, Schulte M (2009) Characterisation of porous materials for bioseparation. J Chromatogr A 1216:6906–6916. doi:10.1016/j.chroma.2009.07.075
14. Kamath N, D'Souza SF (1991) Immobilization of ureolytic cells through flocculation and adhesion on cotton cloth using polyethylenimine. Enzyme Microb Technol 13:935–938. doi:10.1016/0141-0229(91)90112-N
15. Ovenden C, Xiao H (2002) Flocculation behaviour and mechanisms of cationic inorganic microparticle/polymer systems. Colloids and Surfaces A 197:225–234. doi:10.1016/S0927-7757(01)00903-7
16. Hönig W, Kula RM (1976) Selectivity of protein precipitation with polyethylene glycol fractions of various molecular weights. Anal Biochem 72:502–512. doi:10.1016/0003-2697(76)90560-1
17. Gervais DP, Pfeiffer KA (2010) (Pfizer Limited) US patent 20100204455, August 12

18. Fahrner R, Franklin J, McDonald P, Peram T, Sisodiya V, Victa C (2008) (Genentech, Inc.) International patent WO/2008/091,740, January 10

19. Gronke RS, Jaquez OA (2009) (Biogen Idec MA Inc.) US Patent 12/425,328, April 16

20. Ramanan S, Stenson R (2008) (Amgen Inc.) International patent WO/2008/100,578, August 21

21. McDonald P, Victa C, Carter-Franklin JN, Fahrner R (2009) Selective antibody precipitation using polyelectrolytes: a novel approach to the purification of monoclonal antibodies. Biotechnol Bioeng 102:1141–1151. doi:10.1002/bit.22127

22. Peram T, McDonald P, Carter-Franklin J, Fahrner R (2010) Monoclonal antibody purification using cationic polyelectrolytes: an alternative to column chromatography. Biotechnol Prog 26:1322–1331. doi:10.1002/btpr.437

23. Netz RR, Joanny JF (1999) Complexation between a semiflexible polyelectrolyte and an oppositely charged sphere. Macromolecules 32:9026–9040. doi:10.1021/ma990264+

24. Carlsson F, Linse P, Malmsten M (2001) Monte Carlo simulations of polyelectrolyte–protein complexation. J Phys Chem B 105:9040–9049. doi:10.1021/jp010360o

25. Seyrek E, Dubin PL, Tribet C, Gamble EA (2003) Ionic strength dependence of protein–polyelectrolyte interactions. Biomacromolecules 4:273–282. doi:10.1021/bm025664a

26. Hattori T, Hallberg R, Dubin PL (2000) Roles of electrostatic interaction and polymer structure in the binding of β-lactoglobulin to anionic polyelectrolytes: measurement of binding constants by frontal analysis continuous capillary electrophoresis. Langmuir 16:9738–9743. doi:10.1021/la000648p

27. Dobrynin AV, Rubinstein M (2003) Effect of short-range interactions on polyelectrolyte adsorption at charged surfaces. J Phys Chem B 107:8260–8269. doi:10.1021/jp0225323

28. Moss JM, VanDamme MP, Murphy WH, Preston BN (1997) Dependence of salt concentration on glycosaminoglycan–lysozyme interactions in cartilage. Arch Biochem Biophys 348:49–55. doi:10.1006/abbi.1997.0365

29. Marky NL, Manning GS (2000) An interpretation of small-ion effects on the electrostatics of the λ repressor DNA complex. J Am Chem Soc 122:6057–6066. doi:10.1021/ja9942437

30. Antonov M, Mazzawi M, Dubin PL (2009) Entering and exiting the protein–polyelectrolyte coacervate phase via nonmonotonic salt dependence of critical conditions. Biomacromolecules 11:51–59. doi:10.1021/bm900886k

31. Schiessel H, Pincus P (1998) Counterion-condensation-induced collapse of highly charged polyelectrolytes. Macromolecules 31:7953–7959. doi:10.1021/ma980823x

32. Stoll S, Chodanowski P (2002) Polyelectrolyte adsorption on an oppositely charged spherical particle Chain Rigidity Effects Macromolecules 35:9556–9562. doi:10.1021/ma020272h

33. Cooper CL, Dubin PL, Kayitmazer AB, Turksen S (2005) Polyelectrolyte–protein complexes. Curr Opin Colloid Interface Sci 10:52–78. doi:10.1016/j.cocis.2005.05.007

34. Liao Q, Dobrynin AV, Rubinstein M (2003) Molecular dynamics simulations of polyelectrolyte solutions: nonuniform stretching of chains and scaling behavior. Macromolecules 36:3386–3398. doi:10.1021/ma025995f

35. Baeurle SA, Nogovitsin EA (2007) Challenging scaling laws of flexible polyelectrolyte solutions with effective renormalization concepts. Polymer 48:4883–4899. doi:10.1016/j.polymer.2007.05.080

36. Carlsson F, Malmsten M, Linse P (2003) Protein–polyelectrolyte cluster formation and redissolution: a Monte Carlo study. J Am Chem Soc 125:3140–3149. doi:10.1021/ja020935a

37. de Gennes PG, Pincus P, Velasco RM, Brochard F (1976) Remarks on polyelectrolyte conformation. J Physique 37:1461–1473. doi:10.1051/jphys:0197600370120146100

38. Jonsson M, Linse P (2001) Polyelectrolyte–macroion complexation. II. Effect of chain flexibility. J Chem Phys 115:10975–10985. doi:10.1063/1.1417508

39. Akinchina A, Linse P (2002) Monte Carlo simulations of polyion–macroion complexes. 1. Equal absolute polyion and macroion charges. Macromolecules 35:5183–5193. doi:10.1021/ma012052u

40. Skepö M, Linse P (2003) Complexation, phase separation, and redissolution in polyelectrolyte–macroion solutions. Macromolecules 36:508–519. doi:10.1021/ma020634l

41. Kayitmazer AB, Seyrek E, Dubin PL, Staggemeier BA (2003) Influence of chain stiffness on the interaction of polyelectrolytes with oppositely charged micelles and proteins. J Phys Chem B 107:8158–8165. doi:10.1021/jp034065a

42. Barrat JL, Joanny JF (1993) Persistence length of polyelectrolyte chains Europhys Lett 24:333–338. doi:10.1209/0295-5075/24/5/003

43. Drifford M, Delsanti M (2001) Polyelectrolyte solutions with multivalent added salts: stability, structure, and dynamics. In: Radeva T (ed) Physical chemistry of polyelectrolytes, surfactant science series. Marcel Dekker, New York, pp 149–161

44. Chodanowski P, Stoll S (2001) Polyelectrolyte adsorption on charged particles in the Debye–Hückel approximation. A Monte Carlo approach. Macromolecules 34:2320–2328. doi:10.1021/ma000482z

45. von Goeler F, Muthukumar M (1995) Polyelectrolyte brush density profiles. Macromolecules 28:6608–6617. doi:10.1021/ma00123a031

46. Kong CY, Muthukumar M (1998) Monte Carlo study of adsorption of a polyelectrolyte onto charged surfaces. J Chem Phys 109:1522–1527. doi:10.1063/1.476703

47. Minakata A, Takahashi H, Nishio T, Nagaya J, Tanioka A (2002) Effect of salts on the conductance of polyelectrolyte solutions. Colloids Surf A 209:213–218

48. Guex N, Peitsch MC (1997) SWISS-MODEL and the Swiss-Pdb Viewer: an environment for comparative protein modeling. Electrophoresis 18:2714–2723. doi:10.1002/elps.1150181505

49. Kiefer F, Arnold K, Künzli M, Bordoli L, Schwede T (2009) The SWISS-MODEL repository and associated resources. Nucleic Acids Res 37:D387–D392

50. Bordoli L, Kiefer F, Arnold K, Benkert P, Battey J, Schwede T (2008) Protein structure homology modeling using SWISS-MODEL workspace. Nat Protocols 4:1–13. doi:10.1038/nprot.2008.197

51. Daura X, Mark AE, van Gunsteren WF (1998) Parametrization of aliphatic CHn united atoms of GROMOS96 force field. J Comput Chem 19:535–547. doi:10.1002/(SICI)1096-987X(19980415

52. Scott WRP, Hünenberger PH, Tironi IG, Mark AE, Billeter SR, Fennen J, Torda AE, Huber T, Krüger P, van Gunsteren WF (1999) The GROMOS biomolecular simulation program package. J Phys Chem A 103:3596–3607. doi:10.1021/jp984217f

53. Tanford C, Kirkwood JG (1957) Theory of protein titration curves. I. General equations for impenetrable spheres. J Am Chem Soc 79:5333–5347. doi:10.1021/ja01577a001

54. Kogej K, Skerjanc J (2001) Surfactant binding to polyelectrolytes. In: Radeva T (ed) Physical chemistry of polyelectrolytes, surfactant science series. Marcel Dekker, New York, pp 793–828

55. Matsunami H, Kikuchi R, Ogawa K, Kokufuta E (2007) Light scattering study of complex formation between protein and polyelectrolyte at various ionic strengths Colloids Surf B 56:142–148. doi:10.1016/j.colsurfb.2006.10.003

56. Tribet C (2001) Complexation between amphiphilic polyelectrolytes and proteins: from necklaces to gels. In: Radeva T (ed) Physical chemistry of polyelectrolytes, surfactant science series. Marcel Dekker, New York, pp 687–742

57. Petit F, Audebert R, Iliopoulos I (1995) Interactions of hydro-phobically modified poly(sodium acrylate) with globular proteins. Colloid Polym Sci 273:777–781. doi:10.1007/BF00658756

58. Tribet C, Porcar I, Bonnefont PA, Audebert R (1998) Association between hydrophobically modified polyanions and negatively charged bovine serum albumin. J Phys Chem B 102:1327–1333. doi:10.1021/jp973022p

59. Tricot M (1984) Comparison of experimental and theoretical per-sistence length of some polyelectrolytes at various ionic strengths. Macromolecules 17:1698–1704. doi:10.1021/ma00139a010

60. Le Bret M (1982) Electrostatic contribution to the persistence length of a polyelectrolyte. J Chem Phys 76:6243–6255. doi:10.1063/1.443027

61. Cooper CL, Goulding A, Kayitmazer AB, Ulrich S, Stoll S, Turksen S, Yusa S, Kumar A, Dubin PL (2006) Effects of poly-electrolyte chain stiffness, charge mobility, and charge sequences on binding to proteins and micelles. Biomacromolecules 7:1025–1035. doi:10.1021/bm050592j

62. Förster S, Schmidt M (1995) Polyelectrolytes in solution. Adv Polym Sci 120:52–128. doi:10.1007/3-540-58704-7_2

3.3. Effects of polymer chain length on precipitation

Paper: Determining the defined length of a polymer chain required per precipitated protein molecule: studying interactions between anionic polymers and four physicochemically different proteins

Florian Capito, Harald Kolmar, Bernd Stanislawski and Romas Skudas

Short summary:

In order to understand effects of polymer chain length on precipitation, different polymer standards with defined chain lengths were used for precipitation of four different proteins. The polymer chain length required per precipitated protein molecule (L_{def}) during protein-polymer interaction was found to be up to 25-times larger than the diameter of the corresponding protein, depending on the surface charge distribution of the protein, its isoelectric point as well as the charge density of the polymer. Electrophoretic light scattering showed a qualitative correlation of the zeta potential of analyzed polymers with their corresponding L_{def} values. If polymer chain length fell below a certain threshold, precipitation was sub-optimal and L_{def} required for precipitation was larger compared to polymers of same type with longer chain lengths. These findings support proposed mechanisms of polymer wrapping and loop formation for optimal charge neutralization during precipitation and are helpful for developing the later intended protein precipitation process.

Determining the defined length of a polymer chain required per precipitated protein molecule: studying interactions between anionic polymers and four physicochemically different proteins

Florian Capito[1][2]*, Harald Kolmar[1], Bernd Stanislawski[2], Romas Skudas[2]

[1] Clemens-Schöpf Institute, Technical University of Darmstadt, Germany

[2] Merck KGaA, Frankfurter Strasse 250, 64293 Darmstadt, Germany

Correspondence to: Florian Capito (E-mail: florian.capito@external.merckgroup.com)

phone: 0049 6151 72 7168

fax: 0049 6151 72 917510

ABSTRACT

Protein precipitation using non-charged and charged polymers is a common method for protein purification, gaining broader interest among manufacturers in downstream processing. While during polymer- surface interactions, the formation of loops, tails and trains has been known for quite a long time, details of polymer conformation and chain length, interacting with the protein during protein precipitation are not fully discovered. Our research presents deeper understanding of polymer-protein interaction, combining fluorescence and infrared spectroscopic measurements of proteins and well-defined polymer standards with well defined chain length to confirm different models of protein-polymer interaction. Lysozyme, chymotrypsinogen A, myoglobin and a monoclonal antibody, all of different molecular weight, isoelectric point and charge distribution at the protein surface, were used for protein-polymer precipitation. The use of polymers of various charge density and chain length showed that the polymer chain length required per precipitated protein (L_{def}) is up to 25-times larger than the diameter of the corresponding protein, depending on the surface charge distribution of the protein, its isoelectric point as well as the charge density of the polymer. Our results support proposed mechanisms of polymer wrapping and loop formation for optimal charge neutralization during complexation and imply the involvement of several polymer chains per precipitated protein molecule. Electrophoretic light scattering showed a qualitative correlation of the zeta potential of analyzed polymers with their corresponding L_{def} values. Comparing protein precipitation behavior of long and short polymer chains, the latter exhibited reduced precipitation efficiency, visible as elevated L_{def}.

Cumulative part- Experimental 99

INTRODUCTION

The formation of an initial protein-polymer complex with several proteins bound per polymer chain at a specific pH depends on ionic strength, polymer charge density, flexibility as well as polymer chain length and charge distribution of the protein [1-7]. The complexity of this interaction is being explained by various *in silico* simulations, indicating a winding of polymers around macroions of opposite charge, while other results show a gel-like structure with polymers connecting proteins which act as cross-linkers [8-11]. Additional studies showed the formation of trains, loops and tails in polymer conformation, the loops interacting with the macroion, *e.g.* protein while the latter are extending from the macroion surface [12-15]. It was shown that in cases where polymer chain length was significantly longer than the diameter of the macroion, only few monomers are binding to the macroion, associated with a high degree of tail formation of the polymer chain [16-17]. Deeper insights into polymer- protein interaction are vital to improve understanding of precipitation processes [18-19]. Therefore, an investigation of various bioactive molecules, different in size as well as in the surface charge distribution would be of great value and importance. For a better understanding of complex formation during protein-polyelectrolyte precipitation, electrophoretic light scattering (ELS) and mobility measurement of protein-polyelectrolyte complexes can be applied [5, 20], as the electrophoretic mobility of polymers correlates qualitatively with their charge density [20]. Additionally as FTIR can e.g. be used to analyze polymers [21], it has been used to quantify polymer amounts in protein-polymer pellet after precipitation.

Thus, we show protein-polymer precipitation applications, combining fluorescence measurements, infrared spectroscopy, modeling and ELS to determine polymer-protein ratios during precipitation and get deeper insights into polymer and protein conformation, relating precipitation strength to polymer chain length, polymer charge density, the isoelectric point (*pI*) of the protein as well as protein surface charge distribution.

EXPERIMENTAL

Proteins

Lysozyme (M_w 14.3 kDa) was obtained from Merck KGaA, Darmstadt, Germany; IgG1 monoclonal antibody mAb A (M_w 150 kDa) was obtained from Merck Millipore, Bedford, USA; myoglobin (M_w 17.05 kDa) from horse skeletal muscle was obtained from Calbiochem, Merck KGaA, Darmstadt, Germany; chymotrypsinogen A (M_w 25 kDa) from bovine pancreas was obtained from Biotrend Chemikalien, Cologne, Germany. Lysozyme, myoglobin and chymotrypsinogen A were obtained as

lyophilized powder after purification via repeated crystallization (purity > 98 % as determined by SDS-PAGE), mAb A was derived from drug substance solution to ensure high degree of purity).

Polymers

Polymers poly- (styrenesulfonic acid) (PSS) with weight average molecular weights of Mw = 1,360 g mol^{-1}, 2,260 g mol^{-1}, 6,530 g mol^{-1}, 10,600 g mol^{-1}, 15,200 g mol^{-1}, 43,300 g mol^{-1} and 976,000 g mol^{-1}, respectively, as well as polymers poly- (acrylic acid) (PAA) with weight average molecular weights of Mw = 1,930 g mol^{-1}, 3,800 g mol^{-1}, 8,300 g mol^{-1}, 18,100 g mol^{-1}, 36,900 g mol^{-1}, 123,000 g mol^{-1} and 958,000 g mol^{-1} respectively, were obtained as polymer standards with polydispersity indices < 1.20 from Polymer Standard Service, Mainz, Germany. Poly- (vinylsulfonic acid) (PVS) with weight average molecular weight of Mw = 2,100 g mol^{-1} was obtained from Polysciences, Warrington, USA; poly- (anetholesulfonic acid) (PASA) with weight average molecular weight of 30,537 g mol^{-1} as determined by SEC, was obtained from Sigma Aldrich, Steinheim, Germany.

Buffers

Precipitation was performed in 20 mM Na-acetate buffer pH 5.0 with a salt concentration of 20 mM NaCl.

Labeling of proteins

Proteins lysozyme, myoglobin, chymotrypsinogen A and mAb A were labeled using the succinimidyl ester Alexa fluor® 546 from Invitrogen, Carlsbad, USA. Labeling was done by dissolving the fluorophore in 500 µL DMSO and adding it to 1g protein, dissolved in Milli-Q water. Unbound fluorophore was removed using a PD-10 column (Amersham Biosciences, Uppsala, Sweden) with Sephadex G25 column material for gel filtration. pH of labeled proteins was then adjusted to pH 5.0 and concentration adjusted to 2 mg ml^{-1} protein. Ionic strength of adjusted labeled protein solutions was in the range of 0.1- 0.4 mS cm^{-1}.

Labeling of poly- (acrylic acid)

Poly- (acrylic acid) was labeled using fluorophore Cascade ® Blue (Invitrogen, Carlsbad, USA) and 1-Ethyl-3-[3-dimethylaminopropyl]carbodiimide hydrochloride (Merck KGaA, Darmstadt, Germany) coupling according to manufacturers protocol to obtain a degree of labeling of approximately two fluorophores per polymer chain.

Unbound fluorophore was removed using gel filtration and a PD-10 column (Amersham Biosciences, Uppsala, Sweden), before adjusting pH of PAA polymer to pH 5.0.

Determination of accumulating PSS, PVS and PASA using Fourier transform infrared spectroscopy (FTIR)

Accumulation of PSS, PVS or PASA within protein-polymer pellet was determined using FTIR to measure peak intensities within the spectrum attributed to sulphonic acid groups in comparison to polymer standards of the same polymer. Supernatant of samples was measured using attenuated total reflection- FTIR using GoldenGate™ ATR MkII series (Specac Inc, Cranston, RI, USA). Spectra were measured at 20 °C with 20 mM Na-acetate buffer and 20 mM NaCl as background. Spectra were recorded in absorbance mode on Bruker Tensor 27 (Bruker Optik GmbH, Ettlingen, Germany) using a 120 scans at spectral resolution of 4.0, employing a Bruker LN-MCT photovoltaic internal detector (Bruker Optik GmbH, Ettlingen, Germany), with an aperture set to 6 mm. After spectra recording and subtraction of the background spectrum, automatic atmospheric compensation was performed and samples smoothed using 17 smoothing points. Data were merged as mean values of multiple measurements. Residual polymer in supernatant was determined using Quant 1 method within OPUS spectral processing software v. 6.0 (Bruker Optik GmbH, Ettlingen, Germany), measuring the height of peaks corresponding to: PSS (1,024- 1,035 cm^{-1}); PVS (1,195- 1,180 cm^{-1}) and PASA (1,180 and 1,100 cm^{-1}). Thereby residual polymer within supernatant was determined, allowing quantification of the polymer fraction of initial polymer, which accumulated within the pellet.

Estimation of protein diameter and protein charge density at pH 5.0

Protein diameters were calculated using Deep View version 4.0.1 (Swiss Institute of Bioinformatics) and used to estimate the end-to-end distance of proteins lysozyme (2lyz), myoglobin (1mbo) and chymotrypsinogen A (1ex3), using the pdb- files (pdb codes in brackets) from protein data bank. Protein diameters were estimated measuring the largest possible distance between two residues in the protein. mAb A diameter was estimated after performing a homology model based on the primary sequence of the antibody (known but not enclosed). The template for the homology model was a crystal structure of a monoclonal antibody from protein data bank (pdb code 1igt). A homology model was built performing an "iterative magic fit" in program Deep View using a PAM200 matrix and minimizing the RMS deviation of the carbon alpha and backbone atoms of model and template followed by a structural alignment to optimize the homology model using Swiss Model protein structure homology- modeling server [22-24]. Protein charge density at pH 5.0 was estimated using corresponding pdb-files, including homology model, from Swiss-Model homology- modeling server within program Adaptive Poisson- Boltzmann Solver (APBS), after assigning protonation states to residues at pH 5.0, using program propka within pdb-pqr converter [25-30]. Charge densities at pH 5.0

were presented using program Chimera, which enabled visualization of electrostatic calculations done by APBS [31-32].

Protein precipitation

Pilot experiments were carried out to determine the optimum polymer amount to be added to achieve highest precipitation yields with a given protein- polymer pair. These experiments were set up at pH 5.0 and 20 mM NaCl as standard conditions to adjust polymer concentration accordingly, allowing for determination of molar ratios of protein and polymer at optimum protein-polymer ratios. Experiments were conducted as follows:

Precipitation was done by adding 300 μL of labeled protein solution (pH 5.0) to 120 μL of 120 mM (five-times concentrated) Na-acetate buffer pH 5.0 with 20 mM NaCl final concentration. To start precipitation, 180 μL of polymer solution, adjusted to pH 5.0, (labeled or non-labeled) were added to the mixture and placed on a shaker at 300 rpm for 60 minutes. Afterwards the sample was centrifuged at 2500 rcf for 15 minutes and the supernatant was transferred to microtiter plates (Nunc GmbH, Langenselbold, Germany). pH was measured immediately after mixing and additionally in the supernatant after centrifugation. Fluorescence counts of protein and, in case of labeled PAA polymer, of polymer were determined and compared to standards with known protein and polymer amount, using Tecan Reader Infinite M200 (Tecan Group Ltd., Männedorf, Switzerland). The amount of precipitated protein was calculated by comparing the fluorescence decrease from the supernatant after precipitation with the initial fluorescence. For fluorescently labeled polymer, the same procedure was applied to determine the amount of precipitated polymer.

Calculation of molar ratios of protein to polymer

Protein to polymer molar ratios were calculated for optimum polymer concentrations, corresponding to the highest precipitation yield, using polymer Mw and the protein Mw. Calculation was performed taking into account the overall polymer concentration, and the protein concentration within the pellet in the samples as determined by fluorescence count decrease in the supernatant, using labeled protein:

Although an error was introduced in this calculation by using the overall polymer concentration for calculating the molar ratios, instead of using the fraction of polymer accumulated in the pellet, this error was minimized by calculating molar ratios at polymer concentrations, where most (> 80- 90 %) of initial polymer accumulated within the protein- polymer pellet (see results).

Calculation of the defined polymer chain length required per precipitated protein molecule (L_{def})

Knowing the molecular weight of the monomers in each polymer, the number of monomers in an average polymer chain was calculated, dividing polymer Mw by the molecular weight of the monomer. Assuming a bond length of 154 pm per C-C bond and an angle of 108°, each monomer requires ~ 2.9 Å of chain length in the polymer chain. $((sin108) * (1.54 + 1.54 * 0.5 + 1.54* 0.5)) = 2.93$ Å

The number of monomers in each polymer was multiplied with the length of each monomer to get the overall length based on 108° angles.

Determination of polymer charge density using electrophoretic mobility measurements

Electrophoretic mobility and zeta potential of polymer stock solutions (5 mg ml^{-1}) of PASA, PSS, PAA and PVS of different Mw was measured using Zetasizer Nano (Malvern Instruments GmbH, Herrenberg, Germany) at pH 5.0 to compare charge density of different polymers at precipitation conditions.

Determination of protein charge density using electrophoretic mobility measurements

Electrophoretic mobility and zeta potential of proteins lysozyme, myoglobin, chymotrypsinogen A and mAb A was measured at a protein concentration of 2-5 mg ml^{-1}, using Zetasizer Nano (Malvern Instruments GmbH, Herrenberg, Germany) at pH 5.0 to compare charge density of proteins at pH equal to pH during precipitation conditions with *in silico* surface charge distribution estimations.

RESULTS AND DISCUSSION

Pilot experiments to determine optimum ratio of protein and polymer

Optimum polymer amounts to be added for a given protein-polymer pair were determined using pilot experiments. pH measurements of protein-polymer mixtures during precipitation and after centrifugation, using the supernatant, revealed no pH-change compared to protein and polymer solutions before starting precipitation.

Precipitation conditions

To analyze optimal precipitation conditions and allow calculation of molar ratios as well as polymer lengths per precipitated protein, protein diameters were estimated using Deep View and the corresponding crystallographic data of lysozyme, myoglobin, chymotrypsinogen A and, in case of mAb A, a homology model (Fig. 4). As a reference value the largest possible distance between two residues in the protein was considered. For lysozyme, 50 Å were measured, in contrast to the 31-32 Å

as stated in the literature [33-34], yet, considering that the longest distance was measured, instead of an average value, these numbers are still in acceptable agreement. For myoglobin, 44 Å were measured which were comparable to the 35 Å stated by Papadopoulos et al. [2000] [35]. For chymotrypsinogen A and mAb A, obtained diameters were also in acceptable agreement with reference values. For mAb A, measured diameter was 160 Å, compared to the stated 140 Å by Striemer et al. (2007) [36]. For chymotrypsinogen A, measured diameter was 42 Å, comparable to the 38.6 Å as determined by Roth and Lenhoff (1995) [33].

Determination of the optimum polymer concentration enabling highest precipitation yields, using PSS or PAA polymers was done. Maximum precipitation yields of 82- 90 %, at polymer concentrations of 0.15- 0.75 mg ml^{-1}, depending on the Mw of PSS or PAA, were obtained (data not shown). Further increase of the polymer concentration led to a decrease in precipitation yield due to overcharging, observed during *in silico* and *in vitro* experiments [37-38].

To calculate the molar ratios of protein vs. polymer within the pellet, the relative fraction of polymer accumulating within the pellet after precipitation, was determined. Results analyzing PAA accumulation when precipitating mAb A showed that the relative fraction of polymer in the pellet, compared to the initially added polymer concentration, decreased with increasing polymer concentration added to the reaction solution (Fig. 1). Additionally, measurements using FTIR and fluorescently labeled polymer to determine PAA, PSS, PASA and PVS accumulation in the pellet after precipitation with either lysozyme, mAb A, chymotrypsinogen A or myoglobin, respectively, showed a > 80- 90 % polymer accumulation within the pellet if polymer concentrations were below the pre-selected optimum polymer concentration range for each of these polymers, corresponding to highest precipitation yields, respectively (Fig. 1, S1 in supplementary material). Therefore, molar ratios of polymer and protein were calculated based on polymer concentrations below the respective optimum concentration to minimize the error within the calculations due to overestimation of polymer within the pellet. The resulting error within calculations, based on the pre-selected polymer concentration range, was below 20 %, with most of the calculations showing an error below 10 % regarding polymer overestimation.

Using polymer Mw and the molecular weight of proteins, the molar ratio of protein to polymer was calculated according to formula 1 (table 1). Potential errors due to polymer overestimation in the pellet could be minimized, taking only the amount of protein in the pellet into account and calculating molar ratios of protein and polymer at polymer concentrations below the optimum concentration as described above.

Calculating the molar ratios of protein/polymer based on the procedures described above, a chain length dependent precipitation behavior of lysozyme, myoglobin, chymotrypsinogen A, and mAb A,

using PSS polymers, was observed. As soon as a threshold of Mw = 2,220g mol^{-1} is exceeded, the molar ratio is independent of the chain length. Below that threshold, the molar ratio of precipitated protein per polymer molecule is lower than expected.

While a polymer chain of PSS with a weight average molecular weight of 43,300g mol^{-1} is around 6.63- times longer than one of PSS with 6,530g mol^{-1}, it led to approximately 5.8- 8.3 -times more protein per polymer chain compared to the shorter chain (Fig. 2a, 3a). These results, except for the low molecular weight PSS standard, are similar to findings, showing a PSS polymer chain length independent precipitation behavior, when titrating papain in the so-called "colloid titration" [39]. Likewise, PAA polymers with Mw of 8,300g mol^{-1} to 958,000g mol^{-1} showed chain length independent precipitation behavior, correlating with increasing polymer chain length (Fig. 2b, 3b), while low molecular weight PAA polymers showed a lower molar ratio than expected.

Eventually, PAA958,000 is approximately 115 times longer than PAA8300, showing a 113- 123 fold higher ratio of protein per polymer chain. PVS2,100 in comparison with PSS2,220 and PAA1,930, all of similar Mw, showed an approximately 2.6-times higher ratio of lysozyme per polymer with strong anionic polymer PVS and a 10 % higher ratio of lysozyme to polymer with polymer PSS, compared to the weak anionic polymer PAA (table 1). While the former two polymers likely exhibit sufficient electrostatic attraction potential to precipitate the protein, PAA shows a weaker electrostatic potential and thereby lower yield of bound or interacting protein per polymer chain. Comparing PASA30,537 (Mw determined by SEC) with hypothetical PAA and PSS polymer, all of same Mw, we saw ratios of lysozyme to polymer of 11.82 for PASA compared to 9.74 for PSS and 9.58 for PAA.

Summarizing these findings, we concluded that for a polymer which exceeds a certain "threshold"-length, the amount of protein precipitated per defined polymer chain length L$_{def}$, would be independent of the overall polymer chain length.

Defined polymer chain length required per precipitated protein molecule (L$_{def}$)

The overall calculated average polymer chain lengths, based on (a) the weight average molecular weights, (b) the amount of monomers and (c) assuming bond angles of 108° at the backbone chain, are shown in table 2. Our calculation for a PSS70000 polymer yielded 99.5 nm which is comparable to 102 nm published by Adamczyk et al. [40], based on results by Donath et al. [41]. Thus, the error in our calculation is comparable to Adamczyk's approach.

Dividing the overall polymer chain length by the number of bound protein per polymer chain, derived from the molar ratios in table 1, the defined polymer chain length required per precipitated protein molecule, L$_{def}$ was obtained (table 2). A comparison of these values with the estimated protein diameter as determined from crystallographic data showed similar or even larger L$_{def}$ than the actual

diameters of the corresponding proteins. This led us to the question why there were differences in L_{def} between different polymer types and whether they correlated with polymer charge density or protein charge surface charge potential or protein isoelectric point. To elucidate this, L_{def} of different polymer types was compared between mAb A and lysozyme.

Comparison L_{def} for lysozyme and mAb A

L_{def} for lysozyme

While lysozyme has an estimated protein diameter of around 50 Å (Fig. 4), L_{def} of PSS polymers tested was in the range of 48- 60 Å (table 2), implying the idea of PSS polymers to anneal linearly to the lysozyme molecule upon precipitation, leading to a necklace-like structure. L_{def} for PSS polymers with M_w less than 6,530 Da increased compared to longer polymer chains and was even longer than the length of the polymer chains.

This indicates reduced precipitation efficiency, also shown by Bohidar et al. [42], who analyzed coacervation and liquid-liquid separation depending on polyelectrolyte chain length, showing that polymers with Mw less than 1000 g mol^{-1} did not allow for coacervation. Although we did not employ copolymers of that small Mw in our studies, both, PAA1,930 and PSS1,360 exhibited much higher L_{def} compared to longer polymer chains, indicating reduced precipitation ability of short polymer chains and thus strongly supporting results by Bohidar et al.

For short polymer chains, chain length might not be long enough to achieve optimal annealing and interaction with the positively charged surface areas of the tested proteins seen in Fig. 5. Therefore, several polymer chains might be required to achieve strong interaction, form bridges and thus high precipitation yields, being reflected in the elevated L_{def} values. Compared to PSS, PAA polymers had L_{def} that was by a factor ~ 2.0- 2.8 higher (table 2). A reason might be that PAA is a weak polymer compared to the strong polyanion PSS, with only 82 % of carboxy-groups being deprotonated at pH 5.0, according to Henderson-Hasselbalch equation. Thereby for an intimate contact between polymer and protein, a longer interaction distance might be required, reflected in a larger L_{def}. Alternatively, more polymer chains interacting with the protein are required to achieve similar precipitation yields compared to PSS. Additionally, differences in persistence length of both polymer types also affect precipitation efficiency, explaining differences in observed L_{def}. Compared to PAA, PSS exhibits a smaller persistence length, facilitating annealing of the polymer chain to the protein surface, allowing for more efficient precipitation [3, 43-45]. Similar results were shown by Bohidar et al., observing reduced DNA- polyion coacervation for polyions with increased persistence length [46].

PAA958,000 showed a slightly reduced L_{def}, however, the difficulty in obtaining the exact molar ratio of protein per polymer using high molecular weight species, due to measurement errors, might account

for this finding. Comparing similar long polymers PVS2,100, PSS2,220 and PAA1,930, L_{def} of PVS was 68 % of the L_{def} of PSS and only 27 % of the L_{def} of PAA, when using lysozyme as target protein. This reflects the strength of the polyanions, and the amount of length required to achieve precipitation of a protein molecule. Comparing polymer chains of similar length, PASA with Mw 30,357, PSS43,300 and PAA36,900, PASA displayed a lower L_{def} than PSS and PAA, implying that the interaction strength between PASA and lysozyme is higher compared to the latter polymers and thus revealed an L_{def} value that is smaller than the diameter of lysozyme.

Considering a polymer- protein interaction as a wrapping and winding of the polymer around the protein as predicted in Monte Carlo simulations [10, 47], the distance between positively charged residues in lysozyme was measured, starting from one side and circulating around the protein several times while passing as many positively charged residues as possible until all positively charged residues which were most likely available to the polymer, were passed (Fig. 4, Fig. 5a and b), leading to a path length of approximately 150 Å.

Considering PAA covering most of the positively charged residues in lysozyme by wrapping around the protein as well as forming loops, tails and trains as seen in simulations, leading to rosette-like multiloop conformations [13, 15], a similar L_{def} than the assumed 150 Å from model calculations could be required. Thus, our experimental results with an L_{def} of ~ 130 Å for PAA fit into this proposed model of protein-polymer interaction.

According to the molar ratio calculations and considering the length of a PAA 1,930 g mol^{-1} polymer chain equaling 79 Å, approximately two PAA-polymer molecules of this length are required to achieve precipitation of one lysozyme molecule. While one molecule might wrap or anneal to the protein, the other one might be required to build a gel like-network connecting proteins which may serve as cross-linkers as seen in other experiments [8-9, 11]. For PASA and PVS, the L_{def} required was less than the diameter of the protein, indicating that only part of the protein is interacting with the polymer chain, most likely due to the higher charge density of these polymers compared to PAA and the resulting stronger interaction.

L_{def} for mAb A

While the diameter of mAb A is approximately 160 Å, all polymers, except of PASA showed L_{def} -values of at least 264 Å or even higher per precipitated mAb A molecule (table 2). The longer L_{def} might be due to annealing of the polymers to positively charged protein areas (marked in blue in Fig. 5c) as well as due to required space between two mAbs interacting with the same polymer chain. Another explanation might be the formation of trains, loops and tails of the polymer when annealing to the antibody as seen in other experiments [13, 15]. In comparison, PASA showed a L_{def} of 173 Å, equal to the diameter of the protein.

While PSS polymers above 10,600g mol^{-1} showed L_{def} of ~270 Å, this value increased if polymer chain length decreased below a certain threshold (table 2). L_{def} increased already for PSS6,530 and even further for PSS1,360, again, to our understanding, supporting results by Bohidar et al., indicating a chain length of less than 1,000g mol^{-1} being insufficient for successful precipitation. Similar results were obtained with PAA polymers, showing an increase of L_{def} if polymer M_w is below 8,300g mol^{-1}. The minor deviations of L_{def} with PAA123,000 and PAA36,900 might be due to experimental inaccuracy and difficulty in determining the optimum molar ratio of mAb A to polymer. The effect of increasing L_{def} with small PAA polymer chains is also reflected when plotting the molar ratio of mAb A to PAA vs. the chain length, showing a lower ratio of mAb A per polymer chain than expected for PAA1,930 and PAA3,800. Reason might be that the polymer chain length of "short" PAA as well as PSS polymers is not long enough to achieve optimal annealing to positively charged protein surface areas at pH 5.0, depicted in Fig. 4 and 5c and thus several chains are required.

Comparing L_{def} of PVS2,100, PSS2,220 and PAA1,930, PVS needs a shorter L_{def} compared to PSS2,220 to achieve precipitation. PAA required an even longer interaction distance between the polymer and mAb A. Similar to results observed with lysozyme, mAb A precipitation displayed a factor 1.6 higher L_{def} for PSS compared to PASA and a factor 3.0 times higher L_{def} for PAA compared to PASA.

Dependence of L_{def} on polymer and protein charge density

The zeta potential of polymer solutions was measured (S2 supplementary material) to compare polymer charge density with required L_{def} values. As zeta-potential measurements were affected by chain-length of the polymers, likely changing viscosity and thereby influencing calculations, zeta potential of polymers of similar chain length was compared. While strong polymer PSS2,220 obtained a zeta potential of -21.9 mV, revealing a high charge density, polymer PVS2,100 with a zeta potential of -29.3 mV showed an even higher charge density, also visible in electrophoretic light scattering measurements by Xia et al. [20], all at pH 5.0. The charge density of PAA1,930 was lower, shown by a less negative zeta potential of -14.2 mV at pH 5.0. Comparing the similar long polymers PASA with Mw 30,537 g mol^{-1}, PAA36,900 and PSS43,300, the zeta potential of PSS43,300 was more negative than the one of PAA, with PASA obtaining the most negative zeta potential, indicating a higher charge density. A general comparison between PSS and PAA polymers at similar chain length showed a more negative potential for PSS compared to PAA polymers.

A comparison of the estimated L_{def} for mAb A or lysozyme, respectively, with zeta potential measurements was done. Although no quantitative correlation can be seen, it is obvious that an increase of L_{def} qualitatively correlates with a decrease in the zeta potential of the corresponding

polymer (table 3). This is clearly indicated when comparing the precipitation results of mAb A and lysozyme with different polymers. Therefore, we were able to qualitatively correlate obtained L_{def} with polymer charge densities determined by ELS.

Furthermore, comparing the ratio of L_{def}/ estimated protein diameter (table 4), the precipitation strength depending on the protein could be determined. While the ratio was lowest for lysozyme, it increased with chymotrypsinogen A and mAb A and was highest with myoglobin. This tendency was seen with PSS and to a less pronounced extent also with PAA polymers, the latter showing a higher ratio, most likely due to the lower charge density and thus requiring a longer distance to anneal and interact with positive surface charge areas of the protein. For PSS polymers, the increase of the ratio L_{def}/ estimated protein diameter correlated with the decrease of the *pI* of the corresponding proteins, *i.e.* proteins with a lower *pI* showed less positive surface charge and thus the polymer required a longer L_{def} to achieve sufficient precipitation. The ratio of L_{def}/ estimated protein diameter correlated also with the measured zeta potential of the proteins, confirming the dependence of protein precipitation strength on protein charge density and distribution (table 4). For PAA polymers, this was also true, however, the difference in L_{def}/ estimated protein diameter was less straight-forward for mAb A and chymotrypsinogen A. Although their *pI* and zeta potential showed differences, both proteins obtained L_{def}/ estimated protein diameter values of around 3.2. Nevertheless, for mAb A this value was slightly higher, being 3.22, while chymotrypsinogen A exhibited 3.18.

Fig. 4 shows protein surface charge distributions at pH 5.0, to compare charge distribution at precipitation conditions. While lysozyme is mainly positively charged, chymotrypsinogen A shows a positively charged frontside and a negatively charged backside. Thus, it can be precipitated in a necklace-like precipitation, exhibiting its positive surface to the negatively charged polymer chain. mAb A shows a large stretch of negative surface charge at the Fc part. Although the variable part of the antibody is mainly positively charged, it also exhibits negatively charged stretches, mainly at one side of the mAb. The polymer chain likely anneals in a similar fashion compared to myoglobin, however might also anneal in such a conformation, that it achieves strong interaction with the positively charged surface area while at the same time circumnavigating the negatively charged area by loop formation, which could explain the larger L_{def}/ protein diameter values compared to lysozyme and chymotrypsinogen A. While myoglobin does also exhibit negative and positive charged surface areas, those are evenly distributed, and not separated in a front and backside unlike chymotrypsinogen A and mAb A. Therefore, the L_{def} and subsequently the ratio of L_{def}/ diameter of myoglobin are higher compared to the other proteins as the polymer putatively needs to build large loops to anneal only to the positively charged areas and "circumnavigate" the negatively charged areas (Fig. 4, table 4).

CONCLUSION

Precipitation results using various anionic polymers showed a polymer-type dependent precipitation behavior. Comparing polymer standards PAA and PSS, molar ratios of protein per polymer were less than expected, also leading to higher L_{def}, if polymer chain lengths were below a threshold. Above this value PSS and PAA polymers exhibited a chain-length independent precipitation behavior. A comparison of L_{def} showed differences between PVS, PSS and PAA polymers of same molecular weight. The weak polyanion PAA required a significantly larger L_{def} for precipitating a single protein compared to the strong polyions PVS and PSS. This difference was most likely due to charge density differences of the polymers, indicated by electrophoretic light scattering measurements of the zeta potential. Weak polymers are most likely required to have a longer and thereby stronger interaction with the protein to achieve similar precipitation yields compared to strong polymers. With some polymers, L_{def} was longer than the corresponding protein diameter. We concluded the formation of polymer trains, tails and loops as seen on charged surfaces, as a cause for these results. Another explanation might be that polymers precipitate by wrapping around the protein and build a network consisting of several polymer chains per precipitated protein. Comparing the ratio of L_{def} to estimated protein diameters, we were able to measure precipitation strength and correlate this to the *pI* and surface charge distribution of the corresponding proteins at precipitation pH as well as to protein charge density determined by electrophoretic light scattering.

ACKNOWLEDGEMENTS

REFERENCES

1. Capito F, Skudas R, Stanislawski B, Kolmar H (2013) Colloid Polym Sci 1-11
2. Cooper CL, Goulding A, Kayitmazer AB, Ulrich S, Stoll S, Turksen S, Dubin PL (2006) Biomacromolecules 7:1025-1035
3. Cooper CL, Dubin PL, Kayitmazer AB, Turksen S (2005) Curr Opin Colloid Interface Sci 10:52–78
4. Benmansour K, Medjahed, K, Tennouga L, Mansri A (2003) Euro Polym J 39:1443-1449
5. Mattison KW, Dubin PL, Brittain IJ (1998) J Phys Chem B 102:3830-3836
6. Mattison KW, Brittain IJ, Dubin PL (1995) Biotechnol Prog 11:632-637
7. Park J, Muhoberac BB, Dubin PL, Xia J (1992) Macromolecules 25:290-295
8. Gummel J, Cousin F, Boué F (2008) Macromolecules 41:2898-2907
9. Bohidar H, Dubin PL, Majhi PR, Tribet C, Jaeger W (2005) Biomacromolecules 6:1573-1585

10. Nguyen, TT, Shklovskii BI (2001) J Chem Phys 114:5905–5916
11. Borrega R, Tribet C, Audebert R (1999) Macromolecules 32:7798-7806
12. Ulrich S, Laguecir A, Stoll S (2005) Macromolecules 38:8939-8949
13. Akinchina A, Linse P (2002) Macromolecules 35:5183-5193
14. Brynda M, Chodanowski P, Stoll S (2002) Colloid Polym Sci 280:789-797
15. Schiessel H, Rudnick J, Bruinsma R, Gelbart WM (2000) Europhys Lett 51:237
16. Chodanowski P, Stoll S (2001) J Chem Phys 115:4951–4960
17. Chodanowski P, Stoll S (2001) Macromolecules 34:2320–2328
18. Thömmes J, Etzel M (2007) Biotechnol Prog 23:42-45
19. Low D, O'Leary R, Pujar NS (2007) J Chrom B 848:48-63
20. Xia J, Dubin PL, Kim Y, Muhoberac BB, Klimkowski VJ (1993) J Phys Chem 97:4528-4534
21. Singh J, Dutta PK (2009) J Polym Res 16:231-238
22. Kiefer F, Arnold K, Künzli M, Bordoli L, Schwede T (2009) Nucleic Acids Res 37:387-392
23. Arnold K, Bordoli L, Kopp J, Schwede T (2006) Bioinformatics 22:195-201
24. Peitsch MC (1995) Bio/Technology 13:658-660
25. Olsson MH, Søndergaard CR, Rostkowski M, Jensen JH (2011) J Chem Theory Comput 7:525-537
26. Bas DC, Rogers DM, Jensen JH (2008) Proteins: Struct Funct Bioinf 73:765-783
27. Dolinsky TJ, Czodrowski P, Li H, Nielsen JE, Jensen JH, Klebe G, Baker NA (2007) Nucleic Acids Res 35:522-525
28. Li H, Robertson AD, Jensen JH (2005) Proteins: Struct Funct Bioinf 61:704-721
29. Dolinsky TJ, Nielsen JE, McCammon JA, Baker NA (2004) Nucleic Acids Res 32:665-667
30. Baker NA, Sept D, Joseph S, Holst MJ, McCammon JA (2001) Proc Natl Acad Sci USA 98:10037-10041
31. Yang Z, Lasker K, Schneidman-Duhovny D, Webb B, Huang CC, Pettersen EF, Goddard TD, Meng EC, Sali A, Ferrin TE (2012) J Struct Biol 179:269-278
32. Pettersen EF, Goddard TD, Huang CC, Couch GS, Greenblatt DM, Meng EC, Ferrin TE (2004) J Comput Chem 25:1605-1612
33. Roth CM, Lenhoff AM (1995) Langmuir 11:3500-3509
34. Kisler JM, Stevens GW, O Connor AJ (2001) Mat Phy Mech 4:89-93
35. Papadopoulos S, Jürgens KD, Gros G (2000) Biophys J 79:2084-2094
36. Striemer CC, Gaborski TR, McGrath JL, Fauchet PM (2007) Nature 445:749-753
37. McDonald P, Victa C, Carter-Franklin JN, Fahrner R (2009) Biotechnol Bioeng 102:1141-1151
38. Carlsson F, Malmsten M, Linse P (2003) J Am Chem Soc 125:3140-3149
39. Izumi T, Hirata M, Kokufuta E, Cha HJ, Frank CW (1994) J Macromol Sci Pure Appl Chem 31:31-37
40. Adamczyk Z, Zembala M, Warszýnski P, Jachimska B (2004) Langmuir 20:10517-10525
41. Donath E, Walther D, Shilov VN, Knippel E, Budde A, Lowack K, Helm CA, Möhwald H (1997) Langmuir 13:5294-5305
42. Pawar N, Bohidar HB (2010) Phys Rev E 82:36107
43. Tricot M (1984) Macromolecules 17:1698–1704
44. Le Bret M (1982) J Chem Phys 76:6243–6255
45 Gummel J, Cousin F, Boué F (2008) Macromolecules 41:2898-2907
46. Rawat K, Pathak J, Bohidar HB (2013) Phys Chem Chem Phys 15:12262-12273
47. Messina R, Holm C, Kremer K (2003) Langmuir 19:4473

Table 1: Molar ratio of protein to polymer and precipitation yield of proteins depending on the chain length and type of polymer as well as type of protein. n.d. means not determined

Polymer	molar ratio lysozyme /polymer using fraction of precipitated protein	% precip. lysozyme at pH 5.0 20 mM NaCl	molar ratio myoglobin /polymer using fraction of precipitated protein	% precip. myoglobin at pH 5.0 20 mM NaCl	molar ratio chymotrypsinogen A /polymer using fraction of precipitated protein	% precip. chymotrypsinogen A at pH 5.0 20 mM NaCl	molar ratio mAb A/polymer using fraction of precipitated protein	% precip. mAb A at pH 5.0 20 mM NaCl
PSS1360	0.36	93.9	0.15	71.8	0.07	25.0	0.04	90.5
PSS2220	0.67	93.6	0.24	69.4	0.39	46.0	0.07	96.8
PSS6530	2.15	94.2	0.90	62.6	2.04	62.4	0.30	94.5
PSS10600	3.48	94.5	1.40	54.2	3.00	67.8	0.61	92.4
PSS15200	4.90	94.2	2.00	57.9	4.76	69.3	0.91	92.7
PSS43300	13.82	93.1	5.50	55.5	11.90	70.5	2.51	92.4
PSS976000	320.5	94.3	129.58	56.6	307.30	71.6	56.25	92.3
PAA1930	0.6	91.4	0.14	53.2	0.10	18.2	0.02	91.2
PAA3800	1.20	93.9	0.42	78.3	0.50	37.7	0.13	95.9
PAA8300	2.72	93.9	1.00	76.7	2.40	54.3	0.66	96.5
PAA18100	5.80	93.9	2.20	74.1	5.40	66.2	1.43	97.3
PAA36900	11.58	93.6	4.46	77.3	11.16	69.6	2.93	96.5
PAA123000	39.14	91.0	14.40	79.2	38.31	70.5	9.93	97.4
PAA958000	308.84	94.6	114.00	78.5	296.00	69.5	74.39	97.9
PVS2100	1.6	94.4	n.d.	n.d.	n.d.	n.d.	0.15	95.0
PASA30537	11.82	93.0	n.d.	n.d.	n.d.	n.d.	2.25	94.1

Table 2: Overall average polymer chain length and L_{def} to achieve optimal interaction with proteins. n.d.: not determined

Table 2: Polymer	overall average polymer chain length in Å	L_{def} based on protein fraction (lysozyme)	L_{def} based on protein fraction (myoglobin)	L_{def} based on protein fraction (chymotrypsinogen A)	L_{def} based on protein fraction (mAb Å)
PSS1360	21.6	60.00	144.00	308.57	540.00
PSS2220	35.2	52.54	146.67	90.26	502.86
PSS6530	103.5	48.14	115.00	50.73	345.00
PSS10600	168.0	48.28	120.00	56.00	275.41
PSS15200	240.9	49.16	120.45	50.61	264.73
PSS43300	686.2	49.65	124.76	57.66	273.39
PSS976000	15,466.7	48.26	119.36	50.33	274.96
PAA1930	78.8	131.33	562.86	788.00	3,940.00
PAA3800	155.2	129.33	369.52	310.40	1,193.85
PAA8300	339.0	124.63	339.00	141.25	513.64
PAA18100	739.3	127.47	336.05	136.91	516.99
PAA36900	1,507.2	130.16	337.94	135.05	514.40
PAA123000	5,023.9	128.36	348.88	131.14	505.93
PAA958000	39,129.6	126.70	343.24	132.19	526.00
PVS2100	57.5	35.94	n.d.	n.d.	383.33
PASA	388.4	32.86	n.d.	n.d.	172.62

Table 3: Comparison of polymer charge density of similar long polymers, expressed as zeta potential at pH 5.0, with required L_{def} of those polymers for precipitating mAb A and lysozyme (Lys)

high charge density	L_{def} mAb A	L_{def} Lys	Zeta potential [mV]
PASA	172.6	32.9	-58.5
PVS	383.3	35.9	-29.3
PSS	502.9	52.5	-21.9
PAA	3,940.0	131.3	-14.2
low charge density			

Table 4: Ratio of L_{def} to estimated protein diameter as mean value for PSS and PAA polymers, respectively, in comparison to *pI* and measured zeta potential at pH 5.0 of corresponding protein. The ratio is indicative for the precipitation strength and correlates with the *pI* as well as with the zeta potential of the protein at pH 5.0

Polymer	lysozyme	chymotrypsinogen A	mAb A	myoglobin
L_{def}/ protein diameter PSS	1.0	1.3	1.8	2.7
L_{def}/ protein diameter PAA	2.6	3.2	3.2	7.8
isoelectric point (*pI*)	**10.7**	**8.8- 9.6**	**8.5**	**7.5**
zeta potential at pH 5.0 [mV]	**16.71**	**5.48**	**5.22**	**1.16**

List of figures:

Fig. 3 Relative accumulation of polymer in the pellet and protein precipitation yield of mAb A, depending on initial polymer concentration and type of polymer added to the sample. Concentrations for calculating molar ratios of protein and polymer were taken in the "red" area, below the optimum precipitation conditions (highlighted in green) to minimize the error of overestimating polymer concentrations within the pellet. Error bars represent triplicate experiments

Fig. 2 Plot of molar ratio of lysozyme molecules per PSS polymer molecule (a) or PAA polymer molecule (b) vs. the precipitation yield achieved at this ratio. Polymer designation according to weight average molecular weight in g mol^{-1}. Ratio was calculated for overall reaction solutions

Fig. 3 Plot of molar ratio of mAb A molecules per PSS polymer molecule (a) or PAA polymer molecule (b) vs. the precipitation yield achieved at this ratio. Polymer designation according to weight average molecular weight in g mol^{-1}. Ratio was calculated for overall reaction solutions

Fig. 4 Surface charge distribution of proteins lysozyme, myoglobin, chymotrypsinogen A and homology model of mAb A at pH 5.0, Snapshots taken from different angles to compare protein frontside with backside. Red: negative surface charge; blue: positive surface charge. Pink: largest measured distances for diameter estimation in Deep View, for clarity not directly shown in protein structure but added as schematic overlay. Proteins sorted according to degree of positive surface charge with lysozyme showing most of positive charge and myoglobin showing least positive charge (according to isoelectric point and zeta potential at pH 5.0). Contour plot using +/- 2 k_BT e^{-1}; proteins not to scale

Fig. 5 (a): lysozyme surface overview in Deep View, positively charged amino acids labeled in blue. (b): Stick view of lysozyme carbon alpha and backbone atoms, positively charged residues labeled in blue. Distance between residues measured and labeled in white. (v): mAb A homology model surface overview in Deep View, positively charged amino acids labeled in blue. Distance in residues measured and labeled in white

Figure 1

a precipitation with PSS at 20 mM NaCl pH 5.0

Legend: PSS1360, PSS2220, PSS6530, PSS10600, PSS15200, PSS43300, PSS976000

b precipitation with PAA at 20 mM NaCl pH 5.0

Legend: PAA1930, PAA3800, PAA8300, PAA18100, PAA36900, PAA123000, PAA958000

Figure 2

a precipitation with PSS at 20 mM NaCl pH 5.0

Legend: PSS1360, PSS2220, PSS6530, PSS10600, PSS15200, PSS43300, PSS976000

b precipitation with PAA at 20 mM NaCl pH 5.0
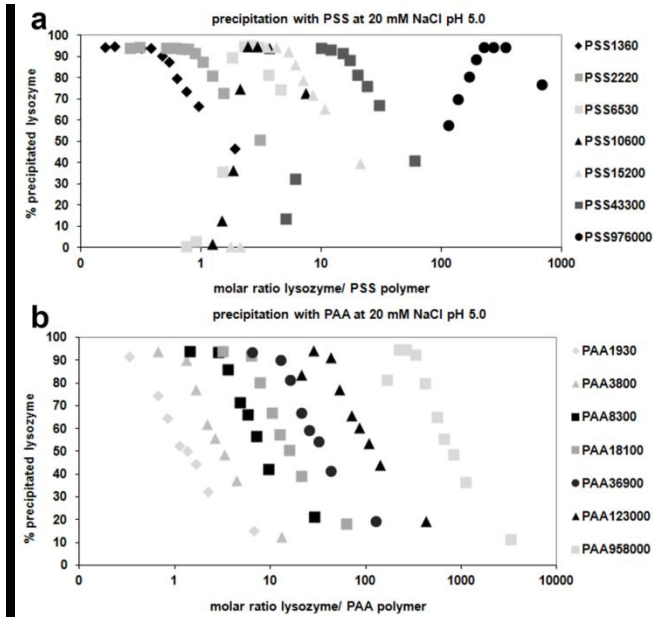
Legend: PAA1930, PAA3800, PAA8300, PAA18100, PAA36900, PAA123000, PAA958000
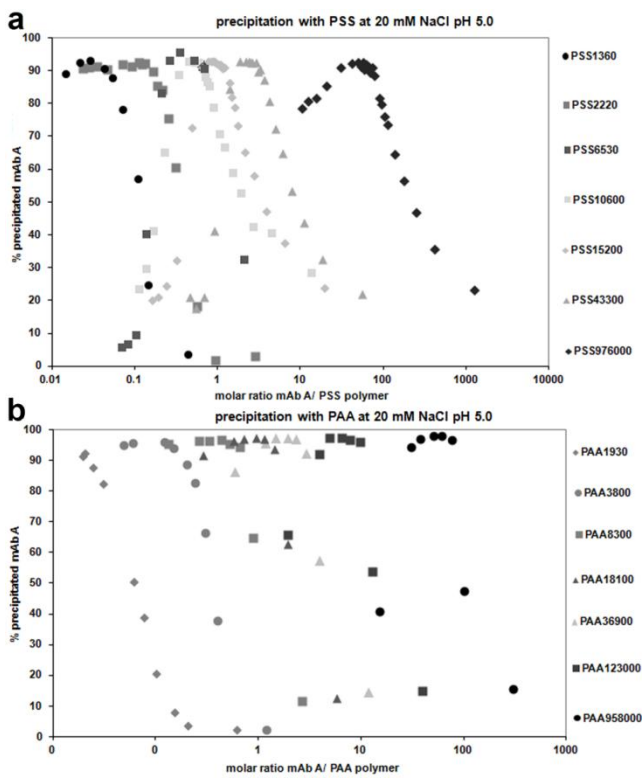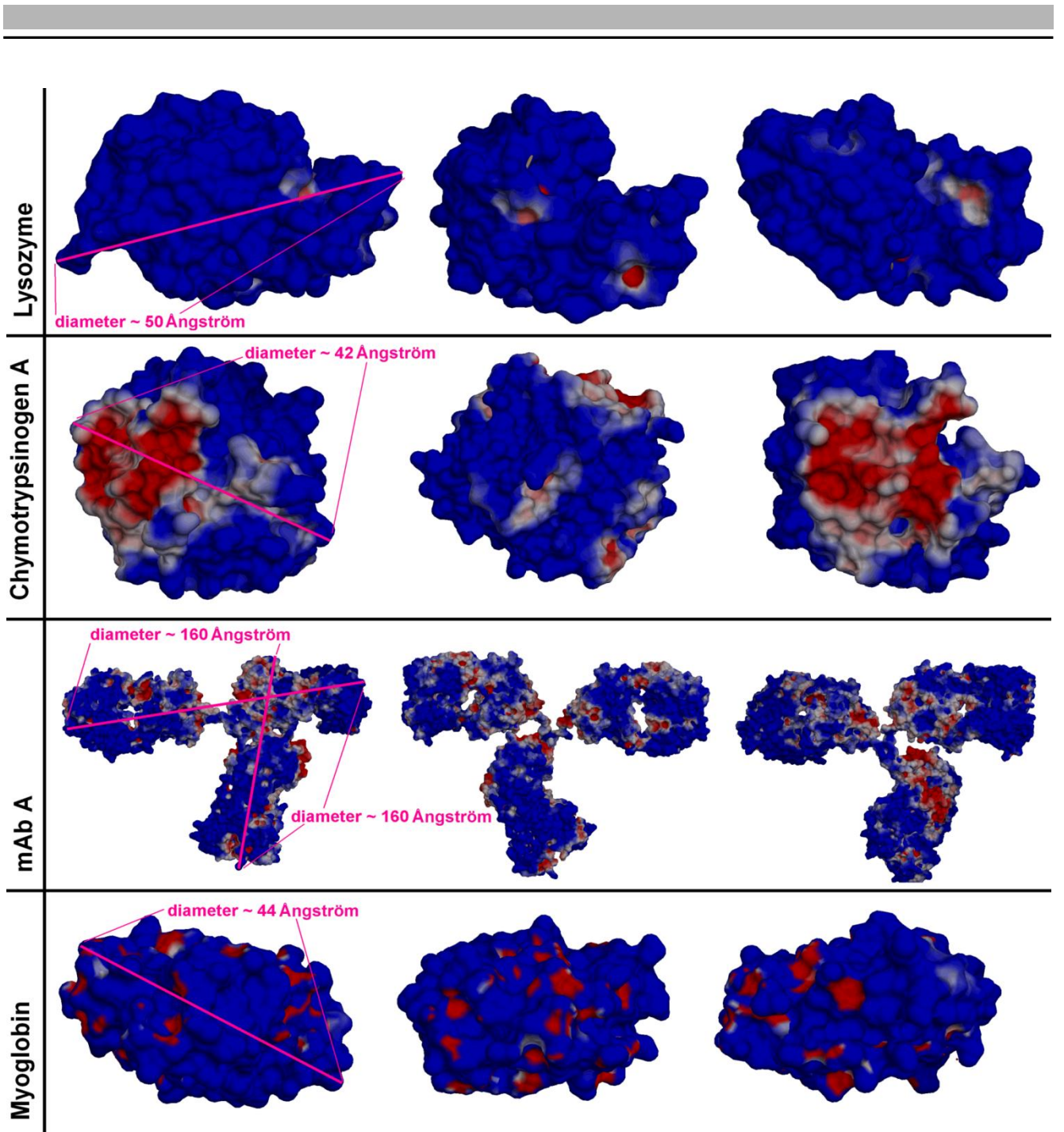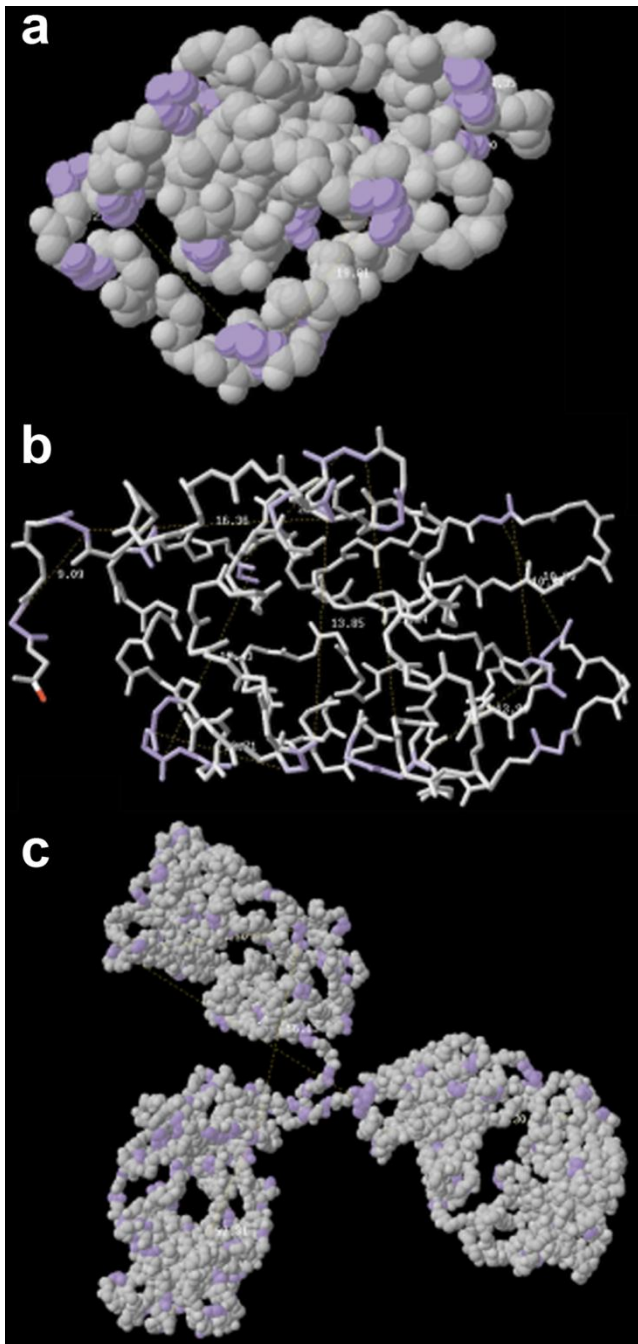
Figure 3

Figure 4

Figure 5

3.4. Effects of copolymer composition on protein precipitation: mAb-BSA protein model systems to optimize precipitation yield and selectivity

Paper: Customization of copolymers to optimize selectivity and yield in polymer-driven antibody purification processes

Florian Capito, Romas Skudas, Harald Kolmar and Bernd Stanislawski

Short Summary:

After preparatory work, elucidating how ionic strength and polymer chain length affect protein precipitation behavior, a test-system was established, analyzing how polymer composition would affect precipitation, using two different proteins per system. While one of several mAbs served as target protein, BSA was used as an impurity protein for analyzing precipitation yield and selectivity. Depending on the physico-chemical properties of the protein, different copolymer compositions were required to obtain maximum precipitation yields and alter selectivity. Results revealed copolymer composition as the major driving force for precipitation selectivity. By adjusting composition and chain length of the precipitant for each of the mAbs, conditions were found that allowed for high precipitation yield and selectivity. These findings do also help in the final development of the protein precipitation process.

Customization of Copolymers to Optimize Selectivity and Yield in Polymer-Driven Antibody Purification Processes

Florian Capito

Institute for Organic Chemistry and Biochemistry, Technische Universität Darmstadt, 64287 Darmstadt, Germany

Merck KGaA, PTD, Frankfurter Strasse 250, 64293 Darmstadt, Germany

Romas Skudas and Bernd Stanislawski

Merck KGaA, PTD, Frankfurter Strasse 250, 64293 Darmstadt, Germany

Harald Kolmar

Institute for Organic Chemistry and Biochemistry, Technische Universität Darmstadt, 64287 Darmstadt, Germany

This manuscript describes customization of copolymers to be used for polymer-driven protein purification in bioprocessing. To understand how copolymer customization can be used for fine-tuning, precipitation behavior was analyzed for five target antibodies (mAbs) and BSA as model impurity protein, at ionic strength similar to undiluted cell culture fluid. In contrast to the use of standardized homopolymers, customized copolymers, composed of 2-acrylamido-2-methylpropane sulfonic acid (AMPS) and 4-(acryloylamino)benzoic acid (ABZ), exhibited antibody precipitation yields exceeding 90%. Additionally, copolymer average molecular weight (M_w) was varied and its influence on precipitation yield and contaminant coprecipitation was investigated. Results revealed copolymer composition as the major driving force for precipitation selectivity, which was also dependent on protein hydrophobicity. By adjusting ABZ content and M_w of the precipitant for each of the mAbs, conditions were found that allowed for high precipitation yield and selectivity. These findings may open up new avenues for using polymers in antibody purification processes. © 2013 American Institute of Chemical Engineers Biotechnol. Prog., 000:000–000, 2013
Keywords: antibody precipitation, copolymer, selectivity, downstream processing

Introduction

Cell culture titers in production of biotherapeutic proteins are rising, resulting in large batch volumes to be purified.[1] This requires the development of new purification strategies to handle these volumes and avoid bottlenecks in purification trains.[2] Within the last few years, protein purification via semiselective precipitation with polyelectrolytes has gained increased interest among manufacturers of therapeutic proteins, as a means to facilitate downstream processing, obtain higher throughput and reduce purification costs.[3–11]

Protein precipitation is thought to be governed mainly by electrostatic interactions with polyelectrolytes. Nevertheless, hydrophobic interactions can be involved in polyelectrolyte-driven precipitation processes, indicating conjoint effects with electrostatic interactions.[12–14] Semiselective precipitation of the protein of interest using anionic polyelectrolytes is achieved via choosing a pH below the isoelectric point (*pI*) of the target protein and above the *pI*'s of most of the proteins present in solution that are considered as impurities. Using cationic polyelectrolytes under similar conditions,

mainly the impurity proteins are precipitated while the target protein remains in solution.[4]

To enable a widespread application of precipitation for large-scale purification, thereby reducing downstream processing costs, it is important to obtain high yields and maintain precipitation selectivity over a wide range of conditions, including various pH- and solvent conductivity ranges.[15,16] Because precipitation is preferably performed directly from the cell culture medium after cell removal by centrifugation, the protein solution is within the pH-range of 5–6.5 with conductivity ranging from 10 to 25 mS cm^{-1}. As a consequence, the use of polyelectrolytes in this case requires extensive dilution of physiological ionic strength cell culture media, as otherwise the electrostatic interaction would not be strong enough to allow for high yield protein precipitation.[3–5]

Experiments by Seyrek et al. (2003) comparing the precipitation behavior of various poly-(acrylic acid) (PAA) polymers, using BSA as test protein, indicated higher precipitation efficiency if the polymer was hydrophobically modified aimed at enhancing hydrophobic interaction as the driving force for target protein precipitation, since it is less dependent on solvent ionic strength. As a consequence, one straightforward strategy to improve precipitation yields of particular target proteins may be the use of customized
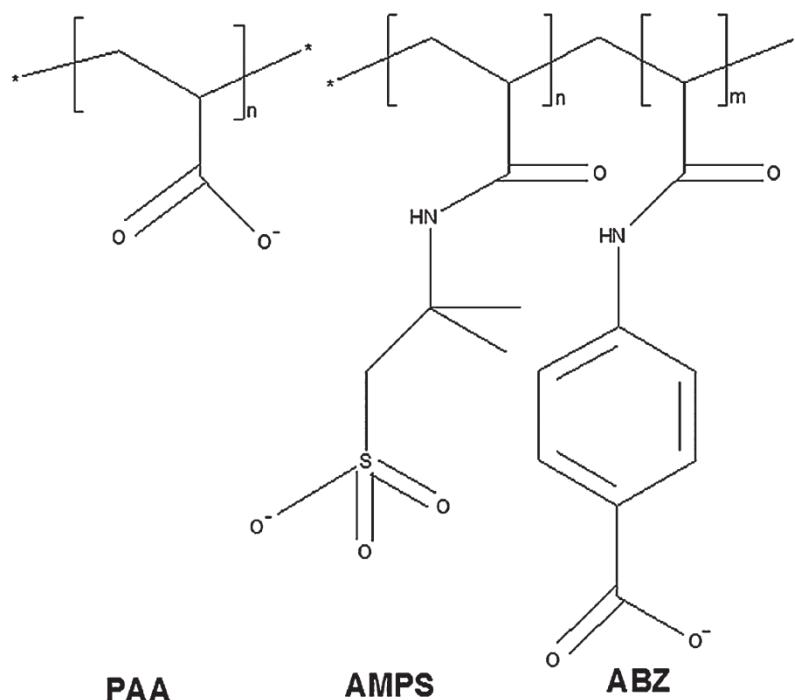

1

Figure 1. Structure and composition of copolymers and homopolymer used for experiments.

copolymers mediating simultaneously both hydrophobic and electrostatic interactions. In addition to ionic strength and polyelectrolyte hydrophobicity, polyelectrolyte weight average molecular weight (M_w) and charge density were also shown to influence polyelectrolyte-driven protein precipitation behavior, thereby enabling control of precipitation selectivity if adjusted accordingly.[17–19]

In this article, we investigated the effects of polyelectrolyte charge density, hydrophobicity and M_w on precipitation yield and selectivity when performing precipitation at physiological ionic strength, allowing us to customize copolymers for respective target proteins. The precipitation behavior of various antibodies with differences in pI and protein hydrophobicity was investigated using anionic homopolymers 2-acrylamido-2-methylpropane sulfonic acid (AMPS) and poly-(acrylic acid) (PAA), and was compared to the precipitation behavior using anionic-hydrophobic copolymers composed of 4-(acryloylamino)benzoic acid (ABZ) and AMPS.

Results show that selectivity and yield can be fine-tuned by customizing polymer composition and M_w, thereby promoting the widespread applicability of polyelectrolytes for large-scale protein purification form cell culture supernatants.

Materials and Methods

Copolymers and homopolymers

Copolymers consisting of varying amounts of ABZ and AMPS (Figure 1), respectively, were synthesized using 50 % (v/v) dimethylformamide (DMF)-water as solvent and $Na_2O_8S_2$ as initiator. The reaction was performed in N_2 conditions at pH 9.0 and 80°C for 5 h before cooling to room temperature. By varying the relative amount of the two monomers, copolymers with different composition were obtained. Varying concentrations of initiator ranging from 0.14 to 3.17% (w/w) were used, with the aim of controlling

copolymer chain length. Additionally, AMPS homopolymer was synthesized using the synthesis method described above. PAA homopolymer with weight average molecular weight (M_w) of 60,000 g mol^{-1} was purchased from Polysciences, Warrington, USA.

Gel permeation chromatography

Molecular weight of copolymers and AMPS homopolymer was determined using gel permeation chromatography (GPC) on LaChrom Elite (VWR-Hitachi, Darmstadt, Germany) (Injection volume 200 µL; calibration with polystyrene sulfonate in 20 % AcCN; elution buffer: 10 mM Na_2HPO_4, 50 mM $NaNO_3$, 20 % AcCN; column 1: MCX 10 µm precolumn; column 2: MCX 1 µm 106 Å; column 3: MCX 10 µm 103 Å; detectors: LaChrom refractive index detector L-2490 and Licrograph L-2400 UV detector; injection by autosampler L-2200; system temperature 40°C at a flow rate of 1 mL min^{-1}).

Attenuated total reflection spectroscopy

Copolymer composition was determined using attenuated total reflection spectroscopy (ATR) and compared to defined monomer blends of ABZ and AMPS, using H_2O as reference. Nearly 20 µL of each polymer sample (C = 5 mg mL^{-1}) were measured on GoldenGate^{TM} MkII series ATR (Specac, Cranston, RI), using a diamond (type IIa, 45°C, refractive index at 1000 cm^{-1}: 2.4; 0.8 mm diameter of active sampling area; 2 µm penetration depth for a sample of refractive index 1.5 at 1000 cm^{-1}; diameter 2 mm × 2 mm) at 20°C. Spectra were recorded with a Bruker Tensor 27 (Bruker Optik GmbH, Ettlingen, Germany); samples were scanned in absorbance mode with 120 scans at a spectral resolution of 4.0. Detector was a Bruker LN-MCT photovoltaic internal detector (Bruker Optik GmbH, Ettlingen, Germany), aperture was set to 6 mm. Atmospheric

Table 1. Physicochemical Properties of Monoclonal Antibodies Employed in This Study

	mAb A	mAb B	mAb C	mAb D	mAb E
Isoelectric point (range)	8.0–8.6	8.15–8.7	8.2–8.5	8.45–8.65	7.2–7.8
M_w (kDa)	144.4	145.8	144.4	145.9	145.2
salinity/ionic strength of pure mAb solution at pH 5.0	<3 mScm^{-1}	<3 mScm^{-1}	<3 mScm^{-1}	<3 mScm^{-1}	<3 mScm^{-1}
IgG-class	IgG$_1$	IgG$_1$	IgG$_1$	IgG$_1$	IgG$_2$

compensation was performed and samples smoothed using 17 smoothing points.

Precipitation experiments

Copolymer Solutions. Prior to use, residual DMF solvent was removed during size exclusion chromatography (PD-10 column; Sephadex G25 column material; Amersham Biosciences AB, Uppsala) and copolymers were adjusted to pH 5.0 before performing precipitation experiments.

Protein Solutions. BSA with fat content < 0.2% was obtained from Merck KGaA (Albumin fraction V; product no. 1.12018.0100), Darmstadt, Germany. Five monoclonal antibodies (mAb) with slightly different physicochemical properties were obtained from Merck Millipore, Darmstadt, Germany as internal standards (Table 1). BSA was labeled with Alexa fluor® 680 fluorophore (Invitrogen, Carlsbad, USA). For labeling, 1 mg of fluorophore was dissolved in 500 μL DMSO and added to 1 g of protein, dissolved in aqueous buffer solution at a final protein concentration of 25 mg ml^{-1}. After stirring for 1 h, unbound fluorophore was removed by gel filtration using a PD-10 column (Amersham Biosciences AB, Uppsala, Sweden) filled with Sephadex G25. Monoclonal antibodies were labeled with Alexa fluor® 546 fluorophore (Invitrogen, Carlsbad, USA), using the same conditions. All protein solutions were adjusted to pH 5.0.

Comparison of protein surface charge distribution at different pH

Protein surface charge distribution of BSA and mAb B was exemplary analyzed at different pH to compare precipitation results with charge distributions. Although the use of computer models in this case would be based on assumptions and modeling parameters, the idea was to obtain a surface charge and hydrophobicity model supporting the understanding of potentially underlying principles for precipitation between protein and copolymers. Consequently, protein charge distribution at different pH-conditions was calculated on the basis of the crystal structure of BSA (protein data bank entry ID 3V03). Structure of BSA was used as input to the program Adaptive Poisson-Boltzmann Solver (APBS), after assigning protonation states to residues at pH values between 5.0 and 5.7, using program propka within pdb-pqr converter.[20–25] Charge distributions at specific pH were visualized using program Chimera and program internal threshold for coloring electrostatic potential, set to: red: ≤ -2.0 k$_B$T e^{-1}; blue: $\geq +2.0$ k$_B$T e^{-1}.[26,27] For determination of protein surface charge distribution of mAb B at different pH that served as model antibody molecule, a structural homology model was generated using Deep View version 4.0.1 (Swiss Institute of Bioinformatics) based on the primary sequence of the antibody.[28]

The crystal structure of a monoclonal antibody from protein data bank (protein data bank entry ID 1IGT) served as structural template. A homology model was built via per-

forming an "iterative magic fit" in program Deep View using a PAM200 matrix and minimizing the RMS deviation of the carbon alpha and backbone atoms of model and template, followed by a structural alignment to optimize the homology model using Swiss Model protein structure homology-modeling server.[29–31] Afterward, mAb B homology model charge distribution was determined and visualized same as described for BSA. Additionally, structures of BSA and the mAb B homology model were used within program Chimera and surface hydrophobicity colored according to Kyte-Doolittle hydropathy scale, using threshold ±1.0.[32]

Determination of antibody hydrophobicity

Monoclonal antibody hydrophobicity was derived from hydrophobic interaction chromatography (HIC) (see review Ref. 33), using Fractogel® EMD Phenyl(S) (Merck KGaA, Darmstadt, Germany) on ÄKTApurifier (GE Healthcare Biosciences AB, Uppsala, Sweden). Monoclonal antibodies were loaded onto column, using 1 M (NH$_4$)$_2$SO$_4$ in 20 mM sodium phosphate. Elution was performed via reducing the concentration of (NH$_4$)$_2$SO$_4$ from 1 to 0 M over 20 column volumes. Monoclonal antibody hydrophobicity was then determined via comparing the ionic strength required for mAb elution. Chromatograms for all mAbs, except for mAb E were obtained from Merck Millipore, Darmstadt, Germany. Additionally, mAb E hydrophobicity was determined using the dye 2-*p*-toluidinonaphthalene-6-sulfonic acid (TNS) (Hydrophobic Protein Analysis Kit, Marker Gene Technologies, Eugene, USA) which exhibits a strong fluorescence increase upon binding to hydrophobic protein surfaces, thus allowing quantification of protein surface hydrophobicity via excitation wavelength at 360 nm and emission at 465 nm.[34] This dye was also used for all other mAbs to allow comparison to mAb E, according to manufacturer's protocol at a concentration of 1 mM, and with mAbs diluted to concentrations between 1 mg mL^{-1} and 62.5 μg mL^{-1}. Fluorescence increase was measured in a fluorescence plate reader M200 (Tecan Instruments, Mannedorf, Switzerland).

Precipitation experiments

Precipitation experiments were performed in Eppendorf tubes using 600 μL of defined protein stock solution, 240 μL of 750 mM NaCl, 100 mM Na acetate buffer pH 5.0, and 360 μL of polyelectrolyte solutions. Final concentrations in each sample were 150 mM NaCl, 20 mM Na acetate buffer pH 5.0, and polyelectrolyte concentrations ranging from 0.1 to 1.5 g per g of antibody. Buffer, polyelectrolyte, and protein were mixed and incubated on a lab shaker. From initial experiments it was known that precipitation is a time-dependent process, reaching a plateau-phase after 20–30 min. To have a safety margin and to allow comparison of results under standardized conditions, this incubation time was set to 1 h at 300 rpm. Afterward, samples were
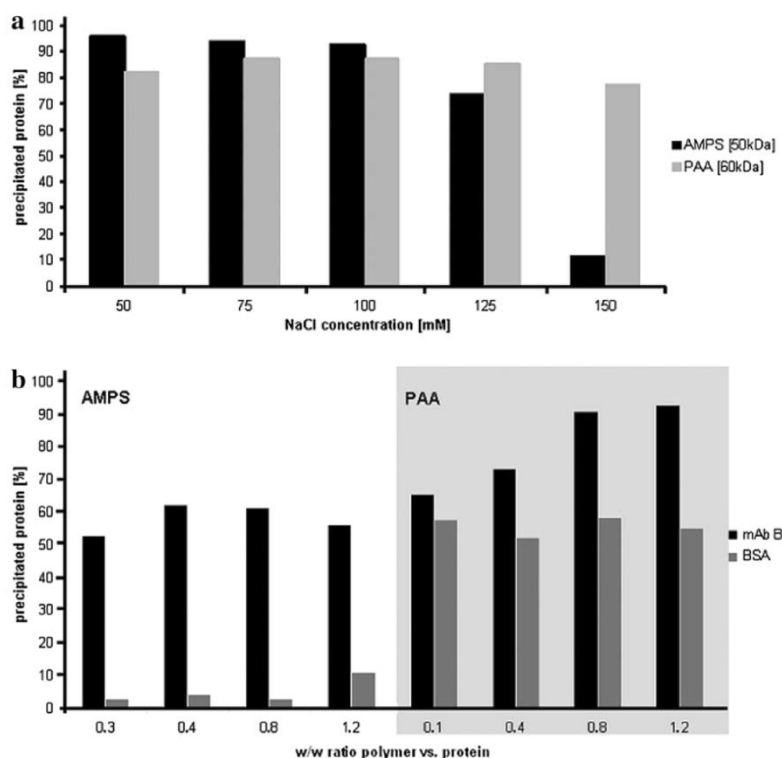
Figure 2. (a): mAb B precipitation using homopolymers AMPS and PAA at 0.4% (w/w) ratio polymer vs. mAb. (b): mAb B and BSA precipitation using AMPS or PAA polymer at pH 5.0.

centrifuged at 2500 rcf for 15 min and the supernatant was transferred to microtiter plates (Nunc, Langenselbold, Germany). Protein concentration in the supernatant was determined by fluorescence measurements in comparison to calibration standards using a Tecan fluorescence plate reader M200 (Tecan Instruments, Mannedorf, Switzerland). The decrease in protein concentration in the supernatant, in comparison to initial protein concentration, was used to calculate the percentage of precipitated protein. Precipitation yield for all mAbs and selectivity in combination with BSA was elucidated using a binary protein system comprised of BSA (serving as an "impurity protein") and one of the five mAbs, both with the same concentration, respectively. BSA was used to enable establishment of a simple test-system, allowing the straightforward identification of correlations in selectivity and yield depending on different parameters. Although host cell proteins represent more realistic impurities in a later process, they were not chosen for this work due to their heterogeneity in physicochemical attributes and different subpopulations, which would likely make it more difficult to understand how copolymers can be customized, as was the focus of this manuscript. Monoclonal antibody concentration in the supernatant was measured using 540 nm as excitation wavelength and 590 nm as emission wavelength. BSA concentration was determined simultaneously using 660 nm as excitation wavelength and 710 nm as emission wavelength.

Results and Discussion

Polyelectrolyte M_w and composition

Various copolymers were synthesized by varying the amount of AMPS and ABZ as well as varying their M_w. Gel permeation chromatography analysis of copolymers and AMPS homopolymer solutions revealed an average M_w from 9000 to 185,000 g mol^{-1}. In copolymers the percentage of ABZ ranged between 0 and 81% (mol%) ABZ, as determined by ATR composition analysis.

Precipitation with homo-polymers AMPS and PAA

For mAb B at pH 5.0 using AMPS homopolymer (M_w 50,000 g mol^{-1}) or PAA homopolymer (M_w 60,000 g mol^{-1}), which are of similar length, as precipitant, precipitation yields in the range of 80–95% were observed, respectively. The precipitation yield using AMPS as polyanionic precipitant declined with increasing ionic strength (Figure 2a), most likely due to counterion screening and consequent reduction in the electrostatic attraction between polyelectrolyte and the protein under consideration. Additionally, possible self-contraction of polymer chains due to screening of Coulomb forces between polyelectrolyte monomer units might also contribute to the observed reduced precipitation efficiency.[35] With increase of ionic strength in the precipitation buffer, only a minor decline in precipitation yield was observed using PAA as precipitant (Figure 2a), while yields of precipitated protein were strongly reduced using AMPS at a NaCl concentration above 100 mM.

Precipitation experiments were carried out at pH 5.0: Because the pK_a of PAA is close to that pH, a significant fraction of the carboxylic acid groups within the polymer remained protonated, thus exhibiting no electrostatic interaction.[36] However, PAA displays intrinsic hydrophobic properties as well, which become more pronounced as ionic strength increases.[14] Considering that protein precipitation is dependent on conjoint hydrophobic and electrostatic forces,

this implies that hydrophobic forces are strengthened with increasing ionic strength, while electrostatic forces are reduced.[14] Accordingly, we observed no differences in the precipitation behavior of PAA between low and high ionic strength (Figure 2a). In contrast, AMPS, with its sulfonic acid groups being dissociated over almost the entire pH-range,[37] shows no dedicated hydrophobic properties at pH 5.0, but exhibits mainly electrostatic interactions. As a consequence of reduced electrostatic interactions with increasing ionic strength and lack of hydrophobic interactions, overall precipitation yield declined (Figure 2a).

Additionally, AMPS and PAA were analyzed for precipitation efficiency in binary mAb-BSA protein systems (Figure 2b). BSA was considered here as an impurity protein since it displays a *pI* close to the typical *pI*-range of most host cell culture proteins.[38,39] Moreover, BSA has been used as a supplement in cell culture media in the past and is still sometimes used today.[40] Because of the low precipitation strength of AMPS at 150 mM NaCl, AMPS was used at 125 mM NaCl while PAA was evaluated at 150 mM NaCl, due to later intended use of precipitation at physiological salt concentrations (Figure 2b). Using these conditions, AMPS showed higher selectivity toward mAb binding compared to PAA, whereas BSA coprecipitation using AMPS varied between 3 and 11%. Using PAA, in contrast, high yield BSA coprecipitation in the range of 50–60% was observed. However, overall precipitation yield for mAbs were higher with PAA compared to AMPS when precipitating mAbs without added BSA (Figure 2a). The hydrophobicity of PAA at pH 5.0 may account for its low selectivity since BSA is known to contain hydrophobic patches on its surface.[41] AMPS, however, mainly exerting electrostatic interactions, did not precipitate BSA, which is expected to be largely uncharged at a pH 5.0 (*pI* 4.7). In contrast, the mAb with a *pI* between 8 and 9 exhibited sufficient positive surface potential to become precipitated via electrostatic interaction with the AMPS homopolymer.

In view of these results, it seemed feasible to consider copolymers that allow for combined hydrophobic and electrostatic interactions with the target proteins, eventually providing optimal conditions with respect to precipitation yield and selectivity, even at physiological ionic strength. While a defined degree of hydrophobicity and electrostatic interaction within the copolymers could be established via variation of their composition, this would not be possible with AMPS homopolymer and not easily achievable with PAA, as it could only be modulated by pH adjustment, which on the other hand would also affect protein charge density.

Influence of polyelectrolyte composition and weight average molecular weight on precipitation selectivity

To elucidate the effect of different M_w and different degrees of hydrophobicity within a polymer on precipitation yield and selectivity, various AMPS–ABZ copolymers of different M_w and different ABZ content were synthesized and used for precipitation experiments with five different mAbs and BSA at 150 mM NaCl and pH 5.0 (Figure 3).

Generally, both mAb and BSA precipitation increased with increasing M_w and increasing ABZ content of copolymers. While with mAb C, precipitation yields of >80% were observed that were independent of M_w and percentage of ABZ, the other mAbs required at least 40–50% ABZ to achieve precipitation yields of 60–80% and higher. As an exception, with mAb E a similar yield was already obtained
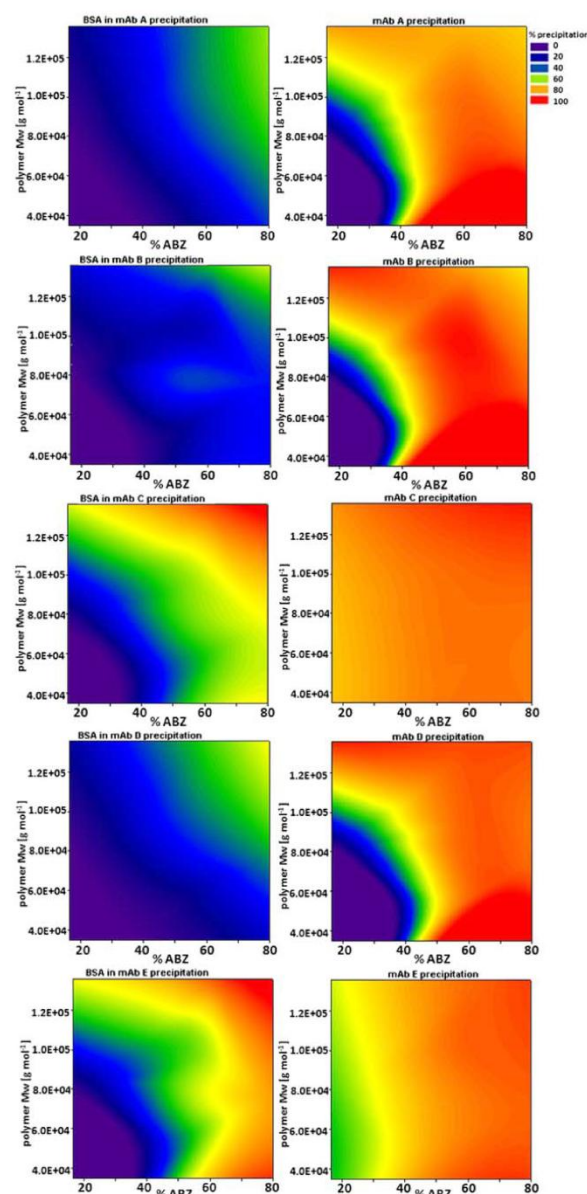
Figure 3. Contour plot of BSA and mAb precipitation in a binary BSA-mAb protein system, using copolymers of different 4-(acryloylamino)benzoic acid (ABZ) content and weight average molecular weight.

with 30–40% ABZ. A further increase of the ABZ content within the copolymer resulted in mAb precipitation yields close to 100%, likely due to conjoint effects of hydrophobic and electrostatic interactions.[12,14,18,42] A Mw between 40,000 and 100,000 g mol^{-1} was beneficial to obtaining high precipitation yields (Figure 3), indicating a chain length dependency of precipitation as has been seen with other experiments, where entropy effects were considered a presumable reason.[38] A correlation between polyelectrolyte M_w and protein–polyelectrolyte cluster formation was also seen in Monte Carlo simulations and *in vitro* experiments.[42–47] However, BSA coprecipitation also increased with increasing ABZ content or increasing copolymer M_w. A reason for this unwanted effect (BSA acts as an impurity protein) might be an increased likelihood of BSA (M_w 66 kDa) to become

Figure 4. (a): Correlation between required ABZ content within copolymer to obtain mAb precipitation >80% and relative mAb hydrophobicity, compared to mAb C hydrophobicity set to 100%. (b): Comparison of mAb A, mAb B and mAb D precipitation yields depending on ABZ content.
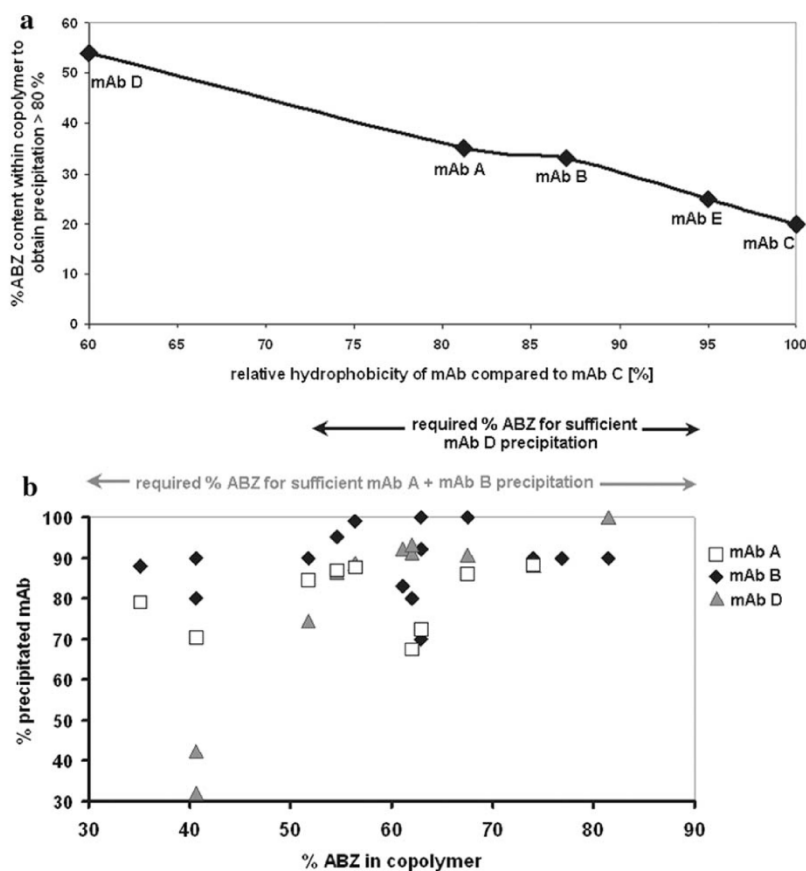
entrapped within the mAb-polyelectrolyte complex when using longer polyelectrolytes.[48] Additionally, for copolymers with higher ABZ content and thus higher hydrophobicity, a higher BSA precipitation was observed, an effect that is most likely due to enhanced hydrophobic interaction.[12]

With mAb C and mAb E, BSA coprecipitation was higher than for the other mAbs, and coprecipitation yields were 60% and higher using a copolymer containing >50% ABZ. For the other mAb-BSA systems, BSA precipitation varied between 20 and 40%, except for copolymer with both high ABZ content and M_w larger than 50,000 g mol^{-1} (mAb A), 70,000 g mol^{-1} (mAb D) and 100,000 g mol^{-1} (mAb B), respectively.

Summarizing these results, for all mAb-BSA systems there is a trade-off between high mAb precipitation yields and elevated BSA coprecipitation, depending on M_w and copolymer composition. However, when comparing the contour plots for each mAB/BSA pair, employing a copolymer of defined M_w and ABZ content, high mAb yield can be obtained while at the same time BSA coprecipitation is minimized. Generally, this window is between 40 and 60% ABZ content and up to a M_w of 100,000 g mol^{-1}, depending on the mAb used.

Influence of mAb hydrophobicity on precipitation behavior

A correlation was observed between antibody hydrophobicity and the ABZ content of the copolymer to achieve at least 80% precipitation (Figure 4a). Monoclonal antibody C

and mAb E are more hydrophobic than the other antibodies, according to HIC and hydrophobicity determination by TNS. For these mAbs, high precipitation yields were achieved already at low ABZ content of the copolymer. Furthermore, BSA coprecipitation was elevated compared to the other mAbs, with hydrophobic interaction between BSA and the mAbs likely playing a role. For mAb A, mAb B, and mAb D, precipitation was compared in relation to ABZ content of employed copolymers (Figure 4b). It should be mentioned that the copolymers used not only differed in their ABZ content but also in their M_w, which may additionally influence precipitation yields. Using copolymers of <50% ABZ content, mAb D precipitation yields were lower than 70% (Figure 4b), in contrast to the two other antibodies. These results correlate with HIC data, showing a significantly lower hydrophobicity for mAb D compared to mAb B and mAb A, which display similar hydrophobicity.

Thus, these results indicate an inverse correlation between mAb hydrophobicity and the required ABZ content within the copolymer to obtain high mAb precipitation yields. Hydrophobic mAbs required less hydrophobic copolymer to achieve acceptable yields compared to less hydrophobic mAbs.

Influence of pH on precipitation selectivity

The copolymers discussed above are intended to be used for protein purification in downstream processing using a near
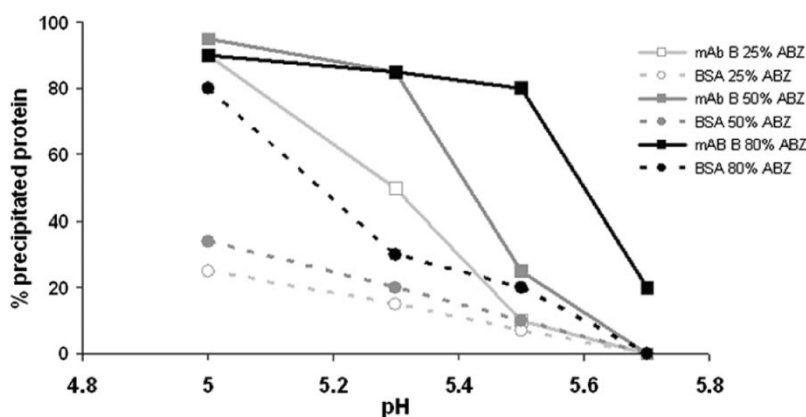
Figure 5. Precipitation yield of mAb B and BSA in a binary protein system, depending on pH and copolymer composition.

physiological pH range of 5–6. These conditions are above the *pI* of most of the impurity proteins, which might help to reduce their coprecipitation. While for mAbs A and C-E, only a limited number of experiments regarding influence of pH on selectivity were performed, detailed effects of pH on precipitation yield and selectivity at 150 mM NaCl were analyzed for mAb B and BSA. Monoclonal antibody B was chosen as a representative for most of the mAbs employed in this study, and a surface hydrophobicity model of this mAb is included in the discussion. Three different copolymers with 25, 50, and 80% ABZ content and a similar M_w of ~100,000 ± 6,000 g mol^{-1} (Figure 5) were employed.

Generally, higher pH reduced BSA co-precipitation; however it also led to lower mAb precipitation yields, as seen in experiments with other mAbs (data not shown). While copolymers with 25 and 50% ABZ, respectively, led to <40% BSA precipitation at pH 5.0, this was reduced to almost 0% at pH 5.7 (Figure 5). Similar to results observed in experiments with mAbs A and C-E (not shown), mAb precipitation yield was reduced from 90% at pH 5.0 to <30% at pH 5.5. However, the copolymer with 25% ABZ content showed significant reduction of precipitation yield already between pH 5.0 and 5.3, in contrast to the 50% ABZ copolymer, which enabled >70% mAb precipitation up to a pH of 5.4. In comparison, usage of copolymer with 80% ABZ content as precipitant allowed for antibody precipitation yields of >80% up to pH 5.5, which were reduced to 20–30% at pH 5.7. Concomitantly, BSA coprecipitation was elevated to 80% at pH 5.0 and reduced to 50% at pH 5.3 (Figure 5). Applying formula 1 (based on Ref. 49) to Figure 5, taking pH 5.5 as basis for comparison, an increase in selectivity from around 1, using 25% ABZ content, to 27, using 80% ABZ content, can be observed.

$$\text{Selectivity } S = \frac{\text{mAb}_{\text{precip}} \ / \ \text{BSA}_{\text{precip}}}{\text{mAb}_{\text{supernatant}} / \text{BSA}_{\text{supernatant}}} \quad (1)$$

Assuming this precipitation behavior to be mainly based on hydrophobic and electrostatic interactions, 80% ABZ content within the copolymer likely enabled strong hydrophobic interaction at pH 5.0, which is close to the pK_a of acrylamidobenzoic acid. This was manifested in high BSA coprecipitation. Increasing the pH resulted in reduction of hydrophobicity of the copolymer due to moving away from the pK_a of ABZ, deprotonating the carboxylic acid group,

and instead exhibiting a negatively charged side chain that caused electrostatic repulsion. Accordingly, BSA coprecipitation was reduced to 50% at pH 5.3 and 10% at pH 5.5. In contrast with the other two copolymers with 25 and 50% ABZ content, respectively, protein precipitation is likely mainly caused by electrostatic interaction. This is corroborated by the finding that only a small decrease in BSA precipitation yield was observed when shifting from pH 5.0 to 5.3. If hydrophobic interactions were the main driving force for protein precipitation using this copolymer, one would have expected a decline of coprecipitation yield with an increase of pH beyond 5.0 due to deprotonation of the carboxylic acid groups.

While so far, the discussed differences in precipitation behavior at different pH were linked to different degrees of copolymer ABZ content and thus hydrophobicity, also intrinsic differences in surface charge and hydrophobicity between mAb and BSA most likely contribute to the observed effects. Monoclonal antibody precipitation decreased with increasing pH, likely due to protein surface charge being reduced when approaching the *pI* of the mAb (Figure 6). While at pH 5.0 low amounts of negative surface charge are present, the increase in net charge at pH 5.7 likely contributes to the observed decrease of precipitation yield which may be attributed to electrostatic repulsion.

For BSA, using a pH above its *pI* (4.7) results in a mainly negative surface charge (Figure 6), and, therefore, in an electrostatic repulsion of the negatively charged protein surface and the anionic polyelectrolyte. As a consequence, the unwanted co-precipitation of BSA is significantly reduced above pH 5.3 and nearly absent at pH 5.7 (Figures 5 and 6). In Figure 7, the surface hydrophobicity of BSA and mAb B is shown according to the Kyte-Doolittle hydropathy scale, which is based on water vapor transfer free energies (pH 7.0) and interior/ exterior distribution of amino acid side chains in proteins.[32] In the mAb, contiguous patches of hydrophobic residues are rare and mainly located in the Fc portion.[50,51] For BSA, several hydrophobic patches are present and more evenly spread across the entire protein surface. This likely allows stronger hydrophobic interaction with the copolymer compared to copolymer and mAb. Additionally, BSA precipitation was performed at pH 5.0, thus being close to its *pI*, allowing for protonation of some of its carboxylic acid groups. This would have resulted in even higher intrinsic hydrophobicity compared to the calculated
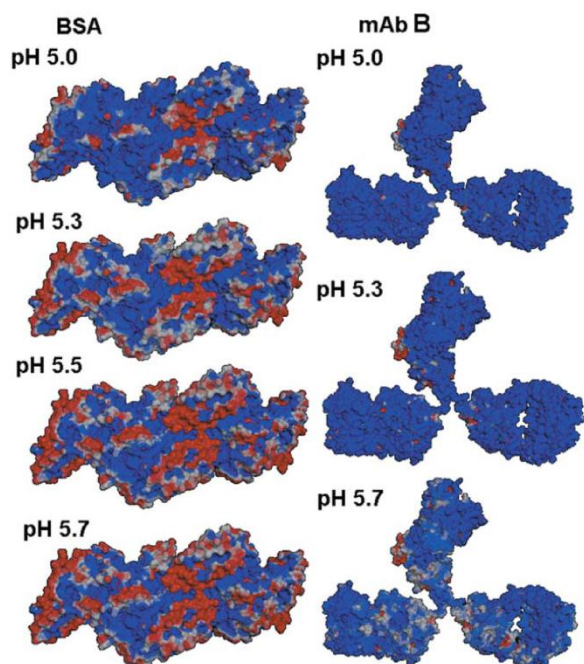
Figure 6. Surface charge distribution of BSA and mAb B, depending on pH, visualized in Chimera using program threshold for coloring electrostatic potential: red: $\leq -2.0\ k_B T\ e^{-1}$; blue: $\geq +2.0\ k_B T\ e^{-1}$.
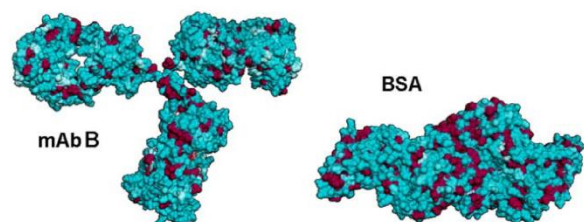

Figure 7. Hydrophobic patches of mAb B (left) and BSA (right). Protein surface labeled according to Kyte–Doolittle scale, using threshold ±1.0. Hydrophobic residues labeled in maroon and hydrophilic residues labeled in cyan, using Chimera.

hydrophobicity pattern at pH 7.0 shown in Figure 7. The finding that BSA co-precipitation decreases with increasing pH corroborates the notion that conjoint hydrophobic and electrostatic interactions are mainly responsible for the pH-dependent precipitation behavior of that protein.

Scalability and possible use of copolymers within a purification process

These customized copolymers, due to ease in scalability, may be added as highly concentrated solution to e.g. cell culture fluid in a bioreactor, allowing precipitation of the target protein after prior pH-adjustment. Nonprecipitated protein could then be removed using e.g. flow-through centrifuges or filtration, and the protein–polymer pellet could be redissolved. This has been shown in experiments by our group, confirming the reversibility of precipitation and redissolution due to pH-adjustments, and has also been shown by

Matsudo et al. (2003) and Lombardi et al. (2013).[9,52] If antibody and polymer have the same net charge, the protein–polymer pellet can be redissolved. Polymer can then be removed by suitable strategies, e.g. using silica flakes with cationic properties that allow capture of the negatively charged polymer while leaving the positively charged antibody in solution. Initial experiments revealed the feasibility of this strategy. While most of the copolymer can be removed using this strategy, only 10% of precipitated antibody are lost in subsequent redissolution and polymer removal processes, resulting in a final yield of around 80–90% (data not shown here).

Conclusion

Compared to homopolymers AMPS and PAA that have intrinsic restrictions with respect to salt-tolerance, yield, and selectivity, AMPS-ABZ copolymers enabled mAb precipitation yields of up to 90–100% in a model mAb and BSA system, likely due to conjoint hydrophobic and electrostatic interactions. Our results using binary mAb–BSA protein matrices indicate that increasing the copolymer chain length, via the M_w, or using copolymers with higher degrees of hydrophobicity due to varied ABZ content, results in enhanced coprecipitation of the model impurity protein BSA, while also increasing the precipitation yield of the mAb target protein. However, depending on the mAb, copolymers with a defined Mw and defined degree of ABZ content can be identified, allowing for high mAb precipitation and low BSA coprecipitation, yielding high mAb purity. Hence, it is possible to fine-tune precipitation selectivity while maintaining high yields by altering Mw and composition of copolymers, the latter factor being more important for adjusting selectivity and being dependent on protein hydrophobicity. While it has to be elucidated whether these observations apply to all antibodies, at least for antibody proteins similar to those tested here, similar observations are expected. Our results provide a deeper understanding of polymer–protein interaction and thus might contribute to a broader applicability of polymer-driven protein precipitation for large-scale protein purification.

Literature Cited

1. Marichal-Gallardo PA, Alvarez MM. State-of-the-art in downstream processing of monoclonal antibodies: process trends in design and validation. *Biotechnol Prog*. 2012;28:899–916.
2. Kelley B. Very large scale monoclonal antibody purification: the case for conventional unit operations. *Biotechnol Prog*. 2007;23:995–1008.
3. Peram T, McDonald P, Carter-Franklin J, Fahrner R. Monoclonal antibody purification using cationic polyelectrolytes: an alternative to column chromatography. *Biotechnol Prog*. 2010;26:1322–1331.
4. Ma J, Hoang H, Myint T, Peram T, Fahrner R, Chou JH. Using precipitation by polyamines as an alternative to chromatographic separation in antibody purification processes. *J Chromatogr B*. 2010;878:798–806.

5. McDonald P, Victa C, Carter-Franklin JN, Fahrner R. Selective antibody precipitation using polyelectrolytes: a novel approach to the purification of monoclonal antibodies. *Biotechnol Bioeng.* 2009;102:1141–1151.

6. Wang YF, Gao JY, Dubin PL. Protein separation via polyelectrolyte coacervation: selectivity and efficiency. *Biotechnol Prog.* 1996;12:356–362.

7. Boeris V, Romanini D, Farruggia B, Picó G. Purification of chymotrypsin from bovine pancreas using precipitation with a strong anionic polyelectrolyte. *Process Biochem.* 2009;44:588–592.

8. Porfiri MC, Braia M, Farruggia B, Picó G, Romanini D. Precipitation with poly acrylic acid as a trypsin bioseparation strategy. *Process Biochem.* 2009;44:1046–1049.

9. Lombardi J, Valetti NW, Picó G, Boeris V. Obtainment of a highly concentrated pancreatic serine proteases extract from bovine pancreas by precipitation with polyacrylate. *Sep Purif Technol.* 2013;116:170–174.

10. Boeris V, Spelzini D, Salgado JP, Picó G, Romanini D, Farruggia B. Chymotrypsin–poly vinyl sulfonate interaction studied by dynamic light scattering and turbidimetric approaches. *Biochim Biophys Acta.* 2008;1780:1032–1037.

11. Mondal K, Mehta P, Gupta MN. Affinity precipitation of *Aspergillus niger* pectinase by microwave-treated alginate. *Protein Expres Purif.* 2004;33:104–109.

12. Tribet C. Complexation between amphiphilic polyelectrolytes and proteins: from necklaces to gels. In: Radeva T, editor. Physical Chemistry of Polyelectrolytes, Surfactant Science Series. New York: Marcel Dekker; 2001:687–742.

13. Hattori T, Hallberg R, Dubin PL. Roles of electrostatic interaction and polymer structure in the binding of β-lactoglobulin to anionic polyelectrolytes: measurement of binding constants by frontal analysis continuous capillary electrophoresis. *Langmuir.* 2000;16:9738–9743.

14. Seyrek E, Dubin PL, Tribet C, Gamble EA. Ionic strength dependence of protein–polyelectrolyte interactions. *Biomacromolecules.* 2003;4:273–282.

15. Thommes J, Etzel M. Alternatives to chromatographic separations. *Biotechnol Prog.* 2007;23:42–45.

16. Low D, O'Leary R, Pujar NS. Future of antibody purification. *J Chromatogr B.* 2007;848:48–63.

17. Cooper CL, Goulding A, Kayitmazer AB, Ulrich S, Stoll S, Turksen S, Yusa Si, Kumar A, Dubin PL. Effects of polyelectrolyte chain stiffness, charge mobility, and charge sequences on binding to proteins and micelles. *Biomacromolecules.* 2006;7:1025–1035.

18. Cooper CL, Dubin PL, Kayitmazer AB, Turksen S. Polyelectrolyte–protein complexes. *Curr Opin Colloid Interface Sci.* 2005;10:52–78.

19. Benmansour K, Medjahed K, Tennouga L, Mansri A. Ionic conductivity of poly[*N*-(3,6,9-trioxadecyl)-4-vinylpyridinium)] salts with univalent counter-ions in aqueous solutions. *Eur Polym J.* 2003;39:1443–1449.

20. Baker NA, Sept D, Joseph S, Holst MJ, McCammon JA. Electrostatics of nanosystems: application to microtubules and the ribosome. *Proc Natl Acad Sci USA* 2001;98:10037–10041.

21. Li H, Robertson AD, Jensen JH. Very fast empirical prediction and rationalization of protein pKa values. *Proteins Struct Funct Bioinf.* 2005;61:704–721.

22. Bas DC, Rogers DM, Jensen JH. Very fast prediction and rationalization of pKa values for protein–ligand complexes. *Proteins Struct Funct Bioinf.* 2008;73:765–783.

23. Olsson MHM, Sondergaard CR, Rostkowski M, Jensen JH. PROPKA3: consistent treatment of internal and surface residues in empirical pKa predictions. *J Chem Theory Comput.* 2011;7:525–537.

24. Dolinsky TJ, Czodrowski P, Li H, Nielsen JE, Jensen JH, Klebe G, Baker NA. PDB2PQR: expanding and upgrading automated preparation of biomolecular structures for molecular simulations. *Nucleic Acids Res.* 2007;35:522–525.

25. Dolinsky TJ, Nielsen JE, McCammon JA, Baker NA. PDB2PQR: an automated pipeline for the setup, execution, and analysis of Poisson–Boltzmann electrostatics calculations. *Nucleic Acids Res.* 2004;32:665–667.

26. Yang Z, Lasker K, Schneidman-Duhovny D, Webb B, Huang CC, Pettersen EF, Goddard TD, Meng EC, Sali A, Ferrin TE. UCSF Chimera, MODELLER, and IMP: an integrated modeling system. *J Struct Biol.* 2012;179:269–278.

27. Pettersen EF, Goddard TD, Huang CC, Couch GS, Greenblatt DM, Meng EC, Ferrin TE. UCSF Chimera—a visualization system for exploratory research and analysis. *J Comput Chem.* 2004;25:1605–1612.

28. Guex N, Peitsch MC. SWISS-MODEL and the Swiss-PdbViewer: an environment for comparative protein modeling. *Electrophoresis.* 1997;18:2714–2723.

29. Kiefer F, Arnold K, Kunzli M, Bordoli L, Schwede T. The SWISS-MODEL repository and associated resources. *Nucleic Acids Res.* 2009;37:387–392.

30. Arnold K, Bordoli L, Kopp Jr, Schwede T. The SWISS-MODEL workspace: a web-based environment for protein structure homology modelling. *Bioinformatics.* 2006;22:195–201.

31. Bordoli L, Kiefer F, Arnold K, Benkert P, Battey J, Schwede T. Protein structure homology modeling using SWISS-MODEL workspace. *Nat Protocols.* 2008;4:1–13.

32. Kyte J, Doolittle RF. A simple method for displaying the hydropathic character of a protein. *J Mol Biol.* 1982;157:105–132.

33. Roettger BF, Ladisch MR. Hydrophobic interaction chromatography. *Biotechnol Adv.* 1989;1:15–29.

34. McClure WO, Edelman GM. Fluorescent probes for conformational states of proteins. I. Mechanism of fluorescence of 2-*p*-toluidinylnaphthalene-6-sulfonate: a hydrophobic probe. *Biochemistry.* 1966;5:1908–1919.

35. De Gennes PG, Pincus P, Velasco RM, Brochard F. Remarks on polyelectrolyte conformation. *J Phys France.* 1976;37:1461–1473.

36. Fujiwara M, Grubbs RH, Baldeschwieler JD. Characterization of pH-dependent poly(acrylic acid) complexation with phospholipid vesicles. *J Colloid Interface Sci.* 1997;185:210–216.

37. Durmaz S, Okay O. Acrylamide/2-acrylamido-2-methylpropane sulfonic acid sodium salt-based hydrogels: synthesis and characterization. *Polymer.* 2000;41:3693–3704.

38. Champion KM, Arnott D, Henzel WJ, Hermes S, Weikert S, Stults J, Vanderlaan M, Krummen L. A two-dimensional protein map of Chinese hamster ovary cells. *Electrophoresis.* 1999;20:994–1000.

39. Pezzini J, Joucla G, Gantier R, Toueille M, Lomenech AM, Le Sénéchal C, Garbay B, Santarelli X, Cabanne C. Antibody capture by mixed-mode chromatography: a comprehensive study from determination of optimal purification conditions to identification of contaminating host cell proteins. *J Chromatogr A* 2011;45:8197–8208.

40. van der Valk J, Brunner D, De Smet K, Fex Svenningsen A, Honegger P, Knudsen LE, Lindl T, Noraberg J, Price A, Scarino ML, Gstraunthaler G. Optimization of chemically defined cell culture media-replacing fetal bovine serum in mammalian in vitro methods. *Toxicol In Vitro.* 2010;24:1053–1063.

41. Xiao J, Shi J, Cao H, Wu S, Ren F, Xu M. Analysis of binding interaction between puerarin and bovine serum albumin by multi-spectroscopic method. *J Pharm Biomed Anal.* 2007;45:609–615.

42. Carlsson F, Malmsten M, Linse P. Protein-polyelectrolyte cluster formation and redissolution: a Monte Carlo study. *J Am Chem Soc.* 2003;125:3140–3149.

43. Izmrudov V, Galaev I, Mattiasson B. Polycomplexes-potential for bioseparation. *Bioseparation.* 1998;7:207–220.

44. Tsuchida E, Abe K. Polyelelctrolyte complexes. In: Wilson AD, Prosser HJ. Developments in Ionic Polymers-2. New York: Elsevier; 1986:191–263.

45. Papisov LM, Litmanovich AA, Billingham NC, Calvert PD, Kurimura Y. Conducting Polymers/Molecular Recognition. Berlin: Springer; 1989:139–179.

46. Shieh JY, Glatz CE, Dubin P, Bock J, Davis R, Schulz DN, Thies C. Macromolecular Complexes in Chemistry and Biology. *Berlin: Springer*; 1994:273–284.

47. Pergushov DV, Izumrudov VA, Zezin AB, Kabanov VA. Stability of interpolyelectrolyte complexes in aqueous saline solutions: effect of the degree of polymerization of polyions, *J. Polym. Sci. A.* 1995;37:1081–1087.

48. Blintsov AN, Dzantiev BB, Bobkova AF, Izumrudov VA, Zezin AB, Atabekov IG. A new method for enzyme immunoassay of

phytoviruses, based on interpolyelectrolyte reactions. *Doklady Biochem.* 1995;345:175–178.

49. Strege MA, Dubin PL, West JS, Flinta CD. Protein separation via polyelectrolyte complexation. In: Ladisch M, Willson RC, Paint CC, Builder SE, editors. Protein Purification: From Molecular Mechanisms to Large-Scale Processes. ACS symposium series. Washington, DC: American Chemical Society; 1990:427–466.

50. Boschetti E. Antibody separation by hydrophobic charge induction chromatography. *Trends Biotechnol.* 2002,20:333–337.

51. Guerrier L, Flayeux I, Boschetti E. A dual-mode approach to the selective separation of antibodies and their fragments. *J Chrom B.* 2001;755:37–46.

52. Matsudo T, Ogawa K, Kokufuta E. Complex formation of protein with different water-soluble synthetic polymers. *Biomacro-molecules* 2003;4:1794–1799.

3.5. Mid infrared spectroscopy as tool in protein precipitation process development and aided monitoring of critical process parameters in protein production

3.5.1 Host cell protein quantification using MIR

Paper: Host cell protein quantification by fourier transform mid infrared spectroscopy (FT-MIR)

Florian Capito, Romas Skudas, Harald Kolmar and Bernd Stanislawski

Short Summary:

Mid infrared spectroscopy (MIR) was evaluated the first time as tool for quantifying host cell impurity proteins in samples containing polymer, representing polymer-treated process samples. Promising results were obtained for a host cell protein level between 20,000- 200,000 ng ml^{-1}, comparable to an ELISA assay. Yet, this concentration range makes the application only partly suitable for use within the development of a precipitation process. However, the use of MIR for host cell protein quantification is suitable especially for monitoring of process development steps with higher host cell protein concentrations, allowing direct measurement without further dilution and dilution-errors as with ELISA.

Fig. 4: Typical mammalian cell culture process in a small-scale bioreactor. Source: Figure taken at Merck Site Martillac.

Host Cell Protein Quantification by Fourier Transform Mid Infrared Spectroscopy (FT-MIR)

Florian Capito,[1,2] Romas Skudas,[2] Harald Kolmar,[1] Bernd Stanislawski[2]

[1]Institute for Organic Chemistry and Biochemistry, Technische Universität Darmstadt, Darmstadt, Germany

[2]Merck KGaA, Frankfurter Strasse 250, 64293 Darmstadt, Germany; telephone: 49-6151-727168; fax: 0049 6151 72 917510; e-mail: florian.capito@external.merckgroup.com

ABSTRACT: Process development in up- and downstream processing requires enhanced, non-time-consuming, and non-expensive monitoring techniques to track product purity, for example, the level of endotoxins, viral particles, and host cell proteins (HCPs). Currently, HCP amounts are measured by laborious and expensive HCP-enzyme-linked immunosorbent assay (ELISA) assays best suited for measuring HCP amounts in the low concentration regime. The measurement of higher HCP amounts using this method requires dilution steps, adding dilution errors to the measurement. In this work we evaluated the suitability of attenuated total reflection spectroscopy for HCP quantification in process development, using clarified cell culture fluid from monoclonal antibody producing Chinese hamster ovary-cells after treatment with different polyelectrolytes for semi-selective clarification. Forty undiluted samples were chosen for multivariate data analysis in the middle infrared range and predicted HCP-values were in good agreement with results obtained by an ELISA-assay, suggesting the suitability of this new method for HCP-quantification. As this method is able to quantify HCP titers ranging from approximately at least 20,000–200,000 ng mL^{-1}, it is suitable especially for monitoring of process development steps with higher HCP concentrations, omitting dilution errors associated with ELISA assays.

Biotechnol. Bioeng. 2013;110: 252–259.

© 2012 Wiley Periodicals, Inc.

KEYWORDS: host cell proteins; attenuated total reflection; Fourier transform infrared spectroscopy; partial least squares regression; process development; bioanalytics

Introduction

Host cell proteins (HCPs) represent a major process related impurity group present in cell culture supernatant during the production of biopharmaceuticals. Their removal and quantification during various steps of up- and downstream processing is required as HCPs possess potentially antigenic functions (Champion et al., 2005; Dotzel, 1999; Zoon, 1997). Process development makes use of different, orthogonal purification methods to remove and measure HCPs, reflecting their vast biochemical and biophysical heterogeneity (Wang et al., 2009). To elucidate the potential of fermentation and purification methods for HCP clearance as well as effects of cell culture parameters on HCP presence during process development, many HCP analyses are necessary. Furthermore, constant analysis of HCP titers in cell cultures at different downstream processing steps helps to monitor the efficacy of the chosen purification method and adapt to changes in real-time.

Up-to-date HCP quantification is mainly done by not real-time enzyme-linked immunosorbent assays (ELISA) or 2D polyacrylamide gel electrophoresis (2D-SDS–PAGE) combined with western blotting (Flatman et al., 2007; Wang et al., 2009).

Some alternative technique addressing the drawbacks of time-consuming and expensive HCP-analysis, is HPLC, which has the potential to be done at- or online to the bioreactor, though at low sensitivity, and results being subjective to interpretation (Hoffman, 2000). Additionally, online sensors, used to measure analytes face the problem of sterility and long-term stability (Rhiel et al., 2002).

An alternative non-invasive technology is Fourier transform infrared spectroscopy (FT-IR), which provides an opportunity to measure directly in the fermenter or in a bypass without destroying the analytes. FT-IR makes use of the interaction between irradiation and matter at different wavenumbers (Kong and Shaoning, 2007).

A sample-specific spectrum provides opportunity for identifying functional groups and molecules (Griffiths and

Haseth, 2007), for example, proteins. For quantitative and qualitative analysis of proteins, nine characteristic bands in the infrared spectra can be analyzed (Amide A, Amide B, and Amide 1–7), whereby mainly the Amide I and II bands are used (Krimm et al., 1986).

The application of FT-IR for complex sample characterization is not straight forward, since cell cultures consist of various components (vitamins, amino acids, cholesterol, growth factors, lipids, nucleic acids, proteins, and antibiotics; Chu and Robinson, 2001). These complex analytes with non-specified components show overlapping spectra, therefore data processing such as first and second derivative, Fourier self-deconvolution and normalization can help to increase resolution and reveal information, for example, about secondary structure elements of proteins (Dong et al., 2002; Kong and Shaoning, 2007; Li et al., 1996). Principal component analysis (PCA) and partial least squares regression (PLS) models help to extract chemical information from spectra and elucidate information about single components (Esbensen, 2002; Martens and Naes, 1989; Wold et al., 2001).

Additionally, FT-IR has been used to obtain protein secondary structure (Arrondo et al., 1993; Barth, 2007; Goormaghtigh et al., 2006; Jackson and Mantsch, 1995; Siebert, 1995), to identify in situ compounds in different cell culture compositions (Doak and Phillips, 1999; Mazarevica et al., 2004), and to analyze single amino acids in a composition in the millimolar range (Barth, 2007; Riley et al., 2001). New strategies involving FT-IR are classification of microorganisms (Winder et al., 2004), recombinant protein quantification in microbial cell cultures (Gross-Selbeck et al., 2007; McGovern et al., 1999) and determination of antibody or human antithrombin III titers in mammalian cell cultures (Harthun et al., 1997; Sellick et al., 2010).

In our approach, we applied FT-IR while differentiating between different proteins, HCPs on one hand and antibodies on the other hand, quantifying the amount of HCPs. To evaluate the potential of FT-IR for HCP quantification during process development, we used multivariate data analysis in conjunction with antibody producing Chinese hamster ovary (CHO) cells, subjected to semi-selective HCP and antibody removal in the supernatant in order to meet a robustness criterion. Samples were precipitated with different polyelectrolytes to evaluate the ability of the method, to quantify HCPs against a background of polyelectrolyte and antibody.

Our method of choice was attenuated total reflection (ATR; Fahrenfort, 1961; Harrick, 1960), already been used for fuel and fermentation analysis (Pillonel et al., 2003; Pimentel et al., 2006), able to perform in situ analysis without intensive sample preparation, furthermore, providing a possibility to obtain a constant in real-time monitoring of cell culture.

The objective of this study was to elucidate the potential of FT-IR to assist in cell culture analysis during process development and predict HCP titers. HCP analysis was compared to ELISA assays; HCP prediction was done using chemometric PCA and PLS models for an antibody

producing CHO cell line. Calibration model was evaluated analyzing prediction error and robustness.

Materials and Methods

Cell Lines

CHO cells producing IgG1 antibody were used for the experiments, produced by Merck Millipore and obtained from Merck KGaA, Darmstadt, Germany as internal standard derived from serum free cell culture media.

Polyelectrolytes

Poly(anethole sulfonic acid; Sigma–Aldrich (Sigma–Aldrich Chemie GmbH, Steinheim, Germany), poly(styrene sulfonic acid; Polymer Standards Service, Mainz, Germany), poly(vinyl sulfonic acid; Polysciences, Warrington), poly-(acrylic acid; Polysciences), and dextran sulfate (DS; Sigma–Aldrich) were used for semi-selective precipitation after adjusting adequate polyelectrolyte stock solutions to pH 5.0.

Preparation of Calibration Samples

Cell culture was harvested, clarified, and adjusted to pH 5.0 using a 20 mM Na-acetate buffer (Merck KGaA, Darmstadt, Germany), polyelectrolytes of different composition and concentration were added to remove different HCP subpopulations and antibody to varying, not correlating, degrees, and simulate a differing chemical background. Thereby we avoided the risk of colinearity of protein concentrations in the samples (Martens and Naes, 1989; Scarff et al., 2006; Warnes et al., 1996) and were able to cover a wide space of the calibration area (Isaksson and Naes, 1990). Also, the use of different polyelectrolytes minimized possible influence of polyelectrolytes on the calibration model. After an incubation step, samples were centrifuged and supernatant transferred to new tubes.

Antibody Concentration Determination by Affinity Chromatography

Protein A analytical affinity chromatography was used to determine monoclonal antibody (mAb) concentration in the samples. All experiments were run on the LaChrom Merck Hitachi HPLC system (VWR, Darmstadt, Germany) using Poros A20 ($4.6 \times 50\,mm^2$) column (Applied Biosystems, Foster City). UV detection was carried out at 280 nm and sample injection volume was 100 μL. Two different buffer solutions were used: 25 mM sodium dihydrogen phosphate and 300 mM sodium chloride pH 7.2 as adsorption buffer and 150 mM acetic acid pH 2.7 as a desorption buffer. System was calibrated with known concentration mAb samples. The measurements of the chosen samples were carried out three times. Mean values from three independent runs of each sample were taken.

HCP Analysis by ELISA

HCP concentration in all supernatants of polyelectrolyte-treated samples was analyzed using HCP-ELISA (3rd Generation CHO–HCP ELISA kit; Cygnus Technologies, Wrentham, MA) according to the manufacturer's manual. Samples were measured multiple times. Interference of either antibody or polyelectrolytes on assay results was analyzed mixing 1/5 of 100 ng mL^{-1} HCP standard with 4/5 of antibody or polyelectrolyte, respectively, to obtain 20 ng mL^{-1} HCP standards.

HCP Analysis by ATR

Unlike for ELISA, samples were used without prior serial dilution to ensure they met higher limit of quantification in spectroscopy. Twenty microliters of each sample were measured on GoldenGate^{TM} MkII series ATR (Specac Inc, Cranston, RI), using a diamond (type IIa, 45°C, diameter 2 mm × 2 mm; refractive index at 1,000 cm^{-1}: 2.4; 0.8 mm diameter of active sampling area; 2 m penetration depth for a sample of refractive index 1.5 at 1,000 cm^{-1}) at 20°C with H$_2$O as background. Diamond was open to atmosphere and head space purged with N$_2$. Spectra were recorded with a Bruker Tensor 27 (Bruker Optik GmbH, Ettlingen, Germany); samples were scanned in absorbance mode with 120 scans at a spectral resolution of 4.0. Detector was a Bruker LN-MCT photovoltaic internal detector (Bruker Optik GmbH), aperture was set to 6 mm. Atmospheric compensation was performed and samples smoothed using 25 smoothing points.

Principal Component Analysis

Principal component analysis was performed analyzing all samples with Unscrambler Software (Camo Process AS, Norway, 2002.). 1st derivative based on Savitzky–Golay algorithm using 17 smoothing points was performed and PCA done to find spectral outliers to be excluded from model building as well as define different groups of samples to be compared.

PLS-Model Using Quant

A multivariate calibration model was established using Quant2 method within OPUS spectral processing software v. 6.0 (Bruker) for multivariate data analysis using PLS with PLS1 algorithm (Höskuldsson, 1988). Samples were measured and Quant2 model established using HCP values calculated as merged mean values from ELISA assay results from corresponding samples. HCP concentrations of the samples used for the model were between 6,800 and 180,000 ng mL^{-1} according to ELISA. PLS model was calculated using one-out-cross-validation after splitting the data set into a training and a cross-validation set, comprising 35 samples; and an independent test-set, comprising five samples (Osten, 1988). By using the

independent test-set, overtraining of the model should be analyzed and the model robustness be evaluated (Brereton, 1992). Different mathematical data pre-treatment steps (multiplicative scatter correction, first and second derivative, vector normalization) were evaluated to improve PLS model according to root mean square error of cross-validation (RMSECV) and coefficient of determination (R^2) of cross-validation using automatic optimization mode of OPUS software. The initial wavenumber range for model optimization comprised the amide bands from 1,700 to 1,500 cm^{-1} with intervals of 20 cm^{-1} adding and removing wavenumber regions within 1,700–1,500 cm^{-1} to improve model accuracy. In an attempt to improve model quality, additional visual inspection of spectra revealed a correlation between peak intensities and HCP concentrations measured by ELISA in the wavenumber area of 1557.49–1546.88; 1514.092–1505.412; 1424.403–1417.653, 1410.9–1395.47, and 1352.07–1341.47 cm^{-1}.

These areas were chosen for data pre-treatment using first derivative with Savitzky–Golay algorithm and 17 smoothing points. Other wavenumber areas between the measured 4,000 and 900 cm^{-1} were not chosen, Amide I band was disregarded to avoid possible interference with antibody protein in samples. As it was known that polyelectrolytes used for sample pre-treatment show absorbance peaks in the wavenumber area of 1,390–1,360 cm^{-1} and between 1,100 and 1,000 cm^{-1}, these areas were also excluded from data pre-treatment. Final PLS model was validated (overview see Fig. 1) and analyzed using the independent test-set data.

Results and Discussion

HCP-ELISA

In order to estimate the HCP amounts in the chosen 40 samples, including the independent test-set samples, an ELISA assay was performed. A wide spread of HCP titers between 6,800 and 182,000 ng mL^{-1} was detected in the supernatant of the 40 samples, subjected to precipitation, improving the robustness of the calibration model. All samples contained different amounts of antibody which was precipitated to various degrees. The polyelectrolytes themselves as well as samples with only antibody did not show any influence on the ELISA assay, the influence test revealed 20 ng mL^{-1} ± less than 25% variation of observed values from expected values and was therefore within the limitations of the assay (according to manufacturers manual).

Comparison HCP and Antibody Precipitation

Comparing the relative HCP and antibody concentration, determined by ELISA and Protein A chromatography, respectively, no correlation was seen. HCP concentration varied from 6,800 to 180,000 ng mL^{-1} while antibody concentration was mainly between 0.005 and 0.5 mg mL^{-1}
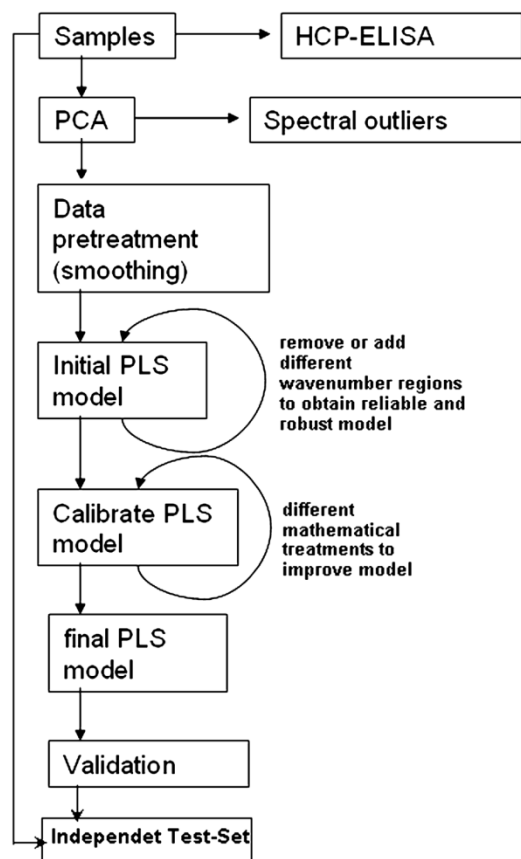
Figure 1. PLS model development.

Figure 2. **A**: HCP and mAb titers in samples as measured by ELISA and affinity chromatography. **B**: Concentration of polyelectrolytes added to the 40 samples for semi-selective HCP removal.

(Fig. 2A). As no correlation between antibody and HCP precipitation occurred, there was also no colinearity of concentration change between antibody and HCPs in the samples.

Polyelectrolyte concentration added to samples varied between 0.2 and 1 mg mL^{-1} (Fig. 2B). No correlation of added polyelectrolyte concentration with mAb and HCP concentration within the samples was seen.

HCP Quantification by FT-IR

MIR Spectra

Spectra of all analyzed 40 samples showed a high degree of overlapping peaks, also in the Amide I and II region. From previous experiments, it was known that peaks around 1,390

and 1,100–1,000 cm^{-1} can be assigned to polyelectrolytes (areas highlighted in magenta in Fig. 4). The wavenumber area below 1,200 cm^{-1} showed strong peaks, assigned to polyelectrolytes. Amide I and II bands were clearly visible and C–O–H bending vibration was seen in the peak around 1,400 cm^{-1}. Yet, previous experiments (Harthun et al., 1997; Sellick et al., 2010) show the ability of multivariate data analysis to distinct different proteins within infrared spectra using cell cultures and subsequently quantify recombinant protein in the cell culture. The ability of overall protein quantification using mid infrared spectroscopy (MIR) and ATR is shown by Etzion et al. (2004).

Principal Component Analysis

After doing IR spectroscopic analysis, a PCA was performed to compare different samples and find possible outliers not suitable for the calibration. Results after initial PCA comprising wavenumbers 4,000–1,400 cm^{-1} showed no outliers, keeping all 40 samples for further PLS model calibration and subsequent test-set validation. Final PCA with manually chosen peaks comprising wavenumber areas of 1557.49–1546.88; 1514.092–1505.412; 1424.403–1417.653, 1410.9–1395.47, and 1352.07–1341.47 cm^{-1} showed a separation correlating with HCP concentrations in the samples at principal component 1 (Fig. 3).
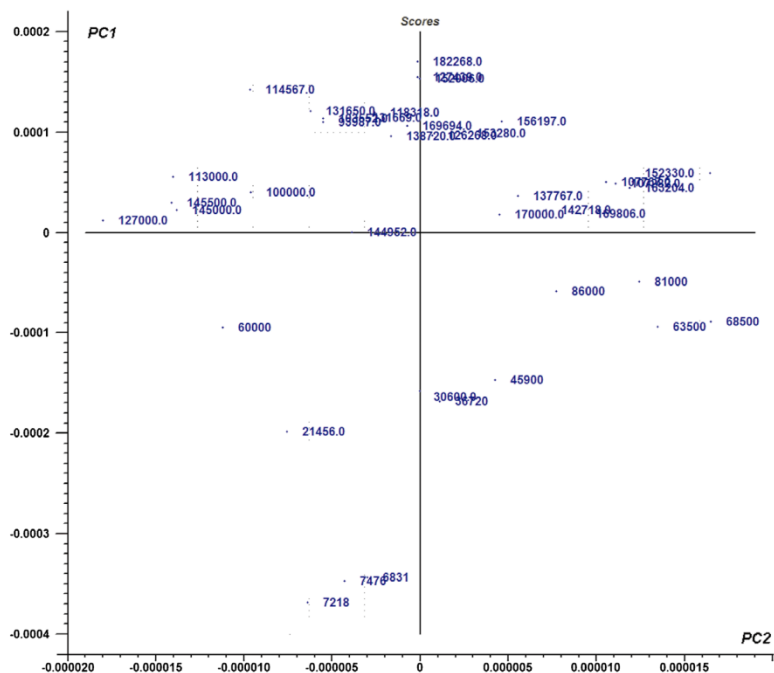
Figure 3. Principal component analysis of samples, PC1 correlates with HCP concentration within the samples.

Figure 4. Overview of second derivative (17 smoothing points) of FT-IR spectra: amide peaks, polyelectrolyte peak, and C–O–H bending peak highlighted in magenta; wavenumber areas used for model calibration framed and designated as 1–5.

PLS-Calibration Model

Assigned Functional Groups and Model Quality

An initial PLS model using wavenumber range between 4,000 and 1,400 cm^{-1} evaluating different mathematical treatment steps was established and proven to be inaccurate.

The automatic optimization of the model using wavenumber ranges 1,700–1,500 cm^{-1} in intervals of 20 cm^{-1} led to a rank of 3 with coefficient of determination of 82.3% and RMSECV of 19,200 ng mL^{-1}. In contrast, using manually chosen wavenumber ranges (framed areas in spectral overview of second derivative spectra, designated as 1–5 in Fig. 4) by visual inspection for the PLS1 calibration model, a R^2-value of 88.75% for the first rank was obtained, showing a RMSECV of 17,500 ng mL^{-1}, after removing one outlier not detected by PCA. Models with fewer factors, i.e., ranks, are more robust as they avoid overfitting of the model to a certain set of calibration standards, they also avoid incorporation of spectral noise ratios into the chemometric model (Martens and Naes, 1989). Therefore, our model can be seen as more reliable. HCP titers determined from ELISA, correlated with the peak intensities of the chosen wavenumber range, the RPD (quotient of standard

Table I. Functional groups assigned to wavenumbers used for the model building.

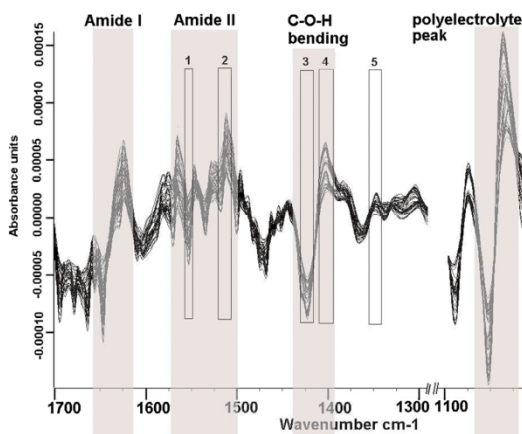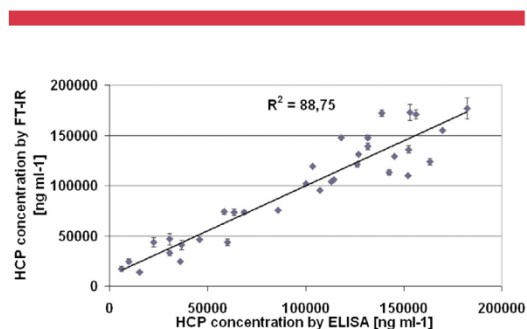| Designation in Figure 4	Wavenumber range (cm^{-1})	Assigned
1	1,557–1,545	Amide II
2	1,514–1,505	Amide II
3	1,424–1,417	C–O–H bending
4	1,410–1,394	C–O–H
5	1,352–1,341	C–O carboxylic acid

Figure 5. Comparison of HCP values determined by ELISA (X-axis) and determined by ATR (Y-axis) showing a degree of correlation of 88.75% for the added trendline (black). Standard deviation of multiple ELISA measurements shown as error bars.

deviation and standard estimation error) was 2.98. Assigning the wavenumber ranges used for the calibration, two of the wavenumber ranges chosen (1,557–1,545 cm^{-1} and 1,514–1,505 cm^{-1}), may be assigned to the Amide II band at 1,575–1,480 cm^{-1}, corresponding to CN stretching and NH bending vibrations as well as minor contributions from CO bending and CC stretching (Barth, 2007). Two other ranges (1,424–1,417 cm^{-1} and 1,410–1,394 cm^{-1}) may be assigned to C–O–H bending (Table I). The wavenumber range 1,352—1,341 cm^{-1} may be assigned to a carboxyl group.

A validation of the predicted HCP values from the Quant2 analysis and the "real" HCP values from the ELISA

was done for 34 calibration and validation samples not including the previously removed outlier as well as the five independent test-set samples (Fig. 5). Twenty-seven out of 34 samples were within the limitations of the ELISA assay (<25% CV according to manufacturers manual), 15 out of 34 samples showed coefficients of variation less than 10%, the precision of the ELISA (according to manufactureres manual). As the model is based on the HCP values from the ELISA assay, it cannot be better than the ELISA concerning precision. Yet, the model seems suitable for predicting HCP titers between at least 20,000 and 200,000 ng mL^{-1}. Samples with lower HCP concentrations than 20,000 ng mL^{-1} showed a higher deviation, however, as other publications showed the ability to measure amino acids in the millimolar range (Barth, 2007; Riley et al., 2001), the limit of quantification for HCP using ATR should be around 10,000 ng mL^{-1}, using more samples with low HCP concentration for model calibration.

Five samples were chosen to evaluate the prediction accuracy of the model (Table II). These samples were not used for model calibration and validation. HCP prediction for four of the five samples was within the limitation of the ELISA assay. Prediction of four test-set samples showed a precision compared to ELISA-determined HCP values of less than 10% CV, with the test-set sample comprising a low HCP concentration, showing a CV slightly larger than the limitation of ELISA.

Interference of Antibody and Polyelectrolytes

The chosen wavenumber ranges as well as the use of various polyelectrolytes at different concentrations (Fig. 2B) minimized interference from polyelectrolytes present in the sample. A contour plot shows that polyelectrolyte concentrations added to achieve various antibody and HCP concentrations in the samples do not correlate (Fig. 2B) and specific HCP concentrations can be achieved using either high, medium or low concentrations of (different) polyelectrolytes (Fig. 6). The ability of FT-IR to distinguish and quantify different amino acids in the millimolar range down to 0.3 mM (approximately 0.02 mg mL^{-1}; Riley et al., 2001) indicates the feasibility of our experimental results, distinguishing HCP and mAb proteins. If mAb and polyelectrolyte peaks were incorporated into the model

Table II. Prediction accuracy of calibration model for independent test-set samples.

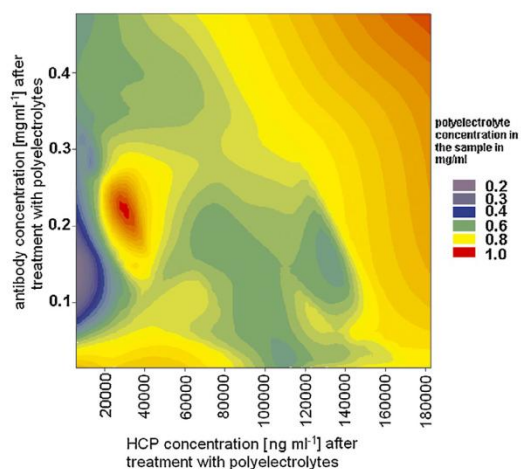| Sample	HCP titer determined by ELISA (ng mL^{-1})	HCP titer predicted with model (ng mL^{-1})	Precision: % CV (*ELISA precision < 10% CV)	Within limitation of ELISA
1	7,476	9,188	22.89	Yes
2	21,456	23,155	7.93	Yes
3	81,000	82,715	2.12	Yes
4	107,767	113,000	4.86	Yes
5	145,000	148,530	2.43	Yes

Figure 6. Contour plot of HCP concentration and antibody concentration in samples depending on polyelectrolyte concentration in samples. *X*-axis: HCP concentration in samples in ng mL^{-1} as determined by ELISA. *Y*-axis: antibody concentration in samples in mg mL^{-1} as determined by affinity chromatography. *Z*-axis: polyelectrolyte concentration in samples ranging from 0.2 mg mL^{-1} (blue contour) to 1 mg mL^{-1} (red contour).

calibration data, the good agreement of HCP prediction results from the calibration model with the results obtained by ELISA should not be possible, as polyelectrolytes as well as mAb composition and concentration did not show any influence on ELISA assay results.

Conclusion

FT-IR can be used for quantitative determination of HCPs during process development. Compared to ELISA, its prediction accuracy is comparable and well within the limitation of ELISA, if HCP titers exceed 20,000 ng mL^{-1}. Comparing the precision, it obtains slightly lower, yet acceptable, precision shown by few samples with a larger coefficient of variation. Although, in contrast to western blot and ELISA, the sensitivity of FT-IR using ATR is much lower, it is a useful tool for fast analysis of process parameters and their impact on HCP removal. FT-IR has the ability to do measurements in situ, without exhaustive sample preparation steps, preventing dilution errors. The measurement itself does not consume any enzymes, in contrast to ELISA and western blot, and is therefore quite inexpensive. It is faster than HPLC analysis without any buffer consumption. FT-IR might also be suitable for HCP quantification of titers lower than 20,000 ng mL^{-1}. However, as only very few samples within that HCP concentration range were available for model calibration, further research elucidating the limit of quantification for HCPs should be done.

References

Arrondo JL, Muga A, Castresana J, Goñi FM. 1993. Quantitative studies of the structure of proteins in solution by Fourier-transform infrared spectroscopy. Prog Biophys Mol Biol 59:23–56.

Barth A. 2007. Infrared spectroscopy of proteins. Biochim Biophys Acta Bioenerg 1767(9):1073–1101.

Brereton G. 1992. Multivariate pattern recognition in chemometrics, illustrated by case studies. Amsterdam: Elsevier Science Publishers B.V.

Champion K, Madden H, Dougherty J, Shacter E. 2005. Defining your product profile and maintaining control over it, part 2. Bioprocess Int 5(9):52–57.

Chu L, Robinson DK. 2001. Industrial choices for protein production by large-scale cell culture. Curr Opin Biotechnol 12(2):180–187.

Doak DL, Phillips JA. 1999. In situ monitoring of an *Escherichia coli* fermentation using a diamond composition ATR probe and mid-infrared spectroscopy. Biotechnol Prog 15(3):529–539.

Dong A, Malecki JM, Lee L, Carpenter JF, Lee JC. 2002. Ligand-induced conformational and structural dynamics changes in *Escherichia coli* cyclic AMP receptor protein. Biochem 41(21):6660–6667.

Dotzel MM. 1999. International conference on harmonisation of technical requirements for registration of pharmaceuticals for human use, "Guidance on Specifications: Test Procedures and Acceptance Criteria for Biotechnological/Biological Products" (Geneva, Switzerland). Fed Regist 64:44928–44935.

Esbensen KH. 2002. Multivariate data analysis—In practice: An introduction to multivariate data analysis and experimental design. Oslo: Camo Process AS.

Etzion Y, Linker R, Cogan U, Shmulevich I. 2004. Determination of protein concentration in raw milk by mid-infrared Fourier transform infrared/attenuated total reflectance spectroscopy. J Dairy Sci 87(9):2779–2788.

Fahrenfort J. 1961. Attenuated total reflection: A new principle for the production of useful infra-red reflection spectra of organic compounds. Spectrochim Acta 17(7):698–709.

Flatman S, Alam I, Gerard J, Mussa N. 2007. Process analytics for purification of monoclonal antibodies. J Chromatogr B 848(1):79–87.

Goormaghtigh E, Ruysschaert J-M, Raussens V. 2006. Evaluation of the information content in infrared spectra for protein secondary structure determination. Biophys J 90(8):2946–2957.

Griffiths PR, Haseth J. 2007. Fourier transform infrared spectroscopy. 2nd edn. Hoboken, New Jersey: Wiley Interscience.

Gross-Selbeck S, Margreiter G, Obinger C, Bayer K. 2007. Fast quantification of recombinant protein inclusion bodies within intact cells by FT-IR spectroscopy. Biotechnol Prog 23(3):762–766.

Harrick NJ. 1960. Surface chemistry from spectral analysis of totally internally reflected radiation. J Phys Chem 64(9):1110–1114.

Harthun S, Matischak K, Friedl P. 1997. Determination of recombinant protein in animal cell culture supernatant by near-infrared spectroscopy. Anal Biochem 251(1):73–78.

Hoffman K. 2000. Strategies for host cell protein analysis. Biopharm 13(6):38–45.

Höskuldsson A. 1988. PLS regression methods. J Chemom 2(3):211–228.

Isaksson T, Naes T. 1990. Selection of samples for calibration in near-infrared spectroscopy. Part II: Selection based on spectral measurements. Appl Spectrosc 44(7):1152–1158.

Jackson M, Mantsch HH. 1995. The use and misuse of FTIR spectroscopy in the determination of protein structure. Crit Rev Biochem Mol Biol 30(1995):95–120.

Kong J, Shaoning YU. 2007. Fourier transform infrared spectroscopic analysis of protein secondary structures. Acta Biochim Biophys Sin 39(8):549–559.

Krimm S, Bandekar JCB, Anfinsen JTE, Frederic MR. 1986. Vibrational spectroscopy and conformation of peptides, polypeptides, and proteins. Advances in protein chemistry. Orlando: Academic Press. p 181–364.

Li W, Goovaerts P, Meurens M. 1996. Quantitative analysis of individual sugars and acids in orange juices by near-infrared spectroscopy of dry extract. J Agric Food Chem 44(8):2252–2259.

Martens H, Naes T. 1989. Multivariate calibration. Chichester: John Wiley & Sons.

Mazarevica G, Diewok J, Baena JR, Rosenberg E, Lendl B. 2004. On-line fermentation monitoring by mid-infrared spectroscopy. Appl Spectrosc 58(7):804–810.

McGovern AC, Ernill R, Kara BV, Kell DB, Goodacre R. 1999. Rapid analysis of the expression of heterologous proteins in *Escherichia coli* using pyrolysis mass spectrometry and Fourier transform infrared spectroscopy with chemometrics: Application to a2-interferon production. J Biotechnol 72(3):157–168.

Osten DW. 1988. Selection of optimal regression models via cross-validation. J Chemom 2(1):39–48.

Pillonel LP, Luginbühl WL, Picque DP, Schaller ES, Tabacchi RT, Bosset JB. 2003. Analytical methods for the determination of the geographic origin of Emmental cheese: Mid- and near-infrared spectroscopy. Eur Food Res Technol 216(2):174–178.

Pimentel MF, Ribeiro GMGS, da Cruz RS, Stragevitch L, Pacheco Filho JGA, Teixeira LSG. 2006. Determination of biodiesel content when blended with mineral diesel fuel using infrared spectroscopy and multivariate calibration. Microchem J 82(2):201–206.

Rhiel M, Cohen MB, Murhammer DW, Arnold MA. 2002. Nondestructive near-infrared spectroscopic measurement of multiple analytes in un-diluted samples of serum-based cell culture media. Biotechnol Bioeng 77(1):73–82.

Riley MR, Crider HM, Nite ME, Garcia RA, Woo J, Wegge RM. 2001. Simultaneous measurement of 19 components in serum-containing animal cell culture media by Fourier transform near-infrared spectroscopy. Biotechnol Prog 17(2):376–378.

Scarff M, Arnold SA, Harvey LM, McNeil B. 2006. Near infrared spectroscopy for bioprocess monitoring and control: Current status and future trends. Crit Rev Biotechnol 26:17–39.

Sellick CA, Hansen R, Jarvis RM, Maqsood AR, Stephens GM, Dickson AJ, Goodacre R. 2010. Rapid monitoring of recombinant antibody production by mammalian cell cultures using Fourier transform infrared spectroscopy and chemometrics. Biotechnol Bioeng 106(3):432–442.

Siebert F. 1995. Infrared spectroscopy applied to biochemical and biological problems. Methods in Enzymology, Academic Press. Volume 246: 501–526.

Wang X, Hunter AK, Mozier NM. 2009. Host cell proteins in biologics development: Identification, quantitation and risk assessment. Biotechnol Bioeng 103(3):446–458.

Warnes MR, Glassey J, Montague GA, Kara B. 1996. On data-based modelling techniques for fermentation processes. Process Biochem 31(2):147–155.

Winder CL, Carr E, Goodacre R, Seviour R. 2004. The rapid identification of *Acinetobacter* species using Fourier transform infrared spectroscopy. J Appl Microbiol 96(2):328–339.

Wold S, Sjöström M, Eriksson L. 2001. PLS-regression: A basic tool of chemometrics. Chemom Intell Lab Syst 58(2):109–130.

Zoon KC. 1997. Points to consider in the manufacture and testing of monoclonal antibody products for human. Rockville: Center for Biologics Evaluation and Research, FDA.

Cumulative part- Experimental 141

3.5.2 mAb titer and host cell protein level quantification using MIR

Paper: Matrix effects during monitoring of antibody and host cell proteins using attenuated total reflection spectroscopy

Florian Capito, Romas Skudas, Bernd Stanislawski and Harald Kolmar

Short summary:

MIR spectroscopy was further advanced for quantification of host cell protein levels as well as antibody titer in samples containing polymer. The underlying idea was to use MIR spectroscopy as a cost-effective tool for quantification of target protein level (mAb) and host cell impurity proteins when performing polymer-driven protein purification. Especially for host cell protein quantification, costly ELISA assays could be replaced by this new application for MIR. Compared to the previous publication, limit of quantification for host cell proteins could be improved. However, results suggest that only part of the precipitation process development samples can be analyzed by MIR, due to the relatively high limit of quantification for host cell proteins of 2,000 ng ml^{-1} and the only acceptable accuracy for mAb quantification. Yet, though not mentioned explicitly in this paper, this technique is still helpful when estimating the precipitation yield and selectivity during development of a protein precipitation process.

Matrix Effects During Monitoring of Antibody and Host Cell Proteins Using Attenuated Total Reflection Spectroscopy

Florian Capito

Clemens-Schoepf-Institute for Organic Chemistry and Biochemistry, Technical University Darmstadt, D-64289 Darmstadt

Merck KGaA, Frankfurter Strasse 250, 64293 Darmstadt, Germany

Romas Skudas and Bernd Stanislawski

Merck KGaA, Frankfurter Strasse 250, 64293 Darmstadt, Germany

Harald Kolmar

Clemens-Schoepf-Institute for Organic Chemistry and Biochemistry, Technical University Darmstadt, D-64289 Darmstadt

Production of recombinant proteins, e.g. antibodies, requires constant real-time monitoring to optimize yield and quality attributes and to respond to changing production conditions, such as host cell protein (HCP) titers. To date, this monitoring of mammalian cell culture-based processes is done using laborious and time consuming enzyme-linked immunosorbent assays (ELISA), two-dimensional sodium dodecylsulphate polyacrylamide gel electrophoresis, and chromatography-based systems. Measurements are usually performed offline, requiring regular sample withdrawal associated with increased contamination risk. As information is obtained retrospectively, the reaction time to adapt to process changes is too long, leading to lower yield and higher costs. To address the resulting demand for continuous online-monitoring systems, we present a feasibility study using attenuated total reflection spectroscopy (ATR) to monitor mAb and HCP levels of NS0 cell culture in situ, taking matrix effects into account. Fifty-six NS0 cell culture samples were treated with polyelectrolytes for semi-selective protein precipitation. Additionally, part of the samples was subjected to filtration prior to analysis, to change the background matrix and evaluate effects on chemometric quantification models. General models to quantify HCP and mAb in both filtered and unfiltered matrix showed lower prediction accuracy compared to models designed for a specific matrix. HCP quantification in the range of 2,000–55,000 ng mL^{-1} using specific models was accurate for most samples, with results within the accepted limit of an ELISA assay. In contrast, mAb prediction was less accurate, predicting mAb in the range of 0.2–1.7 g L^{-1}. As some samples deviated substantially from reference values, further investigations elucidating the suitability of ATR for monitoring are required. © 2012 American Institute of Chemical Engineers Biotechnol. Prog., 29: 265–274, 2013
Keywords: attenuated total reflection, monitoring, antibody, host cell proteins, matrix effects

Introduction

Almost all pharmaceutical antibodies are now produced using mammalian cell culture-based fermentation processes. Though the process is widely integrated, the process control strategy still relies on various real-time monitored parameters. For example, during fermentation, secretion of host cell proteins (HCPs) and monoclonal antibody (mAb) production has to be monitored to define the optimum harvesting point and optimize fermentation conditions.[1] Monitoring can be done in situ directly in the reactor or ex situ in a bypass or loop, making use of filters to remove cells and unwanted particles prior to sample analysis. However, sensors used for online monitoring present contamination and long-term sta-

bility risks, requiring the implementation of non-invasive sensors.[2–4] Ex-situ monitoring methods are well established, e.g. HCP quantification using enzyme-linked immunosorbent assays (ELISA) or two-dimensional sodium dodecylsulphate polyacrylamide gel electrophoresis (2D-SDS-PAGE). However, such methods are time-requiring and may require appropriate pre-dilution steps.[5]

A prolonged analysis time (> 2 h) due to sample and assay preparation and incubation can lead to insufficient knowledge about the actual fermentation process because information is obtained retrospectively. The delay increases the difficulty of finding the optimum time for harvesting the bioreactor.[5,6] Furthermore, during pilot-runs of recombinant protein production in bioreactors, parameter settings need to rely on historical data and optimization is done in a trial-and-error manner as actual information about the fermentation process is available only at a later point of time.[1] Using

265

high performance liquid chromatography as an ex-situ method for monitoring mAb production overcomes some of these constraints. It enables constant monitoring and fast data interpretation, yet the separation time required increases the time to react to conditions during fermentation. Moreover, relatively large amounts of buffer are required, which adds further to the waste load. Furthermore, results may be subject to interpretation and affected by interactions between the mAb and the matrix that lead to peak broadening.[5,7–9] Capillary electrophoresis systems may also be used for automated mAb analysis. However, they have only recently gained acceptance among manufacturers.[5] As a consequence, a fast non-invasive method which combines HCP and mAb quantification would help to adapt to fermentation changes in real-time by constant monitoring of protein levels.[8]

A non-invasive technique such as Fourier transform infrared spectroscopy (FTIR) could be used for in situ or ex situ analysis. The former method using immersion probes, e.g. autoclavable attenuated total reflection (FTIR-ATR) probes fitting into a fermenter port, or glass fibers (e.g., made from Telur, Arsen and Selen) passing through the bioreactor while the ex situ technique uses a flow-through cell.[10–12]

FTIR in the mid-infrared range has already been used for in situ monitoring of glucose, fructose, and acetic acid levels as well as nitrogen and carbon sources during fermentation processes.[10,11,13–16] Schenk et al. used this technique to analyze pH and methanol production in bacterial cell cultures[17,18] while in another experiment quantification of glucose and lactic acid in the low millimolar range using plasma samples was possible.[19] FTIR can be used to study protein in the millimolar range as well as distinguish different amino acids due to specific vibration frequencies in the mid-infrared range.[20] The applicability of this technique to off-line quantification of protein expression during *Escherichia coli* and mammalian cell culture fermentation was shown by McGovern et al.[21] and Gross-Selbeck et al.[22] while Timmins et al.[23] used FTIR for discriminating different baker's yeast strains.

ATR as one FTIR technique[24,25] is applicable for cell culture composition analysis, classification of microorganisms as well as amino acid and protein analysis, e.g. distinguishing proteins according to differences in their secondary structure as reflected by different peak positions within an infrared spectrum.[10,11,26–28] The use of FTIR-ATR for overall protein quantification in milk was also successfully demonstrated.[29] Mazarevica et al.[30] used synthetic samples as well as samples withdrawn during fermentation of baker's yeast, to determine glucose and ethanol concentrations throughout fermentation using FTIR-ATR while Roychoudhury et al.[16] used this technique for online monitoring of ammonium, glucose, and biomass during fermentation.

While a combination of above mentioned applications of FTIR in general and FTIR-ATR should enable constant monitoring of protein expression, the challenge is to distinguish between background matrices (such as different proteins, media background influences, vitamins, amino acids, cholesterol, growth factors, lipids, antibiotics, and nucleic acids).[31] With the help of appropriate data processing and resolution-enhancing techniques[32,33] as well as principal component analysis (PCA) and partial least squares regression (PLS),[34–36] protein quantification based on FTIR in the mid-infrared range in mammalian cell cultures against differing background matrices was shown to be promising. Sellick et al. quantified mAb production rates against a HCP impurity

background, using several NS0 or CHO cell lines as differing background matrix.[37] In previous experiments, Capito et al. showed the ability of FTIR-ATR to successfully quantify HCP titers in CHO cell culture.[38]

Based on their and our experiments and the need for a fast, non-invasive method, combining HCP and mAb quantification, we tried to elucidate the influence of differing background matrices on HCP and mAb quantification by using FTIR-ATR in the mid-infrared range in conjunction with appropriate chemometric models involving PCA and PLS. Furthermore, we evaluated the potential of this technique for monitoring the production of antibody as well as HCPs in cell culture fluid and assessed its future use in online monitoring of fermentation processes. HCP and mAb levels of initially 66 cell culture fluid samples, which were split into a calibration set, a validation set, and an independent test-set, were adjusted using a polyelectrolyte-treatment procedure to remove different amounts of antibody as well as different subpopulations of HCPs from the samples. The use of polyelectrolytes for semi-selective precipitation was to avoid correlating titer changes and thereby colinearity within the samples, e.g. occurring when using dilution steps, thereby enabling the establishment of a robust chemometric system.[34,39] Additionally, to simulate different background matrices, we filtered part of the samples before measurement and compared quantification models based on matrices of both filtered and unfiltered samples with models based on only filtered or only unfiltered samples. HCP monitoring suitability was compared to ELISA assays and the suitability for mAb monitoring was compared to quantification using fluorophore-labeled mAb.

Materials and Methods

Polyelectrolytes

The following were used for semi-selective protein removal after adjusting adequate dilutions of polyelectrolyte stock solutions to pH 5.0: Poly(styrene sulfonic acid) with weight average molecular weights of $M_w = 1,360$ g mol^{-1}, 10,600 g mol^{-1}, 15,200 g mol^{-1} and 976,000 g mol^{-1} (Polymer Standards Service, Mainz, Germany); poly(vinyl sulfonic acid) with weight average molecular weight of $M_w = 2,100$ g mol^{-1} (Polysciences, Warrington, USA); poly(anethole sulfonic acid), weight average molecular weight not determined (Sigma-Aldrich, Steinheim, Germany); dextran sulfate (DS), weight average molecular weight not determined (Sigma-Aldrich, Steinheim, Germany); and poly(acrylic acid) (Polysciences, Warrington, USA) with weight average molecular weights of $M_w = 1,930$ g mol^{-1}, 3,800 g mol^{-1}, 123,000 g mol^{-1}, and 958,000 g mol^{-1}.

Cell line

A murine myeloma cell line producing an IgG2 antibody (mAb) was used for the experiments and kindly provided by Merck Serono, Darmstadt, Germany.

Cell culture fluid and pre-treatment conditions

After harvesting and clarification of cell culture, the pH was adjusted to pH 5.0 using a 25 mM sodium-acetate buffer (Merck KGaA, Darmstadt, Germany). The pH-adjusted cell culture was split into two groups representing ex situ and in situ samples. Ex situ samples were produced by filtration through a 0.2 μm sterile filter (Minisart 0.2 μm sterile filter,

Sartorius Stedim Biotech, Göttingen, Germany) to evaluate background matrix effects on the chemometric model induced by filters. The other group was not subjected to filtration. This set should simulate in situ analysis of proteins. About 7% (wt/wt) with a fluorophore (Alexa Fluor® 546, Invitrogen Molecular Probes, Grand Island, USA) labeled IgG2 antibody was added to filtered and non-filtered cell culture fluid, in the cell culture fluid. Afterwards, various polyelectrolytes of different concentrations were added to the cell culture fluids to semi-selectively remove different HCPs and thereby obtain various HCP subpopulations in the cell cultures as well as remove antibody to various levels. A total of 29 different sample variants (polyelectrolyte composition and concentration) were obtained using the filtered cell culture fluid. Using non-filtered cell culture fluid, a total of 37 different sample variants (polyelectrolyte composition and concentration) were obtained. After an incubation step, samples were centrifuged and the supernatant was transferred to new tubes.

Antibody concentration determination by fluorescence

IgG2 antibody of NS0 cell culture was purified using Protein A chromatography and labeled with the fluorophore Alexa Fluor® 546 (Invitrogen Molecular Probes, Grand Island, USA). About 1 g of antibody was labeled with 1 mg of fluorophore in sodium-carbonate buffer pH 9.0 using slow stirring for 1 h. Afterwards, non-bound fluorophore was removed using a Sephadex G25 column (GE Healthcare, Uppsala, Sweden) for size exclusion chromatography. Concentration of labeled purified IgG2 antibody was determined using photometry with the appropriate extinction coefficient and pH adjusted to pH 5.0 using sodium acetate buffer (Merck KGaA, Darmstadt, Germany). Non-labeled cell culture fluid containing non-labeled IgG2 antibody was spiked adding labeled IgG2 antibody to obtain a final 7% (wt/wt) of labeled antibody in the cell culture fluid. After the polyelectrolyte treatment and centrifugation, the supernatant was transferred to microtiterplates (Nunc, Langenselbold, Germany) and fluorescence counts in supernatant measured in comparison to IgG2 standards using 540 nm as excitation wavelength and 590 nm as emission wavelength in a Tecan Reader (Tecan Infinite M200, Tecan Deutschland GmbH, Crailsheim, Germany). The IgG2 concentration present in the supernatant of each sample was calculated as mean value from triplicate measurements.

HCP quantification using HCP-ELISA

In order to obtain calibration standards for the chemometric model, the HCP content in supernatant of all 66 samples was determined as mean value from triplicate measurements using NS0-HCP ELISA kit (Cygnus technologies, Southport, USA). Appropriate dilution steps were performed prior to ELISA according to the manufacturers' manual to ensure that samples were within the quantification range of the assay. Possible interference of mAb or polyelectrolytes on the assay was evaluated by mixing 1/5 of 100 ng mL^{-1} HCP standard with 4/5 of mAb or polyelectrolyte, respectively, to obtain 20 ng mL^{-1} standards.

Antibody and HCP quantification using ATR

In contrast to ELISA, samples were used without prior dilution steps to ensure they met the higher quantification limit of FTIR-ATR spectroscopy. About 20 μL of each sam-

ple were applied to crystal of GoldenGate™ ATR MkII series (Specac, Cranston, RI) and measured at 20°C using H$_2$O as background. Spectra were recorded in absorbance mode on a Bruker Tensor 27 (Bruker Optik GmbH, Ettlingen, Germany) using a sample scan number of 120 scans at a spectral resolution of 4.0. The detector used was a Bruker LN-MCT photovoltaic internal detector (Bruker Optik GmbH, Ettlingen, Germany), with an aperture set to 6 mm.

After spectra recording and dividing by the background spectrum, automatic atmospheric compensation within OPUS spectral processing software v. 6.0 (Bruker Optik GmbH, Ettlingen, Germany) was performed, dividing the single channel sample spectrum by the single channel background spectrum to obtain a spectrum which does not contain H$_2$O or CO$_2$ bands using an algorithm within OPUS software. Afterwards samples were smoothed using 25 smoothing points and data were merged as mean values of corresponding triplicate measurements.

Principal component analysis

In order to find possible spectral outliers to be excluded from model design and evaluate differences between sample treatment (type of polyelectrolyte, filtered samples vs. non-filtered cell culture fluid), a PCA was performed. PCA thereby converts the observations of putatively correlated variables using orthogonal transformation into linearly not correlated principal components. The first principal component has most of the variance within the data set, whereby the succeeding principal components have less variance and are all independent from the preceding principal components.[35,40] Therefore, PCA was used to find outliers by comparing the first principal components and looking for data which differed a lot from other spectra.[35]

The procedure was carried out using the Unscrambler (Camo Process AS, Oslo, Norway). All samples were subjected to 1st derivative based on Savitzky–Golay algorithm with 25 smoothing points and only the first and second principal components, which explain much of variance within the data, were analyzed.

Partial least squares regression model

Performing multivariate data analysis using PLS with PLS1, a Quant2 method was prepared using OPUS spectral processing software v. 6.0 (Bruker Optik GmbH, Ettlingen, Germany).

Using PCA, the PLS algorithm extracts variables T and U by compressing the information from factors X (e.g., spectral intensities within spectra, formula 1) and the results Y (reference values determined e.g. by HCP-ELISA, formula 2), respectively. Disregarding irrelevant residual information E and f, the score matrix T is used to predict the U matrix, containing the Y-scores and thereby predict the results Y.[41] Loadings P and q, estimated by regression, describe how T-matrix and U-matrix are related to X and Y, respectively. While the first PLS component, or first rank (in OPUS) is used to explain most of the covariance, succeeding components explain less covariance and may also explain spectral noise.[35,41] Using PLS within OPUS, we tried to find only the relevant information within the spectra, most likely explaining the results, while obtaining high degrees of correlation and avoiding overfitting, minimizing number of ranks during PLS model design.[34–36]
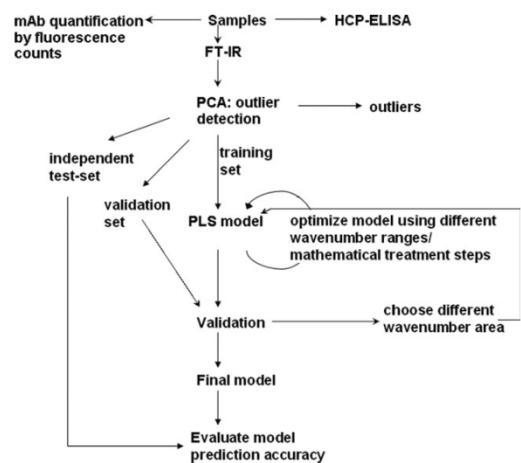
Figure 1. Steps for chemometric model development within OPUS software.

$$X = T \times P^T + E \tag{1}$$

$$Y = U \times q^T + f \tag{2}$$

Sixty-six samples were measured with ATR and Quant2 model established using HCP concentrations obtained from ELISA assay from corresponding samples as well as mAb concentration measured using Tecan reader and fluorescence counts.

PLS models were designed using one-out-cross validation after splitting the data set into a training and cross-validation set.[42] Additionally, an independent test-set was used to analyze overtraining effects of the models and evaluate the robustness as the models have never "seen" these test-set samples for calibration nor validation.[43] The test-set comprised 20 randomly chosen samples for the general models with both, filtered and unfiltered background matrix. For the specific models the size of the test-set had to be limited due to the overall limited number of sample population, hence 10 randomly chosen samples were used to elucidate model robustness for models specific to unfiltered or filtered matrix, respectively.

An initial PLS model (for overview of model development, see Figure 1) was designed using the Amide I and II bands for antibody and HCP quantification. Optimization of the chemometric models was done to find the best rank(s) for the respective PLS model, where an increase in the rank did not lead to significantly reduced predictive error sum of squares (PRESS). The number of ranks used for the model was kept as low as possible to obtain a higher robustness and avoid incorporation of noise into the models.

The model was optimized independently for mAb and HCP quantification using different groups of spectral similarity according to PCA clustering. Afterwards, spectra were transformed using first and second derivative, vector normalization, and subtraction of a line (automatic mode in OPUS by fitting a line to the chosen spectral area and subtracting that line to correct tilted spectra) in an attempt to optimize the initial PLS model according to root mean square error of cross validation (RMSECV) and coefficient of determination

(R^2) of cross-validation using automatic optimization mode of OPUS software (overview see Figure 1). Wavenumber ranges between 1,000 and 1,100 cm^{-1} and between 1,360 and 1,390 cm^{-1} were excluded from any model calculation as it was known from previous experiments that polyelectrolytes showed high absorbance peaks in this area and might interfere with model calculations.

mAb quantification

The initial model was started using the range 1,500–1,700 cm^{-1} comprising the protein associated Amide I and II bands. Filtered and unfiltered samples were used for the model design. Initial wavenumber range between 1,500 and 1,700 cm^{-1} was split into intervals of 20 cm^{-1} and used for automatic model optimization within OPUS software regarding improvement of prediction quality and reliability when using only specific wavenumber regions of the initial wavenumber area. The automatic optimization mode systematically used these 20 cm^{-1} wavenumber areas to perform one-out cross-validation after using different pre-treatment steps and calculated RMSECV, rank, and RPD together with a plot of predicted vs. true values. Wavenumber range was then narrowed in 10 cm^{-1} intervals covering the Amide I band between 1,600 and 1,700 cm^{-1}. As antibodies are known to show a high beta-sheet content, the wavenumber ranges indicative for elevated beta-sheet content in proteins (1,620–1,635 cm^{-1} and 1,675–1,695 cm^{-1}) were evaluated for mAb quantification.[44] Furthermore, different optimization strategies using first and second derivative and visual inspection of peaks that correlated with mAb levels were used. To elucidate possible matrix effects, all procedures were evaluated using filtered and unfiltered samples, only filtered, or only unfiltered samples, respectively, to "simulate" in situ analysis as well as ex situ analysis of fermentation broth after filtration in a bypass.

Data treatment for final model used first derivative with Savitzky–Golay algorithm and 25 smoothing points. For mAb quantification, the wavenumber range 1,614–1,660 cm^{-1} and 1,680–1,690 was chosen to exclude polysaccharide associated peaks below 1,610 cm^{-1} and cover peaks indicative for secondary structure elements.

HCP quantification

For HCP quantification, the initial model was designed encompassing relevant Amide I and II bands with wavenumber ranges 1,500–1,700 cm^{-1}. Further optimization strategies were evaluated using the first and second derivative. Manual inspection of spectra revealed several peaks which correlated with HCP concentration levels determined from ELISA. These peaks were used for optimization of the model trying to involve as many data points as possible to improve the chemometric model.[35] All procedures were evaluated for HCP quantification using filtered and unfiltered samples, only filtered, or only unfiltered samples, respectively, to "simulate" in situ analysis as well as ex situ analysis of fermentation broth after filtration in a bypass and analyze possible associated matrix effects. Data treatment for final model used first derivative with Savitzky–Golay algorithm and 25 smoothing points for filtered or non-filtered samples only, respectively. Final model involving both filtered and non-filtered samples used first derivative with Savitzky–Golay algorithm and 25 smoothing points, followed by subtraction of a line by automatically adding a line to the spectral area
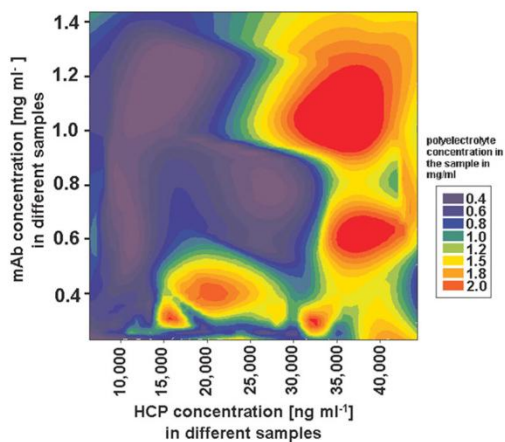
Figure 2. Contour plot showing HCP and mAb concentration depending on polyelectrolyte concentration in samples.

X-axis: HCP concentration in ng mL^{-1} (showing only samples up to 45,000 ng mL^{-1}; higher HCP titers in standards used for ELISA calibration and also included in calibration of the PLS model were not presented in the contour plot as they did not contain polyelectrolyte); *y*-axis: mAb concentration in mg mL^{-1} (showing only samples from 0.2 to 1.4 mg mL^{-1}; standards used for ELISA calibration and also included in calibration of the PLS model were not presented in the contour plot as they did not contain polyelectrolyte); *z*-axis: contours of polyelectrolyte concentration in corresponding samples ranging from 0.4 mg mL^{-1} (violet) to 2.0 mg mL^{-1} (red).

and subtracting that line to correct tilted spectra as suggested by OPUS software.

Results and Discussion

HCP-ELISA

The measurement of the HCP concentrations in the 66 samples using an ELISA indicated that the different polyelectrolytes or antibody concentrations did not influence the assay results. All influence tests yielded 20 ng mL^{-1} with a deviation from this standard less than the limitation of the ELISA assay [< 25% coefficients of variation (CV) according to manufacturer's manual]. HCP concentration levels ranged from 1,000 to approximately 55,000 ng mL^{-1}.

Antibody concentration measurements using fluorescence

Determination of antibody concentrations of cell culture samples that were spiked with fluorophore-labeled mAb gave different mAb levels within the different samples ranging from 0.17 to 1.7 g L^{-1}. As seen in previous experiments (data not shown), the precipitation behavior of labeled antibody was equal to that of unlabeled mAb. Therefore mAb concentration determination by measuring the change of only the labeled mAb fraction in the samples corresponds to the change of the entire mAb population (labeled and non-labeled).

Comparison of HCP and antibody concentration changes in samples

A comparison of the HCP and mAb concentration in the different samples analyzed using ELISA and with fluorescent

mAb spiked cell culture revealed no correlation of concentration changes in the samples. The HCP concentration in samples was between 1,000 and 55,000 ng mL^{-1}. The antibody concentration varied between 0.17 and 1.7 g L^{-1}, being relatively representative for corresponding protein titers during fermentation as deduced from initial experiments.

Colinearity evaluation of polyelectrolyte concentration and corresponding protein concentrations in samples

Plotting the concentration of mAb and HCPs in the different samples vs. the polyelectrolyte concentration added to the samples showed no correlation (Figure 2). Hence, the effects of colinearity and residual polyelectrolyte influence on the chemometric model were minimized. Also, the use of polyelectrolytes of different chemical nature and the additional use of filtered and non-filtered sample standards without added polyelectrolyte for model cross-validation and testing minimized possible interference further.

HCP and mAb quantification by FTIR-ATR

Principal component analysis. PCA was done to detect possible outliers as well as obvious differences between the samples. Plotting principal component 1 and 2 of wavenumber range 1,150–1,700 cm^{-1} accounts for more than 97% variance. It was obvious that ten filtered samples differed compared to the unfiltered as well as other filtered samples. During the course of the experiments, we found out that the reason was due to measurement of these ten samples with insufficiently cooled IR-detector, leading to a lower signal-to-noise ratio of those samples compared to the rest of the sample population. A removal of these outliers and repetition of the PCA showed no further outliers to be excluded from the model design.

Mid infrared spectra. An initial inspection of the remaining 56 spectra of analyzed samples showed overlapping peaks. As protein analysis using IR is mainly focusing on the Amide I and II bands, spectra were compared in this area in the wavenumber range from 1,500 to 1,700 cm^{-1}, extending to 1,340 cm^{-1} to include peaks associated with HCP concentration used in the PLS models. Peaks in the wavenumber range between 1,360 and 1,390 cm^{-1} and between 1,000 and 1,100 cm^{-1} were disregarded as they can likely be assigned to polyelectrolytes (data not shown).

Protein specific Amide I and II bands were chosen for treatment with multivariate data analysis methods PCA and PLS to elucidate mAb and HCP quantification, as these bands showed only a minor overlap in the spectra (Figure 3). For quantifying protein levels in the low microgram scale per milliliter in cell culture against a HCP and media background, this approach has been successfully employed already.[37] Likewise, the approach quantifying HCP against a mAb and media background should be achievable and was shown in previous experiments[38]; particularly since protein secondary structure can be compared using IR and antibody secondary structure exhibits exceptionally high content of beta-sheet.[44]

PLS-calibration model

Minimizing matrix effects by model optimization for mAb and HCP quantification. Optimization of the models for HCP quantification using the PRESS-method decreased the
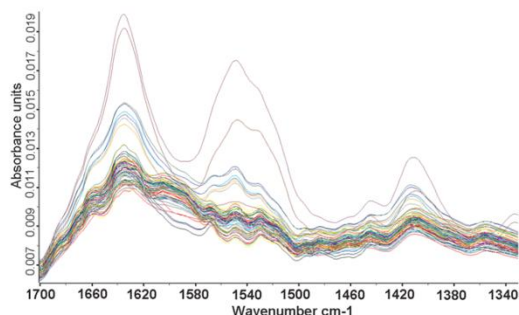
Figure 3. IR spectra of 56 NS0 cell culture fluid samples, after excluding outliers, showing wavenumber range from 1340 to 1,700 cm^{-1}.

Protein-structure associated peaks around 1,550 (Amide II) and 1,650 were considered for mAb and HCP quantification.

Figure 4. Comparison of correlation of HCP titers predicted using ELISA and ATR by application of different PLS models.

Models optimized for only unfiltered samples (A) or filtered samples (B) show an acceptable correlation in contrast to a general model applied to samples of differing chemical background (C).

ranks from 6 to 2. For mAb quantification, the rank decreased from 3 or 5, respectively, to 2. Models using fewer ranks, i.e. less factors reduce the risk of overfitting and incorporation of spectral noise fractions into the model. Therefore a factor number of 2 can be seen as more reliable compared to the initial model(s).[35]

A comparison of the HCP titers determined by ELISA and HCP concentration predicted using FTIR-ATR revealed an increasing correlation during model optimization. The final models showed a higher robustness if optimized for similar background matrices, comprising either only unfiltered (Figure 4A, R^2 87%) or only filtered samples (Figure 4B, R^2 93%). An optimization of the model for HCP quantification using a combination of different background matrices (filtered and unfiltered samples; Figure 4C) showed a R^2 of 83.6% and a factor 1.5–2.5 higher root mean square error compared to models optimized for samples of only filtered or non-filtered type.

A comparison of the mAb concentrations determined by fluorescence with the predicted values using FTIR-ATR showed an increasing correlation during model optimization and slightly reduced interference from different background matrix effects compared to HCP quantification. Initial models comprised wavenumber regions 1,500 to 1,700 cm^{-1} to cover Amide I and II bands. Optimization was achieved using secondary structure specific wavenumber regions within the Amide I band, which correlate with alpha-helix and beta-sheet content of proteins, to quantify the antibody. The optimized model for quantification of mAb in unfiltered samples showed a correlation coefficient of 92.9% (Figure 5A). The PLS model optimized for a background matrix of filtered samples showed a higher correlation coefficient of 97.9% (Figure 5B) while the general model optimized for both filtered and unfiltered samples showed a correlation coefficient of 91.1% and had a factor 1.3–1.65 higher root mean square error compared to the specific models (Figure 5C).

Minimizing interference of other substances within the cell culture fluid by using protein-assigned wavenumber regions

In the initial model for HCP quantification, the wavenumber ranges used comprised the Amide I and II bands and can be assigned to C—O and C—N stretching as well as NH bending. To avoid interference of our results with other sub-stances within the cell culture fluid, e.g. lipids, DNA, and media components, we excluded certain wavenumber regions for model development, e.g. those indicative for lipids such as 1330 cm^{-1}, around 1460 cm^{-1}, and > 1700 cm^{-1}.[45] Wavenumber regions indicative for nucleic acid-associated sugar-phosphate vibrations were also not used for model development.[46] However, although most of the chosen wavenumber regions for HCP quantification did not overlap with associated base-sugar vibrations, some interference as well as due to polysaccharide C—O stretching[47] cannot totally be excluded from being a possible explanation for the high rank required for the initial model.[46]
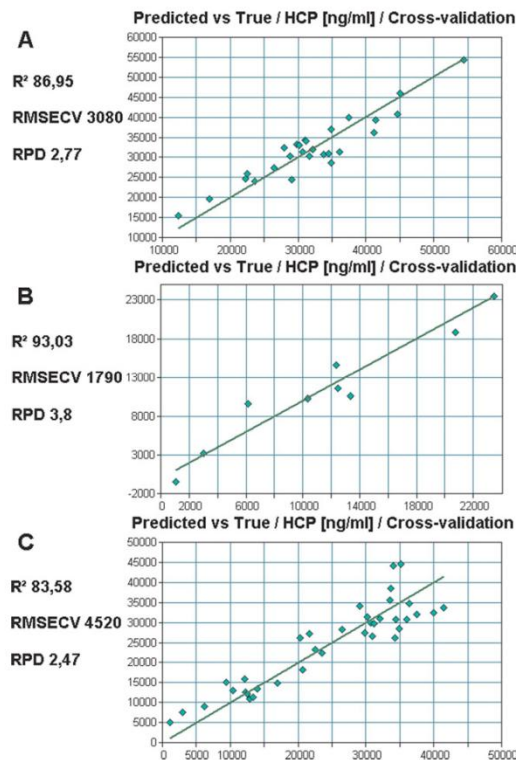
Therefore, after manual inspection of peaks in the spectra, we decided to choose those that seemed to correlate with HCP concentration change and hence minimize interference from other substances such as additives within the cell culture media. These wavenumbers comprised the Amide II band as well as bands most likely originating from C—O—H bending and other vibrations of carboxygroups (Table 1) and excluded most of the above described wavenumber regions. In the initial model for mAb quantification, the chosen wavenumber ranges comprised the Amide I and II bands associated with C—O and C—N stretching, NH bending, and to minor contributions of CO bending and CC stretching (Table 2).[26] In an effort to

Figure 5. Comparison of correlation of mAb titers predicted using PLS models covering Amide I region and ELISA.

A: mAb quantification PLS model to measure mAb titers in unfiltered samples. B: PLS model for mAb quantification in filtered samples. C: PLS model for measuring mAb titer in both, filtered and unfiltered samples.

Table 1. Assigned Functional Groups to Chosen Wavenumbers Used for Initial and Optimized Model for HCP Quantification

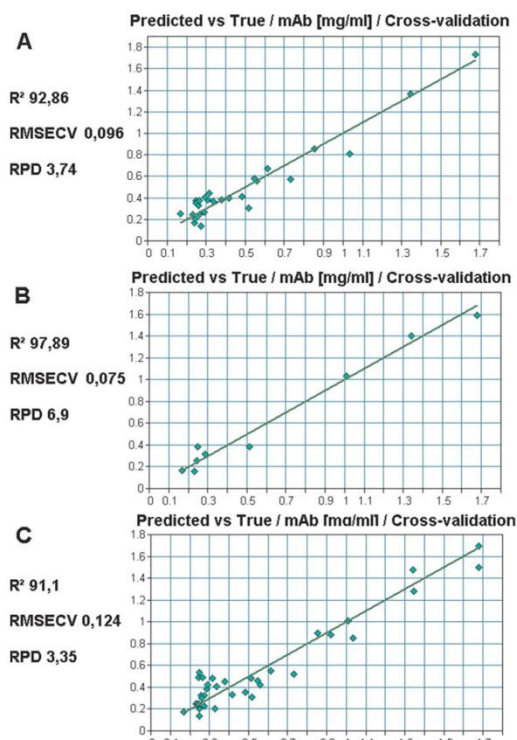| Model	Wavenumber range (cm^{-1})	Assigned
Initial model	1,500–1,700	Amide I and II (C=O stretching, CN stretching, NH bending, CO bending, CC stretching)
Final optimized model	1,545–1,557	Amide II (CN stretching, NH bending, CO bending, CC stretching)
	1,505–1,514	Amide II (CN stretching, NH bending, CO bending, CC stretching)
	1,417–1,424	C—O—H bending
	1,394–1,410	C—O—H
	1,341–1,352	C—O carboxylic acid

Table 2. Assigned Functional Groups to Chosen Wavenumbers Used for Initial and Optimized Model for mAb Quantification

Model	Wavenumber range (cm^{-1})	Assigned
Initial model	1,500–1,700	Amide I and II (C=O stretching, CN stretching, NH bending, CO bending, CC stretching)
Final optimized model	1,650–1,660	Amide I (indicative for turns, loops and alpha-helix)
	1,680–1,690	Amide I (indicative for beta-sheet and irregular)
	1,614–1,642	

Choice of samples for model calibration

HCP-quantification. Although we tried to achieve an evenly distribution of samples within our calibration area, most samples were in the center area of the calibration. The HCP concentration in the samples ranged from 1,000 to 55,000 ng mL^{-1} (Figures 4A–C), which might be increased further to improve the comparison to HCP titers during fermentation.

mAb-quantification. Samples showed mAb titers in the range of 0.17–1.7 g L^{-1}, also covering the mAb titers found in NS0 cell culture during fermentation.[49,50] As many mAb containing samples revealed mAb titers of 0.2 g L^{-1}, four of those samples were randomly removed in the general model to achieve better sample coverage across the calibration area thereby avoiding an influence on the calibration model.[35] For the optimized models, no additional samples were removed besides test-set samples and "outliers" as identified earlier by PCA. The calibration lines for all three models obtained coefficients of determination between 91.1 and 97.9% with a rank of 2 (Figures 5A–C).

Test-set validation

Prediction ability and robustness of models for mAb and HCP quantification were evaluated using independent test-set samples comprising unfiltered and filtered samples, which were not used during model development. Twenty test-set samples were used to verify the prediction accuracy of the general HCP and mAb model, 10 test-set samples, respectively, were used to verify the prediction accuracy of models specific to either unfiltered or filtered matrix.

The models optimized for matrices of filtered or unfiltered samples showed good HCP concentration prediction ability. About 70–80% of test-set samples showed CV of less than 25%, the limitation of the ELISA assay, with slightly higher prediction accuracy for the model optimized for filtered sample matrices. In comparison, the general model resulted in only

improve the rank and coefficient of correlation of the model, the optimized models encompassed only structural vibrations associated with the Amide I band and excluded interference of nucleic acid-associated base-sugar vibrations, sugar-phosphate vibrations as well as sugar vibrations and lipid-associated vibrations.[45,46] Further optimization was achieved focusing on Amide I peak areas that are indicative for certain secondary structure elements (compare to Goormaghtigh et al., 2006) in proteins (Table 2)[33,48] and excluding peaks assigned to interfering substances, e.g. 1,610 cm^{-1}, assigned to polysaccharide stretching vibration modes[47] as well as polyelectrolyte peaks at 1,000–1,100 cm^{-1} and around 1,390 cm^{-1}.

Antibodies are known for their elevated beta-sheet content and low amount of alpha-helices; therefore a focus on spectral areas indicative for protein structures with high beta-sheet content seemed feasible. Additionally, peaks indicative for alpha-helix were incorporated into the model to correlate low intensities of these peaks due to high alpha helix absence in mAbs with mAb concentration. Using these wavenumber regions, we were able to minimize interference of different background matrices. An improvement of models optimized for either unfiltered or filtered samples as well as the general model for both filtered and unfiltered samples was achieved.

Cumulative part- Experimental

50% of the 20 test-set samples being predicted within the limitation of the ELISA assay, yielding CVs between 2.6 and 24%.

For the mAb quantification models, the model optimized for filtered samples yielded 70% of test-set samples with CV < 25%, while the model optimized for unfiltered samples yielded 60% of test-set samples with CV < 25%. The general model showed lower accuracy with only 50% of test-set samples being predicted with a CV < 25%.

Model robustness comparing filtered and non-filtered background matrices

Compared to the paper of Sellick et al.,[37] which described a feasibility study on using several chemometric models that were optimized to quantify mAb, glucose, and lactate in CHO and NS0 cells, our models showed similar, slightly reduced relative RMSECV between 4.5 and 7.5% during cross-validation for mAb quantification. However, our results show higher RMSECV for independent test-set samples. While Sellick et al. used different CHO or NS0 cell lines, respectively, we focused on designing a general, more robust model based on one cell line with different background matrices (e.g., due to filtration and with various polyelectrolytes as background). We used the same wavenumber regions and ranks for different sample clusters to obtain one general model for quantifying mAb and another general model for quantifying HCPs at the cost of lower prediction accuracies. Also, by minimizing the number of ranks we reduced the risk of incorporation of spectral noise into our models thereby preventing overfitting. For some models this resulted in slightly lower degrees of correlation.

However, our models for mAb and HCP quantification, optimized on filtered or non-filtered samples, respectively, showed moderate to good degrees of correlation and prediction accuracy. About 70–80% of test-set samples were predicted with CV < 25% using the specific HCP models. In comparison, only 60–70% of independent test-set samples were predicted with CV < 25% when specific mAb prediction models were used.

The general model for mAb quantification in filtered and unfiltered samples achieved a prediction accuracy with a R^2 of 91.1% (Figure 5C). The results were slightly influenced by matrix effects due to the filtration step, which is similar to the results reported by Rodrigues et al.[51] They quantified an active pharmaceutical ingredient at similar relative concentration ranges compared to our mAb by using a near-infrared based PLS model after applying different filtration techniques. Yet, only 50% of test-set samples were predicted with CV < 25%, similar to the general HCP quantification model, the latter having a lower accuracy during cross-validation due to being influenced by matrix effects (Figure 4C) and resulting in 50% of independent test-set samples predicted with CV < 25%.

Putative causes for the lower accuracy of the general models compared to specific models might be matrix effects of different chemical background of the cell culture media. By filtering the cell culture fluid, some particles and compounds might be removed thereby changing the background and accounting for difficulties in applying a quantification model optimized for filtered samples on non-filtered samples and *vice versa*. While the effect of matrix influence was larger with the general HCP model, possibly due to the lower HCP concentration in the samples compared to mAb, the matrix influence on the general mAb model was less pronounced when compared to specific mAb models.

Conclusions

The results of this feasibility study on using FTIR-ATR for mAb and HCP quantification in cell culture imply its potential use for in situ monitoring of mAb and HCP titers during fermentation processes, but also indicate the need for further performance elucidations. To evaluate matrix effects and elucidate the effect of filters sometimes used in bypass-systems for protein quantification, we designed optimized models as well as a general model for comparing mAb and HCP titers in filtered and unfiltered samples of a cell culture where wavenumber regions were chosen to minimize interference from nucleic acids, lipids, and media components. Compared to the protein concentrations determined by ELISA, HCP prediction for the independent test-set samples using models designed for specific background matrices was fairly accurate for the range of approximately 2,000–55,000 ng mL^{-1}, with 70–80% of test-set samples being predicted within the limitation of the ELISA. Additionally, the quantification range might be increased to cover the relevant HCP titers during fermentation. Yet, a direct comparison of HCP titers using one single model for filtered and non-filtered samples achieved a slightly lower coefficient of determination and was influenced by background matrix effects, resulting in only 50% of test-set samples being predicted within the limitation of the ELISA assay. This indicates the need for separate models depending on the corresponding matrix, optimized for ex situ or in situ monitoring of HCP secretion. Furthermore, the use of larger sample populations could help to improve the models and especially for the models optimized for filtered or unfiltered sample matrix. Using larger test-set sample populations, the prediction accuracy and robustness of the models could be more precisely evaluated, although the results presented here indicate the potential suitability of our method for predicting HCP titer.

The prediction of mAb was not as accurate as antibody concentration determination by fluorescence counts (CV ∼ 10%) when analyzing the mAb concentration range of 0.17–1.7 g L^{-1} and covering the relevant mAb titers during fermentation using NS0 cell cultures. The overall prediction accuracy for the test-set samples was lower compared to HCP prediction and test-set spectra validation yielded some substantial deviations compared to reference values. Optimized models yielded only 60–70% of test-set samples predicted with CV < 25%, while the general model showed reduced prediction accuracy with only 50% of test-set samples being predicted with CV < 25%.

These results show that to obtain more precise models, further optimization is required concerning the selected wavenumber regions and the size of sample population. Having a more evenly distributed antibody concentration within the samples would also be beneficial where in this case, most of the samples contained mAb at the low end of the concentration range and thus made the model design more difficult.

Similarly to HCP models, PLS models optimized for ex situ monitoring of mAb production in a bypass using a filter should not be applied to in situ measurements of antibody concentrations using probes directly in the bioreactor and *vice versa*. Yet, our feasibility study shows the potential of FTIR-ATR to quantify protein in different background matrices using a non-invasive analysis that can enable the real-time monitoring of fermentation. Further research on determining the specifications and limitations of this method with

respect to the matrix effects associated with different cell cultures, fermentation systems, as well as processing steps may lead to improved prediction accuracies.

Literature Cited

1. Bowering LC, Bracewell DG, Kesharvarz-Moore E, Hoare M, Weir ANC. Comparison of techniques for monitoring antibody fragment production in *E. coli* fermentation cultures. *Biotechnol Prog*. 2002;18:1431–1438.
2. Garn M, Gisin M, Thommen C, Cevey P. A flow injection analysis system for fermentation monitoring and control. *Biotechnol Bioeng*. 1989;34:423–428.
3. Vojinovic V, Cabral JMS, Fonseca LP. Real-time bioprocess monitoring. I. In situ sensors. *Sens Actuators B*. 2006;114:1083–1091.
4. Rhiel M, Cohen MB, Murhammer DW, Arnold MA. Nondestructive near-infrared spectroscopic measurement of multiple analytes in undiluted samples of serum-based cell culture media. *Biotechnol Bioeng*. 2002;77:73–82.
5. Flatman S, Alam I, Gerard J, Mussa N. Process analytics for purification of monoclonal antibodies. *J Chromatogr B*. 2007;848:79–87.
6. Gill A, Bracewell DG, Maule CH, Lowe PA, Hoare M. Bioprocess monitoring: An optical biosensor for rapid bioproduct analysis. *J Biotechnol*. 1998;65:69–80.
7. Hoffman K. Strategies for Host Cell Protein Analysis. *BioPharm*. 2000;13:38–45.
8. Wang X, Hunter AK, Mozier NM. Host cell proteins in biologics development: Identification, quantitation and risk assessment. *Biotechnol Bioeng*. 2009;103:446–458.
9. Zhang J, Zhou H, Ji Z, Regnier F. Monoclonal antibody production with on-line harvesting and process monitoring. *J Chromatogr B*. 1998;707:257–265.
10. Doak DL, Phillips JA. In situ monitoring of an escherichia coli fermentation using a diamond composition ATR probe and mid-infrared spectroscopy. *Biotechnol Prog*. 1999;15:529–539.
11. Landgrebe D, Haake C, Höpfner T, Beutel S, Hitzmann B, Scheper T, Rhiel M, Reardon K. On-line infrared spectroscopy for bioprocess monitoring. *Appl Microbiol Biotechnol*. 2010;88:11–22.
12. Le Coq D, Michel K, Keirsse J, Boussard-Plédel C, Fonteneau G, Bureau B, Le Quéré JM, Sire O, Lucas J. Infrared glass fibers for in-situ sensing, chemical and biochemical reactions. *Comptes Rendus Chim*. 2002;5:907–913.
13. Kornmann H, Rhiel M, Cannizzaro C, Marison I, von Stockar U. Methodology for real-time, multianalyte monitoring of fermentations using an in-situ mid-infrared sensor. *Biotechnol Bioeng*. 2003;82:702–709.
14. Franco VG, Perín JC, Mantovani VcE, Goicoechea HcC. Monitoring substrate and products in a bioprocess with FTIR spectroscopy coupled to artificial neural networks enhanced with a genetic-algorithm-based method for wavelength selection. *Talanta*. 2006;68:1005–1012.
15. Sivakesava S, Irudayaraj J, Ali D. Simultaneous determination of multiple components in lactic acid fermentation using FT-MIR, NIR, and FT-Raman spectroscopic techniques. *Process Biochem*. 2001;37:371–378.
16. Roychoudhury P, Harvey LM, McNeil B. At-line monitoring of ammonium, glucose, methyl oleate and biomass in a complex antibiotic fermentation process using attenuated total reflec-

tance-mid-infrared (ATR-MIR) spectroscopy. *Anal Chim Acta*. 2006;561:218–224.
17. Schenk J, Marison IW, von Stockar U. A simple method to monitor and control methanol feeding of *Pichia pastoris* fermentations using mid-IR spectroscopy. *J Biotechnol*. 2007;128:344–353.
18. Schenk J, Marison IW, von Stockar U. pH prediction and control in bioprocesses using mid-infrared spectroscopy. *Biotechnol Bioeng*. 2008;100:82–93.
19. Petibois C, Gionnet K, Goncalves M, Perromat A, Moenner M, Deleris G. Analytical performances of FT-IR spectrometry and imaging for concentration measurements within biological fluids, cells, and tissues. *Analyst*. 2006;131:640–647.
20. Berthomieu C, Hienerwadel R. Fourier transform infrared (FTIR) spectroscopy. *Photosynth Res*. 2009;101:157–170.
21. McGovern AC, Ernill R, Kara BV, Kell DB, Goodacre R. Rapid analysis of the expression of heterologous proteins in *Escherichia coli* using pyrolysis mass spectrometry and Fourier transform infrared spectroscopy with chemometrics: application to a-interferon production. *J Biotechnol*. 1999;72:157–168.
22. Gross-Selbeck S, Margreiter G, Obinger C, Bayer K. Fast quantification of recombinant protein inclusion bodies within intact cells by FT-IR spectroscopy. *Biotechnol Prog*. 2007;23:762–766.
23. Timmins ÉM, Quain DE, Goodacre R. Differentiation of brewing yeast strains by pyrolysis mass spectrometry and Fourier transform infrared spectroscopy. *Yeast*. 1998;14:885–893.
24. Fahrenfort J. Attenuated total reflection: a new principle for the production of useful infra-red reflection spectra of organic compounds. *Spectrochim Acta*. 1961;17:698–709.
25. Harrick NJ. Surface chemistry from spectral analysis of totally internally reflected radiation. *J Phys Chem*. 1960;64:1110–1114.
26. Barth A. Infrared spectroscopy of proteins. *Biochim Biophys Acta*. 2007;1767:1073–1101.
27. Goormaghtigh E, Ruysschaert J-M, Raussens V. Evaluation of the information content in infrared spectra for protein secondary structure determination. *Biophys J*. 2006;90:2946–2957.
28. Jackson M, Mantsch HH. The use and misuse of FTIR spectroscopy in the determination of protein structure. *Crit Rev Biochem Mol Biol*. 1995;30:95–120.
29. Etzion Y, Linker R, Cogan U, Shmulevich I. Determination of protein concentration in raw milk by mid-infrared fourier transform infrared/attenuated total reflectance spectroscopy. *J Dairy Sci*. 2004;87:2779–2788.
30. Mazarevica G, Diewok J, Baena JR, Rosenberg E, Lendl B. On-line fermentation monitoring by mid-infrared spectroscopy. *Appl Spectrosc*. 2004;58:804–810.
31. Chu L, Robinson DK. Industrial choices for protein production by large-scale cell culture. *Curr Opin Biotechnol*. 2001;12:180–187.
32. Kong J, Yu S. Fourier transform infrared spectroscopic analysis of protein secondary structures. *Acta Biochim Biophys Sin*. 2007;39:549–559.
33. Dong A, Malecki JM, Lee L, Carpenter JF, Lee JC. Ligand-induced conformational and structural dynamics changes in *Escherichia coli* cyclic AMP receptor protein. *Biochemistry*. 2002;41:6660–6667.
34. Martens H, Martens M. *Multivariate Analysis of Quality*. Chichester: Wiley;2001.
35. Naes T. *Multivariate Calibration and Classification*. Chichester: NIR Publications;2002.
36. Wold S, Martens H, Wold H, Kågström B, Ruhe, A. The multivariate calibration problem in chemistry solved by the PLS method. *Matrix Pencils*. 1983;973:286–293.
37. Sellick, CA, Hansen R, Jarvis RM, Maqsood AR, Stephens GM, Dickson AJ, Goodacre R. Rapid monitoring of recombinant antibody production by mammalian cell cultures using Fourier transform infrared spectroscopy and chemometrics. *Biotechnol Bioeng*. 2010;106:432–442.
38. Capito F, Skudas R, Kolmar H, Stanislawski B. Host cell protein quantification by Fourier transform mid infrared spectroscopy (FT-MIR). *Biotechnol Bioeng*. In press. DOI: 10.1002/bit.24611
39. Warnes MR, Glassey J, Montague GA, Kara B. On data-based modelling techniques for fermentation processes. *Process Biochem*. 1996;31:147–155.

40. Wold S, Esbensen K, Geladi P. Principal component analysis. *Chemom Intell Lab Syst.* 1987;2:37–52.

41. Sjöström M, Wold S, Lindberg W, Persson JÃk, Martens H. A multivariate calibration problem in analytical chemistry solved by partial least-squares models in latent variables. *Anal Chim Acta.* 1983;150:61–70.

42. Osten DW. Selection of optimal regression models via cross-validation. *J Chemom.* 1988;2:39–48.

43. Brereton G. *Multivariate Pattern Recognition in Chemometrics, Illustrated by Case Studies.* Amsterdam: Elsevier Science Publishers B.V.;1992.

44. Hering JA, Innocent PR, Haris PI. Automatic amide I frequency selection for rapid quantification of protein secondary structure from Fourier transform infrared spectra of proteins. *Proteomics.* 2002;2:839–849.

45. Goormaghtigh E, Raussens V, Ruysschaert JM. Attenuated total reflection infrared spectroscopy of proteins and lipids in biological membranes. *Biochim Biophys Acta.* 1999;1422: 105–185.

46. Banyay M, Sarkar M, Gräslund A. A library of IR bands of nucleic acids in solution. *Biophys Chem.* 2003;104:477–488.

47. Marcotte L, Kegelaer Gg, Sandt C, Barbeau J, Lafleur M. An alternative infrared spectroscopy assay for the quantification of polysaccharides in bacterial samples. *Anal Biochem.* 2007;361:7–14.

48. Oberg KA, Ruysschaert J-M, Goormaghtigh E. The optimization of protein secondary structure determination with infrared and circular dichroism spectra. *Eur J Biochem.* 2004;271:2937–2948.

49. Burky JE, Wesson MC, Young A, Farnsworth S, Dionne B, Zhu Y, Hartman TE, Qu L, Zhou W, Sauer PW. Protein-free fed-batch culture of non-GS NS0 cell lines for production of recombinant antibodies. *Biotechnol Bioeng.* 2007;96:281–293.

50. Dempsey J, Ruddock S, Osborne M, Ridley A, Sturt S, Field R. Improved fermentation processes for NS0 cell lines expressing human antibodies and glutamine synthetase. *Biotechnol Prog.* 2003;19:175–178.

51. Rodrigues LO, Cardoso JP, Menezes JC. Applying near-infrared spectroscopy in downstream processing: one calibration for multiple clarification processes of fermentation media. *Biotechnol Prog.* 2008;24:432–435.

3.5.3 Antibody aggregate quantification using MIR

Technical Report: Mid-infrared spectroscopy-based antibody aggregate quantification in cell culture fluids

Florian Capito, Romas Skudas, Harald Kolmar and Christian Hunzinger

Copyright © WILEY-VCH Verlag GmbH & Co. KGaA, Weinheim, 2013

Short summary:

The feasibility of using MIR for antibody aggregate quantification is shown, using different antibodies and process samples. The idea is to use the knowledge of this paper and employ MIR, in a similar manner, for analysis of mAb structure and aggregate formation, when performing protein precipitation using copolymers. By that, harmful effects of precipitation on protein structure can be elucidated.
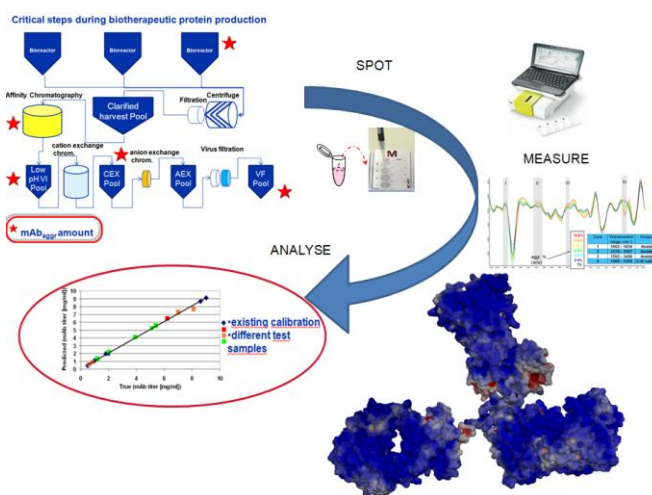
Fig. 5: Graphical abstract; Reproduced by permission of WILEY-VCH Verlag GmbH & Co. KGaA, Weinheim.

Technical Report

Mid-infrared spectroscopy-based antibody aggregate quantification in cell culture fluids

Florian Capito[1, 2], Romas Skudas[2], Harald Kolmar[1] and Christian Hunzinger[2]

[1] Institute for Organic Chemistry and Biochemistry, Technische Universität Darmstadt, Germany
[2] Merck KGaA, Darmstadt, Germany

Therapeutic antibody purification involves several steps which potentially induce antibody aggregation. Currently, aggregate monitoring mainly employs chromatographic, SDS-PAGE and light scattering techniques. In this study, the feasibility of mid-infrared spectroscopy (MIR) for the quantification of soluble antibody aggregates was investigated. Several multivariate models were evaluated to quantify antibody aggregation in chromatography elution streams and in clarified CHO cell culture supernatants (a surrogate for bioreactor output). A general model was established that is applicable for aggregate quantification directly from different cell culture solutions. Real-process samples and process-sample mimics were used to verify the general aggregate quantification model using two different antibodies. Results showed good prediction ability down to 1% aggregate content. Together with recently published results using MIR for host cell protein and target protein quantification, the results presented here indicate that MIR could provide multi-parameter process information from a single, fast, cost-effective and straightforward measurement. In conclusion, our study demonstrates that MIR is suitable for aggregate quantification in therapeutic antibody purification processes.

Supporting information
available online

1 Introduction

Purification of therapeutic antibodies is usually performed using a set of orthogonal purification techniques, typically starting with centrifugation and filtration to remove cellular debris and large particulates. This process is then usually followed by protein A affinity chromatography for selective antibody capture, a low-pH virus inactivation step, and ion-exchange chromatography and/or hydrophobic interaction chromatography (as orthogonal techniques). After final polishing, antibodies are formulated using different excipients to enhance long-term stability. However, several of the aforementioned procedures may cause antibody aggregate formation, particularly via filtration-associated shear stress and stress due to agitation, aeration and stirring [1, 2]. In addition, exposure to low-pH conditions during affinity chromatography elution and virus inactivation can also precipitate aggregation [3, 4]. pH shifts occurring during purification and formulation, lyophilization, long-term storage or freeze-thaw, and concentration-induced aggregate formation stemming from high antibody levels in the final product are other possible sources of protein aggregation [5, 6]. Aggregate levels can vary between 0.5 and 60%, depending on the external stress factors at play, intrinsic properties of the antibody and purification steps employed [5].

As antibody aggregates are associated with increased immunogenicity, anaphylactic side reactions and even renal failure, high aggregate levels must be avoided in the final drug product [7, 10]. A common acceptance criteri-

Correspondence: Florian Capito, MM-PTD-D, A003/101, Merck KGaA, Frankfurter Str. 250, 64293 Darmstadt, Germany
E-mail: florian.capito@external.merckgroup.com

Abbreviations: CHO, Chinese hamster ovary cell culture; **mAb**, monoclonal antibody; **MIR**, mid-infrared spectroscopy; **PLS**, partial least squares regression; **RMSE-CV**, root mean square error of cross-validation; **RMSE-IT**, root mean square error of the independent test-set; **SDS-PAGE**, sodium dodecyl sulfate polyacrylamide gel electrophoresis; **SEC**, size exclusion chromatography; **SEC-HPLC**, size exclusion chromatography high performance liquid chromatography

1

on is to maintain aggregate levels below 5% measured at the end of product shelf life. However, this limit can become more stringent, as indicated by product stability data and the critical operating parameter envelope. Soluble aggregates are primarily quantified using size exclusion chromatography (SEC)-high performance liquid chromatography (HPLC) as the method of choice, and to a minor extent also by sodium dodecyl sulfate polyacrylamide gel (SDS-PAGE) or light scattering [11, 12]. SEC-HPLC has the drawback of requiring large eluent volumes, leading to a high eluent waste load. Furthermore, dilution of samples and column filters for off-line analysis can theoretically lead to a reversal of aggregation, making SEC-HPLC data not always representative of aggregation present in process streams. SDS-PAGE is limited to detecting covalently linked aggregates only, and becomes somewhat time-consuming. Thus this technique is of limited value for biotherapeutic process optimization, although new lab-on-chip techniques allow for faster data analysis [13]. Light scattering provides qualitative information only, instead of generating quantitative results. Mid-infrared spectroscopy (MIR) is one of the most-promising potential techniques for aggregate monitoring, since it possesses a good balance between sensitivity and analysis time [13]. MIR is based on the interaction between matter and irradiation at different wavenumbers, leading to structure specific energy absorbance and a specific infrared spectrum [14]. This allows aggregated antibody to be differentiated from non-aggregated antibody, as well as from other unrelated substances. MIR has been used for quantification of antibody levels and host cell protein impurities (HCP) in cell culture fluid [15–17] and has also been used to analyze the effects of storage and formulation type on antibody structure [18–24]. Moreover, it has also been successfully applied to aggregate analysis [25–29]. However, most of these studies have focussed on qualitative spectra analysis, instead of MIR-based aggregate quantification as required for downstream processing analytics. The aim of this paper is to apply MIR to at-line quantification of soluble aggregates in both pure monoclonal antibody (mAb) solutions and cell culture fluid samples containing mAb, thereby showing the suitability of MIR to analyze multiple parameters (aggregate level as well as antibody and host cell protein content [16]) within a process stream sample using a single measurement.

2 Materials and methods

2.1 Sample preparation

2.1.1 mAb A sample preparation

Purified antibody solution (mAb A) was obtained from Merck KGaA, Darmstadt, Germany. Antibody aggregation was induced by exposing the antibody to cycles of

pH-shift: incubation for 2 hours at pH 5.0, followed by 2 hours incubation at pH 10, before changing pH back to pH 5.0. The pH-shift cycle was repeated four times, adjusting the pH by adding 1 M NaOH or HCl as required. Afterwards, antibody was stored at 4°C for 24 h to allow for sedimentation of large particles. Aggregate formation was analyzed using SEC and fractions containing aggregated mAb were concentrated using Eshmuno S (Merck KGaA, Darmstadt, Germany). The extent of aggregate formation were then determined using SEC after applying dialysis to remove trace buffer levels that otherwise interfering with analysis by infrared spectroscopy. Concentration of samples with aggregated antibody was increased, using centrifugal filter units (Amicon, Merck KGaA, Darmstadt, Germany).

After allowing aggregated antibody to sediment at 4 °C for 24 h, an aliquot of supernatant was taken and injected into pure antibody solution (not subjected to pH shift and thus not exhibiting aggregates, confirmed by SEC). The total antibody amount in each sample was standardised after injection of aggregated antibody, resulting in a final antibody concentration of 10 mg mL^{-1} in all samples. Aggregate levels ranged from 0.02 to 14.8% of total antibody levels. Additionally, aggregated antibody was injected into CHO4 and CHO-DG44 cell culture fluid harvested from non-antibody producing mammalian cell cultures. Similarly to pure antibody solutions, final antibody concentration of culture supernatant samples was standardised to at 4 mg mL^{-1} and aggregate levels were adjusted within a range of 0.02–14.8% (w/w). To observe any changes in aggregation behaviour after aggregate antibody solutions were completed in various milieus, samples were re-analyzed by SEC.

2.1.2 mAb B sample preparation

Additionally, antibody solution (mAb B) was obtained as a process sample, taken directly after affinity chromatography (post protein A mAb solution) with aggregate levels determined by SEC. Non-aggregated mAbB was obtained from Merck KGaA, Darmstadt, Germany.

A process sample, containing 7% (w/w) aggregates (determined by SEC) was added to non-aggregated mAb B solution to obtain final aggregate levels between 1 and 7%.

2.2 MIR analysis

Samples were measured in transmission mode using a Direct Detect™ infrared spectrometer (Merck Millipore, Danvers, USA), applying 2 μL of each sample to Direct Detect™ filter cards before measurement, according to manufacturer's instructions. H$_2$O was used as a reference. Additionally, concentrated aggregated antibody, non-aggregated antibody (mAb A), as well as defined blends of aggregated and non-aggregated antibody were measured for spectral comparison and selection of useful

wavenumber ranges for aggregate quantification (Supporting information, Fig. S1 shows spectral comparison of defined blends of aggregated and non-aggregated antibody and wavenumber ranges used for quantification model design). The same procedure was applied to quantify mAb B aggregation. Obtained spectra were exported from Direct Detect software™ and analyzed using spectral processing software OPUS v 6.5 (Bruker Optik GmbH, Ettlingen, Germany). Afterwards, the second derivative of spectra was calculated to allow for baseline normalization.

3 Results

Two therapeutic monoclonal antibodies, mAb A and mAb B were used as model proteins. Repeated pH-shift of mAb A resulted in the formation of aggregated antibody, present as mostly dimers and to a small percentage as multimers as analyzed by SEC. Aggregated fractions were concentrated using Eshmuno S to obtain final levels of aggregated antibody between 53–54% of total antibody. mAb B was a mid-purification process sample containing 7% antibody aggregates based on total antibody content. Both antibody solutions were added into the respective non-aggregated antibody solution to reach various levels of aggregate content. SEC revealed no changes in the aggregation pattern upon injection into non-aggregated samples and no influence of aliquot size on aggregate amount and distribution.

3.1 MIR analysis

For mAb A and mAb B, spectra of aggregated and non-aggregated antibody were compared, showing large differences in the wavenumber ranges of 1665-1654 cm^{-1}; 1624-1616 cm^{-1}; 1601-1594 cm^{-1}; 1579-1567 cm^{-1}; 1545-1535 cm^{-1}; 1502-1496 cm^{-1}; 1475-1470 cm^{-1}; 1461-1450 cm^{-1}; 1317-1306 cm^{-1}; 1360-1355 cm^{-1} and 914-903 cm^{-1}. The wavenumber range 1300-1100 cm^{-1} was not considered due to absorbance of the filter card used for sample measurement in the Direct Detect™ instrument. Shifts of bands as described in the literature were observed, such as a shift of beta-sheet associated bands from around 1690 cm^{-1} to 1694 cm^{-1} Broadening of bands, associated with disordered structures [18–24] was also noted.

An intense band in the wavenumber range of 1630-1600 cm^{-1} was associated with the presence of aggregated antibody. This band corresponds with intermolecular beta-sheet binding (1619 cm^{-1}) [12] as well as hydrogen-bonding between beta-strands (1622 cm^{-1}) [30]. The wavenumber regions listed above were used within OPUS software as input parameters for automatic optimization mode, to optimize partial least squares regression (PLS)- based models for aggregate amount prediction. The software algorithm initially employed all suggested wavenumber regions to design an aggregate amount prediction model. Wavenumber regions not leading to an improved model quality are then sequentially removed in order to minimize the root mean square error of model cross-validation (RMSE-CV).

Results of the automatic optimization mode in OPUS suggest four wavenumber regions to be used for aggregate quantification using mAb A or mAb B: 1665-1654 cm^{-1}; 1579-1567 cm^{-1}; 1502-1496 cm^{-1} and 1360-1355 cm^{-1}. These wavenumber regions were also identified during the comparison of cell culture fluid samples with different levels of antibody aggregation. Thus, these four wavenumber ranges were used for establishing sev-

Table 1. Overview of PLS models used to quantify aggregates in pure antibody solution and in cell culture fluid (CCF)

Model for predicting aggregate amounts in	mAb	Number of cross-validation samples	Number of independent test-set samples	Number of ranks required for PLS model	Residual predictive deviation (RPD)	Coefficient of correlation (R²)	Root mean square error of cross-validation (RMSE-CV)	Root mean square error of independent test-set (RMSE-IT)
Pure antibody solution[a]	mAb A	19	19	1	8.98	98.8	0.62	0.51
DG44 CCF[b]	mAb A	19	19	1	9.68	98.9	0.54	0.47
CHO4 CCF[c]	mAb A	19	19	1	5.87	97.1	0.97	0.85
DG44 & CHO4 CCF[d]	mAb A	38	38	1	6.50	97.6	0.78	0.95
Pure antibody solution, DG44 & CHO4 CCF[e]	mAb A & mAb B	22	36	5	4.79	95.6	1.00	0.89

a) Model A; b) Model B; c) Model C; d) Modal D; e) Modal E

Table 2. Comparison of mAb A aggregate quantification using Models A-E. Test samples in range 1–15% aggregated antibody content shown

mAb solution			DG44					CHO4				
mAb model (Model A)				DG44- model (Model B)		DG44-CHO4-model (Model D)			CHO4 model (Model C)		General DG44-CHO4-model (Model D)	
True[a]	Predicted	CV[b]	True	Predicted	CV	Predicted	CV	True	Predicted	CV	Predicted	CV
1.00	0.91	6.68	**1.00**	1.28	19.97	0.69	21.92	**1.00**	1.20	14.17	1.47	33.42
2.00	1.94	2.03	**2.00**	1.45	19.36	2.38	13.60	**2.00**	2.14	4.99	2.47	16.77
2.00	2.14	5.11	**4.00**	3.91	1.55	4.56	9.96	**2.00**	1.80	7.00	2.13	4.76
6.00	6.09	1.06	**4.00**	3.94	0.98	4.33	5.78	**4.00**	5.55	27.45	5.08	19.09
6.00	6.36	4.29	**6.00**	6.90	10.61	7.22	14.37	**6.00**	6.32	3.71	6.36	4.22
8.00	8.23	1.99	**8.00**	8.03	0.28	8.91	8.04	**8.00**	6.92	9.5	6.91	9.67
10.00	9.71	2.05	**10.00**	9.23	5.46	10.75	5.30	**8.00**	6.13	16.52	6.29	15.14
12.00	12.60	3.52	**10.00**	10.80	5.65	11.15	8.12	**10.00**	9.93	0.47	10.00	0.00
12.00	11.14	5.07	**12.00**	11.58	2.48	11.52	2.80	**12.00**	11.59	2.43	11.46	3.16
14.00	14.24	1.22	**14.00**	13.95	0.26	14.30	1.50	**14.00**	11.25	13.88	11.16	14.33
14.80	15.38	2.75	**14.80**	15.38	2.75	14.53	1.30	**14.00**	13.18	4.14	12.95	5.32

a) True value measured by SEC
b) CV, coefficient of variation

eral models, based on PLS1 algorithm within Quant 2 method in OPUS software:

(i) model for predicting aggregate amount in pure mAb A solution (model A);
(ii) model for predicting mAbA aggregate amount in DG44 cell culture fluid (model B);
(iii) model for predicting mAb A aggregate amount in CHO4 cell culture fluid (model C);
(iv) general model for predicting mAb A aggregate amount in both, DG44 and CHO4 cell culture fluid (model D); and
(v) general model for predicting mAb A and mAb B aggregate amount, using post protein A elution as real process samples (mAbB), process-sample mimics (mAbA) as well as cell culture fluid (model E).

Sample sets for each of these models were split into a cross-validation set used for one-out-cross validation and an independent test set comprised of samples not used for model design (Table 1). These independent test set samples were used to evaluate the overall prediction ability of the model and avoid any bias on the model during design (Table 1) [31]. Almost all of final obtained PLS models required only the first rank hence minimizing the risk of noise incorporation into the model and preventing over-specification. For the general model to quantify both mAb A and mAb B aggregation, a rank of 5 was determined by minimizing the prediction error sum of squares within OPUS software.

Coefficients of correlation (R^2) of greater than 95.6% and a residual predictive deviation (RPD) of greater than 4.5 indicated all models reliably described the dataset. RMSE-CV and root mean square error of the independent test set (RMSE-IT) showed a prediction error of usually less than 1% , yielding good prediction capabilities that enabled us to monitor antibody aggregation levels down to 1% of the total mAb content with acceptable deviations (Tables 2 and 3). Samples containing less than 1% aggregated antibody could not be predicted successfully and are thus not shown in Tables 2 and 3. The majority of test set samples within the range 1 to 14.8% aggregate content displayed a coefficient of variation (CV) of less than 10% (Tables 2 and 3). Only one of the samples shown in Table 2 and four samples presented in table 3 displayed CV values larger than 25%. Samples containing low percentage of aggregates displayed a larger CV: The lower signal-to-noise ratio in these samples may explain the difficulty in quantifying low levels of aggregations.

4 Discussion

Our results indicated that MIR in combination with PLS-based quantification models can be used to monitor the amount of aggregated antibody in partly purified mAb process streams and in cell culture fluid, a surrogate for purification process input streams. The chosen antibodies, mAb A and mAb B, are slightly different with respect to secondary structure and aggregate distribution. As a consequence differences in wavenumber shifts used to discriminate between the aggregated and the non-aggregated state are exhibited by the two mAb. This is reflected by the prediction ability of the designed models shown in Tables 2 and 3. Model prediction of aggregate levels is improved in the case of single mAb quantification, compared to the prediction of aggregate formation using a general aggregate quantification model as shown in Table 3.

BIOtec visions
www.biotecvisions.com

Table 3. Comparison of aggregate quantification for mAb A and mAb B using a general aggregate quantification model (Model E) including real process samples and process-sample mimics

Sample	True[a]	Predicted	CV[b]	Sample	True	Predicted	CV
mAb B	1.50	0.88	29.15	mAb A in DG44	4.00	4.42	7.45
mAb B	2.00	2.30	10.49	mAb A in DG44	4.00	3.82	3.16
mAb B	2.50	1.80	19.91	mAb A in DG44	6.00	7.05	12.36
mAb B	2.50	2.46	1.19	mAb A in DG44	8.00	9.70	15.02
mAb B	3.00	2.52	11.20	mAb A in DG44	10.00	10.78	5.48
mAb B	3.00	3.32	7.50	mAb A in DG44	12.00	10.53	8.64
mAb B	3.50	4.33	16.69	mAb A in DG44	14.00	14.57	2.88
mAb B	3.50	2.25	25.30	mAb A in DG44	14.80	15.40	2.88
mAb B	4.00	3.85	2.04	mAb A in CHO4	1.00	1.21	14.91
mAb B	4.50	4.31	2.94	mAb A in CHO4	2.00	1.44	19.69
mAb B	4.50	3.74	11.97	mAb A in CHO4	2.00	1.06	33.19
mAb B	5.00	3.54	20.67	mAb A in CHO4	4.00	4.37	6.50
mAb B	5.50	4.24	16.19	mAb A in CHO4	6.00	6.30	3.50
mAb B	5.50	4.66	10.84	mAb A in CHO4	8.00	6.91	9.65
mAb B	6.50	6.85	3.79	mAb A in CHO4	10.00	10.45	3.20
mAb B	6.50	5.12	15.07	mAb A in CHO4	12.00	10.80	7.07
mAb A in DG44	1.00	1.52	37.09	mAb A in CHO4	14.00	10.44	17.98
mAb A in DG44	2.00	2.51	17.85	mAb A in CHO4	14.00	13.17	4.20

a) True value measured by SEC
b) CV, coefficient of variation

MIR and especially Direct Detect™ technology is suitable for fast aggregate quantification, e.g. bioreactor culture samples or various phases of downstream processing, as mimicked by the here presented models using cell culture fluid with antibody addition and also using real process-samples containing mAb B. Specific wavenumber regions used to estimate host cell protein impurities and antibody levels [20, 21] do not overlap with wavenumber ranges selected in this study, except for the region 1665-1654 cm^{-1}, which can also be modified slightly to avoid interference with overall antibody quantification as described [21]. Thus, in principle, this multiple parameter estimation (mAb, host cell protein, mAb aggregation level) can be obtained with a single MIR measurement. Furthermore, once matrix effects have been accounted for [16], a general model seems to be applicable for aggregate quantitation in different cell culture fluids and for different antibodies.

In conclusion, our results demonstrate the suitability of MIR for aggregate quantification using both fermentation (upstream) and purification (downstream) process samples. Spectrum interpretation of aggregation can be performed using a general quantification model applicable to multiple mAb products. Quantification of aggregates was possible down to 1% aggregates content, both in post protein A chromatography process stream samples and in cell culture fluid. For samples in the range 1 to 14% aggregate content, CV calculate for predictive models overwhelmingly fell below 10% and produced a RMSE-IT of 0.47-0.85%. Use of a general quantification model allowed for quantitative determination of aggregate for-

mation down to 1% in CHO4 and CHO-DG44 cell culture fluid, resulting in RMSE-CV in the range 0.79-1.1%. Furthermore, a model combining mAb A and mAb B aggregate quantification, taking real-process samples as well as process-sample mimics into account, achieved similar good results, with slightly decreased prediction ability, a RMSE-CV of 1.0%, RMSE-IT of 0.89% and a higher rank of 5. MIR presents several advantages as aggregate quantification methodology: It reduces sample handling, requires no buffer addition and decreases analysis turnaround. Thus it is ideally placed to support rapid decision making during the manufacturing process of biotherapeutic mAb.

5 References

[1] Mahler, H.-C., Müller, R., Friess, W., Delille, A. et al., Induction and analysis of aggregates in a liquid IgG1-antibody formulation. *Eur. J. Pharm. Sci.* 2005, *59*, 407–417.

[2] Roessl, U., Wiesbauer, J., Leitgeb, S., Birner-Gruenberger, R. et al., Non-native aggregation of recombinant human granulocyte-colony

5

stimulating factor under simulated process stress conditions. *Biotechnol J.* 2012, *7*, 1014–1024.

[3] Chu, L., Robinson, D. K., Industrial choices for protein production by large-scale cell culture. *Curr. Opin. Biotechnol.* 2001, *12*, 180–187.

[4] Vunnum, S., Vedantham, G., Hubbard, B., Protein A-based affinity chromatography. in: Gottschalk,U. (Ed.), *Process scale purification of antibodies*, John Wiley & Sons. Inc., Hoboken, New Jersey 2009, pp. 79–102.

[5] Wang, W., Singh, S., Zeng, D. L., King, K. et al., Antibody structure, instability, and formulation. *J. Pharm. Sci.* 2007, *96*, 1–26.

[6] Shire, S. J., Shahrokh, Z., Liu, J., Challenges in the development of high protein concentration formulations. *J. Pharm. Sci.* 2004, *93*, 1390–1402.

[7] Ryan, M. E., Webster, M. L., Statler, J. D., Adverse effects of intravenous immunoglobuin therapy. *Clin. Pediatr.* 1996, *35*, 23–31.

[8] Demeule, B., Gurny, R., Arvinte, T., Where disease pathogenesis meets protein formulation: Renal deposition of immunoglobulin aggregates. *Eur J Pharm Biopharm.* 2006, *62*, 121–130.

[9] Braun, A., Kwee, L., Labow, M. A., Alsenz, J., Protein aggregates seem to play a key role among the parameters influencing the antigenicity of interferon alpha (IFN-alpha) in normal and transgenic mice. *Pharm Res* 1997, *14*, 1472–1478

[10] Hermeling, S., Crommelin, D. J. A., Schellekens, H., Jiskoot, W., Structure-immunogenicity relationships of therapeutic proteins. *Pharm Res* 2004, *21*, 897–903.

[11] Brorson, K., Phillips, J., Defining your product profile and maintaining control over it. Part 4 Product-related impurities: Tackling aggregates, *BioProcess International* 2005, *3*, 50–54.

[12] Hawe, A., Kasper, J. C., Friess, W., Jiskoot, W., Structural properties of monoclonal antibody aggregates induced by freeze-thawing and thermal stress. *Eur. J. Pharm. Sci.* 2009, *38*, 79–87.

[13] Flatman, S., Alam, I., Gerard, J., Mussa, N., Process analytics for purification of monoclonal antibodies. *J. Chromatogr. B* 2007, *848*, 79–87.

[14] Kong, J., Yu, S., Fourier transform infrared spectroscopic analysis of protein secondary structures. *Acta Biochim. Biophys. Sinica* 2007, *39*, 549–559.

[15] Capito, F., Skudas, R., Kolmar, H., Stanislawski, B., Host cell protein quantification by fourier transform mid-infrared spectroscopy (FT-MIR). *Biotechnol. Bioeng.* 2013, *110*, 252–259.

[16] Capito, F., Skudas, R., Stanislawski, B., Kolmar, H., Matrix effects during monitoring of antibody and host cell proteins using attenuated total reflection spectroscopy. *Biotechnol. Prog.* 2013, *29*, 265–274.

[17] Sellick, C. A., Hansen, R., Jarvis, R. M., Maqsood, A. R. et al., Rapid monitoring of recombinant antibody production by mammalian cell cultures using fourier transform infrared spectroscopy and chemometrics. *Biotechnol. Bioeng.* 2010, *106*, 432–442.

[18] Matheus, S., Friess, W., Mahler, H.-C., FTIR and nDSC as analytical tools for high-concentration protein formulations. *Pharm. Res.* 2006, *23*, 1350–1363.

[19] Breen, E. D., Curley, J. G., Overcashier, D. E., Hsu, C. C. et al., Effect of moisture on the stability of a lyophilized humanized monoclonal antibody formulation. *Pharm. Res.* 2001, *18*, 1345–1353.

[20] Skrdla, P. J., Harrington, C., Lin, Z., Use of real-time FT-IR monitoring of a pharmaceutical compound under stress atmospheric conditions to characterize its solid-state degradation kinetics. *Int. J. Chem. Kinet.* 2010, *42*, 25–36.

[21] Gupta, M. K., Tseng, Y.-C., Goldman, D., Bogner, R. H., Hydrogen bonding with adsorbent during storage governs drug dissolution from solid-dispersion granules. *Pharm. Res.* 2002, *19*, 1663–1672.

[22] Yoshioka, S., Aso, Y., Correlations between molecular mobility and chemical stability during storage of amorphous pharmaceuticals. *J. Pharm. Sci.* 2007, *96*, 960–981.

[23] Surewicz, W. K., Mantsch, H. H., New insight into protein secondary structure from resolution-enhanced infrared spectra. *Biochim Biophys Acta.* 1988, *952*, 115–130.

[24] Andya, J., Hsu, C., Shire, S., Mechanisms of aggregate formation and carbohydrate excipient stabilization of lyophilized humanized monoclonal antibody formulations. *AAPS J.* 2003, *5*, 21–31.

[25] Joubert, M. K., Luo, Q., Nashed-Samuel, Y., Wypych, J. et al., Classification and characterization of therapeutic antibody aggregates. *J. Biol. Chem.* 2011, *286*, 25118–25133.

[26] Seshadri, S., Khurana, R., Fink, A. L., Ronald, W., Fourier transform infrared spectroscopy in analysis of protein deposits. *Methods Enzymol.* 1999, *309*, 559–576.

[27] Ami, D., Natalello, A., Taylor, G., Tonon, G et al., Structural analysis of protein inclusion bodies by Fourier transform infrared microspectroscopy, *Biochim. Biophys. Acta* 2006, *1764*, 793–799.

[28] Dong, A., Prestrelski, S. J., Allison, S. D., Carpenter, J. F., Infrared spectroscopic studies of lyophilization- and temperature-induced protein aggregation. *J. Pharm. Sci.* 1995, *84*, 415–424.

[29] Maruyama, T., Katoh, S., Nakajima, M., Nabetani, H. et al., FT-IR analysis of BSA fouled on ultrafiltration and microfiltration membranes. *J. Membr. Sci.* 2001, *192*, 201–207.

[30] Brych, S. R., Gokarn, Y. R., Hultgen, H., Stevenson, R. J. et al., Characterization of antibody aggregation: Role of buried, unpaired cysteines in particle formation. *J. Pharm. Sci.* 2010, *99*, 764–781.

[31] Brereton, G. (Ed.), *Multivariate pattern recognition in chemometrics, illustrated by case studies*, Elsevier Science Publishers B.V., Amsterdam 1992.

Cumulative part- Experimental

3.6. Development and cost-comparison of a precipitation process for industrial protein purification

Paper: Feasibility study of semi-selective protein precipitation with salt-tolerant copolymers for industrial purification of therapeutic antibodies

Florian Capito, Johann Bauer, Almut Rapp, Christian Schröter, Harald Kolmar and Bernd Stanislawski

Short summary:

A polymer-driven antibody purification strategy is described. Results of all other, in this thesis included papers were used to implement a system, allowing direct precipitation of antibodies from cell culture fluid, even at ionic strength of 22.5 mS cm^{-1}. This can be achieved without dilution of the cell culture fluid, in contrast to previously published results. Precipitation selectivity and yield can be fine-tuned and protein be up-concentrated between 40-100 fold when redissolving it. No harmful effects of precipitation on protein structure and no aggregate formation are visible, as shown by Biolayer Interferometry and MIR analysis. Compared to protein A, yield and purity are lower and loss of mAb is higher. Yet, precipitation was shown to be more cost-effective than protein A chromatography for high-titer mAb systems. While main costs with precipitation are because of mAb loss, protein A costs originate mainly from media costs. Comparing a 10 g l^{-1} batch, precipitation was shown to decrease costs by 30-50% compared to protein A – based mAb purification.

Feasibility Study of Semi-Selective Protein Precipitation With Salt-Tolerant Copolymers for Industrial Purification of Therapeutic Antibodies

Florian Capito,[1,2] Johann Bauer,[2] Almut Rapp,[2] Christian Schröter,[1,2] Harald Kolmar,[1] Bernd Stanislawski[2]

[1]Institute for Organic Chemistry and Biochemistry, Technische Universität Darmstadt, Petersenstrasse 22, 64287 Darmstadt, Germany; telephone: +49-6151-72-7168; fax: +49-6151-72-917510; e-mail: florian.capito@external.merckgroup.com
[2]Merck KGaA, Darmstadt, Germany

ABSTRACT: We present a feasibility study for an antibody capturing process from clarified cell culture fluid using semi-selective protein precipitation with salt-tolerant copolymers. Protein precipitation is mediated by hydrophobic and electrostatic interactions with the copolymer that can be customized for the respective target. Precipitation yield with different copolymers at ionic strength of 2–22.5 mS cm^{-1} and pH 5.0–pH 5.7 was evaluated using pure monoclonal antibody solutions. Optimized parameters were used to elucidate yield and purity of various antibodies precipitated at physiological conditions from cell culture fluid of CHO, NS0, and SP2/0 cell culture fluid. Precipitated protein was easily redissolved in small volume, enabling concentrating mono-clonal antibodies (mAb) more than 40-fold and up to 100-fold, while residual polymer was removed to >98% using cationic polymer attached to silica flakes. mAb recovery of >90% and host cell protein clearance of >80% were achieved, not requiring any pre-dilution of cell culture fluid. Precipitation showed no impact on mAb binding affinity when compared to non-precipitated mAb. The obtained yield and purity were lower compared to a protein A based purification and loss of mAb was factor 1.5–3.0 higher. Yet, for high titer mAb purification processes being implemented in the future, precipitation is an attractive option due to its ease of scalability and cost-effectiveness.

Biotechnol. Bioeng. 2013;xxx: 1–13.

© 2013 Wiley Periodicals, Inc.

KEYWORDS: copolymer; protein precipitation; 2-acrylamido-2-methylpropane sulfonic acid; 4-(acryloylamino)benzoic acid; downstream processing; protein purification

Introduction

Monoclonal antibodies (mAbs) are widely used in clinical applications, diagnostic systems and different research fields. Production of these proteins using mammalian cell expression systems has grown tremendously over the years since the production of the first licensed mAb in 1986 (Kelley, 2009). To date, mainly three different cell lines are used for mAb production: chinese hamster ovary (CHO), murine myeloma (NS0), and SP2/0 cells, while large scale production takes place in bioreactors ranging from 5,000 to 25,000 L. Downstream processing of antibodies and biotherapeutic proteins in general uses a series of purification steps, starting with harvesting of the fermenter using disk stack centrifuges, followed by clarification through depth- and membrane filter systems (Kelley, 2009). Afterwards, several chromatography steps are used, starting from initial capture using affinity chromatography with protein A, followed by anion and/or cation exchange chromatography. Virus inactivation is achieved via low pH incubation and additional filtration to remove residual virus particles (Fahrner et al., 2001; Kelley, 2009; Shukla et al., 2007).

Increasing cell culture expression levels of 5–10 g L^{-1} nowadays compared to 0.1 g L^{-1} 25 years ago as well as rising economic pressure require the need for enhanced purification methods with higher yield and throughput compared to the performance of current chromatography-based systems (Birch and Onakunle, 2005; Kelley, 2009; Sommerfeld and Strube, 2005; Wurm, 2004). These demands for large scale antibody purification may be met by either increasing chromatography column material capacity, dimensions of columns, faster operation using rigid materials or developing alternative means of purification which should give comparable yields and purities, however, decrease costs and be better scalable (Cooper et al., 2005; De Palma, 2009; Gottschalk, 2006, 2008; Low et al., 2007; Thömmes and Etzel, 2007). Such methods include liquid-liquid partitioning, crystallization and precipitation. Due to ease

of scalability, precipitation is gaining more interest, especially for large scale batch purification, where the desired protein is precipitated out of the harvest cell solution. Common methods for protein precipitation are ammonium sulphate precipitation (AS; Venkiteshwaran et al., 2008), polyethylene glycol (PEG) precipitation, or using caprylic acid as precipitant (Temponi et al., 1989; Wang et al., 2009). However, straightforward use of PEG or AS for large-scale purification requires large amounts of these precipitants and higher protein concentrations yielding only moderate purity grades, while producing a high waste load (De Palma, 2009; Farid, 2008; Sommerfeld and Strube, 2005). Nevertheless, optimized precipitation processes would allow to overcome the current drawbacks of limited mAb purification capacity (De Palma, 2009; Thömmes and Etzel, 2007), providing an alternative to protein A affinity chromatography.

A very recent approach is the use of polyelectrolytes as precipitants which might be applied to a greater number of antibodies without the demand for customization (US Patent No. 20100204455, 2010; WO/2008/091740, 2008; US Patent App. 12/425,328, 2009; WO Patent WO/2008/100,578, 2008; De Palma, 2009; McDonald et al., 2009; US WO/2008/079280, 2006). Various polyelectrolytes can be used that allow for tailor-made polymer–protein interactions to selectively precipitate mAbs during capture or intermediate polishing and thereby purify to a desired yield, enabling to omit protein A capture step. In this way, a more economical and easier scalable way of purification could be established. An overview of a purification process using polymers as antibody precipitants is shown in Figure 1. McDonald et al. (2009) described a precipitation process using homopolymers poly-(vinyl sulfonic acid; PVS), poly-(acrylic acid; PAA). and poly-(styrene sulfonic acid; PSS) for antibody purification. This precipitation scheme has some drawbacks as PVS and PAA require dilution of the cell culture fluid to low ionic strength

Figure 1. Overview of purification process using polymers.

prior to polymer addition to achieve acceptable precipitation yields. PSS, in contrast, can be used at high ionic strengths, likely due to conjoint effects of aromatic ring and sulfonic acid groups (Carlsson et al., 2003; Cooper et al., 2005; Tribet, 2001), but it displayed unsatisfactory pellet redissolution behavior after precipitation.

Therefore, the aim of this feasibility study was the design of copolymers with carefully adjusted hydrophobic and anionic properties to allow for precipitation at high ionic strength, omitting large dilution steps, as well as showing good redissolution behavior after precipitation.

Here, we describe the capability of copolymers consisting of 2-acrylamido-2-methylpropane sulfonic acid (AMPS) and 4-(acryloylamino)benzoic acid (ABZ), respectively, for secondary clarification of mAbs in clarified cell culture fluid. We investigated the dependence of purification yields on copolymer weight average molecular weight (Mw) and composition. Host cell protein (HCP) clearance and mAb yields were compared to recently published techniques using anionic homopolymers for secondary clarification McDonald et al. (2009) as well as to a conventional protein A chromatography-based purification step.

Materials and Methods

Copolymer Synthesis and Preparation

4-aminobenzoic acid, acrylic acid chloride, AMPS, solvent dimethylformamide (DMF), acid neutralizer triethylamine, initiator disodium sulfonatooxy sulfate and chain transfer agent (CTA) 1-butanthiol were used as obtained from Merck KGaA, Darmstadt, Germany. Copolymers (Fig. 2) consisting of varying relative amounts of AMPS and 4-(acryloylamino) benzoic acid (ABZ), respectively, were synthesized using $Na_2O_8S_2$ as starter for radical polymerization and DMF-water (50% v/v) as solvent. The reaction was performed at pH 9.0, 80°C under N_2 atmospheric conditions for 5 h before cooling to 20°C. Copolymer chain length was controlled by adjusting starter concentrations and using CTA 1-butanthiol at molar ratios of overall monomer concentration versus CTA between 1:0.0075 and 1:0.12. Copolymer composition was adjusted by varying the relative amount of the two monomers.

Exemplary, synthesis of pol 5 is described, which is also applicable to all other copolymers. In a first step, 4-aminobenzoic acid and acrylic acid chloride were used to synthesize ABZ monomer at 3°C, using triethylamine (TEA) as acid neutralizer during reaction. 82.29 g (0.6 mol) 4-aminobenzoic acid were dissolved in 600 mL DMF while cooling to below 5°C. Maintaining that temperature, 59.49 g (0.588 mol) TEA and 52.68 g (0.582 mol) acrylic acid chloride were slowly added over a period of 80 min. Temperature was kept below 5°C for an additional 3 h and the precipitate was removed by vacuum filtration. The reaction solution was added to 10°C cold water and left at 8°C for 14 h for product to precipitate. Residual solvent was evaporated using a vacuum drying oven at 30°C for 48 h at 40 mbar. In a second step, 10.89 g (52.55 mmol) AMPS were
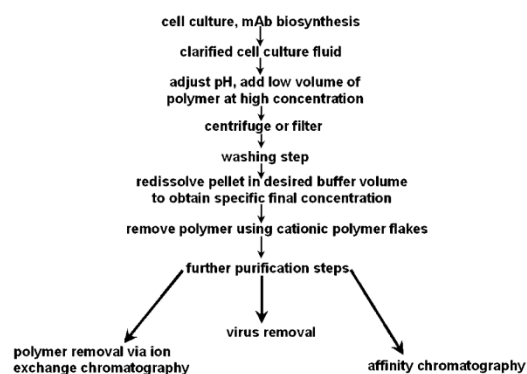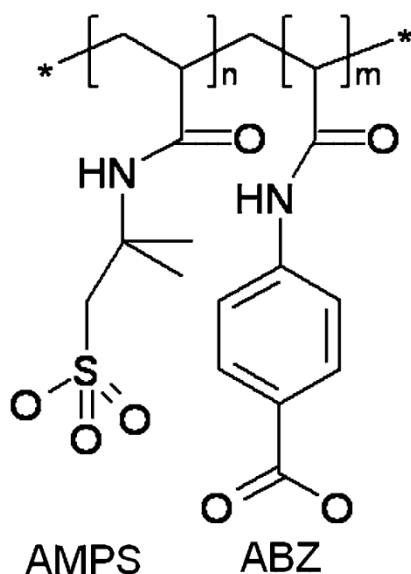
Figure 2. Structure, composition, and weight average molecular weight (Mw) of copolymers used in this study. Mw ranging from 9,800 to 185,000 g mol^{-1}, respective composition within copolymer (mol %): AMPS: 20–100%, ABZ: 0–80%.

dissolved in 215 mL H_2O, maintaining a temperature below 10°C. 6.72 g (35.15 mmol) ABZ were dissolved in 225 mL DMF and added to the AMPS solution. The pH was adjusted to pH 9.0, using NaOH. Reaction solution was degassed using N_2. CTA was added at a molar ratio of 1: 0.03 compared to overall monomer concentration. 0.48 g (2.02 mmol) $Na_2S_2O_8$, dissolved in 10 mL H_2O was added. The reaction solution was heated to 80°C for 5 h under N_2 atmosphere. After 5 h the reaction solution was cooled to room temperature and purified using gel filtration (PD-10 column; Sephadex G25 column material; Amersham Biosciences AB, Uppsala, Sweden), according to the manufacturers instructions.

Additionally, AMPS homopolymer was synthesized using the above described process but omitting the addition of ABZ monomer and CTA.

Triethylamminoethyl (TMAE) modified silica flakes were synthesized using silica flakes coated with glycidyloxipropyl-triethoxysilan with 10–100 μm diameter and adding monomers *N,N*-dimethylethylendiamine (0.225 M), acrylic acid chloride (0.216 M) and dimethylsulphate (0.228 M), using 4.5 mM ammoniumcer-IV-nitrat as initiator. Synthesis was done at 40°C for 3 h and pH 2.0.

Copolymer solution was adjusted to the required pH (pH 5.0, pH 5.4; pH 5.6, or pH 5.7, respectively) using HCl or NaOH before performing precipitation experiments or infrared spectroscopic composition analysis. Additionally,

viscosity of high concentration copolymer solutions was compared to elucidate potential of adding low amount of highly concentrated copolymer to achieve precipitation without excessive sample dilution.

To elucidate polymer removal using TMAE attached to silica flakes, four copolymer samples were labeled with fluorophore Cascade ® Blue (Invitrogen, Carlsbad, CA) using 1-Ethyl-3-[3-dimethylaminopropyl]carbodiimide hydrochloride (Merck KGaA) coupling according to a protocol by Invitrogen to obtain a degree of labeling of approximately two fluorophores per polymer chain. Unbound fluorophore was removed by gel filtration using a PD-10 column (Amersham Biosciences) before adjusting the pH of the copolymer solution to pH 5.0 using HCl.

Analytical Methods

Average molecular weight of copolymers and homopolymer was determined by gel permeation chromatography on a LaChrom Elite chromatography system (VWR-Hitachi, Darmstadt, Germany): injection volume 200 μL; calibration with polystyrenesulfonate in 20% AcCN; elution buffer: 10 mM Na_2HPO_4, 50 mM $NaNO_3$, 20% AcCN; column 1: MCX 10 μm pre-column; column 2: MCX 10 μm 1,000 Å; column 3: MCX 10 μm 10^6 Å; detectors: LaChrom refractive index detector L-2490 and Licrograph L-2400 UV detector; injection by autosampler L-2200; system temperature 40°C at a flow rate of 1 mL min^{-1}. Copolymer composition was determined using attenuated total reflection IR spectroscopy (ATR) and compared to defined monomer blends of 4-ABZ and AMPS, using sulfonic acid associated peak at 1,040 cm^{-1} and 4-ABZ associated peak at 1,390 cm^{-1}. Twenty microliter of each polymer sample ($c = 5$ mg mL^{-1}) were measured on GoldenGate^{TM} MkII series ATR (Specac, Inc., Cranston, RI), using a diamond (type IIa, 45°C, refractive index at 1,000 cm^{-1}: 2.4; 0.8 mm diameter of active sampling area; diameter 2 mm × 2 mm) at 20°C with H_2O as background. All spectra were recorded with a Bruker Tensor 27 (Bruker Optik GmbH, Ettlingen, Germany); samples were scanned in absorbance mode with 120 scans at a spectral resolution of 4.0. Detector was a Bruker LN-MCT photovoltaic internal detector (Bruker Optik GmbH), aperture was set to 6 mm. Atmospheric compensation was performed and samples smoothed using 17 smoothing points.

Antibody and Cell Culture Fluid Solutions

Different IgG-type monoclonal antibodies mAb A, mAb B, mAb C, mAb D, and mAb E were obtained from Merck Millipore, Darmstadt, Germany, as internal standards (Table I). mAbs were labeled with fluorophore Alexa fluor® 546 succinimidylester (Invitrogen), using 1 mg of fluorophore, dissolved in 500 μL DMSO and added to 1 g of protein, dissolved in aqueous buffer solution. After stirring for 1 h, unbound fluorophore was removed using a PD-10 column (Amersham Biosciences AB) for gel filtration with Sephadex G25 column material.

mAb	Isoelectric point	Molecular weight (kDa)	Cell culture fluid
mAb A	8.0–9.0	144.4	NS0
mAb B	8.0–9.0	145.8	SP2/0
mAb C	8.0–9.0	144.4	CHO
mAb D	8.0–9.0	145.9	CHO
mAb E	7.0–8.0	145.2	NS0

For experiments using mAbs in clarified cell culture fluid (CCF), mAbs and their corresponding CCF.

Cell culture fluid (CCF) solutions with defined mAb titer were obtained as clarified cell culture fluid from Merck Millipore (Table I).

CCF solutions were adjusted to pH 5.0 with Na-acetate buffer (Merck KGaA). During the course of the experiments, it was discovered that mAb C showed excellent precipitation behavior, thus mAb C precipitation was also analyzed at pH 5.7 after adequate pH-adjustment using Na-acetate buffer.

Protein A Chromatography (as Comparison)

For comparison reasons, protein A affinity chromatography was additionally used for mAb purification from cell culture fluid. All experiments were run on the LaChrom (Merck Hitachi) HPLC system using Superformance column (10 mm × 50 mm) column packed with ProSep$^{\text{®}}$ Ultra Plus chromatography media (Merck Millipore). UV detection was carried out at 280 nm and sample injection volume was 100 μL. Two different buffer solutions were used: 25 mM sodium di-hydrogen phosphate and 300 mM sodium chloride pH 7.2 as adsorption buffer and 150 mM acetic acid pH 2.7 as a desorption buffer. System was calibrated with known concentration mAb samples. Host cell protein (HCP) concentration in protein A purified product was analyzed using corresponding HCP-ELISA kits: for CHO CCF: 3rd Generation CHO-HCP ELISA kit; for NS0 CCF: NS0-HCP ELISA kit; for SP2/0 CCF: SP2/0-HCP ELISA kit (all kits from Cygnus Technologies, Wrentham, MA). Leaching protein A amount was analyzed using Protein A ELISA kit (RepliGen, Waltham, MA).

Precipitation Experiments

To determine the optimal conditions for CCF experiments, mAb precipitation yield in pure mAb solutions was evaluated in screening experiments varying ionic strength, pH, copolymer concentration, Mw and composition. To this end, different mAb solutions were adjusted to pH 5.0, 5.4, 5.6, and 5.7, respectively. Ionic strength was adjusted to 15, 17.5, 20, 22.5, and 32 mS cm^{-1}, using 20 mM sodium-acetate buffer with the above given pH values and corresponding NaCl concentration. Ionic strength was confirmed using Mettler Toledo Inlab 731 conductivity sensor (Mettler Toledo, Gießen, Germany).

Final mAb concentration after adding copolymer solution and buffer solution was 1 mg mL^{-1} with the above given pH and ionic strength. Initial experiments showed that incubation below 40–50 min resulted in reduced precipitation yields. To account for these relatively slow precipitation kinetics and to allow for high precipitation yields an incubation time of 1 h was chosen for all experiments, to be able to directly compare the precipitation results. Thus, all samples were incubated on a lab shaker for 1 h at 300 rpm to allow for precipitation and then centrifuged at a relative centrifugal force (rcf) of 2,500 for 15 min. The supernatant was discarded and the pellet washed twice with sodium acetate buffer pH 5.0; pH 5.4; pH 5.6, or pH 5.7, respectively before redissolving in defined volume of 80 mM phosphate buffered saline (PBS) pH 7.4 or 50 mM Tris-acetate buffer pH 8.0 (both Merck KGaA), respectively by shaking at 500 rpm for 12 min. Samples were transferred to microtiterplates (Nunc, Langenselbold, Germany). The mAb concentration in buffer of redissolved pellet was determined by fluorescence count measurements in comparison to calibration standards using a Tecan fluorescence plate reader M200 (Tecan Instruments, Männedorf, Switzerland). The percentage of precipitated mAb was calculated by comparing overall mAb concentration in the sample before precipitation and mAb concentration in supernatant after precipitation and subsequent pellet redissolution.

To elucidate mAb precipitation yield in CCF, 10% (w/w) of fluorophore labeled mAb were spiked to corresponding CCF solution, producing the same mAb, to quantify mAb. Precipitation experiments were performed in Eppendorf tubes using 800 μL of spiked CCF solution adjusted to pH 5.0 with fluorophore labeled mAb and 200 μL of polyelectrolyte solutions pH 5.0, respectively. For mAb C CCF, solutions were additionally adjusted to pH 5.7. Final polyelectrolyte concentrations within the samples ranged from 10% to 150% (w/w) copolymer concentration compared to mAb concentration. Conductivity of pH-adjusted CCF solutions was in the range of 13–17 mS cm^{-1} and, except of adding polyelectrolytes, not further reduced.

CCF and polyelectrolyte solution were mixed without adding additional buffer. The procedure was performed as described above for pure mAb solutions and the solution containing the redissolved pellet was analyzed in a fluorescence plate reader (Tecan Instruments) to determine mAb concentration by fluorescence counts measurements in comparison to standards.

Host cell protein (HCP) concentration in buffer of redissolved pellet of all polyelectrolyte-treated CCF samples was analyzed using attenuated total reflection IR spectroscopy (Capito et al., 2013a,b) and corresponding HCP-ELISA kits: for CHO CCF: 3rd Generation CHO-HCP ELISA kit; for NS0 CCF: NS0-HCP ELISA kit; for SP2/0 CCF: SP2/0-HCP ELISA kit (all kits from Cygnus Technologies).

Samples were serially diluted to ensure that they meet the quantification range of the assay and were measured as duplicates. Interference of mAbs or polyelectrolytes on assay results was analyzed mixing 1/5 of 100 ng mL^{-1} HCP

standard with 4/5 of antibody or polyelectrolyte, respectively, to obtain $20\,ng\,mL^{-1}$ HCP standards.

Removal of Residual Copolymer Within CCF Using TMAE Silica Flakes

Using fluorophore-labeled copolymers for precipitation experiments described above, the ability of silica flakes with attached TMAE for copolymer removal was evaluated. After precipitation and centrifugation, supernatant was removed and pellet with precipitated mAb and copolymer was dissolved in either 80 mM PBS pH 7.4 or 50 mM Tris-acetate buffer pH 8.0, respectively. Silica flakes were added to redissolved solution and incubated for 20 min before centrifugation at 2,500 rcf for 10 min. Afterwards, mAb and copolymer concentration in supernatant were determined by fluorescence count measurements on a Tecan reader as described above and compared to standards to determine percentage mAb recovery and percent removed copolymer.

Analysis of Antibody Structural Integrity

To elucidate potential changes and damage to secondary structure, mAb solutions were analyzed via Fourier transform infrared spectroscopy using an AquaSpec^{TM} Flow Cell AS1100 BM with a path length of $7\,\mu m$ (micro-biolytics GmbH, Esslingen, Germany) on a Bruker Tensor (Bruker Optik GmbH). Samples were scanned in absorbance mode with 120 scans at a spectral resolution of 4.0, using Bruker Opus 6.0 software. The detector was a Bruker LN-MCT photovoltaic internal detector (Bruker Optik GmbH), aperture was set to 6 mm. Amide I band regions before and after precipitation were compared to identify spectra changes that are indicative of formation of aggregates, visible as band shifts or appearance of new bands at wave numbers 1,690, 1,655, and $1,619\,cm^{-1}$ (Ami et al., 2006; Dong et al., 1995; Joubert et al., 2011; Maruyama et al., 2001; Seshadri et al., 1999).

To elucidate any effects on mAb integrity due to precipitation, isoelectric focusing (IEF) was done using a broad range pI calibration kit (GE Healthcare, Freiburg, Germany), with a pI range 3–10. $20\,\mu L$ of mAb B and mAb C before and after precipitation as well as pI marker proteins included in the kit were applied to a polyacrylamide thin layer gel according to manufacturer's instructions. Isoelectric focusing was done for 75 min, using maximum power supply settings: 1,000 V, 25 mA, 15 W, coolant temperature 15°C. Following fixing for 1 h in aqueous 10% trichloroacetic acid solution, the gel was stained for 20 min with 0.1% Coomassie Blue (Serva Blue R, Serva Electrophoresis GmbH, Heidelberg, Germany) in 25% methanol, 5% acetic acid (Merck KGaA) and destained in 25% methanol, 5% acetic.

Native PAGE under non-reducing conditions was done to elucidate molecular weight modifications due to precipitation. Novex$^{®}$ NativePAGE^{TM} Bis–Tris 3–12% Gel System (Life Technologies GmbH, Darmstadt, Germany) was used

for mAb A and mAb E using SeeBlue Plus2 Pre-stained Standard (Life Technologies GmbH) and NativePAGE^{TM} Running Buffer Kit (Life Technologies GmbH). Electrophoresis conditions were set to 200 V, 120 mA, 25 W, running time 35 min. Fixing and staining was performed as described for IEF above.

Antibody Binding Kinetics Determination Using Bio-Layer Interferometry (BLI)

Binding assays were performed in 96-well microtiterplates at 25°C and orbital sensor agitation at 1,000 rpm by BLI using an Octet RED system (Pall ForteBio Europe, Portsmouth, UK) and Fortebio Acquisition Software. All measurements were run in $200\,\mu L$ volume. First, Anti Human Fc (AHC) sensor tips were pre-wet for 10 min in PBS immediately prior to use followed by immobilization of antibodies ($10\,\mu g\,mL^{-1}$ PBS) for 600 s. AHC sensors were rinsed in kinetics buffer for 300 s that served as background buffer (PBS pH 7.4, 0.1% BSA, Albumin Fraction V and 0.02% Tween-20 (both Merck KGaA). After rinsing, sensors were moved into wells containing a serial dilution of antigen and association was monitored for 900 s, followed by dissociation in kinetics buffer alone for 900 s. Both assays were run with the same antigen dilution series to ensure comparability. Octet Analysis Software version 6.4 was used for automatic data processing. Data from the 0 nM concentration were used to subtract noise and sensorgrams were fit using a 1:1 binding model.

Results and Discussion

In an effort to improve antibody purification using copolymer precipitants, various copolymers were synthesized and used for antibody precipitation. Influence of ionic strength, pH and copolymer concentration on mAb precipitation yields were first investigated using pure mAb solutions. Optimized conditions were applied to antibody purification from cell culture fluids as described below.

Copolymer Synthesis

Following radical polymerization, 20 different copolymers with different molecular weight and composition were synthesized together with an AMPS-homopolymer (Table II).

Comparing copolymer viscosity, even copolymer concentrations of $90–100\,mg\,mL^{-1}$ showed no dedicated viscosity, thus allowing the application of these copolymers at high dosage to avoid excessive sample dilution.

Protein A Chromatography (as comparison)

Results of using protein A chromatography for purification of mAb B–E in corresponding CCF, thus being fully comparable to precipitation results, showed yields of 93% for mAb capture. HCP amount in protein A purified mAb varied

Table II. Weight average molecular weight (Mw) and composition of exemplary copolymers as well as AMPS-homopolymer used for antibody precipitation experiments.

Polymer	AMPS (% mol by ATR)	ABZ (% mol by ATR)	Mw (g mol^{-1} by RI using SEC)
pol 1	20	80	108,000
pol 2	27	73	75,000
pol 3	35	65	80,000
pol 5	37	63	43,000
pol 7	37	63	43,000
pol 8	43	57	95,000
pol 11	44	56	81,000
pol 12	49	51	59,000
pol 15	59	41	67,000
pol 17	59	41	35,000
pol 18	59	41	61,000
pol 19	65	35	110,000
pol 20	65	35	39,000
Homopolymer	100	0	88,000

Figure 3. Comparison of precipitation yields for mAb A and mAb B using different polymer types and polymer concentrations. Conditions: pH 5.0; 15 mS cm^{-1}. Copolymers (pol 1 and pol 3) show higher yields than AMPS-homopolymer.

between 1,000 and 3,000 ng mg^{-1} of HCP in SP2/0 CCF and between 10 and 2,000 ng mg^{-1} of HCP in either CHO or NS0 CCF. Amount of leaching protein A was in between 0.03 and 0.13 ng mg^{-1}, according to protein A assay.

Evaluation of Precipitation Conditions using Pure mAb Solutions

To evaluate how ionic strength, pH, copolymer concentration and copolymer composition affect precipitation yield, pure mAb solutions were used. Precipitation yields were determined by comparing mAb concentration before precipitation and after pellet redissolution. In addition, precipitation was carried out with fluorophore labeled mAb. These pilot experiments revealed no difference in precipitation behavior between fluorophore labeled and non-labeled mAb thereby validating our method of spiking labeled mAb into CCF solution for later CCF experiments.

Results of different mAb solutions at pH 5.0 and an ionic strength of 15 mS cm^{-1} showed an optimum ratio of mAb to polymer within the range of 0.35–0.9 (w/w; mg polymer/ mg mAb), where highest precipitation yields were obtained (Fig. 3). While at low polymer concentrations mAb precipitation was not efficient, it decreased again when exceeding the optimum polymer concentration range most likely due to overcharging as described in literature (Carlsson et al., 2003; McDonald et al., 2009). Comparing copolymers pol 1 and pol 3 with AMPS-homopolymer, the former showed precipitation yields of >80%, while the pure AMPS polymer yielded only 10–40%. This result indicates that hydrophobic interactions play a significant role in the mAb precipitation process. In contrast to AMPS-ABZ copolymers, AMPS homopolymer lacks hydrophobic properties. Consequently, AMPS homopolymer was not considered further for protein purification. Additionally, when only comparing pol 1 and pol 3 in Figure 3, it was discovered that pol 1 exhibited slightly (5–10%) better precipitation yields than pol 3. This
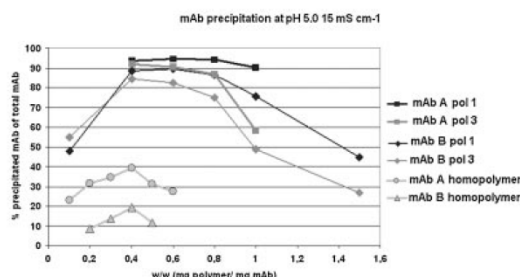
shows that the ratio of AMPS and ABZ groups in the copolymer does influence the mAb precipitation yield. We concluded the higher ABZ content within the composition of pol 1 exhibiting additional hydrophobic interactions and thus increasing precipitation efficiency.

At a pH > 5.4, well below the *pI* of analyzed mAbs (*pI* 7.0– 9.0) and an ionic strength of 15 mS cm^{-1}, precipitation yields decreased significantly. Precipitation of mAb B decreased from >85% at pH 5.0 and 5.4, to 30% at pH 5.7 (Fig. 4A). This is most likely caused by the reduced positive charge of the mAb when approaching its *pI*, which consequently reduces electrostatic interaction between mAb and anionic
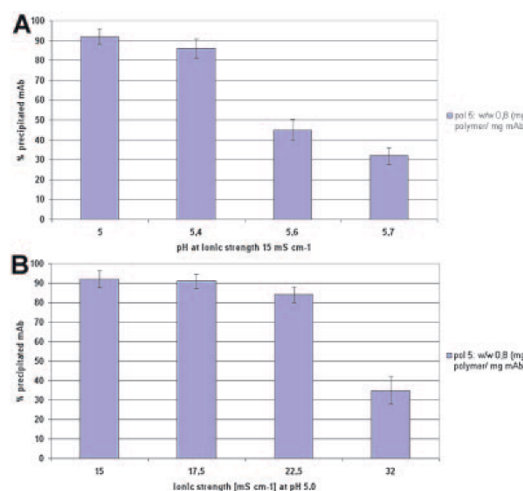

Figure 4. Precipitation yield of pure mAb B solution at different pH (**A**) and ionic strength (**B**). Mean values from triplicates.

copolymer (Izumrudov et al., 1998; McDonald et al., 2009). When varying ionic strength at constant pH (pH 5.0), no significant influence of salt conditions up to an ionic strength of $22.5\,mS\,cm^{-1}$ were observed. At higher ionic strength, precipitation yield of mAb B decreased from initially >90% to around 30% at $32\,mS\,cm^{-1}$ (Fig. 4B). This effect is well-known for polyelectrolytes showing non-monotonic ionic strength precipitation dependence so that precipitation yield decreases at both, very low and very high ionic strength (Antonov et al., 2009; Capito et al., 2013c; Carlsson et al., 2001; Dobrynin and Rubinstein, 2003; Hattori et al., 2000; Marky and Manning, 2000; Moss et al., 1997).

A high ionic strength most likely leads to screening, that is, shielding of positive surface charges of mAbs as well as screening of negative charges of the copolymer (Carlsson et al., 2003; de Gennes et al., 1976). In addition, charged copolymers may collapse at high ionic strength similar to DNA ψ-compactization (Hansen and Löwen, 2000; Kogej and Skerjanc, 2001; Vasilevskaya, 2001). As a result mAb precipitation is reduced at high ionic strength. The decrease in precipitation yield at high ionic strength and high pH (close to the pI), is illustrated in Figure 4, and was observed with all mAbs.

A similar effect has been described by McDonald et al. (2009), using PAA and PVS as polymers for mAb precipitation.

Although their results showed 95% precipitation at pH 7.0, significant dilution of CCF, which is a major disadvantage in application, was required to obtain an ionic strength of $1.5\,mS\,cm^{-1}$ or less.

All of the tested copolymers show a very good salt tolerance which exceeds the ionic strength present in CCF solutions (Fig. 4).

For pure mAb solutions best precipitation results were observed with relative copolymer concentrations between 0.35 and 0.9 mg copolymer/mg mAb at a pH of 5.0 when using an ionic strength between 15 and $17.5\,mS\,cm^{-1}$.

Evaluation of Precipitation Conditions using Cell Culture Fluid Solutions

These above mentioned conditions are used as a starting point for the precipitation experiments with CCF solutions.

Relative copolymer concentrations which achieved highest yields in screening experiments, were used for mAb precipitation in CCF. mAb C precipitation in CCF was additionally evaluated at pH 5.7 due to excellent precipitation behavior at pH 5.0, likely due to a higher hydrophobicity when compared to the other mAbs. Initial experiments with different CCFs, using different mAbs showed that copolymer concentration needed to be increased by a factor 1.5–2.0 to achieve precipitation yields comparable to pure mAb precipitation yields. This is most likely due to impurity proteins in the CCF. Thus copolymer concentration was increased 1.5- to twofold to account for increased polymer "consumption" by impurity proteins, when using CCF.

mAb precipitation was analyzed by fluorescence counts together with HCP co-precipitation, that was determined by attenuated total reflection or HCP-ELISA. No influence of polymer or mAb on ELISA or fluorescence behavior was detected.

mAb precipitation achieved yields between 75% and 99%, with average results of around 90%; similar to results using PAA and PVS, obtained by McDonald et al. (2009), albeit at significantly higher ionic strength of $12–15\,mS\,cm^{-1}$.

Comparing mAb precipitation yield, depending on ABZ content within copolymer or copolymer Mw, yields between 70% and 95% were obtained (Fig. 5A). Comparing copolymers of same ABZ amount within composition, those with higher Mw also resulted in higher precipitation yield. Same was visible when comparing copolymers of similar Mw, for example, 108,000 and $110,000\,g\,mol^{-1}$, but with different ABZ amount in composition (Fig. 5A).

Thus, generally, larger copolymers or copolymers with higher ABZ content resulted in increased precipitation yield. Comparing precipitation yields depending on the mAb, highest yields were observed for mAbs C and D, compared to slightly reduced yields obtained for the other tested mAbs. Possible reasons could be differences in mAb hydrophobicity, for example, mAb C did show a higher intrinsic hydrophobicity than the other mAbs.

The use of copolymers with specific attributes, for example, a Mw of $50,000–60,000\,g\,mol^{-1}$ and a composition of 40–60 mol % ABZ, would allow for a general applicability of copolymer precipitation independent of the type of mAb used. However, while this would omit somewhat laborious mAb-tailored copolymer synthesis, tailor-made adjustment of copolymers could increase yields even further, depending on the mAb.

Overcharging effects that were observed with pure mAb solutions were not detected.

HCP co-precipitation differed among different cell culture fluids (Fig. 5B), likely depending on HCP subpopulations, their pI's and thus their charges at pH 5.0. Generally, HCP co-precipitation, compared to the percent of HCP's originally in the CCF before starting precipitation, mainly varied between 30% and 60%, with exceptions as low as 8% and as high as 85%, also depending on the Mw and hydrophobicity of the copolymers. HCP impurity protein co-precipitation increased significantly with increasing copolymer Mw, leading to higher likelihood of HCP entrapment, or hydrophobicity due to higher ABZ content, likely also leading to more nonspecific HCP co-precipitation and thus reducing purity of the precipitated mAb (Fig. 5B). Generally, it seems that there is a trade-off between high mAb precipitation yields and low HCP co-precipitation, since precipitation yields of both correlate with copolymer hydrophobicity, thus higher ABZ-content of the copolymers.

Therefore, several promising copolymers with defined Mw between 25,000 and $100,000\,g\,mol^{-1}$ and composition of 20–70 mol % ABZ were selected, yielding higher selectivity, favoring mAb precipitation for all the here tested mAbs and limiting HCP co-precipitation. Most promising precipitation
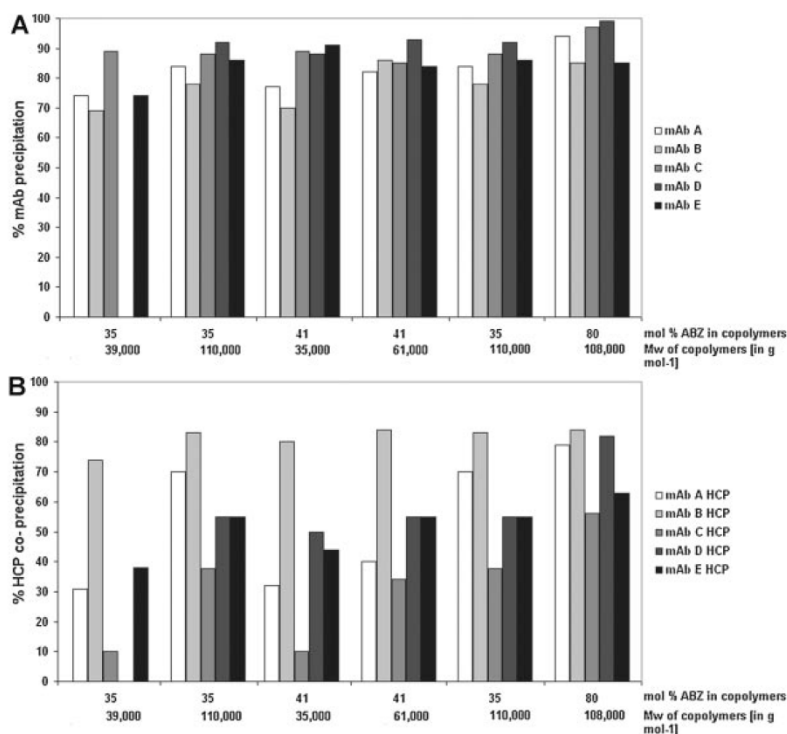
Figure 5. **A**: comparison of mAb precipitation in different CCF solutions using different copolymer compositions and Mw. For mAb C, precipitation was performed at pH 5.7 while other CCFs were used at pH 5.0; absence of columns at specific polymers: mAb not tested with this polymer. **B**: Comparison of HCP co-precipitation in different CCF solutions using different copolymer compositions and Mw. For mAb C, precipitation was performed at pH 5.7 while other CCFs were used at pH 5.0; absence of columns at specific polymers: mAb not tested with this polymer.

results were obtained employing copolymers with Mw between 35,000 and 80,000 g mol^{-1} and a composition of 35–63 mol % ABZ. Regarding HCP co-precipitation, differences were observed between the different CCF solutions. While for mAb C in CHO CCF, HCP co-precipitation was as low as 8%, it increased for different CHO and NS0 CCF's, with thereby lowest observed co-precipitation of 30–40%. SP2/0 CCF did not allow satisfactory precipitation selectivity and thus purity of the precipitated mAb, exhibiting co-precipitation of HCPs of 85%. HCPs in these cell cultures, for example, cytochrome oxidase, thioredoxin, actin, heat shock protein, transferrin and enolase, have acidic *pI*'s in the range of 5.0–6.8, with most HCP's in CCF covering the *pI*-range of 4.0–7.5 (Champion et al., 1999; Smales et al., 2004), however, impurity co-precipitation might have additionally occurred because of precipitation of negatively charged impurity protein that was mediated by anionic copolymers via local positively charged areas of the protein hydrophobic interaction, or non-specific HCP entrapment due to impurity

protein size (Blintsov et al., 1995; Tribet, 2001). The observed difference between SP2/0 CCF and the two other CCFs might be due to different subpopulations of HCPs being present and a different distribution, allowing for elevated co-precipitation.

Thus, compared to McDonald et al. (2009) who reported HCP co-precipitation of 11.7–12.4% within CCF at pH 7.0 and pH 5.0 using PVS homopolymer, we observed higher HCP co-precipitation except for mAb C in CHO CCF being tested at pH 5.7. This may be due to the high protein concentration in contrast to previous studies (McDonald et al., 2009) CCF dilution prior to addition of copolymer was omitted to reduce workload and simplify the precipitation procedure. Another reason for higher HCP co-precipitation observed in our experiments might be the larger Mw of our copolymers that were optimized for mAb precipitation at higher ionic strength as compared to the low Mw PVS polymer used previously (McDonald et al., 2009). This may have caused impurity precipitation to a larger extent likely

due to non-specific HCP entrapment during protein-polymer complex formation (Blintsov et al., 1995; McDonald et al., 2009; Pergushov et al., 1995). When comparing HCP impurities from direct CCF precipitation using high Mw copolymers to PVS homopolymers used for protein precipitation from a post protein A pool (McDonald et al., 2009), HCP co-precipitation was similar being in the range of 21–61%. Precipitated protein is purified by redissolution of the protein-polymer pellets and precipitation of the polymer using TMAE-flakes. Protein-polymer pellets showed excellent redissolution behavior in PBS pH 7.4 after washing in sodium acetate buffer pH 5.0. Additional redissolution experiments using 50 mM Tris-acetate buffer pH 8.0 showed the same results. All pellets were redissolved after shaking for 12 min at 500 rpm. Comparison of the mAb amount in the supernatant after precipitation and in the supernatant of redissolved pellets yielded 100% ± 10% of overall mAb amount with minor deviations due to concentration determination errors.

Copolymers have to be removed from the target protein prior to further processing steps.

TMAE–silica flakes were used to bind suspended polymers, but other techniques, such as ion exchange chromatography can be used as well. However, these flakes have the further advantage of being cost-effective due to low applicable amounts, thus allowing them to be used as single-use copolymer removal system. A single-use system was favored by us, to avoid expensive and laborious re-cycling steps and cleaning-in-place procedures, which would be required to ensure protein removal from both, copolymer and flakes before re-using them.

Usage of TMAE flake suspension (75% w/w flakes in suspension) achieved polymer removal of >98% compared to the initial polymer concentration (Fig. 6). Polymer removal yields showed an optimum using 0.3 mL TMAE

flake suspension per mg of copolymer in the original polymer-protein complex, resulting in 5–20% mAb loss of precipitated mAb, (Fig. 6 highlighted in red), yielding >80% recovery of initial mAb concentration and up to 95% mAb recovery, depending on the initial precipitation step yield and the additional loss of mAb, when using silica flakes (compare Figs. 5A and 6).

Polymer removal yields were similar for the four different copolymers tested.

Using a 5 or 12.5 mL experiment with different mAb concentrations, respectively, for mAb C precipitation, the protein-pellet could be redissolved in a volume as small as 120 μL of PBS pH 7.4 achieving a concentration effect of more than 40-fold and up to 100-fold, respectively, thus reducing buffer consumption and purification time on subsequent chromatography steps. No elevated aggregate formation due to high mAb titer in redissolved solution was visible in infrared spectroscopy. Aggregate formation would result in side chain effects, changes in the hydrogen bonding pattern or formation of intramolecular β-sheets, which would correspond to band shifts in infrared spectroscopy at 1,690, 1,655, and 1,619 cm^{-1} (Andya et al., 2003; Hawe et al., 2009; Surewicz and Mantsch, 1988). Additional size exclusion chromatography data also revealed no evidence for mAb aggregates.

Precipitation Effects on mAb Structure and Binding Kinetics

Binding affinity of mAb A to its target was in the expected nanomolar range; precipitation showed no effect on binding affinity, revealed by BLI sensorgrams before (Fig. 7A) and after (Fig. 7B) precipitation, followed by redissolution. Both, IEF and SDS–PAGE showed no effects on the isoelectric point pattern of the mAbs or on their molecular weight, when comparing samples before precipitation and after precipitation and redissolution.

Spectra of precipitated mAb B and mAb D were compared with non-precipitated mAb B and mAb D, using Fourier transform infrared spectroscopy. No significant differences were seen when comparing the amide I bands within these spectra (Fig. 7C and D). This is consistent with other results in the literature showing unchanged circular dichroism spectra or unchanged specific rotations in mixtures of proteins and polymers (Borrega et al., 1999; Kuramoto et al., 1984; Tribet, 2001; Xia et al., 1999). Precipitation experiments by McDonald et al. (2009) using PVS homopolymers showed 97.3% mAb monomer compared to 99.1% mAb monomer after protein A chromatography. Aggregate formation was slightly elevated for PVS precipitation (3.6%) versus affinity chromatography followed by anion exchange chromatography (AEX; 0.6%; McDonald et al., 2009). Biological activity experiments by McDonald et al. (2009), elucidating the influence of polymer precipitation on mAb activity, revealed activity reduction by 5% after a precipitation-based purification process.
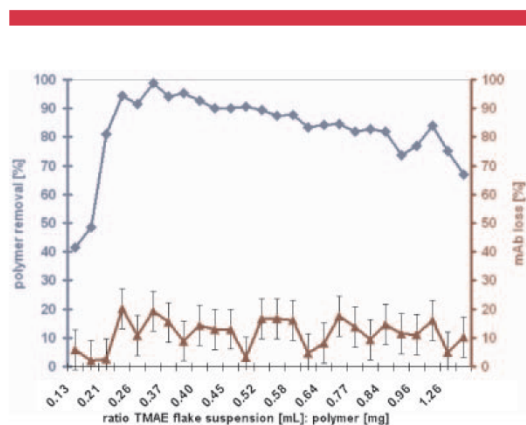

Figure 6. Polymer removal and mAb B loss depending on ratio TMAE flake suspension: polymer. For mAb loss determination, measurement error was around ±7%.
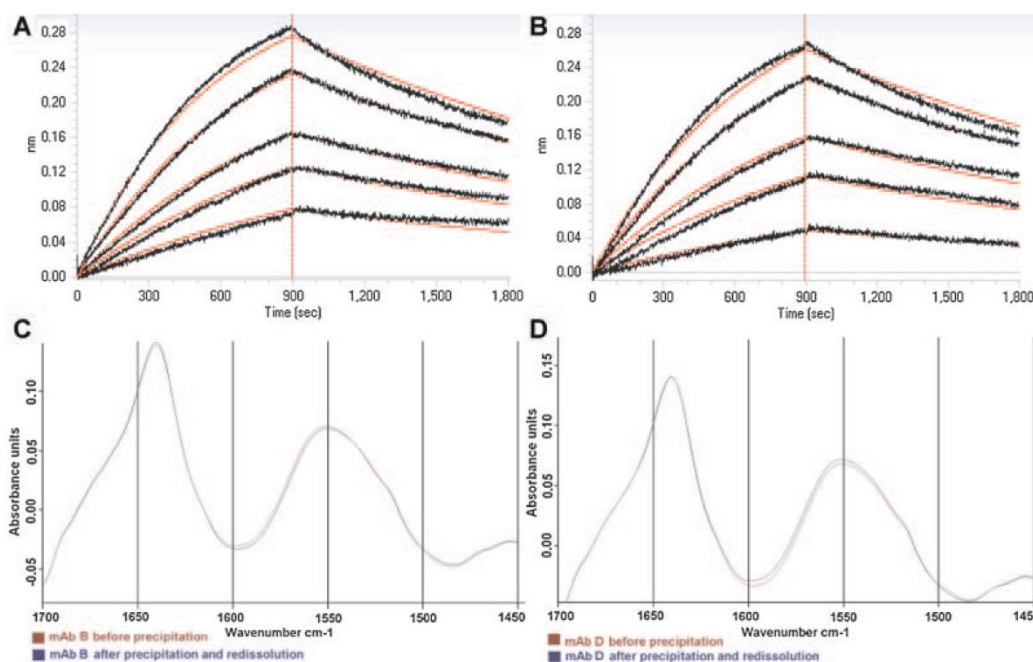
Figure 7. **A** and **B**: BLI kinetic analysis of (A) untreated and (B) precipitated and redissolved mAb A. Anti Human Fc (AHC) Biosensors were pre-wet in PBS for 600 s, and antibodies were coupled for 600 s in PBS. After a 300 s washing step in kinetics buffer (KB), kinetics of non-precipitated and precipitated mAb A were measured in the same antigen containing wells (6, 4, 3, 2, and 1 nM). Red lines represent a global fit of the data to a 1:1 interaction model. Data were collected using Octet Red. **C** and **D**: Amide I and amide II bands of mAb mid infrared spectra before and after precipitation including redissolution step. C: Effect of precipitation with pol 12 at pH 5.0 on mAb B secondary structure. D: Effect of precipitation with pol 17 at pH 5.0 on mAb D secondary structure.

Comparison Precipitation-Based Antibody Purification and Protein A-Based Purification

Antibody purification using protein A affinity chromatography was compared to purification using precipitation. Protein A chromatography showed an average step yield of approximately 93%, with variations between 90.8% for mAb B and up to 95.3% for mAb E. In comparison, the here described precipitation step achieved yields of approximately 80%, assuming an average precipitation yield of 90%, and an additional loss of 10% of that yield, because of copolymer removal. Therefore, yield-wise protein A chromatography was better, although the above stated overall yield of 80% can be regarded as an average value, as even exceptions of up to 90% overall mAb yield, using precipitation were observed (compare Figs. 5A and 6).

Concerning HCP co-purification, protein A eluted samples obtained HCP levels between 1,000 and 3,000 ng mg^{-1} when using SP2/0 as CCF and 10–2,000 ng mg^{-1}, using either CHO or NS0 as CCF. This was equal to a relative HCP co-purification of approximately 0.5% for SP2/0 CCF. For CHO and NS0 CCF, average observed HCP co-purification was around 0.5%, while being lower for most of the samples.

However, these results, showing that protein A leads to purer product than the described precipitation process, are not surprising.

An advantage of precipitation compared to protein A is for purification of high titer mAb cell culture fluids, which are already being established (Kelley, 2009).

This is made clear in the following passage comparing the costs of both techniques depending on mAb titer.

For precipitation, based on in-house cost calculations, taking labor, material, energy costs into account, synthesis of copolymers would amount to production cost of goods of 0.9–1.6 $ per gram of copolymer. However, this value is based on small scale production in the range of 10 kg; therefore it could be reduced if producing larger amounts of copolymer. Production costs for silica flakes were assumed to be 40–50% of those for copolymers per gram of flake. Flakes themselves would thereby contribute the least to these costs due to inexpensive raw materials, justifying their single use, whereby costs would be mainly driven by labor and to a minor factor by monomers used for flake surface modifications. However, these flakes could also be replaced by even more cost-effective materials.
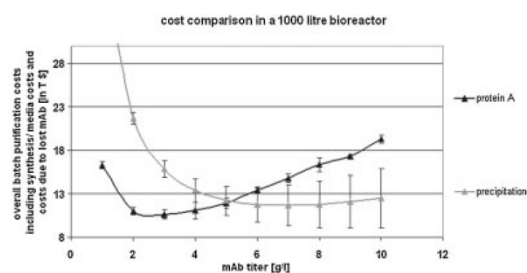
Figure 8. Cost comparison using protein A chromatography and precipitation for mAb purification for a batch volume of 1,000 L, depending on mAb titer. Cost range, depending on assumed costs, indicated as bars on y-axis.

Costs for purification of mAb, depending on the mAb titer, were compared for a 1,000 L batch, either being purified by protein A chromatography or precipitation (Fig. 8).

For protein A chromatography, a loading capacity of $38.7 \, g \, L^{-1}$ was assumed, using a batch loading of 80% of the dynamic binding capacity and a maximum re-using cycle number of 200 before replacing the resin, also including media costs. For precipitation, we assumed an optimum ratio copolymer versus mAb of 80% (w/w), thus leading to copolymer costs per gram of mAb of 0.7–1.3 $.

Flake demand was calculated upon the assumption, to use 0.3 mL flake suspension as optimum per mg copolymer in the sample. As this suspension contained 75% (w/w) flakes, this would equal flake costs per gram of mAb of less than 0.15 $, as for each g of mAb, 0.8 g of copolymer would be required.

Additionally, we also included the financial loss due to lost mAb product, when using the two different purification strategies. For protein A, an average loss of product of 7% during purification would amount to 14 $ loss per liter in CCF with $1 \, g \, L^{-1}$ mAb titer, assuming mAb upstream production costs of 200 $ per liter (in-house costs, also compare Sommerfeld and Strube, 2005). These costs are dependent on the mAb titer, thus using higher titers, the contribution of this loss to overall costs would be minimized. Accordingly, for precipitation we assumed an average loss of 20%, based on 90% precipitation and an additional loss of 10% of these 90%, due to copolymer removal, equaling approximately 40 $ per liter when purifying mAb with a titer of $1 \, g \, L^{-1}$.

Comparison of both techniques, applied to a 1,000 L bioreactor, using different mAb titers, showed that protein A based chromatography is more cost-effective than precipitation, if mAb titers are below $5 \, g \, L^{-1}$ (Fig. 8). Depending on copolymer production costs, used for overall cost calculation (cost range indicated with bars on y-axis Fig. 8), a precipitation process would be economically better than protein A chromatography, if mAb titer exceeded $5 \, g \, L^{-1}$ (Fig. 8). Main cause of costs is hereby the loss of mAb during precipitation (20% assumed in Fig. 8), which accounts for

high costs at low titer, which are then reduced when using high titer CCF. In contrast, protein A chromatography suffers less from mAb-loss associated costs, but mainly from media costs. For the cost comparison, we excluded buffer and workload costs, as this would be rather speculative and the exact amount of buffer consumption during precipitation, protein-pellet washing, redissolution, and copolymer removal would be dependent on the exact conditions, thus not allowing use of a simple number for cost comparison.

However, the results in Figure 8, besides, excluding buffer and labor costs, represent a good initial cost comparison of both processes. Additionally, and not included in the above shown cost analysis; precipitation has the advantage of concentrating a sample, thus allowing to load high titer pre-purified sample onto succeeding chromatography steps, reducing loading time and leading to faster overall purification speed. This could allow to save between 30% and 50% of production costs compared to affinity chromatography, depending on the initial mAb titer and precipitation yield (compare Fig. 8, costs for 1,000 L purification using mAb titer of $10 \, g \, L^{-1}$ using protein A compared to assumed lowest possible costs with precipitation).

Conclusion

It has been shown in this study that AMPS-ABZ copolymers are better suitable for protein precipitation than AMPS homopolymers. Selected copolymers are suitable for precipitation of antibodies from primary clarified undiluted cell culture medium. In this way, the volume of the antibody fraction is reduced by a factor >40, up to factor 100, depending on the mAb concentration, before applying further purification steps. Depending on copolymer ABZ amount and Mw, mAb precipitation can be fine-tuned and optimized, while at the same time reducing impurity protein co-precipitation.

Copolymer-mediated antibody precipitation contributes to reducing the number of purification steps and increasing overall yield. Although initial purity and yield of the precipitant might not be as high as in affinity chromatography, overall yields of up to 90% and higher mAb recovery with as low as 10–20% HCP impurity co-precipitation can be achieved. mAb binding affinity was not affected by polymer-driven protein purification. Comparison of mAb structures before and after precipitation showed no elevated aggregate formation or structural changes due to precipitation. Compared to protein A chromatography, precipitation is easier to scale and can be more cost-effective, when using high mAb titer samples, thereby allowing to save between 30 and 50% of production costs compared to an affinity chromatography based purification approach.

References

Ami D, Natalello A, Taylor G, Tonon G, Maria Doglia S. 2006. Structural analysis of protein inclusion bodies by Fourier transform infrared microspectroscopy. Biochim Biophys Proteins and Proteomics 1764 (4):793–799.

Andya J, Hsu C, Shire S. 2003. Mechanisms of aggregate formation and carbohydrate excipient stabilization of lyophilized humanized monoclonal antibody formulations. AAPS J 5(2):21–31.

Antonov M, Mazzawi M, Dubin PL. 2009. Entering and exiting the protein-polyelectrolyte coacervate phase via nonmonotonic salt dependence of critical conditions. Biomacromolecules 11(1):51–59.

Birch JR, Onakunle Y. 2005. Biopharmaceutical proteins: Opportunities and challenges. In: Smales CM, James DC, editor. Methods in molecular biology, vol. 308: Therapeutic proteins: Methods and protocols. Totowa, NJ: Humana Press, Inc. 1–16.

Blintsov AN, Dzantiev BB, Bobkova AF, Izumrudov VA, Zezin AB, Atabekov IG. 1995. A new method for enzyme immunoassay of phytoviruses, based on interpolyelectrolyte reactions. Doklady Biochem 345:175–178.

Borrega R, Tribet C, Audebert R. 1999. Reversible gelation in hydrophobic polyelectrolyte/protein mixtures: An example of cross-links between soft and hard colloids. Macromolecules 32(23):7798–7806.

Capito F, Skudas R, Kolmar H, Stanislawski B. 2013a. Host cell protein quantification by fourier transform mid infrared spectroscopy (FT-MIR). Biotechnol Bioeng 110(1):252–259.

Capito F, Skudas R, Stanislawski B, Kolmar H. 2013b. Matrix effects during monitoring of antibody and host cell proteins using attenuated total reflection spectroscopy. Biotechnol Prog 29(1):265–274.

Capito F, Skudas R, Stanislawski B, Kolmar H. 2013c. Polyelectrolyte–protein interaction at low ionic strength: Required chain flexibility depending on protein average charge. Colloid Polym Sci 1–11. DOI: 10.1007/s00396-013-2911-3

Carlsson F, Linse P, Malmsten M. 2001. Monte Carlo simulations of polyelectrolyte-protein complexation. J Phys Chem B 105(38):9040–9049.

Carlsson F, Malmsten M, Linse P. 2003. Protein-polyelectrolyte cluster formation and redissolution: A Monte Carlo study. J Am Chem Soc 125 (10):3140–3149.

Champion KM, Arnott D, Henzel WJ, Hermes S, Weikert S, Stults J, Vanderlaan M, Krummen L. 1999. A two-dimensional protein map of Chinese hamster ovary cells. Electrophoresis 20:994–1000.

Cooper CL, Dubin PL, Kayitmazer AB, Turksen S. 2005. Polyelectrolyte-protein complexes. Curr Opin Colloid Interface Sci 10(1–2):52–78.

de Gennes PG, Pincus P, Velasco RM, Brochard F. 1976. Remarks on polyelectrolyte conformation. J Physique 37:1461–1473.

De Palma A. 2009. Getting real with downstream processing. Genet Eng Biotech N 29(13):1–4.

Dobrynin AV, Rubinstein M. 2003. Effect of short-range interactions on polyelectrolyte adsorption at charged surfaces. J Phys Chem B 107 (32):8260–8269.

Dong A, Prestrelski SJ, Allison SD, Carpenter JF. 1995. Infrared spectroscopic studies of lyophilization- and temperature-induced protein aggregation. J Pharm Sci 84(4):415–424.

Fahrner RL, Knudsen HL, Basey CD, Galan W, Feuerhelm D, Vanderlaan M. 2001. Industrial purification of pharmaceutical antibodies: Development, operation and validation of chromatography processes. Biotechnol Genet Eng Rev 18:301–327.

Fahrner R, Franklin J, McDonald P, Peram T, Sisodiya V, Victa C. inventors; Genentech, Inc., assignee. Polyelectrolyte precipitation and purification of antibodies. WO/2008/091740. 2008.

Farid SS. 2008. Economic drivers and trade-offs in antibody purification processes. Biopharm Int. March suppl., 37–42.

Gervais DP, Pfeiffer KA. inventors; Pfizer Limited, assignee. Antibody purification process by precipitation. US Patent No. 20100204455. 2010.

Gottschalk U. 2006. The renaissance of protein purification. Biopharm Int 19(6):8–9.

Gottschalk U. 2008. Bioseparation in antibody manufacturing: The good, the bad and the ugly. Biotechnol Prog 24(3):496–503.

Gronke RS, Jaquez OA. inventors; Biogen Idec MA, Inc., assignee. Method of isolating biomacromolecules using polyalkylene glycol and transition metals. US Patent App. 12/425,328. 2009.

Hansen JP, Löwen H. 2000. Effective interactions between electric double layers. Annu Rev Phys Chem 51:209–242.

Hattori T, Hallberg R, Dubin PL. 2000. Roles of electrostatic interaction and polymer structure in the binding of beta-lactoglobulin to anionic polyelectrolytes: Measurement of binding constants by frontal analysis continuous capillary electrophoresis. Langmuir 16(25):9738–9743.

Hawe A, Kasper JC, Friess W, Jiskoot W. 2009. Structural properties of monoclonal antibody aggregates induced by freeze–thawing and thermal stress. Eur J Pharm Sci 38(2):79–87.

Izumrudov V, Galaev I, Mattiasson B. 1998. Polycomplexes: Potential for bioseparation. Bioseparation 7(4–5):207–220.

Joubert MK, Luo Q, Nashed-Samuel Y, Wypych J, Narhi LO. 2011. Classification and characterization of therapeutic antibody aggregates. J Biol Chem 286(28):25118–25133.

Kelley B. 2009. Industrialization of mAb production technology: The bioprocessing industry at a crossroads. mAbs 1(5):443–452.

Kogej K, Skerjanc J. 2001. Surfactant binding to polyelectrolytes. In: Radeva T, editor. Physical chemistry of polyelectrolytes, surfactant science series, volume 99. 10th edn. New York: Marcel Dekker, Inc. p 793–828.

Kuramoto N, Sakamoto M, Komiyama J, Iijima T. 1984. Complex formation between bovine serum albumin and poly(acrylic acid) as studied by viscometry, circular dichroism, and fluorescence spectroscopy. Macromol Chem Phys 185(7):1419–1427.

Low D, O'Leary R, Pujar NS. 2007. Future of antibody purification. J Chrom B 848(1):48–63.

Marky NL, Manning GS. 2000. An interpretation of small-ion effects on the electrostatics of the λ repressor DNA complex. J Am Chem Soc 122 (25):6057–6066.

Maruyama T, Katoh S, Nakajima M, Nabetani H, Abbott TP, Shono A, Satoh K. 2001. FT-IR analysis of BSA fouled on ultrafiltration and micro-filtration membranes. J Membr Sci 192(1–2):201–207.

McDonald P, Victa C, Carter-Franklin JN, Fahrner R. 2009. Selective antibody precipitation using polyelectrolytes: A novel approach to the purification of monoclonal antibodies. Biotechnol Bioeng 102(4):1141–1151.

Moss JM, Van Damme MPI, Murphy WH, Preston BN. 1997. Dependence of salt concentration on glycosaminoglycan-lysozyme interactions in cartilage. Arch Biochem Biophys 348(1):49–55.

Moya W, Jaber J. inventors; Millipore Corp., assignee. Purification of proteins. United States patent US WO/2008/079280. 2006.

Pergushov DV, Izumrudov VA, Zezin AB, Kabanov VA. 1995. Stability of interpolyelectrolyte complexes in aqueous saline solutions. Polym Sci Ser A 37:1081–1087.

Ramanan S, Stenson R. inventors; Amgen, Inc., assignee. Method of isolating antibodies by precipitation. WO Patent WO/2008/100,578. 2008.

Seshadri S, Khurana R, Fink AL, Ronald W. 1999. Fourier transform infrared spectroscopy in analysis of protein deposits. Meth Enzymol 309:559–576.

Shukla AA, Hubbard B, Tressel T, Gunhan S, Low D. 2007. Downstream processing of monoclonal antibodies-application of platform approaches. J Chrom B 848:29–39.

Smales CM, Dinnis DM, Stansfield SH, Alete D, Sage EA, Birch JR, Racher AJ, Marshall CT, James DC. 2004. Comparative proteomic analysis of GS-NS0 murine myeloma cell lines with varying recombinant monoclonal antibody production rate. Biotechnol Bioeng 88(4):474–488.

Sommerfeld S, Strube J. 2005. Challenges in biotechnology production–generic processes and process optimization for monoclonal antibodies. Chem Eng Prog 44(10):1123–1137.

Surewicz WK, Mantsch HH. 1988. New insight into protein secondary structure from resolution-enhanced infrared spectra. Biochim Biophys Acta 952:115–130.

Temponi M, Kageshita T, Perosa F, Ono R, Okada H, Ferrone S. 1989. Purification of murine IgG monoclonal antibodies by precipitation with

caprylic acid: Comparison with other methods of purification. Hybridoma 8(1):85–95.

Thömmes J, Etzel M. 2007. Alternatives to chromatographic separations. Biotechnol Prog 23(1):42–45.

Tribet C. 2001. Complexation between amphiphilic polyelectrolytes and proteins: From necklaces to gels. In: Radeva T, editor. Physical chemistry of polyelectrolytes, surfactant science series, volume 99. 10th edn. New York: Marcel Dekker, Inc. p 687–743.

Vasilevskaya VV. 2001. Conformational transition in polyelectrolyte molecules: Influence of osmotic pressure of counterions. In: Radeva T, editor. Physical chemistry of polyelectrolytes, surfactant science series, volume 99. 10th edn. New York: Marcel Dekker, Inc. p 181–202.

Venkiteshwaran A, Heider P, Teysseyre L, Belfort G. 2008. Selective precipitation-assisted recovery of immunoglobulins from bovine serum using controlled-fouling crossflow membrane microfiltration. Biotechnol Bioeng 101(5):957–966.

Wang JM, Diehl T, Aguiar D, Dai XP, Arunakumari A. 2009. Precipitation of process-derived impurities in non-Protein A purification schemes for antibodies. BioPharm Int. Oct suppl., Downstream processing 4–10.

Wurm FM. 2004. Production of recombinant protein therapeutics in cultivated mammalian cells. Nat Biotech 22(11):1393–1398.

Xia J, Dubin PL, Kokufuta E, Havel H, Muhoberac BB. 1999. Light scattering, CD, and ligand binding studies of ferrihemoglobin–polyelectrolyte complexes. Biopolymers 50(2):153–161.

4. Summary and conclusion

The studies presented in the cumulative part of this thesis illustrate the different steps to develop a polymer-driven antibody purification process. These peer-reviewed reports show in detail fundamental research, additional method development useful in the development of such a purification process as well as implementation of the final process. A strategy for analyzing copolymers, synthesized by a lab in house, was implemented with particular emphasis on copolymer composition analysis. This was especially important in the context of understanding how copolymer composition affects precipitation yield and selectivity. Compared to ^{1}H-NMR composition analysis, the use of ATR infrared spectroscopy enabled a cost-effective and fast analysis of copolymers and according adjustment of synthesis parameters.[55] Besides the benefits for this project, the similar analytical power of IR compared to NMR was shown, also allowing small-scale companies to use such a technique. Following synthesis and synthesis optimization, basic research experiments were conducted, elucidating how ionic strength, polymer chain length, polymer chain flexibility, pH, pyhsico-chemical properties of copolymer and protein as well as copolymer composition affect precipitation behavior. Similar to relevant work in the literature, cited in the introduction section, increasing ionic strength led to reduced precipitation yields. Additionally to these known aspects, low ionic strength also resulted in reduced precipitation yield.[56] We concluded polyelectrolyte chain conformation being rather stiff at low ionic strength to be the reason for these findings. At low ionic strength, charges at polyelectrolyte sub-units are not sufficiently shielded anymore, leading to a more expanded conformation of the polyelectrolyte. This would then impede interaction with the proteins. Comparing precipitation behavior of different antibodies, the required polyelectrolyte flexibility to allow for high precipitation yields depended on the charge density of the protein.[56] These new insights could also help in the design of polyelectrolytes with defined flexibility to control precipitation selectivity. Another important factor is polymer chain length, which does not only influence yield and selectivity. It also affects precipitation efficiency, meaning the number of polymer chains required to obtain precipitation of an antibody molecule.[57] The use of polymer standards with defined molecular weight distribution revealed that the polymer chain length required per precipitated protein molecule is up to 25-times larger than the actual diameter of the specific protein. Moreover, comparing different types of polymers within this context, the defined length of polymer chain length differed among these copolymers. Under precipitation conditions strongly charged polymers allowed precipitation even with short defined lengths, meaning they enabled efficient precipitation.[57] Moreover, a further adjustment of selectivity and yield can be achieved altering the copolymer composition. Compared to results by other working groups, cited in the introduction section, the use of these copolymers allowed higher salt tolerance and higher yields without prior dilution of the cell culture fluid.[58]

Simultaneously, infrared spectroscopy was used as a process-assessment tool, determining the amount of antibody, host cell proteins as well as aggregated antibody before and after precipitation to analyze selectivity and yield.[59-61] This was particularly important, as e.g. the use of ELISA-assays for HCP quantification is quite costly, especially during process development which requires a large number of these assays to be used. Regarding aggregation analysis and quantification, IR has already been used in the past, as shown by literature cited in the introduction section and was further advanced not only to provide information about the presence of aggregation but also to quantify the amount of aggregates in a sample. The results of these peer-reviewed reports were suitable in the context of this thesis and precipitation process development. Additionally as the here developed quantification procedures for antibody titer, aggregate level and host cell protein amount may also find suitable application as a general fast and cost-effective process-monitoring technique, they are currently under consideration for a patent application. Some further experiments were conducted showing that infrared spectroscopy can be used to distinguish antibodies from other proteins based on differences in secondary structure. These findings were, together with additional denaturation monitoring experiments, submitted for a book chapter. Moreover, they allowed comparison of the secondary structure of monoclonal antibodies before and after precipitation, to elucidate any changes to the protein secondary structure and thus harmful effects of this process.[48] Integration of all these findings helped to implement a protein purification process based on precipitation. This process was then compared to protein A chromatography with respect to costs and effectiveness.[48] The developed process can be used within the purification cascade and may replace at least in part

existing initial chromatography-based purification processes. Compared to protein A affinity chromatography, costs are lower for future high titer cell culture systems used for antibody production.[48] Yet, additional applications beyond antibody production are also feasible.

5. References

[1] Dotzel, M. M. (1999). International conference on harmonisation of technical requirements for registration of pharmaceuticals for human use, ''Guidance on Specifications: Test Procedures and Acceptance Criteria for Biotechnological/Biological Products'' (Geneva, Switzerland). Fed Regist 64:44928–44935.

[2] Zoon, K. C. (1997). Points to consider in the manufacture and testing of monoclonal antibody products for human. Rockville: Center for Biologics Evaluation and Research, FDA.

[3] Maranga, L., Rueda, P., Antonis, A., Vela, C., Langeveld, J., Casal, J., & Carrondo, M. (2002). Large scale production and downstream processing of a recombinant porcine parvovirus vaccine. *Applied microbiology and biotechnology*, *59*(1), 45-50.

[4] Amersham Biosciences AB (2002), Antibody Purification Handbook, Edition AC, pp 19-21, Amersham Biosciences AB, Uppsala, Sweden.

[5] Shukla, A. A., Hubbard, B., Tressel, T., Guhan, S., & Low, D. (2007). Downstream processing of monoclonal antibodies—application of platform approaches. *Journal of Chromatography B*, *848*(1), 28-39.

[6] Zhou, J. X., Tressel, T., Gottschalk, U., Solamo, F., Pastor, A., Dermawan, S., ... & Murphy, M. (2006). New Q membrane scale-down model for process-scale antibody purification. *Journal of Chromatography A*, *1134*(1), 66-73.

[7] Birch, J. R., & Racher, A. J. (2006). Antibody production. *Advanced drug delivery reviews*, *58*(5), 671-685.

[8] Chern, C. S., Lee, C. K., Chen, C. Y., & Yeh, M. J. (1996). Characterization of pH-sensitive polymeric supports for selective precipitation of proteins. *Colloids and Surfaces B: Biointerfaces*, *6*(1), 37-49.

[9] Thömmes, J., & Etzel, M. (2007). Alternatives to chromatographic separations. *Biotechnology Progress*, *23*(1), 42-45.

[10] Sommerfeld, S., & Strube, J. (2005). Challenges in biotechnology production—generic processes and process optimization for monoclonal antibodies. *Chemical Engineering and Processing: Process Intensification*, *44*(10), 1123-1137.

[11] Wurm, F. M. (2004). Production of recombinant protein therapeutics in cultivated mammalian cells. *Nature biotechnology*, *22*(11), 1393-1398.

[12] Low, D., O'Leary, R., & Pujar, N. S. (2007). Future of antibody purification. *Journal of Chromatography B*, *848*(1), 48-63.

[13] Cooper, C. L., Dubin, P. L., Kayitmazer, A. B., & Turksen, S. (2005). Polyelectrolyte–protein complexes. *Current opinion in colloid & interface science*, *10*(1), 52-78.

[14] Shukla, A. A., & Gottschalk, U. (2012). Single-use disposable technologies for biopharmaceutical manufacturing. *Trends in biotechnology*.

[15] Venkiteshwaran, A., Heider, P., Teysseyre, L., & Belfort, G. (2008). Selective precipitation-assisted recovery of immunoglobulins from bovine serum using controlled-fouling crossflow membrane microfiltration. *Biotechnology and bioengineering*, *101*(5), 957-966.

[16] Kuczewski, M., Schirmer, E., Lain, B., & Zarbis-Papastoitsis, G. (2011). A single-use purification process for the production of a monoclonal antibody produced in a PER. C6 human cell line. *Biotechnology Journal*, *6*(1), 56-65.

[17] Temponi, M., Kageshita, T., Perosa, F., Ono, R., Okada, H., & Ferrone, S. (1989). Purification of murine IgG monoclonal antibodies by precipitation with caprylic acid: comparison with other methods of purification. *Hybridoma*, *8*(1), 85-95.

[18] Hilbrig, F., & Freitag, R. (2003). Protein purification by affinity precipitation. *Journal of chromatography B*, *790*(1), 79-90.

[19] Kim, J. Y., Mulchandani, A., & Chen, W. (2005). Temperature-triggered purification of antibodies. *Biotechnology and bioengineering*, *90*(3), 373-379.

[20] Mattiasson, B., Dainyak, M. B., & Galaev, I. Y. (1998). Smart polymers and protein purification. *Polymer–Plastics Technology and Engineering*, *37*(3), 303-308.

[21] Taipa, M. Â., Kaul, R. H., Mattiasson, B., & Cabral, J. M. (2000). Recovery of a monoclonal antibody from hybridoma culture supernatant by affinity precipitation with Eudragit S-100. *Bioseparation*, *9*(5), 291-298.

[22] Izumrudov, V. A., Galaev, I. Y., & Mattiasson, B. (1998). Polycomplexes–potential for bioseparation. *Bioseparation*, *7*(4-5), 207-220.

[23] McDonald, P., Victa, C., Carter-Franklin, J. N., & Fahrner, R. (2009). Selective antibody precipitation using polyelectrolytes: a novel approach to the purification of monoclonal antibodies. *Biotechnology and bioengineering*, *102*(4), 1141-1151.

[24] Juckles, I. R. M. (1971). Fractionation of proteins and viruses with polyethylene glycol. *Biochimica et Biophysica Acta (BBA)-Protein Structure*, *229*(3), 535-546.

[25] Fahie-Wilson, M., & Halsall, D. (2008). Polyethylene glycol precipitation: proceed with care. *Annals of Clinical Biochemistry*, *45*(3), 233-235.

[26] Polson, C., Sarkar, P., Incledon, B., Raguvaran, V., & Grant, R. (2003). Optimization of protein precipitation based upon effectiveness of protein removal and ionization effect in liquid chromatography–tandem mass spectrometry. *Journal of Chromatography B*, *785*(2), 263-275.

[27] Lottspeich, F. & Engels, J. W. (2012). Proteinanalytik p. 20, in *Bioanalytik* (eds. F. Lottspeich & J. W. Engels), Springer-Spektrum, Springer-Verlag Berlin Heidelberg.

[28] Mirica, K. A., Lockett, M. R., Snyder, P. W., Shapiro, N. D., Mack, E. T., Nam, S., & Whitesides, G. M. (2012). Selective precipitation and purification of monovalent proteins using oligovalent ligands and ammonium sulfate. *Bioconjugate Chemistry*, *23*(2), 293-299.

[29] Polson, C., Sarkar, P., Incledon, B., Raguvaran, V., & Grant, R. (2003). Optimization of protein precipitation based upon effectiveness of protein removal and ionization effect in liquid chromatography–tandem mass spectrometry. *Journal of Chromatography B*, *785*(2), 263-275.

[30] Cohn, E. J., Strong, L. E., Hughes, W. L. J., Mulford, D. J., Ashworth, J. N., Melin, M., & Taylor, H. L. (1946). Preparation and Properties of Serum and Plasma Proteins. IV. A System for the Separation into Fractions of the Protein and Lipoprotein Components of Biological Tissues and Fluids1a, b, c, d. *Journal of the American Chemical Society*, *68*(3), 459-475.

[31] Morawetz, H., & Hughes Jr, W. L. (1952). The interaction of proteins with synthetic polyelectrolytes. I. Complexing of bovine serum albumin. *The Journal of Physical Chemistry*, *56*(1), 64-69.

[32] Berdick, M., & Morawetz, H. (1954). The interaction of catalase with synthetic polyelectrolytes. *Journal of Biological Chemistry*, *206*(2), 959-972.

[33] Bozzano, A. G., & Glatz, C. E. (1991). Separation of proteins from polyelectrolytes by ultrafiltration. *Journal of membrane science*, *55*(1), 181-198.

[34] Shahidi, F., Arachchi, J. K. V., & Jeon, Y. J. (1999). Food applications of chitin and chitosans. *Trends in Food Science & Technology*, *10*(2), 37-51.

[35] Bolto, B., & Gregory, J. (2007). Organic polyelectrolytes in water treatment. *Water research*, *41*(11), 2301-2324.

[36] Seyrek, E., Dubin, P. L., Tribet, C., & Gamble, E. A. (2003). Ionic strength dependence of protein-polyelectrolyte interactions. *Biomacromolecules*, *4*(2), 273-282.

[37] Hattori, T., Hallberg, R., & Dubin, P. L. (2000). Roles of electrostatic interaction and polymer structure in the binding of β-lactoglobulin to anionic polyelectrolytes: measurement of binding constants by frontal analysis continuous capillary electrophoresis. *Langmuir*, *16*(25), 9738-9743.

[38] Dobrynin, A. V., & Rubinstein, M. (2003). Effect of short-range interactions on polyelectrolyte adsorption at charged surfaces. *The Journal of Physical Chemistry B*, *107*(32), 8260-8269.

[39] Houska, M., Brynda, E., & Bohatá, K. (2004). The effect of polyelectrolyte chain length on layer-by-layer protein/polyelectrolyte assembly—an experimental study. *Journal of colloid and interface science*, *273*(1), 140-147.

[40] Pergushov, D. V., Izumrudov, V. A., Zezin, A. B., & Kabanov, V. A. (1995). Stability of interpolyelectrolyte complexes in aqueous saline solutions: effect of the degree of polymerization of polyions. *Polymer science. Series A, Chemistry, physics*, *37*(10), 1081-1087.

[41] Kayitmazer, A. B., Seyrek, E., Dubin, P. L., & Staggemeier, B. A. (2003). Influence of chain stiffness on the interaction of polyelectrolytes with oppositely charged micelles and proteins. *The Journal of Physical Chemistry B*, *107*(32), 8158-8165.

[42] Hattori, T., Bat-Aldar, S., Kato, R., Bohidar, H. B., & Dubin, P. L. (2005). Characterization of polyanion–protein complexes by frontal analysis continuous capillary electrophoresis and small angle neutron scattering: Effect of polyanion flexibility. *Analytical biochemistry*, *342*(2), 229-236.

[43]   Carlsson, F., Malmsten, M., & Linse, P. (2003). Protein-polyelectrolyte cluster formation and redissolution: A monte carlo study. *Journal of the American Chemical Society*, *125*(10), 3140-3149.

[44]   Stoll, S., & Chodanowski, P. (2002). Polyelectrolyte adsorption on an oppositely charged spherical particle. Chain rigidity effects. *Macromolecules*, *35*(25), 9556-9562.

[45]   Tsuchida, E., Osada, Y., & Sanada, K. (1972). Interaction of poly (styrene sulfonate) with polycations carrying charges in the chain backbone. *Journal of Polymer Science Part A-1: Polymer Chemistry*, *10*(11), 3397-3404.

[46]   Fahrner R, Franklin J, McDonald P, Peram T, Sisodiya V, Victa C, inventors; Genentech, Inc.,assignee. Polyelectrolyte precipitation and purification of antibodies. WO/2008/091740, 2008.

[47]   Fahrner R, Franklin J, McDonald P, Peram T, Sisodiya V, Victa C, inventors; Genentech, Inc.,assignee. Polyelectrolyte precipitation and purification of proteins. US7947813 B2

[48]   Capito, F., Bauer, J., Rapp, A., Schröter, C., Kolmar, H., & Stanislawski, B. (2013). Feasibility study of semi-selective protein precipitation with salt-tolerant copolymers for industrial purification of therapeutic antibodies. *Biotechnology and bioengineering*, 110(11), 2915-2927.

[49]   Oberg, K. A., Ruysschaert, J. M., & Goormaghtigh, E. (2004). The optimization of protein secondary structure determination with infrared and circular dichroism spectra. *European Journal of Biochemistry*, *271*(14), 2937-2948.

[50]   Barth, A. (2007). Infrared spectroscopy of proteins. *Biochimica et Biophysica Acta (BBA)-Bioenergetics*, *1767*(9), 1073-1101.

[51]   Kong, J., & Yu, S. (2007). Fourier transform infrared spectroscopic analysis of protein secondary structures. *Acta Biochimica et Biophysica Sinica*, *39*(8), 549-559.

[52]   Savitzky, A., & Golay, M. J. (1964). Smoothing and differentiation of data by simplified least squares procedures. *Analytical chemistry, 36*(8), 1627-1639.

[53]   Maddams, W. F., & Mead, W. L. (1982). The measurement of derivative ir spectra—I. Background studies. *Spectrochimica Acta Part A: Molecular Spectroscopy, 38*(4), 437-444.

[54]   Surewicz, W. K., Mantsch, H. H., & Chapman, D. (1993). Determination of protein secondary structure by Fourier transform infrared spectroscopy: a critical assessment. *Biochemistry, 32*(2), 389-394.

[55]   Capito, F., Bauer, J., Rapp, A., Kolmar, H., & Stanislawski, B. (2013). Synthesis and characterization of customized 2-acrylamido-2-methylpropane sulfonic acid - benzylacrylamide /acrylamidobenzoic-acid copolymers for semi-selective protein purification. Journal of Polymer Research. to be submitted

[56]   Capito, F., Skudas, R., Stanislawski, B., & Kolmar, H. (2013). Polyelectrolyte–protein interaction at low ionic strength: required chain flexibility depending on protein average charge. Colloid and Polymer Science, 291(7), 1759-1769.

[57]   Capito, F., Kolmar, H., Stanislawski, B., & Skudas, R. (2013) Determining the defined length of a polymer chain required per precipitated protein molecule: studying interactions between anionic polymers and four physicochemically different proteins. Journal of Polymer Research. submitted

[58]   Capito, F., Skudas, R., Kolmar, H., & Stanislawski, B. (2013) Customization of copolymers to optimize selectivity and yield in polymer-driven antibody purification processes. Biotechnology Progress. in press

[59]   Capito, F., Skudas, R., Kolmar, H., & Stanislawski, B. (2012). Host cell protein quantification by fourier transform mid infrared spectroscopy (FT-MIR). Biotechnology and Bioengineering, 110(1), 252-259.

[60]   Capito, F., Skudas, R., Stanislawski, B., & Kolmar, H. (2012). Matrix effects during monitoring of antibody and host cell proteins using attenuated total reflection spectroscopy. Biotechnology progress, 29(1), 265-274.

[61]   Capito, F., Skudas, R., Kolmar, H., & Hunzinger, C. (2013). Mid-infrared spectroscopy-based antibody aggregate quantification in cell culture fluids. *Biotechnology journal.* 8(8), 912-917.

References   178

Chapter 3.3

Supplementary material to

Determining the defined length of a polymer chain required per precipitated protein molecule: studying interactions between anionic polymers and four physicochemically different proteins – Colloid and Polymer Science
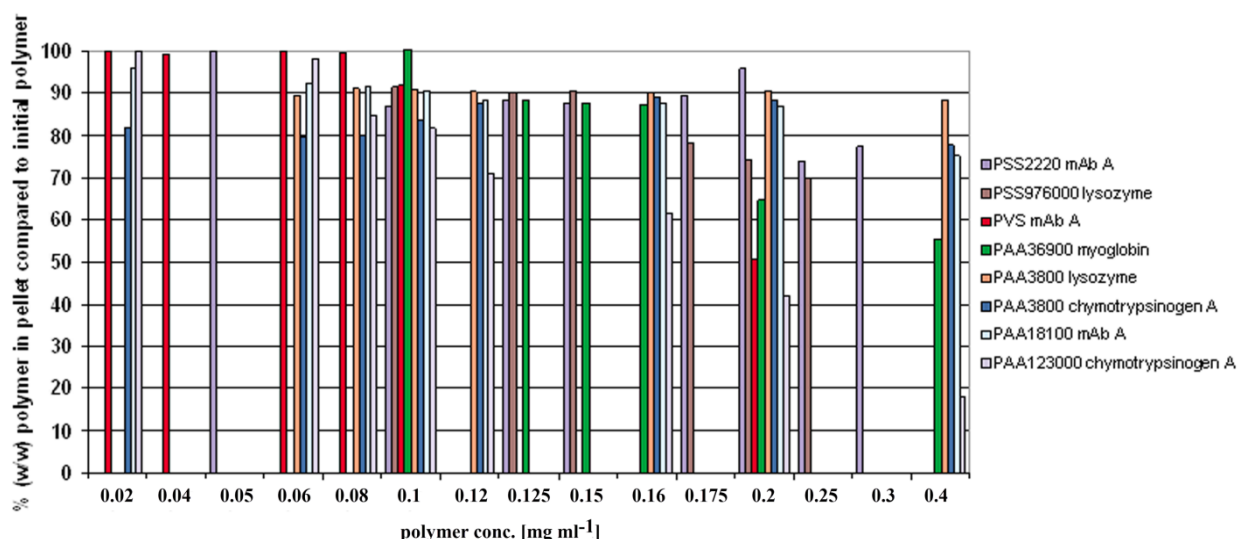
Florian Capito[12], Harald Kolmar[1], Bernd Stanislawski[2] and Romas Skudas[2]

1Clemens-Schöpf Institute, Technical University of Darmstadt, Germany
2 Merck KGaA, Frankfurter Strasse 250, 64293 Darmstadt, Germany
florian.capito@external.merckgroup.com

1 Relative accumulation of polymer in protein-polymer precipitate

S1. Exemplary overview of relative accumulation of polymer in the pellet, when precipitating different proteins, depending on initial polymer concentration. Polymer accumulation was determined using either FTIR (all polymers except PAA) or fluorescently labelled polymer (PAA) for residual polymer determination after precipitation with different proteins. Determination error was 10- 20 % for polymer concentrations less than 0.15 mg ml^{-1}, which were used for pre-selected optimum polymer concentrations. As error was higher for polymer concentrations between 0.15 mg ml^{-1} to 0.4 mg ml^{-1}, this polymer concentration range was not used to calculate molar ratios.

2 Zeta potential of polymers

S2. Zeta potential of polymers measured at pH 5.0.

Polymer and corresponding M_w in g mol^{-1}	Zeta potential [mV]
PASA	-58.5
PSS 1360	-18.1
PSS 2220	-21.9
PSS 6530	-30.2
PSS 10600	-35.6
PSS 15200	-33.3
PSS 43300	-34.4
PSS 976000	-55.2
PVS 2100	-29.3
PAA 1930g mol^{-1}	-14.2
PAA 3800g mol^{-1}	-28.8
PAA 8300g mol^{-1}	-28.1
PAA 18100g mol	-27.6
PAA 36900g mol	-24.5
PAA 123000g mol	-29.2
PAA 958000g mol	-29.4

Biotechnology
Journal

Mid-infrared spectroscopy-based antibody aggregate quantification in cell culture fluids

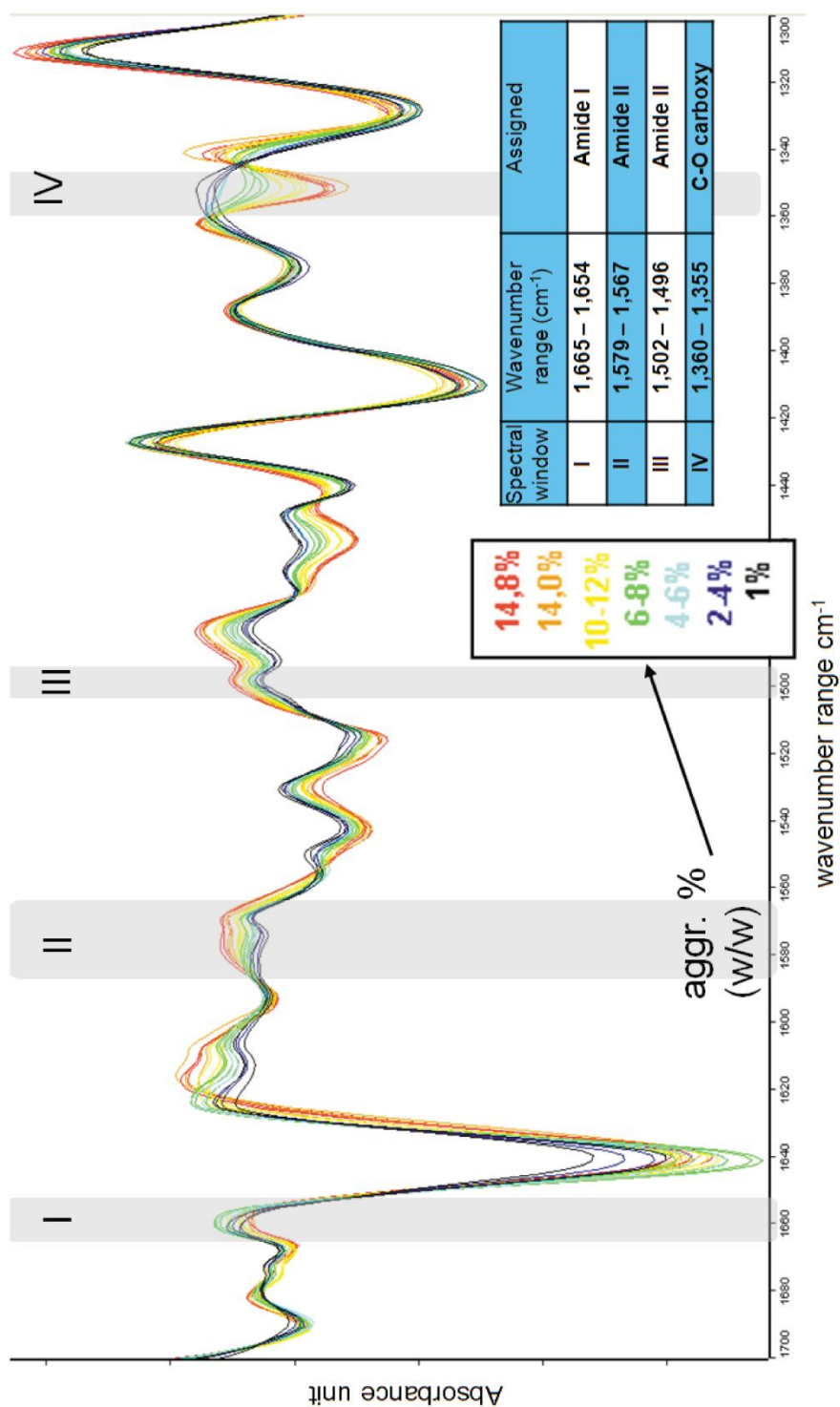*Florian Capito, Romas Skudas, Harald Kolmar and Christian Hunzinger*

Figure 1: Spectral comparison of defined blends of aggregated and non-aggregated antibody. Selected wavenumber ranges used for designing a quantification model, showing a correlation between band intensity and amount of aggregated antibody, are highlighted in grey; explanation and band assignment included in table.

Spectral window	Wavenumber range (cm^{-1})	Assigned
I	1,665 – 1,654	Amide I
II	1,579 – 1,567	Amide II
III	1,502 – 1,496	Amide II
IV	1,360 – 1,355	C-O carboxy

aggr. % (w/w)

14,8%
14,0%
10-12%
6-8%
4-6%
2-4%
1%

M.Sc.   Darmstadt, den 18. Oktober 2013
Florian Capito
Riedeselstrasse 68
64283 Darmstadt
0176- 91376471
florian.capito@gmail.com

Eidesstattliche Erklärung
Ich erkläre hiermit an Eides Statt, dass ich meine Dissertation selbstständig und nur mit
den angegebenen Hilfsmitteln angefertigt habe.

M.Sc. Florian Capito

M.Sc.   Darmstadt, den 18. Oktober 2013

Florian Capito

Riedeselstrasse 68
64283 Darmstadt
0176- 91376471
florian.capito@gmail.com

Erklärung

Ich erkläre hiermit, noch keinen Promotionsversuch unternommen zu haben.

M.Sc. Florian Capito

Curriculum vitae
M.Sc.
Florian Capito
Riedeselstrasse 68
64283 Darmstadt
0176- 91376471
florian.capito@gmail.com

Persönliche Daten

Geburt:	15. Januar 1985 in Mainz
Nationalität:	deutsch
Familienstand:	ledig

Akademischer Werdegang

seit April 2011
Promotion am Clemens-Schöpf-Institut für Organische Chemie und Biochemie der Technischen Universität Darmstadt sowie bei der Merck KGaA unter Betreuung von Prof. Dr. Harald Kolmar, Dr. Bernd Stanislawski sowie Dr. Romas Skudas

August 2009 bis März 2011:
Masterstudium Proteinwissenschaft, Universität Lund, Schweden.
Thema der Masterarbeit:
„Development of a precipitation process for industrial protein purification"
Betreuer: Dr. Bernd Stanislawski (Merck KGaA)
Prof. Dr. Cecilia Cabaleiro-Lago (Universität Lund, Schweden)

August 2007 bis Juli 2008:
Filosofie kandidatexamen (schwedischer Hochschulabschluss) in Molekularbiologie, Universität Lund, Schweden (ERASMUS-Stipendium)

April 2005 bis Juli 2008:
Bachelorstudium in molekularer Biologie, Johannes-Gutenberg Universität Mainz.
Thema der Bachelorarbeit:
"Structure-function relationship of human thymidine kinase 1 mutants"
Betreuer: Prof. Dr. Walter Stöcker
Prof. Dr. Jure Piskur (Universität Lund, Schweden)

Wehrdienst:
Zentrales Institut des Sanitätsdienstes der Bundeswehr, Koblenz, Aussenstelle Mainz, Nährmedienproduktion, Autoklavieren von Laborabfällen

Schulbildung:
1995-2004
Gymnasium zu St. Katharinen, Oppenheim Abschluss: Abitur (Note: 1,6)

Zusatzqualifikationen:	Februar 2013
	Seminar Führunskompetenz für Naturwissenschaftler, Ingenium, TU Darmstadt
	Seit April 2013
	Modul-Kurs „geprüfter Projektmanager Wirtschaftschemie", Gesellschaft Deutscher Chemiker, Universität Münster
	Mai 2013
	Seminar Mitarbeiterführung, Ingenium, TU Darmstadt
Sprachen:	Deutsch (Muttersprache)
	Englisch (verhandlungssicher)
	Schwedisch (fließend)
	Französisch (gute Kenntnisse)

M.Sc. Florian Capito